Using Single Cell RNA Sequencing to Elucidate Mechanisms of Immune Suppression in the Pancreatic Tumor Microenvironment

by

Veerin Rachan Sirihorachai

A dissertation submitted in partial fulfillment
of the requirements for the degree of
Doctor of Philosophy
(Cancer Biology)
in the University of Michigan
2022

Doctoral Committee:

Professor Goutham Narla, Chair
Adjunct Professor Howard Crawford
Assistant Professor Stefanie Galban
Assistant Professor Kyoung E. Lee
Professor Marina Pasca di Magliano
Associate Professor Arvind Rao

Veerin R. Sirihorachai

vrsiri@umich.edu

ORCID iD: 0000-0003-4992-6499

Dedication

To all the people who’ve personally been affected by cancer. Patients, survivors, pre-vivors, the happy families and especially the grieving ones, may this work represent a seed of hope for the future.

Acknowledgements

The following work represents the cumulative efforts of multiple people who have supported the effort in ways ranging from considerable to essential- there were no bit players in this monstrous effort. Professionally, this work would not have been possible had my mentor Dr. Marina Pasca di Magliano not taken a chance on me and given an ambitious single cell sequencing project to the then newest member of the lab. The other members of the Pasca Di Magliano lab were also always helpful. Specifically, this project would not have been possible without Dr. Eileen Carpenter doing the essential work to bridge the gap between the researchers and clinicians. Drs. Nina Steele and Sam Kemp were instrumental in my development as a graduate student, helping me to re-focus and re-engage when I got bogged down in the weeds of the work by sharing their insights and through their ability to re-work seemingly insurmountable tasks into measurable, achievable milestones. Drs. Fil Bednar and Yaqing Zhang repeatedly demonstrated their abilities as senior researchers, making excellent use of their experience to mentor myself and many others through every step of the research process. I'm also grateful to the other postdocs and students in the Pasca Di Magliano lab Dr. Zeribe Nwosu, Dr. Wenting Du, Ashley Velez-Delgado, Mike Scales, Rosa Menjivar, Emily Lasse-Opsahl, Padma Kadiyala, and Ahmed Elhossiny, and a special mention to Katelyn Donahue for being my bay buddy and the other half of the germinal "Pasca Lab Bioinformatics" core. Unfathomable thanks to our lab manager Carlos Espinoza for keeping this veritable cruise liner of people above water.

Over the course of my PhD, I had the pleasure of working with several stellar collaborators. First and foremost, I would like to acknowledge all the members of the pancreatic cancer group at the University of Michigan, the Pancreatic Tumor Eradication Alliance (PanTERA). I have never seen a more engaged group of scientists from different backgrounds come together and have a constructive conversation about their shared interests. The weekly meetings were always informative, supportive, and the camaraderie between all the labs made the weekly meetings a delight to attend. Next, I would like to thank the lab of Dr. Arvind Rao, specifically Stephanie The, who was able to turn the mad, rambling requests of sleep deprived biologists into functional code. The members of my thesis committee were instrumental in keeping me on track as both my project and the world around us took some sharp left turns over the course of my PhD. Thank you to Drs. Howard Crawford, Goutham Narla, Arvind Rao, Kyoung Lee, and Stefanie Galban for your guidance and constructive criticisms, showing me how to lay a path forward when I was overwhelmed and confused about the direction I should be taking my project.

Thank you to everyone in the Cancer Biology program for providing such an amazing graduate school experience. When I visited the University of Michigan for my interview, the feature that drew me first and foremost to the school was the sense of camaraderie in the program. A newer program, with a diverse membership coming from various departments, coming together with both regularity and ease to discuss all types of cancer. I was in awe watching these highly intelligent trainees and faculty members bouncing ideas off each other with an ease and casualness that belayed the fact that these people were based in such different fields they may as well be speaking different

languages. It was the people that fostered the atmosphere of open collaboration and discussion that made my graduate students so enriching.

Personally, I would like to thank my family first and foremost. To my father and sister for being great role models from childhood until today, the people who showed me where hard work, diligence, and ambition can take you. To my brother, who never failed to use his seemingly endless talent and compassion to help me out where he could, whether through building me a new computer to work from home during the pandemic or by refurbishing a scrap car into the vehicle I still drive to this day. To my late mother, who showed me the tenacity and infinite depth of love in the face of insurmountable strife. The ceaseless bouts of laughter, the shared tears, and the delicious meals we've shared over the years have always been the steady foundation on top of which I was able to grow. I wouldn't be the person I am today were it not for your love.

To my friends, old or new, here or there- to all of my friends, thank you for the laughter and warmth. Cancer research is hard, the subject emotionally heavy and at times frustratingly difficult and elusive, and the constant feelings of failure to make appreciable process can take its toll personally and professionally. You were there to make the work not just bearable, but enjoyable even. Movie nights, happy hours, late nights spent laughing or spent huddled together crying over aerosolized capsaicin, I am grateful to have so many people who have meant so much to me.

Thank you to my kids for being little and fluffy and letting me hug and smooch you and only be in trouble for it sometimes. And final thanks to myself for putting one foot in front of the other until you were ready to run.

Table of Contents

List of Tables

List of Figures

List of Appendices

Abstract

Pancreatic ductal adenocarcinoma (PDA) is the third leading cause of cancer related death, with a five-year survival rate of 11%. Not only is PDA often diagnosed at advanced stages, but the standard of care chemotherapy is largely ineffective. The distinctive biologic characteristics of PDA make it difficult to treat. PDA is typically driven by an oncogenic Kras mutation. Oncogenic Kras is required for the maintenance of PDA, but inhibitors for this oncogene are few. Another key feature of PDA is the extensive fibroinflammatory stroma that constitutes the bulk of the tumor volume. The stroma includes fibroblasts, extracellular matrix and abundant infiltrating immune cells. The latter are largely immunosuppressive immune cells, including regulatory T cells, myeloid-derived suppressor cells, and tumor associated macrophages. Data from our laboratory and many others show that immune cells are a key determinant of PDA progression and metastasis. The overarching goal of my project is to understand the nature and regulation of the immune response in the PDA tumor microenvironment by dissecting the crosstalk between tumor cells and immune cells to devise strategies to reverse the immune suppression that characterizes PDA.

First, we performed a multimodal analysis of human PDA tumors and PBMCs, using multiplex immunohistochemistry, mass cytometry, and single cell RNA sequencing to describe the composition of human PDA and hypothesize possible interactions between the various cell types based on abundance, localization, and receptor-ligand expression. The combination of these techniques highlighted the

prevalence of understudied immune checkpoint TIGIT in human PDA compared to normal pancreas. Functionally, we discovered that TIGIT expression is significantly elevated in exhausted CD8 T cells than in effector CD8 T cells, while classical immune checkpoint protein PD-1 was not significantly different. This work demonstrates the efficacy of the discovery pipeline pioneered by members of the lab, using a combination of high resolution techniques to uncover novel and potentially efficacious treatment strategies in PDA.

Secondly, we used single cell RNA sequencing to analyze the transcriptome of the various cell types present in the liver metastases of PDA patients. We characterized the different cell populations and performed differential expression analyses to determine genes upregulated in PDA metastases vs. primary tumors. We then determined putative receptor-ligand interactions based on expression of receptors and ligands on source and target cells in the PDA TME showing preliminary evidence of immune suppression in PDA liver metastases.

Finally, using mouse models of both pancreatic and lung cancer, we studied the effects of oncogenic Kras on the maintenance of the tumor microenvironment in both pancreatic and lung cancers with the goal of discovering the effect oncogenic $Kras^{G12D}$ has on the tumor microenvironment in both primary and metastatic tumors. We verified the functionality of two mouse models of inducible Kras driven pancreas and lung cancer and performed mfIHC on the model of lung cancer to characterize the shifting immune populations in the progression and regression of the lung tumor.

Together, these studies illustrate the importance of understanding cell signaling in the tumor microenvironment. By uncovering previously understudied mechanisms of

immune suppression and elucidating the requirement of KRAS in establishing the TME, our work represents the first step in the identification of interactions required for the maintenance of PDA tumors. Further work is necessary to evaluate the physiological importance of these interactions and subsequently determine their translational potential.

Chapter 1: Introduction

Pancreatic cancer overview

Pancreatic cancer is a fatal malignancy. Using mortality as an indicator of progress against cancer, major strides have been made against many types of cancer during the past several decades, owing to more widespread campaigns for cancer prevention, advancements in early detection, and improvements in both non-targeted treatment with cytotoxic drugs as well as targeted therapies (Siegel et al. 2021). Unfortunately, many of these advances have either not been applied to pancreatic cancer, or the efficacy of the discoveries has not had an appreciable effect on the mortality rate of pancreatic cancer (Figure 1.1A). The mortality rate of pancreatic cancer is so extreme that although pancreatic cancer incidence only makes up for approximately 3% of new cancer cases, pancreatic cancer is projected to be the second leading cause of cancer-related death by 2030 (Rahib et al. 2021). The five-year survival rate, a measure of the percentage of patients that survive five years after diagnosis, for pancreatic cancer patients is the lowest among the ten most common cancers with only a 11% five-year survival rate across all stages. The lethality of pancreatic cancer comes from a variety of sources across the various stages of cancer treatment, starting with the difficulty in diagnosing the disease.

The difficulty in diagnosing pancreatic cancer begins with physiological aspects of the pancreas itself. The pancreas is a dual-function secretory organ that has both

exocrine and endocrine functions (Mizrahi et al. 2020). Acinar cells perform the exocrine functions, secreting digestive pancreatic juice into pancreatic ducts lined by ductal cells. Islet cells perform the endocrine functions, secreting hormones into the bloodstream to regulate blood glucose homeostasis. Disruption of the exocrine functions can lead to inflammation of the pancreas, termed pancreatitis, due to the inappropriate activation of digestive enzymes damaging the cells of the pancreas. Disruption of the endocrine functions can result in diabetes, a group of disorders characterized by impaired blood sugar regulation. Pancreatitis and diabetes are maladies that occur much more commonly than pancreatic cancer and the symptoms of the diseases overlap greatly [see review: (Eibl et al. 2018)]. The symptoms pancreatic cancer patients present with are usually mild, non-specific symptoms such as abdominal or back pain, nausea, and other symptoms common to any sort of gastrointestinal distress, including pancreatitis and diabetes [see review: (Mizrahi et al. 2020)]. To further complicate the relationship between this group of diseases, a history of chronic pancreatitis and/or diabetes is a risk factor of pancreatic cancer, but pancreatitis and new-onset diabetes are also potential symptoms that arise as complications from having pancreatic cancer. The attribution of the symptoms of pancreatic cancer to more common, benign conditions can significantly delay a proper diagnosis until the tumor advances and the symptoms get worse, as the location of the pancreas, nested between the stomach, small intestine, liver and spleen, in the retroperitoneal cavity makes non-invasive imaging or biopsy difficult and time consuming. An in-depth examination of the pancreas does not tend to occur until more serious symptoms such as new-onset diabetes, jaundice, weight loss, and abnormal liver function occur as the tumor grows and metastasizes and begins to significantly

affect the function of the pancreas and/or nearby organs. The delay in diagnosis is reflected in the statistics of pancreatic cancer staging upon diagnosis.

Pancreatic cancer is typically diagnosed at advanced tumor stages where treatment options are limited. 52% of patients are diagnosed with overt metastatic disease, 30% diagnosed with a regionally advanced tumor, and only 11% diagnosed with a localized tumor. Unfortunately, the five-year survival rate for pancreatic cancer significantly decreases once the tumor is advanced beyond a localized tumor with clear margins. The five-year survival rate for localized pancreatic cancer is 39% but decreases to 13% upon regional advancement and further decreases to 3% once the cancer becomes distally advanced (Figure 1.1B and 1.1C)(Siegel et al. 2021). The decrease in the five-year survival rate between localized and regionally advanced tumors is indicative of the fact that the only curative treatment for pancreatic cancer is complete surgical resection via a complicated surgical procedure, combined with adjuvant or neoadjuvant therapy (Carpenter et al. 2021). However, surgical resection of resectable and borderline resectable tumors only has a five-year survival rate of 10-20% with a median disease-free survival time of 7-8 months, the result of unresected margins, undetectable microlesions, and/or possible early metastases (Chikhladze et al. 2019; Versteijne et al. 2020). The current standard of care outside of surgical resection is palliative chemotherapy, with the FOLFIRINOX or gemcitabine/nab-paclitaxel regimens. The new standards of care demonstrate a modest increase in median overall survival, from about 6-7 months with the previous standard of care, gemcitabine monotherapy, to 11.1 months with FOLFIRINOX and 8.5 months with gemcitabine and nab-paclitaxel. While these chemotherapeutic therapies are the current standard of

care, there are multiple other treatment modalities being developed to target the various components of the pancreatic cancer microenvironment, from the tumor cells themselves to the mass of non-tumor cells that make up the bulk of the pancreatic cancer tumor.

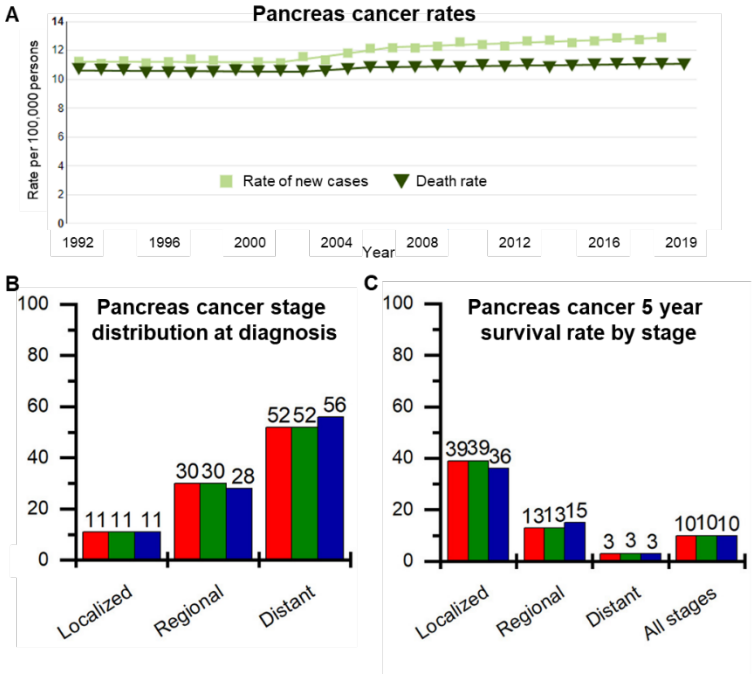

Figure 1.1 Pancreatic cancer statistics
(A) The death rate of pancreatic cancer has not significantly changed in the past two decades as most patients that develop pancreatic cancer will die from the disease. **(B)** Only a small minority of patients are diagnosed with localized disease while most patients are diagnosed with metastatic disease. **(C)** Patients with localized disease have the highest 5-year survival rate, but due to the low percentage of patients diagnosed at this stage and the poor 5-year survival rates of patients diagnosed with regional and metastatic disease, the overall 5-year survival rate of pancreatic cancer remains low.

The pancreatic tumor microenvironment

Pancreatic ductal adenocarcinoma (PDA) is the primary subtype of pancreatic cancer. PDA is the result of the transformation of a cell involved in the exocrine function of the pancreas and represent most pancreatic cancer cases, while the rarer transformations of cells involved in endocrine functions are termed neuroendocrine tumors. The exocrine pancreas includes acinar cells, ductal cells, and centroacinar cells; of those, both acinar and ductal cells have been identified as potential cells of origin for PDA (J.L. Kopp et al. 2011; L. Kopp, Janel et al. 2012; Espinet et al. 2021; Flowers et al. 2021). When the pancreas undergoes an injury from sources including

alcohol abuse, smoking, or duct blockage, the acinar cells transform from their normal secretory state to become a proliferative duct-like cell in order to facilitate tissue repair. This process is called acinar-to-ductal metaplasia (ADM) and is the result of a downregulation of genes that maintain acinar identity such as PTF1A and an upregulation of ductal genes such as SOX9 and CK19 (L. Zhu et al. 2007; L. Kopp, Janel et al. 2012). This trans-differentiation is reversible upon resolution of the injury. However, if the acini or ADM acquire an activating mutation in an oncogene such as KRAS, the cells will remain in the proliferative ADM state even if the source of the injury is resolved (Shi et al. 2009). This persistent, proliferative ADM can give rise to pancreatic intraepithelial neoplasia (PanIN). The presence of PanINs is not predictive of developing PDA, however, also being found in cases of chronic pancreatitis and in healthy individuals, where prevalence increases with age (Basturk et al. 2015). Of note, most cases of PDA in human patients are not linked with a history of diagnosed pancreatitis, thus other routes to cellular transformation are likely to exist. It is through the stepwise accumulation of genetic mutations including the loss of tumor suppressors INK4A/ARF, TP53, CDKN2A, BRCA2, or gain of known oncogenes such as EGFR/HER2, among others, that the PanINs advance from low-grade dysplasia to high-grade dysplasia until they form a carcinoma *in situ*, the most advanced stage of PanIN that is predictive of development of invasive PDA (R. H. Hruban et al. 2000; Biankin et al. 2001; Nowak et al. 2005; Jones et al. 2008; Kanda et al. 2012). This model of the carcinogenesis of PDA has led to the development of multiple genetically engineered mouse models of PDA for use in pre-clinical research.

Mouse models of PDA can be used to model the disease and perform valuable pre-clinical research. There are multiple mouse models of PDA available. Mouse models typically involve expression of Cre-recombinase controlled by a pancreas/acinar cell specific promoter. Expression of the recombinase results in either the activation of oncogenic Kras, or inactivation of a tumor suppressor, or both. The combination of oncogenic Kras and Cre-recombinase (KC) results in age-dependent PanIN progression that will occasionally result in PDA (Hingorani et al. 2003; Ralph H. Hruban et al. 2006). Inactivation of a tumor suppressor such as Ink4a/Arf (KIC) or p53 (KPC) in tandem with the activation of oncogenic Kras accelerates the development of PanINs and increases the occurrence of progression to PDA (Aguirre et al. 2003; Hingorani et al. 2005). While these genetically engineered mouse models do replicate the carcinogenesis of human PDA, one confounding factor is how early these models express oncogenic Kras. The impact of expressing oncogenic Kras early on in embryonic mouse development instead of in an adult mouse both fails to mimic the timeline of human PDA development and can also affect the physiological response of the mouse to the developing tumor. In order to bypass this, an inducible model of the KC was generated.

In the iKras model, activation of the cre-recombinase results in expression of a reverse tetracycline transactivator which can activate transcription of oncogenic Kras only in the presence of doxycycline (Collins et al. 2012; Ying et al. 2012). The later activation of oncogenic Kras results in less PanIN development than in a KC mouse of a comparable age but can be accelerated by inducing acute pancreatitis. This model recapitulates the development of PanINs similar to the KC model, and can also be combined with mutant p53 to develop full blown PDA similar to the KPC model. Another

advantage of the iKras model is the ability to withdraw the doxycycline from the mice and stop expression of oncogenic Kras. There are currently no inhibitors of Kras available but being able to stop expression of oncogenic Kras can be used to mimic inhibition of Kras to analyze how the tumor will respond to the loss of the primary driving oncogene. The mouse models of PDA are incredibly useful for understanding the biology of PDA, though the controlled sequence and combinations of mutations fail to recapitulate the genetic variability of human PDA and the influence that genetic variability can have on the pathology of the tumor.

The subtypes of PDA are characterized by their gene expression profiles and cellular composition, both of which can influence the prognosis and treatment of PDA. RNA sequencing had been performed on PDA tumors to further characterize the mutational profile of PDA. In addition to the genes already found to be important in the carcinogenesis of PDA, gene signatures were found to correlate with both the pathology of the disease as well as patient outcome. Originally, the subtypes were characterized based on bulk RNA sequencing. Bulk RNA sequencing stratified PDA tumors into three subtypes, “Classical”,“Quasimesenchymal”, and “Exocrine-like”, largely based upon the high expression of epithelial genes, mesenchymal genes, and digestive enzyme genes, respectively (Collisson et al. 2011). In addition to describing the differentiation state of the tumor, these subclasses were found to have prognostic value as well. Patients with more classical-type tumors survived longer than those with quasimesenchymal tumors. However, bulk RNA sequencing does not allow for differentiation between tumor epithelium and the surrounding stromal content. One method of circumventing this limitation is virtual microdissection, where the gene signature of normal tissue and

stromal cells can be deconvoluted from the overall expression data to selectively analyze the expression data from the tumor epithelium (Bailey, Chang, Nones, et al. 2016). Using this method, the “exocrine-like” subtype was found to be comprised of either normal tissue with low tumor cellularity, or tumors expressing normal pancreas genes with aberrant methylation patterns. The “quasimesenchymal” subtype was found to be comprised of mostly stromal gene expression, but partially recapitulated a gene signature found in other poorly-differentiated cancers and were re-labeled as “basal-like/squamous”. The limitations with bulk RNA sequencing were ultimately circumvented through the use of laser microdissection, allowing for physical separation of tumor epithelium from the stromal compartment (Moffitt et al. 2015). This advance in technology confirmed the presence of the “classical” and “basal-like” gene signatures present in PDA tumors (Maurer et al. 2019). While sequencing studies have been successful in better understanding the biology of PDA, there has been less success finding an actionable target for PDA treatment.

Clinical trials involving targeted therapies against pathways frequently altered in PDA tumor cells have failed to produce broadly efficacious results. There are two drugs approved by the FDA for treatment of PDA. Erlotinib is an inhibitor of EGFR signaling and has been found to demonstrate an extremely modest survival benefit when combined with gemcitabine, increasing overall survival by weeks (Moore et al. 2007). Olaparib is an inhibitor of PARP that is used to create synthetic lethality in the subgroup of BRCA1/2 mutant PDA tumors and has demonstrated a modest increase in progression free survival on the scale of months but demonstrated no difference in overall survival (Golan et al. 2019). The efficacy of erlotinib and olaparib are

representative of the course most successful clinical trials in PDA have followed. Historically, the drug trials that demonstrated a positive effect, rather than no effect or an adverse effect, were terminated due to demonstrating minimal benefit. However, all the aforementioned trials were targeted towards the PDA tumor cells, ignoring one of unique and most important aspects of the PDA. The tumor cellularity of a PDA tumor is typically quite low, with the bulk of the PDA tumor comprised of stromal components and infiltrating immune cells which provide an exciting avenue for treatment of PDA. The tumor microenvironment (TME) of PDA contains a multitude of cell types capable of performing various functions, both tumor supporting and tumor inhibiting. Reversing the tumor supportive functions of these cell types may be crucial in developing an efficacious treatment regimen for PDA.

Stromal elements

The stromal compartment of the PDA TME is made up of a diverse family of fibroblasts and vascular endothelial cells. The fibroblasts are responsible for the fibrotic nature of the PDA tumor, depositing a dense extracellular matrix (ECM) that both constrains and protects the PDA tumor [see review (Zhang, Crawford, and Pasca di Magliano 2019)]. The mechanical barrier impedes penetration of both anticancer drugs as well as nutrients, further exacerbated by the high interstitial pressure within the PDA tumor (Dufort et al. 2016). PDA tumors are also hypovascular and the vasculature present is largely collapsed due to the interstitial pressure, resulting in poor intratumor oxygen, nutrient, and metabolic waste exchange. This harsh intratumor environment conversely benefits the tumor, as the hypoxic and stressed TME results in the activation of multiple survival pathways, promoting tumor cell survival and metastasis.

Fibroblasts

The bulk of the stromal cells within the PDA tumor are an assortment of fibroblasts [see review:(G. Biffi and Tuveson 2021)]. Fibroblasts are cells that primarily function to deposit extracellular matrix such as collagen, glycoproteins, and proteoglycans, providing structural and mechanical support in connective tissue and during wound healing (Tian et al. 2019). However, in PDA they can have multiple, even contradictory functions. Fibroblasts are one of the first cell populations that expand in preinvasive lesions during the carcinogenesis of PDA (Collins, Bednar, et al. 2012). Upon entering receiving signals from PDA tumor cells, the fibroblasts become polarized and activated, performing different functions based on the signals received. These cancer-associated fibroblasts (CAFs) can be characterized into three groups. The myCAF population functions similarly to an activated myofibroblast by actively depositing ECM. The iCAF population secretes various cytokines that promote inflammation and maintain an immunosuppressive TME. The apCAF population is the most recently described population marked by expression of MHC II, though the function of this population is still being elucidated.

The function of the CAF populations is related to their localization within the tumor. iCAFs are found more distally from the tumor cells, receiving paracrine IL-1 secreted by PDA tumor cells that start an autocrine feedforward loop of JAK/STAT activation (Giulia Biffi et al. 2019). This JAK/STAT signaling is inhibited by TGFβ secreted by PDA tumor cells in a juxtacrine paracrine fashion that also promotes myofibroblastic phenotypes, resulting in the presence of myCAFs surrounding the tumors (Vaughan, Howard, and Tomasek 2000). The resulting deposition of ECM

functions to both protect the tumor and restrain the growth of the tumor (Olive et al. 2009; Özdemir et al. 2014; Rhim et al. 2014). iCAFs are largely considered to be tumor supportive, as most of the cytokines secreted by the cells function in the recruitment and polarization of immunosuppressive cells or suppression and exclusion of effector T cells (Zhang et al. 2013; Feig et al. 2013). The contrasting functions of fibroblasts in tumor promotion and inhibition are reflected in the contradictory responses that occur when fibroblasts are globally inhibited in PDA. Some studies report that inhibition of fibroblasts increases susceptibility of the tumor to treatment, while other studies, including a failed clinical trial, demonstrate that inhibition of fibroblasts accelerates PDA growth and dissemination (Olive et al. 2009; Amakye, Jagani, and Dorsch 2013; Özdemir et al. 2014; Rhim et al. 2014). It is becoming increasingly apparent that the heterogeneity of the fibroblast population should be reflected in the target of treatments, as dosage of fibroblast signaling and the ratio of myCAFs/iCAFs have been shown to influence PDA tumor progression (Mathew et al. 2014; N.G. Steele et al. 2021). Fibroblasts remain an attractive target for therapy, but more needs to be understood about the heterogeneity and function of the cells before any translational work can be done.

Endothelial cells

PDA is a hypovascular tumor, but there is evidence that modulating tumor vasculature can influence PDA tumor growth. As with the fibroblasts, the evidence is similarly contradictory and the biology has to be further investigated before a choice can be made [see review: (Annese et al. 2019)]. Increased vascularization is correlated with more aggressive PDA tumors, so anti-angiogenic treatment could be efficacious if

causality was established between the increased vascularization and the aggressiveness of the disease (Barău et al. 2013). However, increasing vascular perfusion can help potentiate the efficacy of drugs due to the increase in drug delivery (Chauhan et al. 2013). The effect of angiogenesis on hypoxia is another important aspect to consider, as there is evidence of other cancers becoming more aggressively metastatic in response to the increased hypoxia cause by long term anti-angiogenic treatment (Bergers and Hanahan 2008).

Immune compartment

The immune compartment of pancreatic cancer is diverse and complex. The primary population of immune cells are immunosuppressive, actively shutting down any active immune cells. There are multiple populations of myeloid cells that tend to be polarized by the cancer cells to promote tumor growth and inhibit antitumor activity. This is true of the lymphocyte populations as well, with an increase in immunosuppressive B cell subtypes and immunosuppressive T cells subtypes. If effector T cell subtypes are present, they are usually inactivated or rendered exhausted by mechanisms of T cell inhibition. There are both active and passive mechanisms of immunosuppression in PDA. There is expression of immune checkpoint proteins to shut down potential T cell responses, but there is also passive exclusion of various cell types. Only by elucidating the various mechanisms of immune suppression and evasion in PDA can an efficacious combination of treatments be used to treat the disease.

Myeloid compartment

Myeloid cells are a diverse population of cell types that are vital for multiple bodily processes, such as oxygen exchange, wound repair, and the innate immune

response. While they stem from a common progenitor, fully differentiated myeloid cells have multitudes of forms and functions. Erythrocytes, or red blood cells, primarily function in respiration, exchanging oxygen for CO_2. Megakaryocytes are myeloid cells that produce platelets, which are important in blood clotting and wound healing. Mast cells are myeloid cells that primarily function in the allergy response. The final class of myeloid cells are leukocytes, or white blood cells. The primary function of leukocytes are to surveil the body and react to any potential disturbances discovered as part of the innate immune system. There are subpopulations of leukocytes that perform specialized roles, ranging from activation and amplification of immune responses, or promoting an anti-inflammatory response. Leukocytes can be divided into two classes based on the number of lobes developed by their nuclei during myelopoiesis.

Granulocytes are multilobular leukocytes with diverse functions largely dependent on the content of protein granules developed by the cells. The most prominent granulocyte is the neutrophil. Neutrophils are the most abundant leukocyte in human blood. They usually remain in circulation in the blood but are extremely mobile and chemotactically responsive. They are professional phagocytes and contain antimicrobial granules and have a unique mechanism of pathogen killing where the nuclear envelope is dissolved and the mixture of DNA and the cytoplasmic antimicrobial granules are expelled extracellularly to both physically constrain and kill pathogens, called NETosis.

Monocytes are unilobular leukocytes that circulate in the bloodstream. They can directly sense pathogens present in the blood or react to signaling cues from infected or damaged tissue and exit the blood stream to surveil the source of damage. Depending

on the type of disturbance the monocyte encounters and the localization of the interaction, the monocyte can perform any number of actions. If the disturbance is a bacteria, the monocyte can phagocytose the bacteria, additionally releasing cytokines to promote inflammation and recruit additional immune cells. The monocyte can then present antigens found on the digested bacteria to active the adaptive immune response. If the monocyte has extravasated into a tissue, the cell can also mature into a macrophage. Macrophages function very similarly to monocytes but express more receptors that allows for macrophage polarization and a greater range of activity. Macrophages that encounter bacteria or receive pro-inflammatory cytokines from other cells feed forward the pro-inflammatory signaling while increasing anti-microbial activities such as nitric oxide production (iNOS) and increased phagocytosis and antigen presentation. This is termed classically activated, previously M1 polarization. If the macrophage encounters signal from the destruction of tissue, they become anti-inflammatory, secreting cytokines that dampen the immune response to prevent further damage while promoting tissue repair, termed alternatively activated, previously M2 polarization. The classical and alternatively activated designations represent the extremes of the pro/anti-inflammatory macrophage phenotypes, with macrophages existing in a spectrum between the two depending on physiological context. In addition to maturing into macrophages, monocytes also have the capability to mature into dendritic cells. Dendritic cells are major promoters of the adaptive immune response. Dendritic cells are constantly sampling antigens in the environment through phagocytosis, pinocytosis, or receptor-mediated endocytosis. When dendritic cells encounter pathological antigens, they secrete pro-inflammatory signals and can initiate

an adaptive immune response. The diverse biological functions of these myeloid are required for a person to stay healthy but can also be used to initiate and promote tumor growth and metastasis.

Immunosuppressive myeloid cells make up the bulk of immune cells present in the PDA TME. The myeloid cell population can be found expanding in the pancreas during the formation of the premalignant PanIN lesions. Cancer is often colloquialized as “a wound that never heals” which is a fitting description of the mechanism of macrophage polarization in PDA. ADMs are formed due to tissue injury, attracting macrophages which become alternatively activated to facilitate tissue repair. However, in the presence of an oncogenic Kras mutation, the ADM persist and can progress to PanIN and subsequently to PDA, accompanied by macrophages now termed tumor-associated macrophages (TAMs). TAMs are marked by the expression of functional markers such as CCR2 and Arginase. CCR2 is a chemokine receptor that responds to CCL2, a chemokine highly expressed by PDA tumor cells, promoting migration of macrophages to the tumor (Sanford et al. 2013). Multiple cell types in the PDA TME produce M2 promoting cytokines such as CSF1, resulting in TAMs that have immunosuppressive functions, including increased arginase production and immune checkpoint expression (Y. Zhu et al. 2014; Zhang, Yan, et al. 2017; Zhang, Velez-Delgado, et al. 2017). Arginase can deplete the PDA TME of arginine, an amino acid crucial to T cell proliferation, promoting immunosuppression by staunching T cell proliferation (Rodriguez et al. 2004). A phase 1b clinical trial combining CCR2 inhibition with FOLFIRINOX treatment was carried out and was well tolerated and showed

promising efficacy (Nywening et al. 2016). Similarly, neutrophils have also been found to promote an immunosuppressive TME.

An increased neutrophil-lymphocyte ratio in the PDA TME of a patient is a poor prognostic factor (Stotz et al. 2013). This relationship between neutrophils and lymphocytes turned out to be causal, as a population of CXCR2 expressing neutrophils was found to be capable of inhibiting a productive CD8 T cell response against PDA tumors in KPC mice (Stromnes et al. 2014; Chao, Furth, and Vonderheide 2016). Inhibition of CXCR2 or ablation of neutrophils resulted in increased T cell entry and abrogation of metastasis (C.W. Steele et al. 2016). Combination of CCR2 macrophage and CXCR2 neutrophil inhibition demonstrated further benefit, increasing survival of mice treated with FOLFIRINOX (Nywening et al. 2018). In addition to ablation of pro-tumor populations, another treatment modality is to increase the proportion of anti-tumor cells. There is only a small population of dendritic cells in the PDA TME, such that in a mouse model with engineered neo-antigen expression there was no productive CD8 T cell response as there was not significant dendritic cell surveillance (Hegde et al. 2020). Increasing the dendritic cell population in the pancreas slowed down disease progression in the early PanIN lesions and stabilized established PDA tumors and, when combined with an agonist to dendritic cell costimulatory receptor CD40, sensitized them to radiation therapy and increased survival. This occurred in a different mouse model without the engineered neo-antigen, demonstrating that just increasing dendritic cell population and activation requirements can be efficacious in treatment of PDA.

Lymphocytes

Lymphocytes are the other major component of the immune response and function in both the innate and adaptive immune responses. NK cells are the lymphocytes that function in the innate immune response. B cells and T cells are the lymphocytes that function in the adaptive immune response. B cells function in a more supportive role, where, instead of directly killing cells that are recognized by their unique cell surface receptor, they mature and produce one of various classes of antibodies, each of which have their own effects, that is specific to the detected antigen. IgG antibodies are the most common and are used to bind antigens. These antibodies can coat their targets to initiate opsonization and removal via phagocytosis, activate the complement cascade to promote inflammation and subsequent opsonization, or bind the antigens in a way to block their function. T cells act more directly, though their functions can vary based on the combination of cell surface receptors expressed by the T cell, cell polarization from environmental signals, and stimulation from the local cues.

The cell surface receptors that differentiate most T cells are CD8 and CD4. CD8 T cells, known as effector T cells (T_{Eff}), function in killing the cells they recognize, while CD4 T cells, known as helper T cells (T_H), release various cytokines to properly coordinate an immune response in response to recognition of their target. There are several immune checkpoint processes involved in making sure the CD8 T cells are killing the right cells at the right time. First, a CD8 T cell needs to be activated before it can initiate cell killing. A professional antigen presenting cell (APC) such as a dendritic cell or CD4 T cell needs to present the antigen recognized by the CD8 T cell on their MHC class I complex through the T cell receptor (TCR). Once the antigen is recognized,

a costimulatory signal must be sent to the CD8 T cell from the APC to finish activating the CD8 T cell. After this, the T cell undergoes rapid proliferation and is primed to kill its target cells. If a pro-inflammatory cytokine such as IFNγ is present, the CD8 T cell can differentiate into memory CD8 T cells (T_{Mem}) after the proliferative spike. Once the CD8 T cell is activated, it will test the MHC class I complexes of any cells it encounters. If there is antigen recognition, the CD8 T cell will initiate the killing process, preparing to release cytotoxic granules directly towards the cell its bound to. However, this process can be stopped if the CD8 T cell receives any inhibitory immune checkpoint signals, such as PD-L1. These signals result in an exhausted CD8 T cell phenotype (T_{Ex}) where the CD8 T cell is no longer able to function. Regulatory CD4 T cells (T_{Reg}) function specifically to exhaust CD8 T cells and prevent prolonged T_{Eff} activation and autoimmunity. Other CD4 subtypes include pro-inflammatory T_H1 and anti-inflammatory T_H2. Similarly to the macrophage populations which derive their nomenclature from these subtypes, T_H1 and T_H2 cells are polarized by signaling cues in the microenvironment and change the kinds of cytokines released depending on their subtype, all of which serve to amplify the signals that originally polarized the cells. The diversity of CD4 T cells and the immune checkpoints preventing CD8 T cell autoimmunity are both used by tumors to suppress anti-tumor immune responses.

B cells remain relatively understudied in PDA, but they have been implicated in promoting PDA progression. B cells were found to be increased in the PDA TME when compared to normal pancreas (Gunderson et al. 2016; Pylayeva-Gupta et al. 2016). When B cells were depleted in mouse models of PDA, there was suppression of PDA growth (K.E. Lee et al. 2016). Specifically blocking the BTK receptor found on B cells

resulted in an shift from M2 macrophages to more M1 macrophages, promoting T_{Eff} function (Gunderson et al. 2016). Regulatory B cells (B_{Reg}) are a rare subtype of B cells with known immunosuppressive functions and are more prevalent in PDA than normal mouse pancreata (K.E. Lee et al. 2016).

The most prominent CD4 subtypes in PDA are the immunosuppressive subtypes, T_H2 and T_{Reg} (Clark et al. 2007; De Monte et al. 2011; De Monte et al. 2016). Cells in PDA TME secrete chemokines that attract both T_H2 and T_{Reg} (Tan et al. 2009; De Monte et al. 2011). Additionally, the cytokines that can polarize T_H cells into T_H2 and T_{Reg} are expressed by multiple cell types in the PDA TME, including the tumor cells (Prokopchuk et al. 2005; Zhang et al. 2013; De Monte et al. 2016; Giulia Biffi et al. 2019). The CD4 compartment in PDA is largely focused on maintaining an immunosuppressive environment, with cells like TAMs and T_H2 secreting cytokines promoting immune suppression, while the T_{Reg} suppress any attempted T_{Eff} response. Even so, CD8 T cell exhaustion is not the first line of defense the PDA tumor has against a T_{Eff} response. CD8 T cell are excluded from the tumor through expression of certain cytokines or the presence of certain cell types (Feig et al. 2013; Beatty et al. 2015; Steele et al. 2016). Studies have shown that there are neoantigens present in the PDA TME for CD8 T cells to recognize to kill tumor cells, but if since there are so few dendritic cells present in the TME, there is no way to deliver that antigen to a lymph node to initiate a T_{Eff} response (Bailey, Chang, Forget, et al. 2016; Balachandran et al. 2017; Hegde et al. 2020). There are so many layers and complex cellular networks involved in maintaining the immunosuppressive PDA TME. The complexity of the PDA TME has been shown to be functionally redundant, where removing one population of cells can invoke a

compensatory response from another cell population. In some cases this compensatory reaction has accelerated PDA growth, demonstrating that there are cells required for PDA growth as well as cells required for PDA restraint (Zhang et al. 2014; Nywening et al. 2018; Zhang et al. 2020). While there are still multiple underexplored cell types in the PDA TME and much more to elucidate about the ones covered here, there are some actionable targets that should be considered for translation into potential therapies.

Immunotherapy

The appeal of immunotherapy comes from its systemic benefit, as the immune system surveils the entire body and should theoretically be able to clear both the primary tumor and any distant metastases. There are multiple modalities of immunotherapy, but all of them seek to achieve reactivation of the immune system in order to clear PDA. There are mechanisms to overcome immune evasion, making a tumor previously undetectable by the immune system targetable [see review:(Kunk et al. 2016)]. There is boosting general immune function to make an already effective immune response even more effective, to prevent the development of resistance and subsequent progression. And then there are methods to overcome mechanism of immune suppression. Given the immunosuppressive PDA TME, the final modality of overcoming immune suppression has been the major focus of most of the immunotherapy trials.

Immune checkpoint proteins are the target of multiple immunotherapies. The physiological function of immune checkpoint proteins is to prevent excessive T cell activation and subsequent autoimmunity [see review: (Buchbinder and Desai 2016;Marin-Acevedo, Kimbrough, and Lou 2021)]. Two examples of immune checkpoint therapy

that have demonstrated clinical efficacy are CTLA-4 inhibition and PD-1/PD-L1 inhibition. CTLA-4 normally functions to inhibit CD8 T cells during CD8 T cell activation by APCs. In addition to TCR:MHC II recognition, CD8 T cells require co-stimulatory signaling from B7 proteins located on the cell surface of APCs to the CD28 protein on the CD8 T cell. Effective B7:CD28 signaling results in an increase in IL-2 production, a cytokine required for CD8 T cell proliferation. CTLA-4 dampens this co-stimulatory signaling, as it has a higher affinity for binding the B7 proteins than CD28. High levels of CTLA-4 expression, common on T_{Reg}, sequester more B7 protein and prevent CD8 T cell activation. The PD-1/PD-L1 interaction occurs later, as PD-1 expression is only upregulated upon CD8 T cell activation. Both pathways are important in blocking the proliferation and function of self-reactive T cells, as genetic loss of the genes the code these proteins are implicated in autoimmune disorders. However, they can both by used by cancer cells to prevent anti-tumor responses, by promoting polarization of CD4 T cells to T_{Reg} or upregulating expression of PD-1 ligand PD-L1. Immune checkpoint blockade is a modality of immunotherapy designed to overcome this inhibition.

Immune checkpoint blockade has demonstrated success in immunogenic tumors like melanoma, where the high presence of neo-antigens can lead to curative immune clearance once immunosuppression is overcome (Schadendorf et al. 2015). There are many FDA-approved immunotherapy drugs, blocking inhibitory immune checkpoint proteins like the PD-1/PD-L1 axis or CTLA-4 (Vaddepally et al. 2020). However, all these treatments failed to show efficacy in clinical trials of PDA (Royal et al. 2010; Brahmer et al. 2012). There are multiple reasons as to why these single target trials may have failed, as there are multiple mechanisms of immunosuppression present in

the PDA TME. Re-activation of a single pathway of anti-tumor immunity may be compensated for by other immunosuppressive mechanisms, or patients may have variable expression of immune checkpoint proteins. Much like other therapies targeting signaling pathways, combination treatment of immunotherapies may be required to be efficacious. There have also been recent clinical trials demonstrating the efficacy of combining immunotherapy modalities. CD40 agonism is an immunotherapy modality that promotes dendritic cell activation of CD8 T cells [see review: (Vonderheide 2020)]. Increasing CD8 T cell activation and decreasing immune checkpoint inhibition of CD8 T cells have demonstrated early but promising pre-clinical or clinical results (O'Hara et al. 2021; Freed-Pastor et al. 2021). Both a deeper understanding of the broader biology of PDA as well as specific insight into the composition of an individual patient's tumor will be important in developing efficacious treatments against this fatal malignancy.

Thesis Overview

RNA sequencing (RNA-seq) has been a great platform for understanding the biology of cancers as whole as well as individual patient tumors. Major strides have been made in sequencing technology, decreasing costs as well as increasing the resolution. Bulk RNA-seq has been used to make many of the major discoveries in the field, but as previously stated, the whole-tumor resolution makes detection of compartment specific changes difficult. Cell sorting, virtual deconvolution, and laser microdissection have all been functional methods of increasing the specific resolution of sequencing, but even then, most of those strategies are limited by cell numbers and can only assess individual populations, at the loss of detection of smaller or rarer sub-populations. A major stride in RNA-sequencing technology has been the advent of

single cell RNA sequencing (scRNA-seq), allowing for sequencing of individual cells. scRNA-seq has already been used to great effect in many cancer types including PDA, uncovering previously undiscovered cell populations or elucidating the depth of heterogeneity of the cells in the TME and the results that heterogeneity can have on both cancer progression and treatment (Elyada et al. 2019; Peng et al. 2019; J.J. Lee et al. 2021; Raghavan et al. 2021). In this thesis I will present the findings that have come about from our lab's work with scRNA-seq.

In Chapter 2 I present our lab's work in multimodal, comprehensive analysis of the human PDA TME. We focused our analysis on the immune compartment of primary human PDA, specifically looking at the mechanisms and extent of immune checkpoint inhibition present across all the cell types in the PDA TME. This work highlighted the diversity of checkpoint inhibitors expressed across the cells present in the PDA TME, demonstrating why immune checkpoint blockade of a single pathway may not be efficacious. Additionally, we found that understudied immune checkpoint protein TIGIT was the only immune checkpoint protein that was differentially expressed on T_{Ex} compared to T_{Eff}. We then performed a putative ligand-receptor mapping using our scRNA-seq data and found expression of PVR, the cognate receptor of TIGIT, expressed on multiple cell types throughout the PDA TME. This data highlighted the value of single cell RNA sequencing in a cancer as complex as PDA, allowing for a high resolution look at previously understudied populations of cells to generate and test hypotheses that have potential translational value.

In Chapter 3 I use scRNA-seq to characterize the cells present in liver metastases of PDA, comparing them to both primary tumor and adjacent normal

pancreas. As PDA is a disease that is largely diagnosed at the metastatic stage, understanding the biology of metastases is vital for efficacious treatment. As is demonstrated by surgical resection, only eliminating the primary tumor will usually not be curative, as local micrometastases or distal metastases can supplant the primary tumor and lead to recurrence. It was found that the majority of the cell types found in the primary TME were also found in the liver TME, which will allow for comparisons to be drawn between the populations to determine whether therapies effecting the primary tumor will also be efficacious against the metastases or whether a separate treatment strategy has to be developed for PDA metastases.

In Chapter 4 I characterize a mouse model of inducible lung cancer (LC) to be used as a comparison of PDA metastasis to the lung. Preliminary work by another member of our lab has found that activation of oncogenic Kras in the pancreas results in a shift in the lung microenvironment. We plan on using this model of lung cancer to determine the effects of local oncogenic Kras remodeling of the LC TME to compare to the effects of distal pro-metastatic remodeling by distally expressed oncogenic Kras. I functionally confirm that the model of inducible oncogenic Kras functions, developing tumors when Kras is expressed and regressing upon Kras withdrawal, and confirming that inactivation of p53 results in more aggressive tumor development in combination with Kras. Using multiplex immunofluorescence, I characterized the immune composition of the lung mouse model during tumor progression and regression.

In Chapter 5 I cover the implications of my work on the fields of both PDA and LC and discuss the future directions of each project.

References

1. Aguirre, Andrew J., Nabeel Bardeesy, Manisha Sinha, Lyle Lopez, David A. Tuveson, James Horner, Mark S. Redston, and Ronald A. Depinho. 2003. "Activated Kras and Ink4a/Arf deficiency cooperate to produce metastatic pancreatic ductal adenocarcinoma." *Genes & Development* 17 (24): 3112-3126. https://doi.org/10.1101/gad.1158703. http://europepmc.org/articles/pmc305262?pdf=render.
2. Amakye, Dereck, Zainab Jagani, and Marion Dorsch. 2013. "Unraveling the therapeutic potential of the Hedgehog pathway in cancer." *Nature Medicine* 19 (11): 1410-1422. https://doi.org/10.1038/nm.3389.
3. Annese, Tiziana, Roberto Tamma, Simona Ruggieri, and Domenico Ribatti. 2019. "Angiogenesis in Pancreatic Cancer: Pre-Clinical and Clinical Studies." *Cancers* 11 (3): 381. https://doi.org/10.3390/cancers11030381. https://www.mdpi.com/2072-6694/11/3/381/pdf.
4. Bailey, Peter, David K. Chang, Marie-Andrée Forget, Francis A. San Lucas, Hector A. Alvarez, Cara Haymaker, Chandrani Chattopadhyay, Sun-Hee Kim, Suhendan Ekmekcioglu, Elizabeth A. Grimm, Andrew V. Biankin, Patrick Hwu, Anirban Maitra, and Jason Roszik. 2016. "Exploiting the neoantigen landscape for immunotherapy of pancreatic ductal adenocarcinoma." *Scientific Reports* 6 (1): 35848. https://doi.org/10.1038/srep35848. http://europepmc.org/articles/pmc5071896?pdf=render.
5. Bailey, Peter, David K. Chang, Katia Nones, Amber L. Johns, Ann-Marie Patch, Marie-Claude Gingras, David K. Miller, Angelika N. Christ, Tim J. C. Bruxner, Michael C. Quinn, Craig Nourse, L. Charles Murtaugh, Ivon Harliwong, Senel Idrisoglu, Suzanne Manning, Ehsan Nourbakhsh, Shivangi Wani, Lynn Fink, Oliver Holmes, Venessa Chin, Matthew J. Anderson, Stephen Kazakoff, Conrad Leonard, Felicity Newell, Nick Waddell, Scott Wood, Qinying Xu, Peter J. Wilson, Nicole Cloonan, Karin S. Kassahn, Darrin Taylor, Kelly Quek, Alan Robertson, Lorena Pantano, Laura Mincarelli, Luis N. Sanchez, Lisa Evers, Jianmin Wu, Mark Pinese, Mark J. Cowley, Marc D. Jones, Emily K. Colvin, Adnan M. Nagrial, Emily S. Humphrey, Lorraine A. Chantrill, Amanda Mawson, Jeremy Humphris, Angela Chou, Marina Pajic, Christopher J. Scarlett, Andreia V. Pinho, Marc Giry-Laterriere, Ilse Rooman, Jaswinder S. Samra, James G. Kench, Jessica A. Lovell, Neil D. Merrett, Christopher W. Toon, Krishna Epari, Nam Q. Nguyen, Andrew Barbour, Nikolajs Zeps, Kim Moran-Jones, Nigel B. Jamieson, Janet S. Graham, Fraser Duthie, Karin Oien, Jane Hair, Robert Grützmann, Anirban Maitra, Christine A. Iacobuzio-Donahue, Christopher L. Wolfgang, Richard A. Morgan, Rita T. Lawlor, Vincenzo Corbo, Claudio Bassi, Borislav Rusev, Paola Capelli, Roberto Salvia, Giampaolo Tortora, Debabrata Mukhopadhyay, Gloria M. Petersen, Donna M. Munzy, William E. Fisher, Saadia A. Karim, James R. Eshleman, Ralph H. Hruban, Christian Pilarsky, Jennifer P. Morton, Owen J. Sansom, Aldo Scarpa, Elizabeth A. Musgrove, Ulla-Maja Hagbo Bailey, Oliver Hofmann, Robert L. Sutherland, David A. Wheeler, Anthony J. Gill, Richard A. Gibbs, John V. Pearson, Nicola Waddell, Andrew V. Biankin, and Sean M. Grimmond. 2016. "Genomic analyses identify molecular subtypes of pancreatic cancer." *Nature* 531 (7592): 47-52. https://doi.org/10.1038/nature16965.
6. Balachandran, Vinod P., Marta Łuksza, Julia N. Zhao, Vladimir Makarov, John Alec Moral, Romain Remark, Brian Herbst, Gokce Askan, Umesh Bhanot, Yasin Senbabaoglu, Daniel K. Wells, Charles Ian Ormsby Cary, Olivera Grbovic-Huezo, Marc Attiyeh, Benjamin Medina, Jennifer Zhang, Jennifer Loo, Joseph Saglimbeni, Mohsen Abu-Akeel, Roberta Zappasodi, Nadeem Riaz, Martin Smoragiewicz, Z. Larkin Kelley, Olca Basturk, Mithat Gönen, Arnold J. Levine, Peter J. Allen, Douglas T. Fearon, Miriam Merad, Sacha Gnjatic, Christine A. Iacobuzio-Donahue, Jedd D. Wolchok, Ronald P. Dematteo, Timothy A. Chan, Benjamin D. Greenbaum, Taha Merghoub, and Steven D. Leach. 2017. "Identification of unique neoantigen qualities in long-term survivors of pancreatic cancer." *Nature* 551 (7681): 512-516. https://doi.org/10.1038/nature24462. https://www.ncbi.nlm.nih.gov/pmc/articles/PMC6145146.
7. Barău, Anca, Amparo Ruiz-Sauri, Gerardo Valencia, Maria Del Carmen Gómez-Mateo, Luis Sabater, Antonio Ferrandez, and Antonio Llombart-Bosch. 2013. "High microvessel density in pancreatic ductal adenocarcinoma is associated with high grade." *Virchows Archiv* 462 (5): 541-546. https://doi.org/10.1007/s00428-013-1409-1.

8. Basturk, Olca, Seung-Mo Hong, Laura D. Wood, N. Volkan Adsay, Jorge Albores-Saavedra, Andrew V. Biankin, Lodewijk A.A. Brosens, Noriyoshi Fukushima, Michael Goggins, Ralph H. Hruban, Yo Kato, David S. Klimstra, Günter Klöppel, Alyssa Krasinskas, Daniel S. Longnecker, Hanno Matthaei, G. Johan A. Offerhaus, Michio Shimizu, Kyoichi Takaori, Benoit Terris, Shinichi Yachida, Irene Esposito, and Toru Furukawa. 2015. "A Revised Classification System and Recommendations From the Baltimore Consensus Meeting for Neoplastic Precursor Lesions in the Pancreas." *American Journal of Surgical Pathology* 39 (12): 1730-1741. https://doi.org/10.1097/pas.0000000000000533.
9. Beatty, Gregory L., Rafael Winograd, Rebecca A. Evans, Kristen B. Long, Santiago L. Luque, Jae W. Lee, Cynthia Clendenin, Whitney L. Gladney, Dawson M. Knoblock, Patrick D. Guirnalda, and Robert H. Vonderheide. 2015. "Exclusion of T Cells From Pancreatic Carcinomas in Mice Is Regulated by Ly6Clow F4/80+ Extratumoral Macrophages." *Gastroenterology* 149 (1): 201-210. https://doi.org/10.1053/j.gastro.2015.04.010. https://www.ncbi.nlm.nih.gov/pmc/articles/PMC4478138.
10. Bergers, Gabriele, and Douglas Hanahan. 2008. "Modes of resistance to anti-angiogenic therapy." *Nature Reviews Cancer* 8 (8): 592-603. https://doi.org/10.1038/nrc2442. http://europepmc.org/articles/pmc2874834?pdf=render.
11. Biankin, A. V., J. G. Kench, A. L. Morey, C. S. Lee, S. A. Biankin, D. R. Head, T. B. Hugh, S. M. Henshall, and R. L. Sutherland. 2001. "Overexpression of p21(WAF1/CIP1) is an early event in the development of pancreatic intraepithelial neoplasia." *Cancer Res* 61 (24): 8830-7. https://www.ncbi.nlm.nih.gov/pubmed/11751405.
12. Biffi, G., and D. A. Tuveson. 2021. "Diversity and Biology of Cancer-Associated Fibroblasts." *Physiol Rev* 101 (1): 147-176. https://doi.org/10.1152/physrev.00048.2019. https://www.ncbi.nlm.nih.gov/pubmed/32466724.
13. Biffi, Giulia, Tobiloba E. Oni, Benjamin Spielman, Yuan Hao, Ela Elyada, Youngkyu Park, Jonathan Preall, and David A. Tuveson. 2019. "IL1-Induced JAK/STAT Signaling Is Antagonized by TGFβ to Shape CAF Heterogeneity in Pancreatic Ductal Adenocarcinoma." *Cancer Discovery* 9 (2): 282-301. https://doi.org/10.1158/2159-8290.cd-18-0710.
14. Brahmer, Julie R., Scott S. Tykodi, Laura Q.M. Chow, Wen-Jen Hwu, Suzanne L. Topalian, Patrick Hwu, Charles G. Drake, Luis H. Camacho, John Kauh, Kunle Odunsi, Henry C. Pitot, Omid Hamid, Shailender Bhatia, Renato Martins, Keith Eaton, Shuming Chen, Theresa M. Salay, Suresh Alaparthy, Joseph F. Grosso, Alan J. Korman, Susan M. Parker, Shruti Agrawal, Stacie M. Goldberg, Drew M. Pardoll, Ashok Gupta, and Jon M. Wigginton. 2012. "Safety and Activity of Anti–PD-L1 Antibody in Patients with Advanced Cancer." *New England Journal of Medicine* 366 (26): 2455-2465. https://doi.org/10.1056/nejmoa1200694.
15. Buchbinder, Elizabeth I., and Anupam Desai. 2016. "CTLA-4 and PD-1 Pathways." American Journal of Clinical Oncology 39 (1): 98-106. https://doi.org/10.1097/coc.0000000000000239.
16. Carpenter, Eileen, Sarah Nelson, Filip Bednar, Clifford Cho, Hari Nathan, Vaibhav Sahai, Marina Pasca Magliano, and Timothy L. Frankel. 2021. "Immunotherapy for pancreatic ductal adenocarcinoma." *Journal of Surgical Oncology* 123 (3): 751-759. https://doi.org/10.1002/jso.26312.
17. Chao, Timothy, Emma E. Furth, and Robert H. Vonderheide. 2016. "CXCR2-Dependent Accumulation of Tumor-Associated Neutrophils Regulates T-cell Immunity in Pancreatic Ductal Adenocarcinoma." *Cancer Immunology Research* 4 (11): 968-982. https://doi.org/10.1158/2326-6066.cir-16-0188.
18. Chauhan, Vikash P., John D. Martin, Hao Liu, Delphine A. Lacorre, Saloni R. Jain, Sergey V. Kozin, Triantafyllos Stylianopoulos, Ahmed S. Mousa, Xiaoxing Han, Pichet Adstamongkonkul, Zoran Popović, Peigen Huang, Moungi G. Bawendi, Yves Boucher, and Rakesh K. Jain. 2013. "Angiotensin inhibition enhances drug delivery and potentiates chemotherapy by decompressing tumour blood vessels." *Nature Communications* 4 (1). https://doi.org/10.1038/ncomms3516. https://www.ncbi.nlm.nih.gov/pmc/articles/PMC3806395.
19. Chikhladze, Sophia, Ann-Kathrin Lederer, Lampros Kousoulas, Marilena Reinmuth, Olivia Sick, Stefan Fichtner-Feigl, and Uwe A. Wittel. 2019. "Adjuvant chemotherapy after surgery for pancreatic ductal adenocarcinoma: retrospective real-life data." *World Journal of Surgical Oncology* 17 (1). https://doi.org/10.1186/s12957-019-1732-3.

20. Clark, Carolyn E., Sunil R. Hingorani, Rosemarie Mick, Chelsea Combs, David A. Tuveson, and Robert H. Vonderheide. 2007. "Dynamics of the Immune Reaction to Pancreatic Cancer from Inception to Invasion." *Cancer Research* 67 (19): 9518-9527. https://doi.org/10.1158/0008-5472.can-07-0175.
21. Collins, Meredith A., Filip Bednar, Yaqing Zhang, Jean-Christophe Brisset, Stefanie Galbán, Craig J. Galbán, Sabita Rakshit, Karen S. Flannagan, N. Volkan Adsay, and Marina Pasca Di Magliano. 2012. "Oncogenic Kras is required for both the initiation and maintenance of pancreatic cancer in mice." *Journal of Clinical Investigation* 122 (2): 639-653. https://doi.org/10.1172/jci59227.
22. Collisson, Eric A, Anguraj Sadanandam, Peter Olson, William J Gibb, Morgan Truitt, Shenda Gu, Janine Cooc, Jennifer Weinkle, Grace E Kim, Lakshmi Jakkula, Heidi S Feiler, Andrew H Ko, Adam B Olshen, Kathleen L Danenberg, Margaret A Tempero, Paul T Spellman, Douglas Hanahan, and Joe W Gray. 2011. "Subtypes of pancreatic ductal adenocarcinoma and their differing responses to therapy." *Nature Medicine* 17 (4): 500-503. https://doi.org/10.1038/nm.2344. https://www.ncbi.nlm.nih.gov/pmc/articles/PMC3755490.
23. De Monte, Lucia, Michele Reni, Elena Tassi, Daniela Clavenna, Ilenia Papa, Helios Recalde, Marco Braga, Valerio Di Carlo, Claudio Doglioni, and Maria Pia Protti. 2011. "Intratumor T helper type 2 cell infiltrate correlates with cancer-associated fibroblast thymic stromal lymphopoietin production and reduced survival in pancreatic cancer." *Journal of Experimental Medicine* 208 (3): 469-478. https://doi.org/10.1084/jem.20101876. https://www.ncbi.nlm.nih.gov/pmc/articles/PMC3058573.
24. De Monte, Lucia, Sonja Wörmann, Emanuela Brunetto, Silvia Heltai, Gilda Magliacane, Michele Reni, Anna Maria Paganoni, Helios Recalde, Anna Mondino, Massimo Falconi, Francesca Aleotti, Gianpaolo Balzano, Hana Algül, Claudio Doglioni, and Maria Pia Protti. 2016. "Basophil Recruitment into Tumor-Draining Lymph Nodes Correlates with Th2 Inflammation and Reduced Survival in Pancreatic Cancer Patients." *Cancer Research* 76 (7): 1792-1803. https://doi.org/10.1158/0008-5472.can-15-1801-t.
25. Dufort, C., Christopher, E. Delgiorno, Kathleen, A. Carlson, Markus, J. Osgood, Ryan, Chunmei Zhao, Zhongdong Huang, B. Thompson, Curtis, J. Connor, Robert, D. Thanos, Christopher, Scott Brockenbrough, J., P. Provenzano, Paolo, I. Frost, Gregory, Michael Shepard, H., and R. Hingorani, Sunil. 2016. "Interstitial Pressure in Pancreatic Ductal Adenocarcinoma Is Dominated by a Gel-Fluid Phase." *Biophysical Journal* 110 (9): 2106-2119. https://doi.org/10.1016/j.bpj.2016.03.040. http://www.cell.com/article/S0006349516301722/pdf.
26. Eibl, Guido, Zobeida Cruz-Monserrate, Murray Korc, Maxim S. Petrov, Mark O. Goodarzi, William E. Fisher, Aida Habtezion, Aurelia Lugea, Stephen J. Pandol, Phil A. Hart, and Dana K. Andersen. 2018. "Diabetes Mellitus and Obesity as Risk Factors for Pancreatic Cancer." *Journal of the Academy of Nutrition and Dietetics* 118 (4): 555-567. https://doi.org/10.1016/j.jand.2017.07.005. https://scholarworks.iupui.edu/bitstream/1805/20151/1/nihms893453.pdf.
27. Elyada, Ela, Mohan Bolisetty, Pasquale Laise, William F. Flynn, Elise T. Courtois, Richard A. Burkhart, Jonathan A. Teinor, Pascal Belleau, Giulia Biffi, Matthew S. Lucito, Santhosh Sivajothi, Todd D. Armstrong, Dannielle D. Engle, Kenneth H. Yu, Yuan Hao, Christopher L. Wolfgang, Youngkyu Park, Jonathan Preall, Elizabeth M. Jaffee, Andrea Califano, Paul Robson, and David A. Tuveson. 2019. "Cross-Species Single-Cell Analysis of Pancreatic Ductal Adenocarcinoma Reveals Antigen-Presenting Cancer-Associated Fibroblasts." *Cancer Discovery* 9 (8): 1102-1123. https://doi.org/10.1158/2159-8290.cd-19-0094.
28. Espinet, Elisa, Zuguang Gu, Charles D. Imbusch, Nathalia A. Giese, Magdalena Büscher, Mariam Safavi, Silke Weisenburger, Corinna Klein, Vanessa Vogel, Mattia Falcone, Jacob Insua-Rodríguez, Manuel Reitberger, Vera Thiel, Steffi O. Kossi, Alexander Muckenhuber, Karnjit Sarai, Alex Y.L. Lee, Elyne Backx, Soheila Zarei, Matthias M. Gaida, Manuel Rodríguez-Paredes, Elisa Donato, Hsi-Yu Yen, Roland Eils, Matthias Schlesner, Nicole Pfarr, Thilo Hackert, Christoph Plass, Benedikt Brors, Katja Steiger, Dieter Weichenhan, H. Efsun Arda, Ilse Rooman, Janel L. Kopp, Oliver Strobel, Wilko Weichert, Martin R. Sprick, and Andreas Trumpp. 2021. "Aggressive PDACs Show Hypomethylation of Repetitive Elements and the Execution of an Intrinsic IFN Program Linked to a Ductal Cell of Origin." *Cancer Discovery* 11 (3): 638-659. https://doi.org/10.1158/2159-8290.cd-20-1202.

29. Feig, C., J. O. Jones, M. Kraman, R. J. B. Wells, A. Deonarine, D. S. Chan, C. M. Connell, E. W. Roberts, Q. Zhao, O. L. Caballero, S. A. Teichmann, T. Janowitz, D. I. Jodrell, D. A. Tuveson, and D. T. Fearon. 2013. "Targeting CXCL12 from FAP-expressing carcinoma-associated fibroblasts synergizes with anti-PD-L1 immunotherapy in pancreatic cancer." *Proceedings of the National Academy of Sciences* 110 (50): 20212-20217. https://doi.org/10.1073/pnas.1320318110. https://www.ncbi.nlm.nih.gov/pmc/articles/PMC3864274.
30. Flowers, Brittany M., Hang Xu, Abigail S. Mulligan, Kathryn J. Hanson, Jose A. Seoane, Hannes Vogel, Christina Curtis, Laura D. Wood, and Laura D. Attardi. 2021. "Cell of Origin Influences Pancreatic Cancer Subtype." *Cancer Discovery* 11 (3): 660-677. https://doi.org/10.1158/2159-8290.cd-20-0633.
31. Golan, Talia, Pascal Hammel, Michele Reni, Eric Van Cutsem, Teresa Macarulla, Michael J. Hall, Joon-Oh Park, Daniel Hochhauser, Dirk Arnold, Do-Youn Oh, Anke Reinacher-Schick, Giampaolo Tortora, Hana Algül, Eileen M. O'Reilly, David Mcguinness, Karen Y. Cui, Katia Schlienger, Gershon Y. Locker, and Hedy L. Kindler. 2019. "Maintenance Olaparib for Germline BRCA-Mutated Metastatic Pancreatic Cancer." *New England Journal of Medicine* 381 (4): 317-327. https://doi.org/10.1056/nejmoa1903387.
32. Gunderson, Andrew J., Megan M. Kaneda, Takahiro Tsujikawa, Abraham V. Nguyen, Nesrine I. Affara, Brian Ruffell, Sara Gorjestani, Shannon M. Liudahl, Morgan Truitt, Peter Olson, Grace Kim, Douglas Hanahan, Margaret A. Tempero, Brett Sheppard, Bryan Irving, Betty Y. Chang, Judith A. Varner, and Lisa M. Coussens. 2016. "Bruton Tyrosine Kinase–Dependent Immune Cell Cross-talk Drives Pancreas Cancer." *Cancer Discovery* 6 (3): 270-285. https://doi.org/10.1158/2159-8290.cd-15-0827.
33. Hegde, Samarth, Varintra E. Krisnawan, Brett H. Herzog, Chong Zuo, Marcus A. Breden, Brett L. Knolhoff, Graham D. Hogg, Jack P. Tang, John M. Baer, Cedric Mpoy, Kyung Bae Lee, Katherine A. Alexander, Buck E. Rogers, Kenneth M. Murphy, William G. Hawkins, Ryan C. Fields, Carl J. Deselm, Julie K. Schwarz, and David G. Denardo. 2020. "Dendritic Cell Paucity Leads to Dysfunctional Immune Surveillance in Pancreatic Cancer." *Cancer Cell* 37 (3): 289-307.e9. https://doi.org/10.1016/j.ccell.2020.02.008.
34. Hingorani, Sunil R., Emanuel F. Petricoin, Anirban Maitra, Vinodh Rajapakse, Catrina King, Michael A. Jacobetz, Sally Ross, Thomas P. Conrads, Timothy D. Veenstra, Ben A. Hitt, Yoshiya Kawaguchi, Don Johann, Lance A. Liotta, Howard C. Crawford, Mary E. Putt, Tyler Jacks, Christopher V.E. Wright, Ralph H. Hruban, Andrew M. Lowy, and David A. Tuveson. 2003. "Preinvasive and invasive ductal pancreatic cancer and its early detection in the mouse." *Cancer Cell* 4 (6): 437-450. https://doi.org/10.1016/s1535-6108(03)00309-x.
35. Hingorani, Sunil R., Lifu Wang, Asha S. Multani, Chelsea Combs, Therese B. Deramaudt, Ralph H. Hruban, Anil K. Rustgi, Sandy Chang, and David A. Tuveson. 2005. "Trp53R172H and KrasG12D cooperate to promote chromosomal instability and widely metastatic pancreatic ductal adenocarcinoma in mice." *Cancer Cell* 7 (5): 469-483. https://doi.org/10.1016/j.ccr.2005.04.023. https://doi.org/10.1016/j.ccr.2005.04.023.
36. Hruban, R. H., M. Goggins, J. Parsons, and S. E. Kern. 2000. "Progression model for pancreatic cancer." *Clin Cancer Res* 6 (8): 2969-72. https://www.ncbi.nlm.nih.gov/pubmed/10955772.
37. Hruban, Ralph H., N. Volkan Adsay, Jorge Albores-Saavedra, Miriam R. Anver, Andrew V. Biankin, Gregory P. Boivin, Emma E. Furth, Toru Furukawa, Alison Klein, David S. Klimstra, Gűnter Klőppel, Gregory Y. Lauwers, Daniel S. Longnecker, Jutta Lűttges, Anirban Maitra, G. Johan A. Offerhaus, Lucía Pérez-Gallego, Mark Redston, and David A. Tuveson. 2006. "Pathology of Genetically Engineered Mouse Models of Pancreatic Exocrine Cancer: Consensus Report and Recommendations." *Cancer Research* 66 (1): 95-106. https://doi.org/10.1158/0008-5472.can-05-2168.
38. Jones, SiâN, Xiaosong Zhang, D. Williams Parsons, Jimmy Cheng-Ho Lin, Rebecca J. Leary, Philipp Angenendt, Parminder Mankoo, Hannah Carter, Hirohiko Kamiyama, Antonio Jimeno, Seung-Mo Hong, Baojin Fu, Ming-Tseh Lin, Eric S. Calhoun, Mihoko Kamiyama, Kimberly Walter, Tatiana Nikolskaya, Yuri Nikolsky, James Hartigan, Douglas R. Smith, Manuel Hidalgo, Steven D. Leach, Alison P. Klein, Elizabeth M. Jaffee, Michael Goggins, Anirban Maitra, Christine Iacobuzio-Donahue, James R. Eshleman, Scott E. Kern, Ralph H. Hruban, Rachel Karchin, Nickolas Papadopoulos, Giovanni Parmigiani, Bert Vogelstein, Victor E. Velculescu, and Kenneth W. Kinzler. 2008. "Core Signaling Pathways in Human Pancreatic Cancers Revealed by Global

Genomic Analyses." *Science* 321 (5897): 1801-1806. https://doi.org/10.1126/science.1164368. http://europepmc.org/articles/pmc2848990?pdf=render.
39. Kanda, Mitsuro, Hanno Matthaei, Jian Wu, Seung–Mo Hong, Jun Yu, Michael Borges, Ralph H. Hruban, Anirban Maitra, Kenneth Kinzler, Bert Vogelstein, and Michael Goggins. 2012. "Presence of Somatic Mutations in Most Early-Stage Pancreatic Intraepithelial Neoplasia." *Gastroenterology* 142 (4): 730-733.e9. https://doi.org/10.1053/j.gastro.2011.12.042. https://www.ncbi.nlm.nih.gov/pmc/articles/PMC3321090.
40. Kopp, Janel L., Claire L. Dubois, Ashleigh E. Schaffer, Ergeng Hao, Hung Ping Shih, Philip A. Seymour, Jenny Ma, and Maike Sander. 2011. "Sox9+ ductal cells are multipotent progenitors throughout development but do not produce new endocrine cells in the normal or injured adult pancreas." *Development* 138 (4): 653-665. https://doi.org/10.1242/dev.056499. https://www.ncbi.nlm.nih.gov/pmc/articles/PMC3026412/pdf.
41. Kopp, L., Janel, Von Figura, Guido, Erin Mayes, Fen-Fen Liu, L. Dubois, Claire, P. Morris, John, Cheng Pan, Fong, Haruhiko Akiyama, V.E. Wright, Christopher, Kristin Jensen, Matthias Hebrok, and Maike Sander. 2012. "Identification of Sox9-Dependent Acinar-to-Ductal Reprogramming as the Principal Mechanism for Initiation of Pancreatic Ductal Adenocarcinoma." *Cancer Cell* 22 (6): 737-750. https://doi.org/10.1016/j.ccr.2012.10.025. https://www.ncbi.nlm.nih.gov/pmc/articles/PMC3568632.
42. Kunk, Paul R., Todd W. Bauer, Craig L. Slingluff, and Osama E. Rahma. 2016. "From bench to bedside a comprehensive review of pancreatic cancer immunotherapy." *Journal for ImmunoTherapy of Cancer* 4 (1). https://doi.org/10.1186/s40425-016-0119-z. https://www.ncbi.nlm.nih.gov/pmc/articles/PMC4791889.
43. Lee, J. J., V. Bernard, A. Semaan, M. E. Monberg, J. Huang, B. M. Stephens, D. Lin, K. I. Rajapakshe, B. R. Weston, M. S. Bhutani, C. L. Haymaker, C. Bernatchez, C. M. Taniguchi, A. Maitra, and P. A. Guerrero. 2021. "Elucidation of Tumor-Stromal Heterogeneity and the Ligand-Receptor Interactome by Single-Cell Transcriptomics in Real-world Pancreatic Cancer Biopsies." *Clin Cancer Res* 27 (21): 5912-5921. https://doi.org/10.1158/1078-0432.CCR-20-3925. https://www.ncbi.nlm.nih.gov/pubmed/34426439.
44. Lee, Kyoung Eun, Michelle Spata, Lauren J. Bayne, Elizabeth L. Buza, Amy C. Durham, David Allman, Robert H. Vonderheide, and M. Celeste Simon. 2016. "Hif1a Deletion Reveals Pro-Neoplastic Function of B Cells in Pancreatic Neoplasia." *Cancer Discovery* 6 (3): 256-269. https://doi.org/10.1158/2159-8290.cd-15-0822.
45. Marin-Acevedo, Julian A., Erinmarie O. Kimbrough, and Yanyan Lou. 2021. "Next generation of immune checkpoint inhibitors and beyond." Journal of Hematology & Oncology 14 (1). https://doi.org/10.1186/s13045-021-01056-8.
46. Mathew, E., Y. Zhang, A. M. Holtz, K. T. Kane, J. Y. Song, B. L. Allen, and M. Pasca di Magliano. 2014. "Dosage-dependent regulation of pancreatic cancer growth and angiogenesis by hedgehog signaling." *Cell Rep* 9 (2): 484-94. https://doi.org/10.1016/j.celrep.2014.09.010. https://www.ncbi.nlm.nih.gov/pubmed/25310976.
47. Maurer, Carlo, Sam R Holmstrom, Jing He, Pasquale Laise, Tao Su, Aqeel Ahmed, Hanina Hibshoosh, John A Chabot, Paul E Oberstein, Antonia R Sepulveda, Jeanine M Genkinger, Jiapeng Zhang, Alina C Iuga, Mukesh Bansal, Andrea Califano, and Kenneth P Olive. 2019. "Experimental microdissection enables functional harmonisation of pancreatic cancer subtypes." *Gut* 68 (6): 1034-1043. https://doi.org/10.1136/gutjnl-2018-317706.
48. Mizrahi, J. D., R. Surana, J. W. Valle, and R. T. Shroff. 2020. "Pancreatic cancer." *Lancet* 395 (10242): 2008-2020. https://doi.org/10.1016/S0140-6736(20)30974-0. https://www.ncbi.nlm.nih.gov/pubmed/32593337.
49. Moffitt, Richard A, Raoud Marayati, Elizabeth L Flate, Keith E Volmar, S Gabriela Herrera Loeza, Katherine A Hoadley, Naim U Rashid, Lindsay A Williams, Samuel C Eaton, Alexander H Chung, Jadwiga K Smyla, Judy M Anderson, Hong Jin Kim, David J Bentrem, Mark S Talamonti, Christine A Iacobuzio-Donahue, Michael A Hollingsworth, and Jen Jen Yeh. 2015. "Virtual microdissection identifies distinct tumor- and stroma-specific subtypes of pancreatic ductal adenocarcinoma." *Nature Genetics* 47 (10): 1168-1178. https://doi.org/10.1038/ng.3398. https://www.ncbi.nlm.nih.gov/pmc/articles/PMC4912058.
50. Moore, Malcolm J., David Goldstein, John Hamm, Arie Figer, Joel R. Hecht, Steven Gallinger, Heather J. Au, Pawel Murawa, David Walde, Robert A. Wolff, Daniel Campos, Robert Lim, Keyue

Ding, Gary Clark, Theodora Voskoglou-Nomikos, Mieke Ptasynski, and Wendy Parulekar. 2007. "Erlotinib Plus Gemcitabine Compared With Gemcitabine Alone in Patients With Advanced Pancreatic Cancer: A Phase III Trial of the National Cancer Institute of Canada Clinical Trials Group." *Journal of Clinical Oncology* 25 (15): 1960-1966. https://doi.org/10.1200/jco.2006.07.9525.

51. Nowak, N. J., D. Gaile, J. M. Conroy, D. McQuaid, J. Cowell, R. Carter, M. G. Goggins, R. H. Hruban, and A. Maitra. 2005. "Genome-wide aberrations in pancreatic adenocarcinoma." *Cancer Genet Cytogenet* 161 (1): 36-50. https://doi.org/10.1016/j.cancergencyto.2005.01.009. https://www.ncbi.nlm.nih.gov/pubmed/16080956.
52. Nywening, Timothy M, Brian A Belt, Darren R Cullinan, Roheena Z Panni, Booyeon J Han, Dominic E Sanford, Ryan C Jacobs, Jian Ye, Ankit A Patel, William E Gillanders, Ryan C Fields, David G Denardo, William G Hawkins, Peter Goedegebuure, and David C Linehan. 2018. "Targeting both tumour-associated CXCR2+ neutrophils and CCR2+ macrophages disrupts myeloid recruitment and improves chemotherapeutic responses in pancreatic ductal adenocarcinoma." *Gut* 67 (6): 1112-1123. https://doi.org/10.1136/gutjnl-2017-313738. https://digitalcommons.wustl.edu/cgi/viewcontent.cgi?article=7871&context=open_access_pubs.
53. Nywening, Timothy M, Andrea Wang-Gillam, Dominic E Sanford, Brian A Belt, Roheena Z Panni, Brian M Cusworth, Adetunji T Toriola, Rebecca K Nieman, Lori A Worley, Motoyo Yano, Kathryn J Fowler, A Craig Lockhart, Rama Suresh, Benjamin R Tan, Kian-Huat Lim, Ryan C Fields, Steven M Strasberg, William G Hawkins, David G Denardo, S Peter Goedegebuure, and David C Linehan. 2016. "Targeting tumour-associated macrophages with CCR2 inhibition in combination with FOLFIRINOX in patients with borderline resectable and locally advanced pancreatic cancer: a single-centre, open-label, dose-finding, non-randomised, phase 1b trial." *The Lancet Oncology* 17 (5): 651-662. https://doi.org/10.1016/s1470-2045(16)00078-4.
54. O'Hara, M. H., E. M. O'Reilly, G. Varadhachary, R. A. Wolff, Z. A. Wainberg, A. H. Ko, G. Fisher, O. Rahma, J. P. Lyman, C. R. Cabanski, R. Mick, P. F. Gherardini, L. J. Kitch, J. Xu, T. Samuel, J. Karakunnel, J. Fairchild, S. Bucktrout, T. M. LaVallee, C. Selinsky, J. E. Till, E. L. Carpenter, C. Alanio, K. T. Byrne, R. O. Chen, O. C. Trifan, U. Dugan, C. Horak, V. M. Hubbard-Lucey, E. J. Wherry, R. Ibrahim, and R. H. Vonderheide. 2021. "CD40 agonistic monoclonal antibody APX005M (sotigalimab) and chemotherapy, with or without nivolumab, for the treatment of metastatic pancreatic adenocarcinoma: an open-label, multicentre, phase 1b study." Lancet Oncol 22 (1): 118-131. https://doi.org/10.1016/S1470-2045(20)30532-5. https://www.ncbi.nlm.nih.gov/pubmed/33387490.
55. Olive, Kenneth P., Michael A. Jacobetz, Christian J. Davidson, Aarthi Gopinathan, Dominick Mcintyre, Davina Honess, Basetti Madhu, Mae A. Goldgraben, Meredith E. Caldwell, David Allard, Kristopher K. Frese, Gina Denicola, Christine Feig, Chelsea Combs, Stephen P. Winter, Heather Ireland-Zecchini, Stefanie Reichelt, William J. Howat, Alex Chang, Mousumi Dhara, Lifu Wang, Felix Rückert, Robert Grützmann, Christian Pilarsky, Kamel Izeradjene, Sunil R. Hingorani, Pearl Huang, Susan E. Davies, William Plunkett, Merrill Egorin, Ralph H. Hruban, Nigel Whitebread, Karen Mcgovern, Julian Adams, Christine Iacobuzio-Donahue, John Griffiths, and David A. Tuveson. 2009. "Inhibition of Hedgehog Signaling Enhances Delivery of Chemotherapy in a Mouse Model of Pancreatic Cancer." *Science* 324 (5933): 1457-1461. https://doi.org/10.1126/science.1171362. http://europepmc.org/articles/pmc2998180?pdf=render.
56. Peng, Junya, Bao-Fa Sun, Chuan-Yuan Chen, Jia-Yi Zhou, Yu-Sheng Chen, Hao Chen, Lulu Liu, Dan Huang, Jialin Jiang, Guan-Shen Cui, Ying Yang, Wenze Wang, Dan Guo, Menghua Dai, Junchao Guo, Taiping Zhang, Quan Liao, Yi Liu, Yong-Liang Zhao, Da-Li Han, Yupei Zhao, Yun-Gui Yang, and Wenming Wu. 2019. "Single-cell RNA-seq highlights intra-tumoral heterogeneity and malignant progression in pancreatic ductal adenocarcinoma." *Cell Research* 29 (9): 725-738. https://doi.org/10.1038/s41422-019-0195-y.
57. Prokopchuk, O, Y Liu, D Henne-Bruns, and M Kornmann. 2005. "Interleukin-4 enhances proliferation of human pancreatic cancer cells: evidence for autocrine and paracrine actions." *British Journal of Cancer* 92 (5): 921-928. https://doi.org/10.1038/sj.bjc.6602416. https://www.ncbi.nlm.nih.gov/pmc/articles/PMC2361902.
58. Pylayeva-Gupta, Yuliya, Shipra Das, Jesse S. Handler, Cristina H. Hajdu, Maryaline Coffre, Sergei B. Koralov, and Dafna Bar-Sagi. 2016. "IL35-Producing B Cells Promote the Development

of Pancreatic Neoplasia." *Cancer Discovery* 6 (3): 247-255. https://doi.org/10.1158/2159-8290.cd-15-0843.
59. Raghavan, Srivatsan, Peter S. Winter, Andrew W. Navia, Hannah L. Williams, Alan Denadel, Kristen E. Lowder, Jennyfer Galvez-Reyes, Radha L. Kalekar, Nolawit Mulugeta, Kevin S. Kapner, Manisha S. Raghavan, Ashir A. Borah, Nuo Liu, Sara A. Väyrynen, Andressa Dias Costa, Raymond W.S. Ng, Junning Wang, Emma K. Hill, Dorisanne Y. Ragon, Lauren K. Brais, Alex M. Jaeger, Liam F. Spurr, Yvonne Y. Li, Andrew D. Cherniack, Matthew A. Booker, Elizabeth F. Cohen, Michael Y. Tolstorukov, Isaac Wakiro, Asaf Rotem, Bruce E. Johnson, James M. Mcfarland, Ewa T. Sicinska, Tyler E. Jacks, Ryan J. Sullivan, Geoffrey I. Shapiro, Thomas E. Clancy, Kimberly Perez, Douglas A. Rubinson, Kimmie Ng, James M. Cleary, Lorin Crawford, Scott R. Manalis, Jonathan A. Nowak, Brian M. Wolpin, William C. Hahn, Andrew J. Aguirre, and Alex K. Shalek. 2021. "Microenvironment drives cell state, plasticity, and drug response in pancreatic cancer." *Cell* 184 (25): 6119-6137.e26. https://doi.org/10.1016/j.cell.2021.11.017.
60. Rahib, Lola, Mackenzie R. Wehner, Lynn M. Matrisian, and Kevin T. Nead. 2021. "Estimated Projection of US Cancer Incidence and Death to 2040." *JAMA Network Open* 4 (4): e214708. https://doi.org/10.1001/jamanetworkopen.2021.4708.
61. Rhim, D., Andrew, E. Oberstein, Paul, H. Thomas, Dafydd, T. Mirek, Emily, F. Palermo, Carmine, A. Sastra, Stephen, N. Dekleva, Erin, Tyler Saunders, P. Becerra, Claudia, W. Tattersall, Ian, Benedikt Westphalen, C., Jan Kitajewski, G. Fernandez-Barrena, Maite, E. Fernandez-Zapico, Martin, Christine Iacobuzio-Donahue, P. Olive, Kenneth, and Z. Stanger, Ben. 2014. "Stromal Elements Act to Restrain, Rather Than Support, Pancreatic Ductal Adenocarcinoma." *Cancer Cell* 25 (6): 735-747. https://doi.org/10.1016/j.ccr.2014.04.021. http://europepmc.org/articles/pmc4096698?pdf=render.
62. Rodriguez, Paulo C., David G. Quiceno, Jovanny Zabaleta, Blair Ortiz, Arnold H. Zea, Maria B. Piazuelo, Alberto Delgado, Pelayo Correa, Jason Brayer, Eduardo M. Sotomayor, Scott Antonia, Juan B. Ochoa, and Augusto C. Ochoa. 2004. "Arginase I Production in the Tumor Microenvironment by Mature Myeloid Cells Inhibits T-Cell Receptor Expression and Antigen-Specific T-Cell Responses." *Cancer Research* 64 (16): 5839-5849. https://doi.org/10.1158/0008-5472.can-04-0465.
63. Royal, Richard E., Catherine Levy, Keli Turner, Aarti Mathur, Marybeth Hughes, Udai S. Kammula, Richard M. Sherry, Suzanne L. Topalian, James C. Yang, Israel Lowy, and Steven A. Rosenberg. 2010. "Phase 2 Trial of Single Agent Ipilimumab (Anti-CTLA-4) for Locally Advanced or Metastatic Pancreatic Adenocarcinoma." *Journal of Immunotherapy* 33 (8): 828-833. https://doi.org/10.1097/cji.0b013e3181eec14c.
64. Sanford, Dominic E., Brian A. Belt, Roheena Z. Panni, Allese Mayer, Anjali D. Deshpande, Danielle Carpenter, Jonathan B. Mitchem, Stacey M. Plambeck-Suess, Lori A. Worley, Brian D. Goetz, Andrea Wang-Gillam, Timothy J. Eberlein, David G. Denardo, Simon Peter Goedegebuure, and David C. Linehan. 2013. "Inflammatory Monocyte Mobilization Decreases Patient Survival in Pancreatic Cancer: A Role for Targeting the CCL2/CCR2 Axis." *Clinical Cancer Research* 19 (13): 3404-3415. https://doi.org/10.1158/1078-0432.ccr-13-0525.
65. Schadendorf, Dirk, F. Stephen Hodi, Caroline Robert, Jeffrey S. Weber, Kim Margolin, Omid Hamid, Debra Patt, Tai-Tsang Chen, David M. Berman, and Jedd D. Wolchok. 2015. "Pooled Analysis of Long-Term Survival Data From Phase II and Phase III Trials of Ipilimumab in Unresectable or Metastatic Melanoma." *Journal of Clinical Oncology* 33 (17): 1889-1894. https://doi.org/10.1200/jco.2014.56.2736.
66. Shi, Chanjuan, Seung-Mo Hong, Phillip Lim, Hirohiko Kamiyama, Mehtab Khan, Robert A. Anders, Michael Goggins, Ralph H. Hruban, and James R. Eshleman. 2009. "KRAS2 Mutations in Human Pancreatic Acinar-Ductal Metaplastic Lesions Are Limited to Those with PanIN: Implications for the Human Pancreatic Cancer Cell of Origin." *Molecular Cancer Research* 7 (2): 230-236. https://doi.org/10.1158/1541-7786.mcr-08-0206.
67. Siegel, Rebecca L., Kimberly D. Miller, Hannah E. Fuchs, and Ahmedin Jemal. 2021. "Cancer Statistics, 2021." *CA: A Cancer Journal for Clinicians* 71 (1): 7-33. https://doi.org/10.3322/caac.21654.
68. Steele, Colin W., Saadia A. Karim, Joshua D.G. Leach, Peter Bailey, Rosanna Upstill-Goddard, Loveena Rishi, Mona Foth, Sheila Bryson, Karen Mcdaid, Zena Wilson, Catherine Eberlein, Juliana B. Candido, Mairi Clarke, Colin Nixon, John Connelly, Nigel Jamieson, C. Ross Carter,

Frances Balkwill, David K. Chang, T.R. Jeffry Evans, Douglas Strathdee, Andrew V. Biankin, Robert J.B. Nibbs, Simon T. Barry, Owen J. Sansom, and Jennifer P. Morton. 2016. "CXCR2 Inhibition Profoundly Suppresses Metastases and Augments Immunotherapy in Pancreatic Ductal Adenocarcinoma." *Cancer Cell* 29 (6): 832-845. https://doi.org/10.1016/j.ccell.2016.04.014. https://doi.org/10.1016/j.ccell.2016.04.014.

69. Steele, Nina G., Giulia Biffi, Samantha B. Kemp, Yaqing Zhang, Donovan Drouillard, Lijyun Syu, Yuan Hao, Tobiloba E. Oni, Erin Brosnan, Ela Elyada, Abhishek Doshi, Christa Hansma, Carlos Espinoza, Ahmed Abbas, Stephanie The, Valerie Irizarry-Negron, Christopher J. Halbrook, Nicole E. Franks, Megan T. Hoffman, Kristee Brown, Eileen S. Carpenter, Zeribe C. Nwosu, Craig Johnson, Fatima Lima, Michelle A. Anderson, Youngkyu Park, Howard C. Crawford, Costas A. Lyssiotis, Timothy L. Frankel, Arvind Rao, Filip Bednar, Andrzej A. Dlugosz, Jonathan B. Preall, David A. Tuveson, Benjamin L. Allen, and Marina Pasca Di Magliano. 2021. "Inhibition of Hedgehog Signaling Alters Fibroblast Composition in Pancreatic Cancer." *Clinical Cancer Research* 27 (7): 2023-2037. https://doi.org/10.1158/1078-0432.ccr-20-3715.
70. Stotz, M, A Gerger, F Eisner, J Szkandera, H Loibner, A L Ress, P Kornprat, W A Zoughbi, F S Seggewies, C Lackner, T Stojakovic, H Samonigg, G Hoefler, and M Pichler. 2013. "Increased neutrophil-lymphocyte ratio is a poor prognostic factor in patients with primary operable and inoperable pancreatic cancer." *British Journal of Cancer* 109 (2): 416-421. https://doi.org/10.1038/bjc.2013.332. http://europepmc.org/articles/pmc3721392?pdf=render.
71. Stromnes, Ingunn M, J Scott Brockenbrough, Kamel Izeradjene, Markus A Carlson, Carlos Cuevas, Randi M Simmons, Philip D Greenberg, and Sunil R Hingorani. 2014. "Targeted depletion of an MDSC subset unmasks pancreatic ductal adenocarcinoma to adaptive immunity." *Gut* 63 (11): 1769-1781. https://doi.org/10.1136/gutjnl-2013-306271. https://www.ncbi.nlm.nih.gov/pmc/articles/PMC4340484.
72. Tan, Marcus C. B., Peter S. Goedegebuure, Brian A. Belt, Brian Flaherty, Narendra Sankpal, William E. Gillanders, Timothy J. Eberlein, Chyi-Song Hsieh, and David C. Linehan. 2009. "Disruption of CCR5-Dependent Homing of Regulatory T Cells Inhibits Tumor Growth in a Murine Model of Pancreatic Cancer." *The Journal of Immunology* 182 (3): 1746-1755. https://doi.org/10.4049/jimmunol.182.3.1746.
73. Tian, Chenxi, Karl R. Clauser, Daniel Öhlund, Steffen Rickelt, Ying Huang, Mala Gupta, D. R. Mani, Steven A. Carr, David A. Tuveson, and Richard O. Hynes. 2019. "Proteomic analyses of ECM during pancreatic ductal adenocarcinoma progression reveal different contributions by tumor and stromal cells." *Proceedings of the National Academy of Sciences* 116 (39): 19609-19618. https://doi.org/10.1073/pnas.1908626116.
74. Vaddepally, Raju K., Prakash Kharel, Ramesh Pandey, Rohan Garje, and Abhinav B. Chandra. 2020. "Review of Indications of FDA-Approved Immune Checkpoint Inhibitors per NCCN Guidelines with the Level of Evidence." *Cancers* 12 (3): 738. https://doi.org/10.3390/cancers12030738.
75. Vaughan, M. B., E. W. Howard, and J. J. Tomasek. 2000. "Transforming growth factor-beta1 promotes the morphological and functional differentiation of the myofibroblast." *Exp Cell Res* 257 (1): 180-9. https://doi.org/10.1006/excr.2000.4869. https://www.ncbi.nlm.nih.gov/pubmed/10854066.
76. Versteijne, Eva, Mustafa Suker, Karin Groothuis, Janine M. Akkermans-Vogelaar, Marc G. Besselink, Bert A. Bonsing, Jeroen Buijsen, Olivier R. Busch, Geert-Jan M. Creemers, Ronald M. Van Dam, Ferry A.L.M. Eskens, Sebastiaan Festen, Jan Willem B. De Groot, Bas Groot Koerkamp, Ignace H. De Hingh, Marjolein Y.V. Homs, Jeanin E. Van Hooft, Emile D. Kerver, Saskia A.C. Luelmo, Karen J. Neelis, Joost Nuyttens, Gabriel M.R.M. Paardekooper, Gijs A. Patijn, Maurice J.C. Van Der Sangen, Judith De Vos-Geelen, Johanna W. Wilmink, Aeilko H. Zwinderman, Cornelis J. Punt, Casper H. Van Eijck, and Geertjan Van Tienhoven. 2020. "Preoperative Chemoradiotherapy Versus Immediate Surgery for Resectable and Borderline Resectable Pancreatic Cancer: Results of the Dutch Randomized Phase III PREOPANC Trial." *Journal of Clinical Oncology* 38 (16): 1763-1773. https://doi.org/10.1200/jco.19.02274.
77. Vonderheide, Robert H. 2020. "CD40 Agonist Antibodies in Cancer Immunotherapy." Annual Review of Medicine 71 (1): 47-58. https://doi.org/10.1146/annurev-med-062518-045435.
78. Ying, Haoqiang, C. Kimmelman, Alec, A. Lyssiotis, Costas, Sujun Hua, C. Chu, Gerald, Eliot Fletcher-Sananikone, W. Locasale, Jason, Jaekyoung Son, Hailei Zhang, L. Coloff, Jonathan,

Haiyan Yan, Wei Wang, Shujuan Chen, Andrea Viale, Hongwu Zheng, Ji-Hye Paik, Carol Lim, R. Guimaraes, Alexander, S. Martin, Eric, Jeffery Chang, F. Hezel, Aram, R. Perry, Samuel, Jian Hu, Boyi Gan, Yonghong Xiao, M. Asara, John, Ralph Weissleder, Alan Wang, Y., Lynda Chin, C. Cantley, Lewis, and A. Depinho, Ronald. 2012. "Oncogenic Kras Maintains Pancreatic Tumors through Regulation of Anabolic Glucose Metabolism." *Cell* 149 (3): 656-670. https://doi.org/10.1016/j.cell.2012.01.058. https://www.ncbi.nlm.nih.gov/pmc/articles/PMC3472002.

79. Zhang, Y., H. C. Crawford, and M. Pasca di Magliano. 2019. "Epithelial-Stromal Interactions in Pancreatic Cancer." *Annu Rev Physiol* 81: 211-233. https://doi.org/10.1146/annurev-physiol-020518-114515. https://www.ncbi.nlm.nih.gov/pubmed/30418798.
80. Zhang, Y., W. Yan, E. Mathew, K. T. Kane, A. Brannon, M. Adoumie, A. Vinta, H. C. Crawford, and M. Pasca di Magliano. 2017. "Epithelial-Myeloid cell crosstalk regulates acinar cell plasticity and pancreatic remodeling in mice." *Elife* 6. https://doi.org/10.7554/eLife.27388. https://www.ncbi.nlm.nih.gov/pubmed/28980940.
81. Zhang, Yaqing, Jenny Lazarus, Nina G. Steele, Wei Yan, Ho-Joon Lee, Zeribe C. Nwosu, Christopher J. Halbrook, Rosa E. Menjivar, Samantha B. Kemp, Veerin R. Sirihorachai, Ashley Velez-Delgado, Katelyn Donahue, Eileen S. Carpenter, Kristee L. Brown, Valerie Irizarry-Negron, Anna C. Nevison, Alekya Vinta, Michelle A. Anderson, Howard C. Crawford, Costas A. Lyssiotis, Timothy L. Frankel, Filip Bednar, and Marina Pasca Di Magliano. 2020. "Regulatory T-cell Depletion Alters the Tumor Microenvironment and Accelerates Pancreatic Carcinogenesis." *Cancer Discovery* 10 (3): 422-439. https://doi.org/10.1158/2159-8290.cd-19-0958.
82. Zhang, Yaqing, Ashley Velez-Delgado, Esha Mathew, Dongjun Li, Flor M Mendez, Kevin Flannagan, Andrew D Rhim, Diane M Simeone, Gregory L Beatty, and Marina Pasca Di Magliano. 2017. "Myeloid cells are required for PD-1/PD-L1 checkpoint activation and the establishment of an immunosuppressive environment in pancreatic cancer." *Gut* 66 (1): 124-136. https://doi.org/10.1136/gutjnl-2016-312078. https://www.ncbi.nlm.nih.gov/pmc/articles/PMC5256390.
83. Zhang, Yaqing, Wei Yan, Meredith A. Collins, Filip Bednar, Sabita Rakshit, Bruce R. Zetter, Ben Z. Stanger, Ivy Chung, Andrew D. Rhim, and Marina Pasca Di Magliano. 2013. "Interleukin-6 Is Required for Pancreatic Cancer Progression by Promoting MAPK Signaling Activation and Oxidative Stress Resistance." *Cancer Research* 73 (20): 6359-6374. https://doi.org/10.1158/0008-5472.can-13-1558-t.
84. Zhang, Yaqing, Wei Yan, Esha Mathew, Filip Bednar, Shanshan Wan, Meredith A. Collins, Rebecca A. Evans, Theodore H. Welling, Robert H. Vonderheide, and Marina Pasca Di Magliano. 2014. "CD4+ T Lymphocyte Ablation Prevents Pancreatic Carcinogenesis in Mice." *Cancer Immunology Research* 2 (5): 423-435. https://doi.org/10.1158/2326-6066.cir-14-0016-t.
85. Zhu, Liqin, Guanglu Shi, C. Max. Schmidt, Ralph H. Hruban, and Stephen F. Konieczny. 2007. "Acinar Cells Contribute to the Molecular Heterogeneity of Pancreatic Intraepithelial Neoplasia." *The American Journal of Pathology* 171 (1): 263-273. https://doi.org/10.2353/ajpath.2007.061176. https://www.ncbi.nlm.nih.gov/pmc/articles/PMC1941579.
86. Zhu, Yu, Brett L. Knolhoff, Melissa A. Meyer, Timothy M. Nywening, Brian L. West, Jingqin Luo, Andrea Wang-Gillam, S. Peter Goedegebuure, David C. Linehan, and David G. Denardo. 2014. "CSF1/CSF1R Blockade Reprograms Tumor-Infiltrating Macrophages and Improves Response to T-cell Checkpoint Immunotherapy in Pancreatic Cancer Models." *Cancer Research* 74 (18): 5057-5069. https://doi.org/10.1158/0008-5472.can-13-3723.
87. Özdemir, C., Berna, Tsvetelina Pentcheva-Hoang, L. Carstens, Julienne, Xiaofeng Zheng, Chia-Chin Wu, R. Simpson, Tyler, Hanane Laklai, Hikaru Sugimoto, Christoph Kahlert, V. Novitskiy, Sergey, De Jesus-Acosta, Ana, Padmanee Sharma, Pedram Heidari, Umar Mahmood, Lynda Chin, L. Moses, Harold, M. Weaver, Valerie, Anirban Maitra, P. Allison, James, S. Lebleu, Valerie, and Raghu Kalluri. 2014. "Depletion of Carcinoma-Associated Fibroblasts and Fibrosis Induces Immunosuppression and Accelerates Pancreas Cancer with Reduced Survival." *Cancer Cell* 25 (6): 719-734. https://doi.org/10.1016/j.ccr.2014.04.005. https://doi.org/10.1016/j.ccr.2014.04.005.

Chapter 2: Multimodal Mapping of the Tumor and Peripheral Blood Immune Landscape in Human Pancreatic Cancer[1,2]

Abstract

Pancreatic ductal adenocarcinoma (PDA) is characterized by an immune-suppressive tumor microenvironment that renders it largely refractory to immunotherapy. We implemented a multimodal analysis approach to elucidate the immune landscape in PDA. Using a combination of CyTOF, single-cell RNA sequencing, and multiplex immunohistochemistry on patient tumors, matched blood, and non-malignant samples, we uncovered a complex network of immune-suppressive cellular interactions. These experiments revealed heterogeneous expression of immune checkpoint receptors in individual patient's T cells and increased markers of $CD8^+$ T cell dysfunction in advanced disease stage. Tumor-infiltrating $CD8^+$ T cells had an increased proportion of cells expressing an exhausted expression profile that included upregulation of the immune checkpoint TIGIT, a finding that we validated at the protein level. Our findings point to a profound alteration of the immune landscape of tumors,

[1] Data from Chapter 2 have been published in Nature Cancer in a manuscript entitled, "Multimodal Mapping of the Tumor and Peripheral Blood Immune Landscape in Human Pancreatic Cancer" (2020).

[2] Author list: Nina G. Steele[+], Eileen S. Carpenter[+], Samantha B. Kemp[+], Veerin Sirihorachai[+], Stephanie The, Lawrence Delrosario, Jenny Lazarus, El-ad David Amir, Valerie Gunchick, Carlos Espinoza, Samantha Bell, Lindsey Harris, Fatima Lima, Valerie Irizarry-Negron, Daniel Paglia, Justin Macchia, Angel Ka Yan Chu, Heather Schofield, Erik-Jan Wamsteker, Richard Kwon, Allison Schulman, Anoop Prabhu, Ryan Law, Arjun Sondhi, Jessica Yu, Arpan Patel, Katelyn Donahue, Hari Nathan, Clifford Cho, Michelle A. Anderson, Vaibhav Sahai, Costas A. Lyssiotis, Weiping Zou, Benjamin L. Allen, Arvind Rao, Howard C. Crawford*, Filip Bednar*, Timothy L. Frankel*, Marina Pasca di Magliano*

[+] Equal author contribution

*Corresponding authors

and to patient-specific immune changes that should be taken into account as combination immunotherapy becomes available for pancreatic cancer.

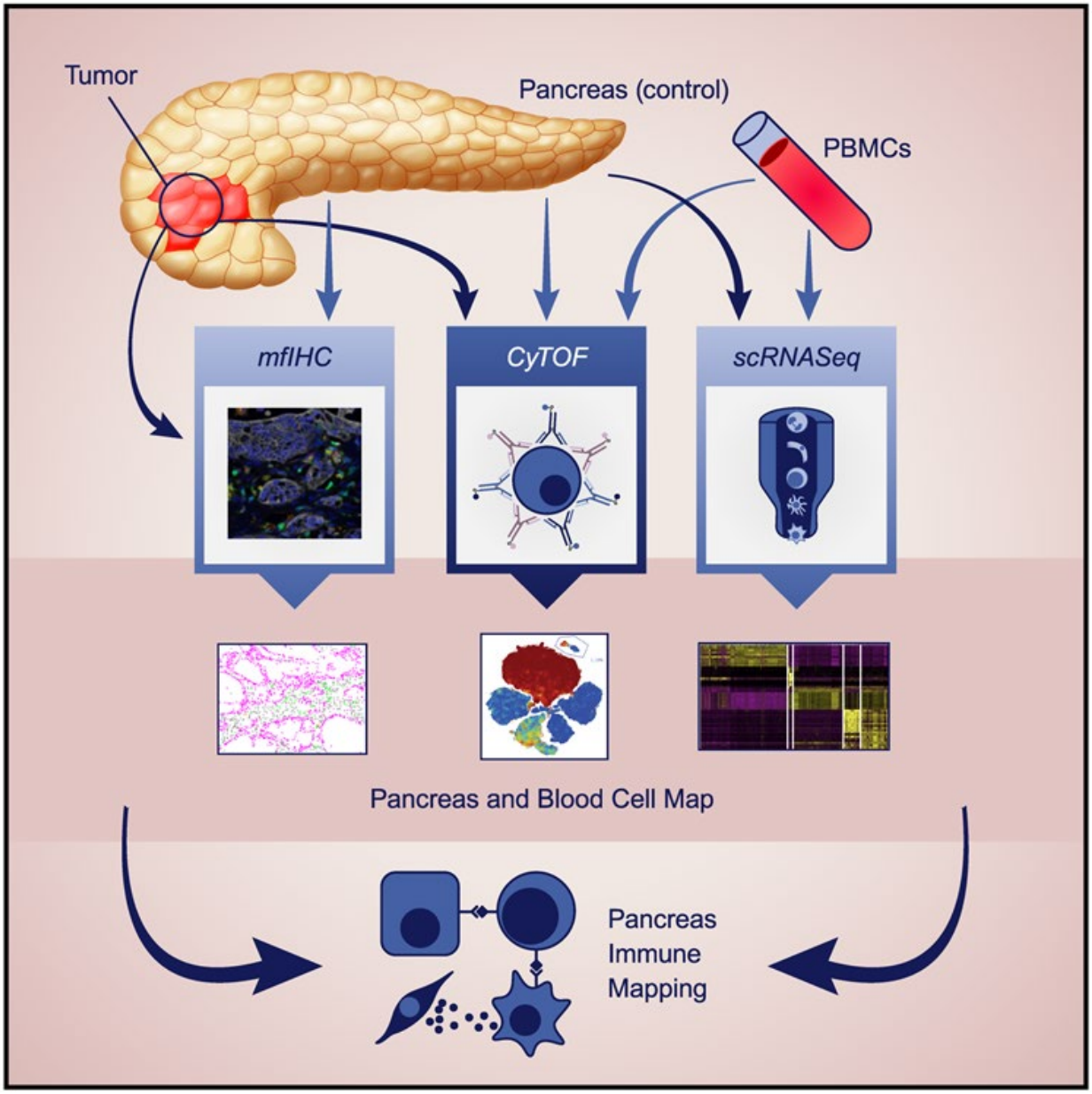

Figure 2.1 Graphical Abstract

Introduction

Pancreatic ductal adenocarcinoma (PDA), one of the deadliest human malignancies, is distinguished by an extensive and complex tumor microenvironment (TME) containing abundant infiltrating immune cells. Immunotherapy clinical trials using checkpoint inhibitors PD-1 and CTLA4 as single agents have been unsuccessful (Royal et al. 2010; Brahmer et al. 2012), but recent clinical trials using combination of immune regulatory agents have shown positive initial results (NCT02588443), indicating the need to target multiple components of the stroma and better understand the immune landscape of human PDA. The prevalence of $CD8^+$ T cells varies across patients (Ingunn M. Stromnes et al. 2017). Deconvolution of bulk RNA sequencing data from The Cancer Genome Atlas (TCGA) stratified tumors based on their cytolytic index, including a high cytolytic index group (Balli et al. 2017). These data indicate that the $CD8^+$ T cell landscape in pancreatic tumors might be more complex than previously believed, and the mechanisms of immune suppression may vary across patients. While pancreatic cancer is most often diagnosed when locally invasive or metastatic, most existing datasets are limited to surgical samples representing earlier stages of the disease.

The presence and distribution of cytotoxic T cells in PDA has important prognostic correlations; $CD8^+$ T cells in proximity to PDA cells correlate with increased overall survival (Carstens et al. 2017). Further, analysis of rare long-term PDA survivors revealed persistence of T cell clones specific to tumor antigens (Balachandran et al. 2017). Conversely, infiltration of myeloid cells, specifically tumor associated macrophages, negatively correlates with prognosis (Tsujikawa et al. 2017), consistent

with an immune-suppressive role of these cells (Vonderheide 2018). $CD4^+$ T cells are abundant within tumors, with a prevalence of regulatory T cells (Clark et al. 2007); their nature in human PDA is currently poorly understood. Similarly, our understanding of other immune cell types within tumors is limited.

Here, we used multiple, complementary approaches [mass cytometry (CyTOF), single-cell RNA sequencing (scRNA seq), and multiplex fluorescent immunohistochemistry (mfIHC)] to investigate the immune landscape of pancreatic tumors from a collection of samples that included both surgical and fine needle biopsy samples, as well as matched patient blood (graphical abstract). Our work adds an in-depth immune characterization to complement recent single cell characterization on pancreatic tumor cells (Moncada et al. 2020; Chan-Seng-Yue et al. 2020) and cancer associated fibroblasts (Elyada et al. 2019; Dominguez et al. 2020). We observed that immune landscapes in each individual patient were heterogeneous, although some common features emerged. Cytotoxic T cells in patients displayed an exhausted gene expression signature, which was progressively more pronounced in advanced disease. The specific combinations of immune checkpoint genes expressed in each patient's $CD8^+$ T cells was unique. Tumor infiltrating $CD8^+$ T cell had a higher proportion of cells expressing genes previously associated with T cell exhaustion, and these cells had enriched expression of the immune checkpoint T-cell immunoglobulin and ITIM domains (TIGIT) (Manieri, Chiang, and Grogan 2017). Predicted interaction analysis (Cohen et al. 2018; Qiming Zhang et al. 2019) revealed multiple potential cellular interactions upregulated in tumors compared with non-malignant tissue. Overall, our study provides a wealth of hypothesis-generating data to benefit the PDA community at large.

Results

CyTOF and multiplex immunohistochemistry mapping reveal heterogeneous immune infiltration in human pancreatic cancer

To map the immune infiltration in pancreatic cancer, we performed CyTOF on 10 pancreatic tumor samples and 8 samples from non-malignant pancreas specimens [Whipple pancreaticoduodenectomy (n=2), distal pancreatectomy (n=4), partial pancreatectomy (n=1) or endoscopic fine needle biopsy (n=3)]. Clinical pathology review provided the diagnosis for samples (Supplemental Figure 2.1A); histology of surgical specimens is shown in Supplemental Figure 2.1B. Our validated antibody panel contained 30 immune markers (Supplemental Table 2.1) (Bendall et al. 2011). We used the Astrolabe Cytometry platform for batch correction to account for differences in the timing of sample acquisition, and selected live singlets for downstream analysis (Nowicka et al. 2019; Amir et al. 2019).

Principal component analysis (PCA) showed a minor shift between adjacent or normal pancreas and tumor samples (Figure 2.2A), indicating differences in immune cell composition. To visualize the distribution of cell populations within individual samples, we utilized unbiased hierarchical clustering algorithms (Nowicka et al. 2019), along with supervised annotation (Figure 2.2B,C and Supplemental Figure 2.1C,D). While adjacent/normal samples contained mostly non-immune cells, tumor samples had an abundance of immune cells (Figure 2.2C). Multiple immune populations were elevated in tumor samples: myeloid cells, B cells, NK cells, $CD4^+$ T cells, regulatory T cells and $CD8^+$ T cells (Figure 2.2D and Supplemental Figure 2.1E). We observed an inverse correlation between the percentage of myeloid cells and $CD8^+$ T cells (Figure 2.2E),

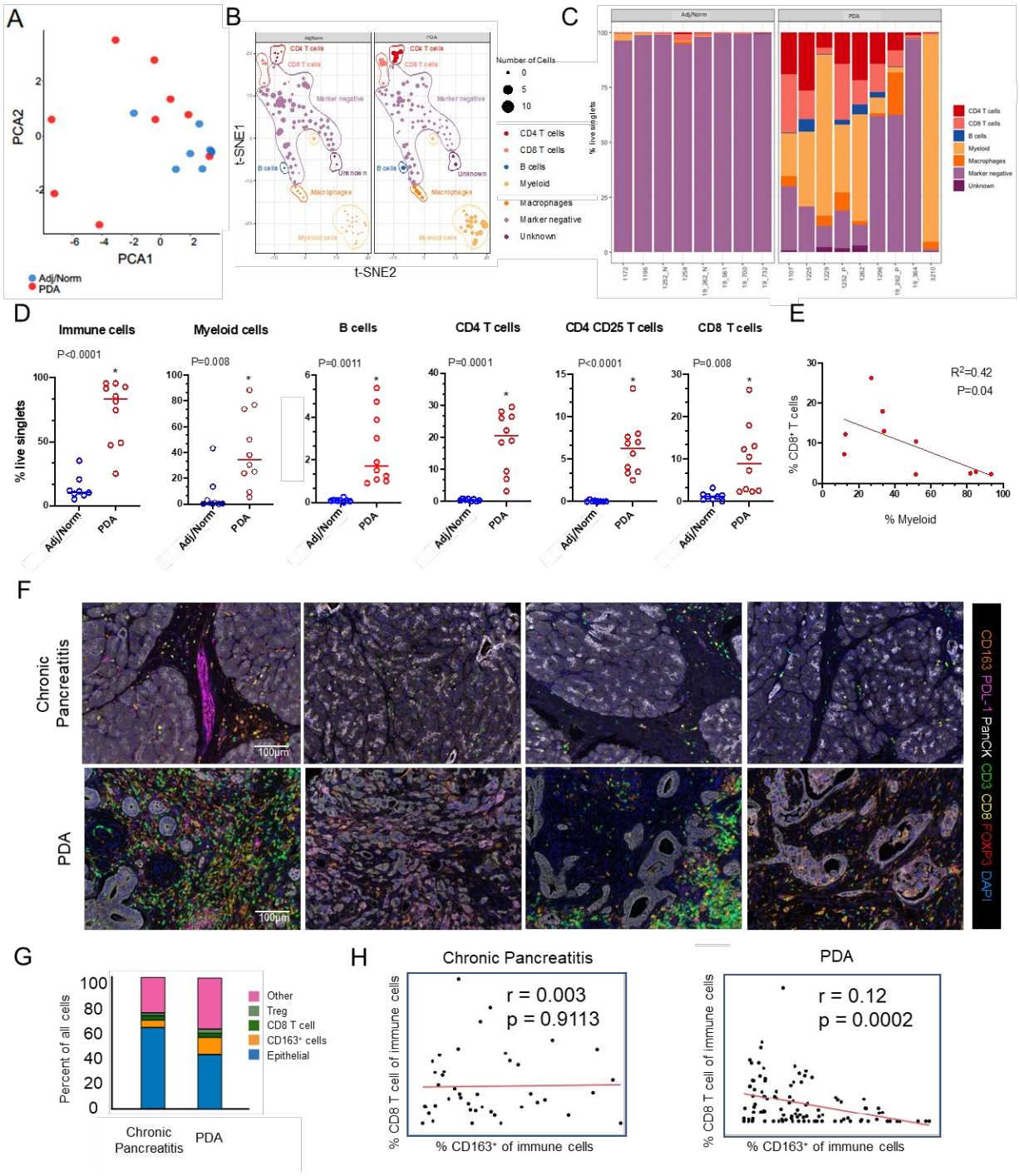

Figure 2.2 CyTOF and multiplex fluorescent immunohistochemistry (mfIHC) mapping reveals heterogeneous immune infiltration in human pancreatic cancer.

(A) PCA analysis comparing intensity of marker staining of n=8 normal or adjacent pancreata tissue samples (blue) compared to n=9 PDA tumor samples (red). **(B)** Merged adj/norm panc (left) and PDA (right) t-SNE analysis of defined cell clusters from CyTOF analysis on tissue samples. The size of the dot represents the number of cells in the cluster. Each color represents a cell population: CD4 T cells (red), CD8 T cells (pink), B cells (blue), Myeloid (light orange), Macrophages (orange), $CD45^-$ cells (light purple), Unknown (purple). (Continued on next page)

(C) Bar plot representation from FlowSOM CyTOF analysis of n=8 adj/norm tissue samples and n=9 PDA tumor samples. Analysis was only performed on samples with greater than 3,000 live singlets. **(D)** Manual quantitation of total immune cells ($CD45^+$), myeloid cells ($CD11b^+$), $CD4^+$ T cells, $CD8^+$ T cells, potential Tregs ($CD4^+$ $CD25^+$), and B cells. Manual gating included n=8 adj/norm patients and n=10 PDA patients per group. Asterisk denotes a p-value less than 0.05 determined by two-sided Student's t-test. **(E)** Correlation plot of total $CD11b^+$ myeloid cells compared to total $CD8^+$ T cells. **(F)** mfIHC composite images of formalin-fixed, paraffin-embedded tissue specimens from four different patients with chronic pancreatitis (top row) and four patients with PDA (bottom row). Antibodies and colors are as follows: CD163 (orange), PD-L1 (magenta), Pancytokeratin (PanCK; white), CD3 (green), CD8 (yellow), FOXP3 (red), and DAPI (blue). **(G)** Comparison of cellular infiltration between n=34 chronic pancreatitis patients and n=71 PDA patients (P-values: Other 0.0001, CD163+ cells 0.020, $CD8^+$ T cells 0.3483, Treg <0.0001, Epithelial <0.0001). **(H)** Correlation between percentage of $CD8^+$ T cells and $CD163^+$ cells in chronic pancreatitis and PDA.

(Ingunn M. Stromnes et al. 2017; Clark et al. 2007; Y. Zhang et al. 2017; Panni et al. 2019; Ingunn M Stromnes et al. 2014).

To measure immune composition in undisturbed tissue and define the spatial relationships between immune cells in the microenvironment, we performed seven-color multiplex fluorescent immunohistochemistry (mfIHC) on a formalin fixed paraffin embedded tissue tumor microarray (TMA) comprised of 71 PDA and 34 chronic pancreatitis samples, as previously described (Lazarus et al. 2018) (Supplemental Figure 2.1F). Representative images from individual samples are shown in Figure 2.2F, Supplemental Figure 2.1G–H. Chronic pancreatitis samples contained a higher epithelial cell component than the PDA samples. Conversely, immune cell infiltration was more abundant in PDA tissue (Figure 2.2G). In agreement with our CyTOF analysis, mfIHC demonstrated an increase in Tregs ($FOXP3^+$) and macrophages ($CD163^+$). However, unlike in the CyTOF data, $CD8^+$ T cells did not change (Figure 2.2G), likely reflecting differences in the control tissues (chronic pancreatitis versus adjacent/normal pancreas). Individual patient tumors were variable in terms of $CD8^+$ T cell infiltration. As in the CyTOF data, we observed a negative correlation between $CD8^+$ T cells and myeloid cells in PDA samples (Figure 2.2H and 2.2E) (Tsujikawa et al.

2017; Clark et al. 2007), supporting a key immunosuppressive role of this cell population (Y. Zhang et al. 2017; Beatty et al. 2015; Sanford et al. 2013; Denardo and Ruffell 2019; Nywening et al. 2018; Zhu et al. 2017; Zhu et al. 2014). Overall, our data show a complex microenvironment and considerable variability across individual patients.

Single cell RNA sequencing reveals a complex immune landscape with heterogeneous expression of immune checkpoints and ligands in the pancreatic cancer microenvironment

We performed single cell RNA sequencing (scRNA seq) on 16 PDA samples, including surgical (n=6) and fine needle biopsy specimens (n=10) (Supplemental Figure 2.2A). All the patients were treatment-naïve at the time of sample acquisition. We also included three non-malignant pancreas samples (1196, 1258, 19732) from patients undergoing surgery for duodenal adenoma, ampullary carcinoma, or adjacent to PDA, respectively, where an uninvolved portion of pancreas was included in the resection (as determined by pathologic evaluation). To capture a window into the systemic immune response in PDA patients, we also collected peripheral blood mononuclear cells (PBMCs) from these patients and healthy subjects (Supplemental Figure 2.2A, right panel).

In total, we sequenced 8541 cells from adjacent/normal samples and 46,244 from PDA, while from the blood samples we sequenced 14,240 cells from 4 healthy subjects, and 55,873 cells from 16 PDA patients. To define and visualize cell subpopulations, we batch corrected our tumor and blood sequencing samples (Supplemental Figure 2.2B) and then used unbiased clustering and a dimensionality

reduction through Uniform Manifold Approximation and Projection (UMAP) (Figure 2.3A and Supplemental Figure 2.3A). We identified each subpopulation based on published lineage markers (Figure 2.3B and Supplemental Figure 2.3B). We observed variability in the total immune cell composition of individual tumors, and in the relative abundance of individual immune cell components similar to CYTOF and mfIHC data (Supplemental Figure 2.2C and 2.2D).

Figure 2.3 Single cell RNA sequencing reveals heterogenous expression of immune checkpoints in PDA tissue.

(A) PCA analysis comparing intensity of marker staining of n=8 normal or adjacent pancreata tissue samples (blue) compared to n=9 PDA tumor samples (red). **(B)** Merged adj/norm panc (left) and PDA (right) t-SNE analysis of defined cell clusters from CyTOF analysis on tissue samples. The size of the dot represents the number of cells in the cluster. Each color represents a cell population: CD4 T cells (red), CD8 T cells (pink), B cells (blue), Myeloid (light orange), Macrophages (orange), $CD45^-$ cells (light purple), Unknown (purple). **(C)** Bar plot representation from FlowSOM CyTOF analysis of n=8 adj/norm tissue samples and n=9 PDA tumor samples. Analysis was only performed on samples with greater than 3,000 live singlets. **(D)** Manual quantitation of total immune cells ($CD45^+$), myeloid cells ($CD11b^+$), $CD4^+$ T cells, $CD8^+$ T cells, potential Tregs ($CD4^+$ $CD25^+$), and B cells. Manual gating included n=8 adj/norm patients and n=10 PDA patients per group. Asterisk denotes a p-value less than 0.05 determined by two-sided Student's t-test. **(E)** Correlation plot of total $CD11b^+$ myeloid cells compared to total $CD8^+$ T cells. **(F)** mfIHC composite images of formalin-fixed, paraffin-embedded tissue specimens from four different patients with chronic pancreatitis (top row) and four patients with PDA (bottom row). Antibodies and colors are as follows: CD163 (orange), PD-L1 (magenta), Pancytokeratin (PanCK; white), CD3 (green), CD8 (yellow), FOXP3 (red), and DAPI (blue). **(G)** Comparison of cellular infiltration between n=34 chronic pancreatitis patients and n=71 PDA patients (P-values: Other 0.0001, $CD163^+$ cells 0.020, $CD8^+$ T cells 0.3483, Treg <0.0001, Epithelial <0.0001). **(H)** Correlation between percentage of $CD8^+$ T cells and $CD163^+$ cells in chronic pancreatitis and PDA.

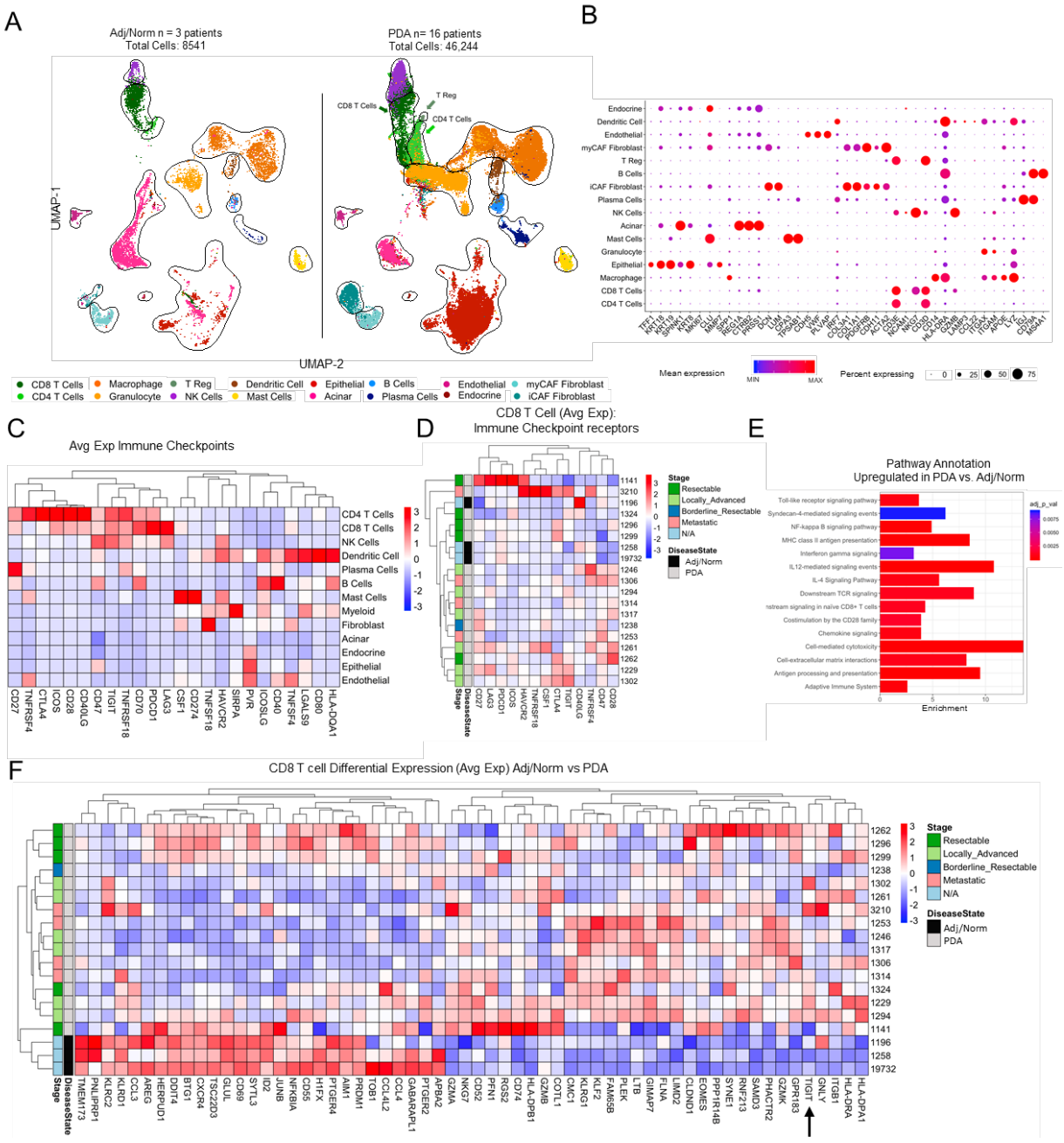

We identified abundant pro-inflammatory cells in the PDA microenvironment including CD8^{+} T cells and natural killer cells (NK) (Figure 2.3A). To gather insight into the possible mechanisms preventing anti-tumor immune responses, we profiled average expression of immune checkpoint receptors and ligands by cell type, both in tumors and

PBMCs of PDA patients (Figure 2.3C and Supplemental Figure 2.3C). We observed expression of multiple immune checkpoint receptors in T and NK cell subsets, while myeloid populations were enriched for their corresponding ligands (Figure 2.3C). $CD8^+$ T cells had elevated ICOS, TIGIT, PDCD1 and LAG3, among others, but relatively low expression of CTLA4. CTLA4, as well as all other checkpoints except for LAG3, was high in $CD4^+$ T cells. NK cells also had elevated CD47, TIGIT, TNFRSF18 and LAG3, and modest expression of PDCD1. The expression of checkpoint ligands was heterogeneous, with epithelial cells mainly expressing PVR and LGALS9 (encoding for PVR and GALECTIN 9, ligands for TIGIT and HAVCR2(TIM3) respectively). Myeloid and dendritic cells expressed several genes encoding checkpoint ligands, including SIRPA, LGALS9, PVR, and ICOSLG (Figure 2.3C). Similarly, in PBMC samples, $CD4^+$ T cells, $CD8^+$ T cells and NK cells had elevated expression of multiple immune checkpoint receptors (TIGIT was elevated in all three cellular compartments), and granulocytes, monocytes and B cells, plasma cells and dendritic cells expressed the ligands (Supplemental Figure 2.3C). We also detected expression of immune checkpoint ligands in other non-immune cell types, which included fibroblasts, endocrine, and endothelial cells (Figure 2.3C). Our single cell data revealed a complex, patient-specific landscape of immune checkpoint ligand and receptor expression across multiple immune and non-immune cell types.

Tumor-infiltrating $CD8^+$ T cells have a distinct gene expression profile, with progressive dysfunction in advanced disease

Cytotoxic T cells are a fundamental component of anti-tumor immune responses and the target of immunotherapy (for review see (Rosenberg 2014)). To gather deeper

insight into the functional status of tumor-infiltrating $CD8^+$ T cells, we investigated their transcriptional profile. To investigate patient-specific variability, we mapped the average expression of immune checkpoint receptors in $CD8^+$ T cells in each individual patient's tumor and blood samples (Figure 2.3D and Supplemental Figure 2.3D). Infiltrating $CD8^+$ T cells expressed markedly distinct immune checkpoint profiles in individual patient samples, both in tumors and blood (Figure 2.3D and Supplemental Figure 2.3D). In tumor samples, LAG3 was elevated in patients 1141, 1294, 1261 and 1229. Patient 1229 (locally advanced) also had high expression of ICOS, CTLA4, TIGIT and CD47. Conversely, patient 1261 (also locally advanced), had elevated CD27, LAG3, PDCD1, HAVCR2, TNFRSF18, CSF1, TIGIT, CD40LG, CD47 and CD28, but not CTLA4. The immune checkpoint landscape did not cluster by disease stage, and while some metastatic patients had high expression of multiple immune checkpoints (3210) others expressed only a limited subset (1253). Analysis of circulating $CD8^+$ T cells revealed a similarly complex landscape, but no clear overall correlation in the expression of individual checkpoints between patient tumor and blood T cells at a gene expression level (Supplemental Figure 2.3D).

We then investigated tumor-infiltrating $CD8^+$ T cells compared to $CD8^+$ T cells in normal/adjacent tissue. By functional annotation, we observed pathways relating to cell cytotoxicity, chemokine signaling, T cell receptor signaling, and antigen processing were significantly enriched in PDA samples, compared to adjacent/normal tissue $CD8^+$ T cells, an indication that immune responses had been elicited in the tumors (Figure 2.3E). We performed unbiased clustering of the $CD8^+$ T cell gene expression signatures in patients. Circulating $CD8^+$ T cells gene expression patterns did not clearly segregate

by disease stage (Supplemental Figure 2.3E). We then performed an unbiased differential expression analysis on the tissue-infiltrating $CD8^+$ T cells in tumors versus adjacent/normal tissue. This analysis revealed distinct expression patterns in healthy versus tumor infiltrating total $CD8^+$ T cells (Figure 2.3F). We noted that the $CD8^+$ T cells in adjacent/normal samples clustered together, while tumor-infiltrating $CD8^+$ T cell signatures spanned a spectrum in individual samples. Some tumor signatures partially resembled non-malignant tissue and others were greatly diverging. Interestingly, upon clinical annotation, we discovered that the divergence from the normal signature was more pronounced in samples from advanced disease stage. When we considered which genes were differentially expressed across the groups, we observed an increase in T cell activation and trafficking markers (GZMB, GZMA, KLF2) (Ingunn M. Stromnes et al. 2017; Balli et al. 2017; Carlson et al. 2006) in tumor $CD8^+$ T cells, compared to adjacent/normal tissues. Further, T cell exhaustion markers such as EOMES and GZMK were low in healthy $CD8^+$ T cells, and elevated in the majority of tumor $CD8^+$ T cell samples (Wherry et al. 2007; Li et al. 2018). The only immune checkpoint receptor identified as differentially overexpressed in tumor-infiltrating $CD8^+$ T cells, compared to $CD8^+$ T cells in adjacent/normal tissue, was TIGIT, a gene encoding a receptor belonging to the Ig superfamily (Manieri, Chiang, and Grogan 2017). Overall, comparison of the transcriptional profile of tumor and adjacent/normal infiltrating $CD8^+$ T cells revealed unique profiles of expression of immune checkpoint genes in individual patients. However, some common features emerged, such as expression of activation markers, as well as an exhausted gene expression signature which progressively increased with advanced disease stage.

Tumor infiltrating $CD8^+$ T cells include an expanded exhausted population characterized by TIGIT expression

Distinct populations of tumor infiltrating $CD8^+$ T cells have been described (Jansen et al. 2019). Given the progressive dysfunction of tumor-infiltrating $CD8^+$ T cells, we hypothesized that the transcriptional profile shift might be caused by changes in $CD8^+$ populations. By unbiased clustering, we distinguished 6 populations of CD8A-expressing T cells in both adjacent/normal and PDA samples (Figure 2.4A). To identify sub-populations, we plotted the top expressed genes per cluster (Figure 2.4B), and compared them with published signatures of $CD8^+$ T cells subtypes (Wherry et al. 2007). We identified two populations of effector $CD8^+$ T cells (T_{eff}), expressing PRF1 and GZMB; a population of likely memory (mem)/ precursor effector (pec) $CD8^+$ T cells ($T_{mem/pec}$) expressing CCR6 (Kondo, Takata, and Takiguchi 2007); and two populations of exhausted $CD8^+$ T cells (T_{ex}) expressing EOMES, GZMK, and TIGIT (Figure 2.4C, Supplemental Figure 2.4A and average expression heatmap in Supplemental Figure 2.4C). Interestingly, comparison of tumor infiltrating versus adjacent/normal $CD8^+$ T cells revealed a relative increase in exhausted T cells and memory T cells, with converse reduction of effector T cell levels (Figure 2.4D and Supplemental Figure 2.4B). We then examined expression of immune checkpoints and immune activation markers across $CD8^+$ T cell subsets, and observed uniform expression of PDCD1, HAVCR2 and LAG3 (Figure 2.4C), while TIGIT was enriched in exhausted and memory $CD8^+$ T cells. We found that 13.3% of effector $CD8^+$ T cells, compared to 44.2% of exhausted $CD8^+$ T cells expressed TIGIT. To compare gene expression changes within distinct clusters of $CD8^+$ T cells, we performed two separate differential expression analyses. We first

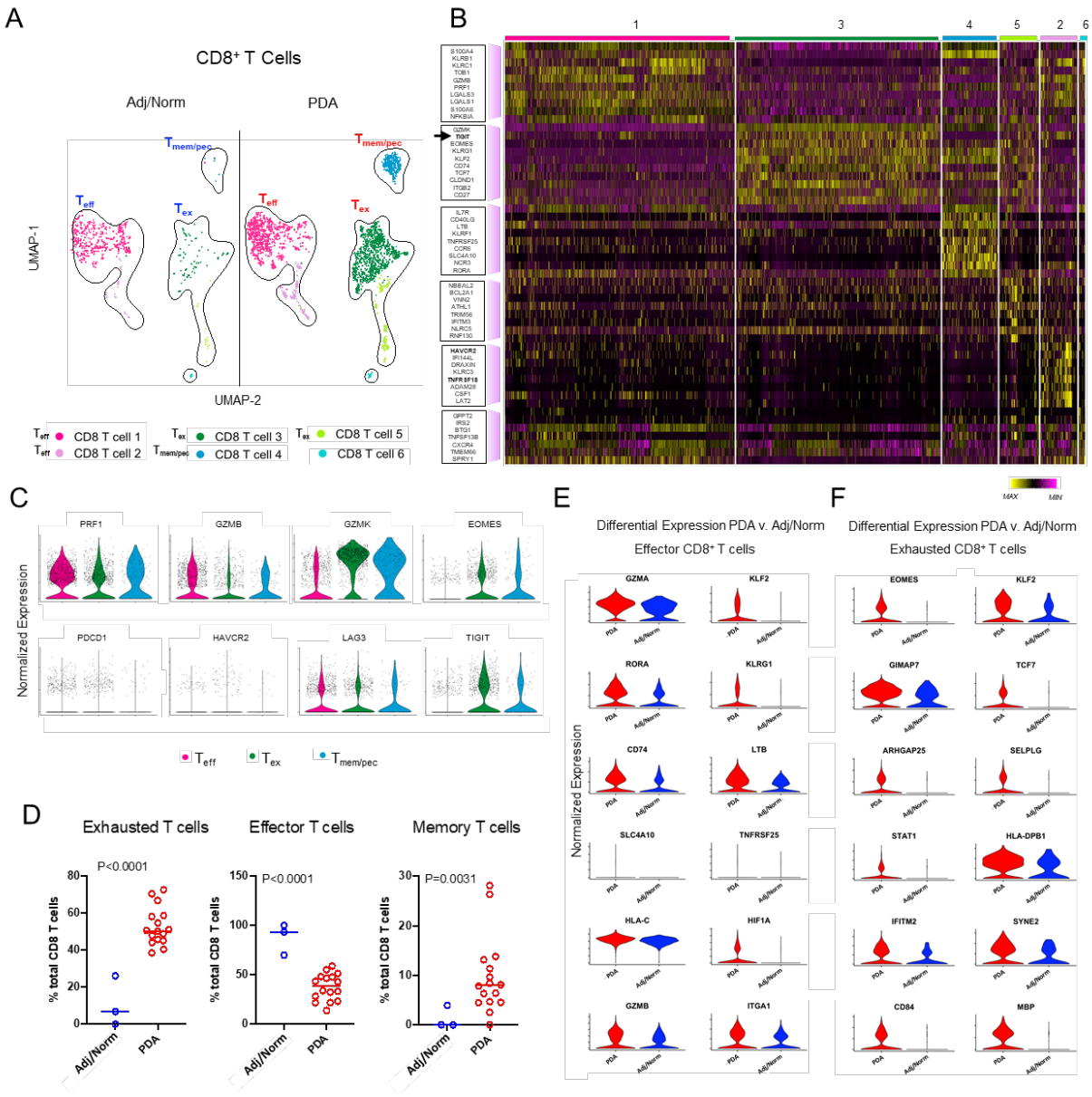

Figure 2.4 Single cell RNA sequencing reveals exhausted CD8+ T cell phenotype in PDA patients is defined by the immune checkpoint TIGIT.

(A) UMAP analysis of CD8+ T cells from n=3 adjacent/normal pancreas samples (left) and n=16 PDA tumors (right). The 6 identified subsets of CD8+ T cells were collapsed into potential memory (blue), effector (pink) and exhausted (green). **(B)** Single cell resolution heatmap analysis of top 10 genes for each identified CD8+ T cell subset. **(C)** Violin plots of normalized expression for selected markers mapped across the CD8+ T cell subsets. **(D)** Quantitation of potential exhausted (p=9.11E-6), effector (p=2.209E-5) and memory (p=0.0031) T cells in adjacent/normal pancreas and PDA patients, plotted as % total CD8+ T cells. Plots represent n=3 adj/norm and n=16 PDA patients. Two-sided Student's t-test was performed to compare between groups and a p value of 0.05 or less was considered statistically significant. Panel of genes differentially expressed in **(E)** effector and **(F)** exhausted CD8+ T cells in PDA (red) compared to adjacent/normal pancreas (blue). Plots represent n=3 adj/norm and n=16 PDA patients. Violin plots are shown as normalized expression. All violin plots in (E) and (F) have an adjusted p-value of $p<0.01$ and are considered statistically significant.

compared PDA effector $CD8^+$ T cells to adjacent/normal effector $CD8^+$ T cells, and we found that GZMA and GZMB were higher in tumor infiltrating effector $CD8^+$ T cells, suggesting T cell activation (Figure 2.4E). RORA expression, a marker associated with effector T cells, was also upregulated (Wherry et al. 2007) (Figure 2.4E), consistent with an ongoing immune response. We then compared PDA exhausted $CD8^+$ T cells to adjacent/normal exhausted $CD8^+$ T cells and tumor infiltrating exhausted $CD8^+$ T cells had higher expression of EOMES and KLF2, markers of exhaustion (Wherry et al. 2007) (Figure 2.4F).

Our data suggest that exhausted $CD8^+$ T cells are abundant in pancreatic tumors, and that their exhausted phenotype is more profound than the equivalent population in adjacent/normal tissue. Further, TIGIT was the sole immune checkpoint Receptor that specifically defined exhausted $CD8^+$ T cells.

A complex landscape of NK and $CD4^+$ T cells cell subsets in pancreatic cancer

Similar to effector $CD8^+$ T cells, NK cells display cytotoxic activity and express immune checkpoint receptor (Figure 2.3C), however these cells are not well defined in human PDA (Ducimetière, Vermeer, and Tugues 2019). Unsupervised sub-clustering of NK cells revealed three populations (Figure 2.5A and 2.5B). Along with the three NK cell

subsets, we found two additional populations that we labeled cluster 1 and 2, which expressed NKG7, CD3E, and CD8A. While these cells did not cluster with the CD8 T cells based on their transcriptional profile, they could potentially be highly cytolytic CD8 T cells expressing some NK markers (Arlettaz et al. 2004; Mcmahon et al. 2002). A "NK" cell population expressing CD8A was identified in a recent PDA scRNA-seq paper (Elyada et al. 2019). Highly variable gene expression analysis highlighted differences among subpopulations (Figure 2.5B). In NK subsets we detected expression of markers of antigen presentation (HLA-DRA), cytolytic activity (PRF1, GZMB), and chemokines/chemokine receptors (CCL3, IL7R), in agreement with a recently published characterization of human NK cells by single cell RNA sequencing (Smith et al. 2020). NK cluster 1 was enriched for immune checkpoint HAVCR2, while NK cluster 3 expressed high levels of immune checkpoint TNFRSF4 (Figure 2.5B and 2.5C). We then performed differential gene expression analysis and unbiased clustering of individual patient samples to compare tumor infiltrating NK cells with NK cells in non-tumor tissue. The signatures of tumor-infiltrating and non-tumor NK cells were not as divergent as was the case for $CD8^+$ T cells, and, with one exception (1324), resectable tumor samples clustered closely with the non-tumor samples (Figure 2.5D). However, advanced disease samples had a different expression signature than healthy counterparts, with increased expression of activation markers such as GZMA and elevated expression of two immune checkpoint genes, TIGIT and HAVCR2. The role of NK cells in PDA is not well understood; our findings set the stage for future functional studies on the role of NK cells in this disease.

Figure 2.5 Single cell RNA sequencing of pancreatic tissues reveals TIGIT is differentially expressed in NK cells from PDA patients and is a defining marker of Tregs.

(A) Merged UMAP of 5 identified subsets of NK cells from adjacent/normal pancreas (left) and PDA (right). Plots represent n=3 adj/norm and n=16 PDA patients. **(B)** Single cell resolution heatmap of each NK cell subset identified. Immune checkpoints (HAVCR2, TNFRSF4) are bolded. **(C)** Violin plots of normalized average expression within NK cell subsets demonstrating specific lineage markers for NK cells (such as NCAM1/FCGR3A) and immune checkpoint receptors. **(D)** Unbiased differential average expression of merged NK cells from adjacent/normal pancreas (black) and PDA (grey). Disease stage is plotted on the left. **(E)** Merged UMAP of all $CD4^+$ T cells with 13 identified cell subsets. Naïve $CD4^+$ T cells are denoted as T_H0 ($CCR7^+$) and Tregs as Tregs ($FOXP3^+$). All other subsets are denoted as CD4 T cells. **(F)** Single cell resolution heatmap of each $CD4^+$ T cell subset. Boxes on the left designate naïve CD4+ T cells (T_H0) and the $CD4^+$ T cell subsets that are defined by immune checkpoint expression (TIGIT, TNFRSF18, PDCD1). **(G)** Feature plots of CTLA4 and TIGIT in regulatory $CD4^+$ T cells (outlined). In all panels, plots represent n=3 adj/norm and n=16 PDA patients.

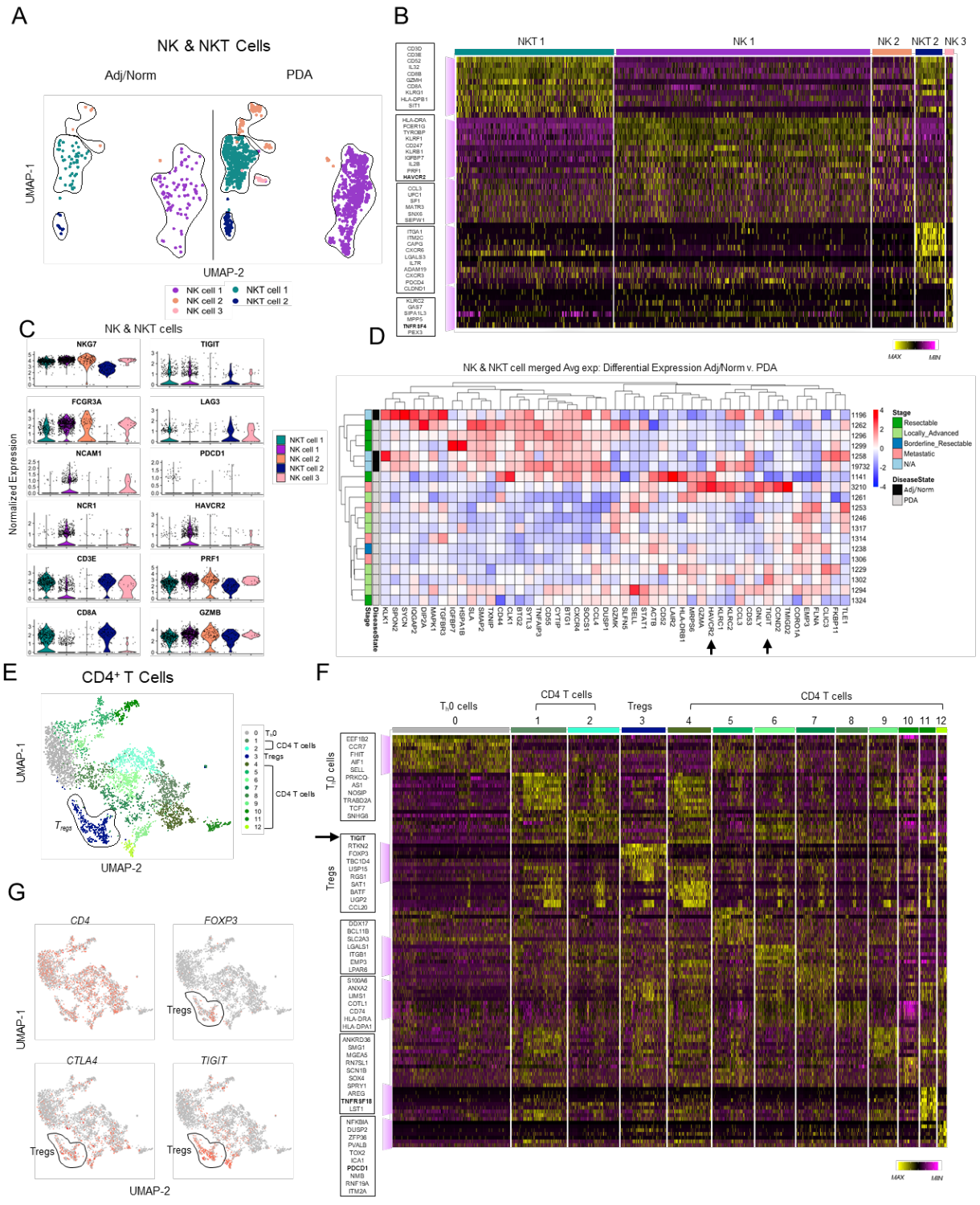
A
NK & NKT Cells
Adj/Norm
PDA
UMAP-1
UMAP-2
NK cell 1
NK cell 2
NK cell 3
NKT cell 1
NKT cell 2
B
NKT 1
NK 1
NK 2
NKT 2
NK 3
C
NK & NKT cells
NKG7
TIGIT
FCGR3A
LAG3
NCAM1
PDCD1
NCR1
HAVCR2
CD3E
PRF1
CD8A
GZMB
Normalized Expression
D
NK & NKT cell merged Avg exp: Differential Expression Adj/Norm v. PDA
Stage
Resectable
Locally_Advanced
Borderline_Resectable
Metastatic
N/A
DiseaseState
Adj/Norm
PDA
E
CD4⁺ T Cells
T0
CD4 T cells
Tregs
F
T0 cells
CD4 T cells
Tregs
G
CD4
FOXP3
CTLA4
TIGIT

We then investigated $CD4^+$ T cells, a complex population that includes regulatory T cells, and plays a fundamental role in regulating pancreatic carcinogenesis (Y. Zhang et al. 2014; Y. Zhang et al. 2020; Jang et al. 2017). Unlike the $CD8^+$ T and NK cells, we could not perform differential expression on $CD4^+$ T cells as we did not capture enough cells from adjacent/normal tissue samples; instead we focused on studying the tumor-infiltrating component. We identified 13 transcriptionally distinct populations of $CD4^+$ T cells, although many of the different clusters tended to merge together (Figure 2.5E). A highly enriched gene analysis of $CD4^+$ subsets revealed expression of naïve T cell markers CCR7 and SELL (Sckisel et al. 2017) in cluster 0 and expression of regulatory T cell marker FOXP3 in cluster 3 (Figure 2.5F). As expected, based on previous studies, CTLA4 was highly expressed within Tregs (Bengsch et al. 2017) (Figure 2.5G). Specific immune checkpoint genes were highly expressed in individual clusters, such as TNFRSF18 and PDCD1. TIGIT appeared as a top expressed gene in Tregs (Figure 2.5F), although it was also expressed in other clusters more sparsely (Figure 2.5G). The other clusters did not correspond to known subsets of $CD4^+$ T cells, and were relatively similar to one another, a possible reflection of low transcriptional activity of non-Treg $CD4^+$ T cells. Taken together, these analyses suggest multiple immune checkpoint receptors are expressed in $CD4^+$ and NK cell subsets. In particular, the immune checkpoint TIGIT was differentially overexpressed on tumor-infiltrating PDA $CD8^+$ T cells, regulatory T cells and NK cells.

<u>Myeloid and dendritic cells are an important source of immune checkpoint ligands in human PDA</u>

We next analyzed myeloid cells, which are an important source of immune checkpoint ligands in PDA. By unbiased clustering, we identified 6 transcriptionally distinct populations of myeloid cells. (Figure 2.6A). We observed an abundant granulocyte population expressing CXCR1 and CXCR2, FCGR3B and S100A8 (Figure 2.6B). Consistent with previous studies (Elyada et al. 2019; Sanford et al. 2013), we detected resident macrophages and alternatively activated macrophages ($MARCO^{+}$), and classical monocytes (Figure 2.6A and 2.6B). We also observed an additional myeloid population, denoted as alternatively activated macrophages 2, that resembled alternatively activated macrophages and was uniquely defined by abundant expression of CHIT1 and multiple immune checkpoint ligands (Figure 2.6A, 2.6B and Supplemental Figure 2.5A). We next mapped immune checkpoint ligand expression within specific myeloid compartments and observed heterogeneous expression of immune checkpoints in specific clusters (Figure 2.6C). Differential expression analysis between adjacent/normal and tumor-infiltrating myeloid sub-clusters revealed multiple upregulated checkpoint ligands. LGALS9, the ligand for HAVCR2 (encoding for TIM3), was significantly increased within alternatively activated macrophages, while SIRPA, the ligand for CD47, was higher in PDA granulocytes compared to granulocytes in adjacent/normal tissue (Figure 2.6D). PVR, the ligand for TIGIT was enriched in total

Macrophages (Figure 2.6D). Average expression heatmaps of macrophages (Supplemental Figure 2.6B) and granulocytes (Supplemental Figure 2.5C) demonstrated that the expression of immune checkpoint ligands was highly variable in individual patients.

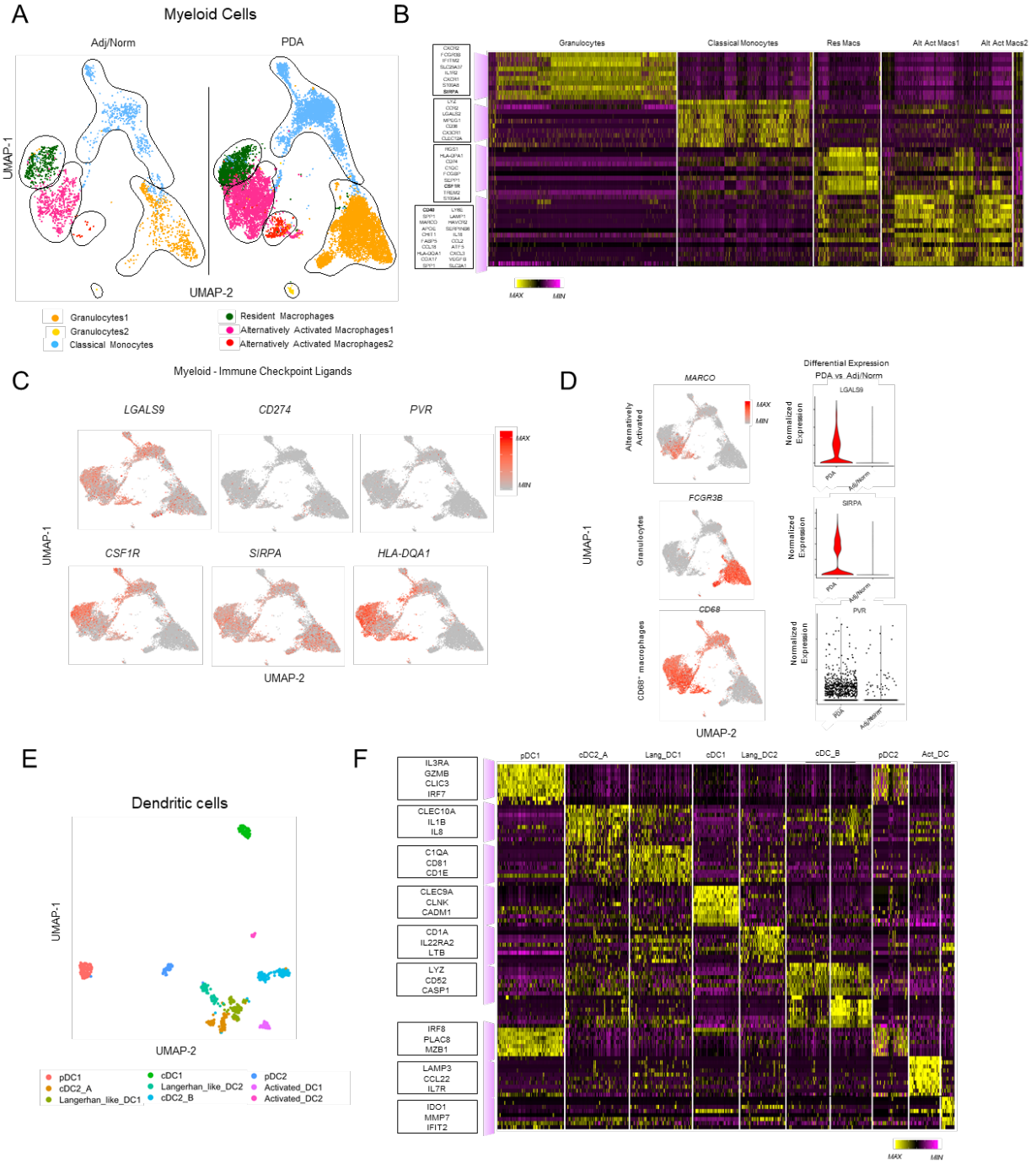

Figure 2.6 Single cell RNA sequencing reveals distinct myeloid and dendritic cell subsets.

(A) Merged UMAP of 6 identified myeloid cell subsets in adjacent/normal pancreas (left) and PDA (right). **(B)** Single cell resolution heatmap of each myeloid cell subset identified. Boxes on the left designate the top expressing genes for each myeloid subset. **(C)** Selected feature plots of the immune checkpoints, LGALS9, CD274, PVR, CSF1R, SIRPA, HLA-DQA1 in myeloid cells. **(D)** Selected feature plots of markers that define alternatively activated macrophages, granulocytes, and total macrophage subsets (left) and violin plots of immune checkpoint ligands that are upregulated in PDA patients (right). **(E)** UMAP analysis of dendritic cells in merged normal/adjacent pancreas and PDA. **(F)** Top ten highly enriched gene signature analysis of dendritic cell subclusters identifying potential DC subsets, including plasmocytoid DCs (pDCs), Langerhans-like DCs (Lang_DCs), conventional DCs (cDCs), and activated DCs (Act_DCs). In all panels, plots represent n=3 adj/norm and n=16 PDA patients.

Dendritic cells (DCs) cells are professional antigen presenting myeloid cells, and support anti-tumor activity by stimulating T cells; their relative rarity in PDA is one of the potential causes for ineffective immune responses in this disease (Hegde et al. 2020). Clustering analysis revealed multiple populations of tumor-infiltrating DCs (Figure 2.6E). We found two populations of plasmacytoid DCs (IRF8, GZMB) and two populations of Langerhans-like DCs (CD207, CD1A) as previously described (Elyada et al. 2019) (Figure 2.6F and 2.7A). Langerhans-like DC2 had robust expression of IL22RA2, also known as IL22BP, and the IL-22-IL22BP axis is known to be a crucial mediator of tumorigenesis in the colon (Huber et al. 2012) and pancreas (Perusina Lanfranca et al. 2020). We also detected a population of conventional DC1s (CLEC9A, IRF8) (Elyada et al. 2019; Collin and Bigley 2018), and two additional populations of potential conventional DC2s that expressed immune checkpoint ligand SIRPA (Figure 2.6F and 2.7A). We also detected two unique populations of activated DCs (LAMP3, CCL22) (Elyada et al. 2019) (Figure 2.6F and 2.7A). We then plotted the average expression of known immune checkpoint ligands in the different DC subsets. We discovered that activated DC1 had elevated expression of nearly all the immune checkpoint ligands, including PVR (Figure 2.7B), suggesting that in pancreatic tumors some subsets of DCs may be immunosuppressive (Veglia and Gabrilovich 2017).

Mapping predicted interactions and tissue heterogeneity in pancreatic cancer samples by single cell sequencing

To explore potential cross-talk between T/NK and myeloid populations, we applied a predicted interaction algorithm (Cohen et al. 2018) based on known ligand-receptor (LR) pairs interacting with high affinity (Ramilowski et al. 2015). We curated the list to specifically add immune checkpoints and limit the receptor-ligand pairs to cytokines, chemokines and specific signaling pathways [for a comprehensive list, see Supplemental Table 2.7]. We first plotted all the receptor-ligand interactions that were statistically higher in tumor versus non-malignant samples, based on the level of ligand expression, and observed a complex landscape of potential interactions involving multiple cell types (Supplemental Figure 2.5D). We then visualized upregulated ligands in macrophages (Figure 2.7C), granulocytes (Figure 2.7D), dendritic cells (Figure 2.7E), endothelial cells (Figure 2.7F) and epithelial cells (Figure 2.7G) and mapped the predicted binding partners in CD4, CD8, and NK cells. Among interactions upregulated in cancer compared to adjacent/normal, we detected known putative immune suppressive interactions, such as those mediated by the chemokine receptors CXCR2 in granulocytes and CCR2 in macrophages (Sanford et al. 2013; Denardo and Ruffell 2019). Predicted interactions mediated by IL1A and IL1B with their receptor encoding genes IL1R1 and IL1R2 were also upregulated, consistent with their known roles in pancreatic cancer (Elyada et al. 2019; Das et al. 2020; Öhlund et al. 2017). Multiple putative interactions linked T and NK cells to myeloid immune checkpoint ligands, which is consistent with a key role for myeloid cells in establishing immune suppression in pancreatic cancer (for review see (Vonderheide 2018)). Predicted immune checkpoint-

mediated interactions such as ICOS/ICOSLG and SIRPA/CD47 were among those upregulated in pancreatic cancer compared to healthy/adjacent tissue. TIGIT/PVR interactions were elevated between macrophages and $CD4^+$ T cells, $CD8^+$ T cells and NK cells (Figure 2.7C). Interestingly, the putative TIGIT/PVR interaction was also elevated between tumor endothelial and epithelial cells, T cell and NK cell subsets (Figure 2.7F and 2.7G). We then endeavored to investigate the expression of other genes involved in the TIGIT pathway. We investigated the expression of TIGIT's costimulatory counter receptor, DNAM1 (CD226), which competes for PVR and PVRL2 and promotes T cell activation (Fourcade et al. 2018). We found that while TIGIT was significantly increased on PDA $CD8^+$ T cells (P= 4.8e-32), CD226 expression was not altered in $CD8^+$ T cells between adjacent/normal and PDA cells (Figure 2.7H). CD96 and PVRIG act similarly to TIGIT, inhibiting T cell activation. Expression analysis showed that mRNA levels of these receptors were not altered between adjacent/normal and PDA $CD8^+$ T cells (Figure 2.7H). PVRL2 encodes a second ligand for TIGIT, although it binds with a lower affinity compared to PVR (Yu et al. 2009). We detected expression of PVRL2 in epithelial, myeloid, and endothelial cells (Figure 2.7I). TIGIT, CD96, PVRIG, and CD226 were mainly expressed by T and NK cells in PDA tissue (Figure 2.7I). We then investigated the Adenosine pathway, because of its immune suppressive role (Maj et al. 2017). We profiled this pathway in tumor samples and found expression of the adenosine receptor ADORA1 in epithelial and mast cells, ADORA2B in epithelial, mast cells, and dendritic cells, ADORA3 in dendritic, mast, and myeloid cells (Supplemental Figure 2.5E).

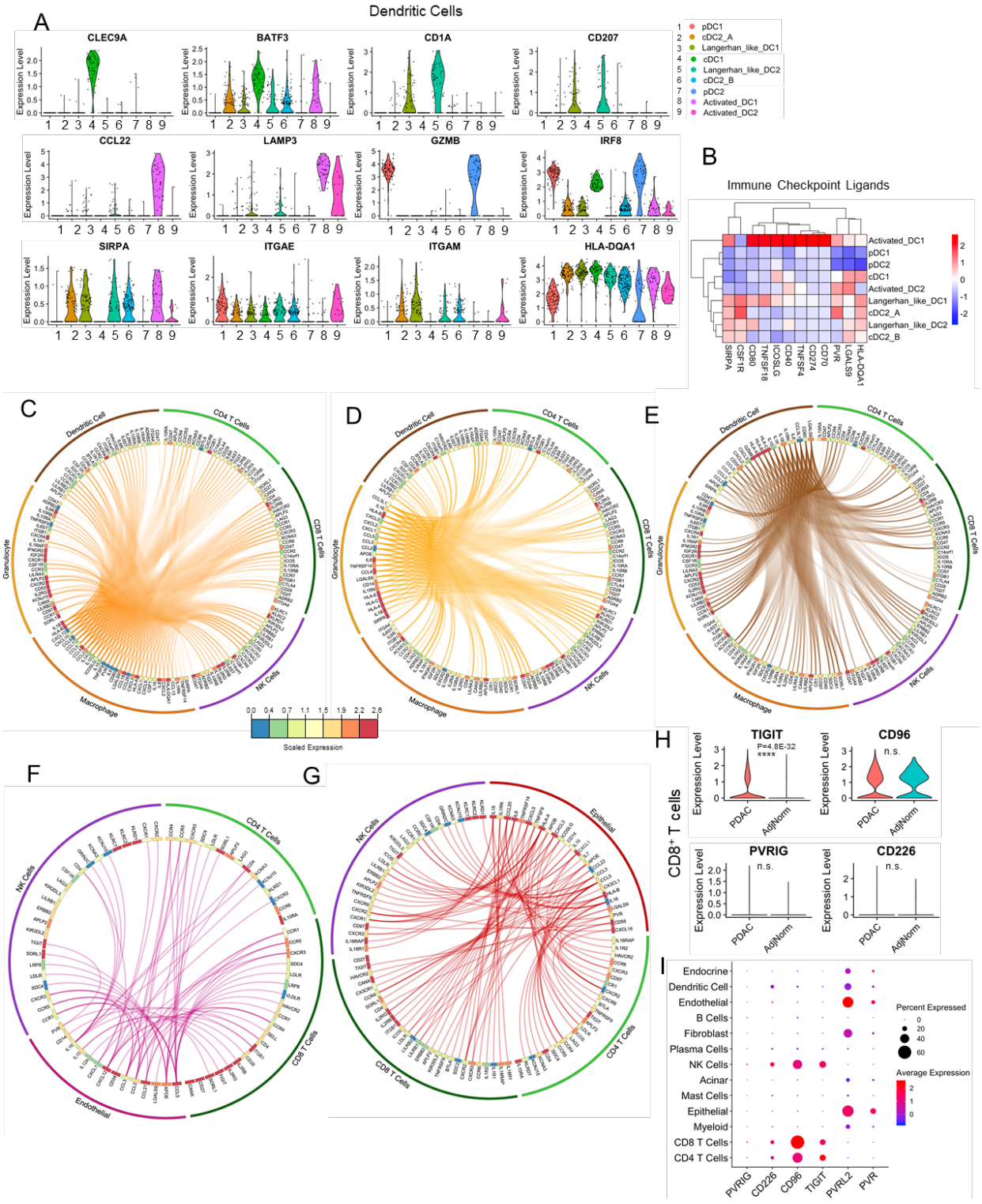
A
Dendritic Cells
CLEC9A
BATF3
CD1A
CD207
CCL22
LAMP3
GZMB
IRF8
SIRPA
ITGAE
ITGAM
HLA-DQA1
Expression Level
1 pDC1
2 cDC2_A
3 Langerhan_like_DC1
4 cDC1
5 Langerhan_like_DC2
6 cDC2_B
7 pDC2
8 Activated_DC1
9 Activated_DC2
B
Immune Checkpoint Ligands
Activated_DC1
pDC1
pDC2
cDC1
Activated_DC2
Langerhan_like_DC1
cDC2_A
Langerhan_like_DC2
cDC2_B
SIRPA
CSF1R
CD80
TNFSF18
ICOSLG
CD40
TNFSF4
CD274
CD70
PVR
LGALS9
HLA-DQA1
C
D
E
Dendritic Cell
CD4 T Cells
CD8 T Cells
NK Cells
Macrophage
Granulocyte
Scaled Expression
F
G
Endothelial
H
CD8+ T cells
TIGIT
P=4.8E-32
****
CD96
n.s.
PVRIG
CD226
PDAC
AdjNorm
I
Endocrine
Dendritic Cell
Endothelial
B Cells
Fibroblast
Plasma Cells
NK Cells
Acinar
Mast Cells
Epithelial
Myeloid
CD8 T Cells
CD4 T Cells
PVRIG
CD226
CD96
TIGIT
PVRL2
PVR
Percent Expressed
Average Expression

Figure 2.7 Predicted ligand receptor mapping in PDA patients demonstrate myeloid and non-immune cell types as sources of immune checkpoint ligands.

(A) Violin plots, where each dot represent a single cell, of select dendritic cell lineage markers across all 9 identified subsets. **(B)** Immune checkpoint ligand expression heatmap within dendritic subclusters. **(C)** Circos plot map of all putative ligand receptor interactions that are upregulated in PDA macrophages, **(D)** granulocytes, **(E)** dendritic cells, **(F)** endothelial cells **(G)** epithelial cells compared to adjacent/normal pancreas visualized by circos plot using the Circos software V0.69-9 (circos.ca). The heatmap within the circos plots is the scaled average expression of each gene within PDA tissue cell populations. The interactions plotted are those in which the expression level of either the ligand, the receptor, or both are increased in expression in PDA samples compared to adjacent/normal tissue. **(H)** Violin plots for the normalized expression of TIGIT, CD96, and CD226 in CD8+ T cells in PDA (red) compared to adjacent/normal pancreas (blue). Between adj/norm and PDA groups, the asterisk indicates P<0.0001, and exact P=4.8E-32. For Figure 6 panels A through H, n=3 adj/norm samples were examined and n=16 PDA patients were analyzed. **(I)** Dot plot analysis of TIGIT family members within PDAC tissue. Color of dot represents average expression, while the size of the dot represents percent expression. Dot plot represent n=16 PDA patients gene expression.

The expression of multiple immune checkpoints has been previously described in pancreatic cancer (Balli et al. 2017). Since a deconvolution approach was used, the specific immune cell types expressing receptors and ligands could not be assessed. In contrast, our analysis provides a comprehensive view of the multiple, redundant potential immune suppressive interactions within the pancreatic cancer microenvironment.

TIGIT protein expression is increased on T and NK cells in pancreatic cancer, and its expression in the tumors correlates with matched blood

To determine whether mRNA expression of immune checkpoints was reflected by protein levels, we performed mass cytometry on tumor and normal/adjacent uninvolved tissue samples (Figure 2.8A). TIGIT expression was elevated in tumor-infiltrating $CD8^+$ T cells in the majority of samples, albeit not all, while PD1 and LAG3 were not significantly altered (Figure 2.8A). Interestingly, we detected an increase in expression in PD-1 ligand, PD-L1, in $CD68^+$ macrophages from PDA patients (Supplemental Figure 2.7B). CTLA4 expression was significantly increased in $CD4^+$ T

cells in most PDA samples versus adjacent/normal tissues (Figure 7B). TIGIT$^+$ CD4$^+$;CD25$^+$ T cells were more frequent in PDA samples, compared to controls (Figure 2.8B). Similarly, TIGIT$^+$ NK cells (CD56$^+$) were more frequent in PDA, although this finding is limited by the small number of samples analyzed (Figure 2.8C). In one patient, where matched tumor and uninvolved adjacent tissue were analyzed, we observed a higher frequency of TIGIT expression on both CD8$^+$ and CD4$^+$ T cells in the tumor (Figure 2.8D). We then performed immunostaining for both TIGIT and PVR on patient tissue in situ (Figure 2.8E) and observed TIGIT in CD8$^+$ T cells, and PVR (red) in epithelial and stromal cells (Figure 2.8E and single channels shown in Supplemental Figure 2.7A).

Lastly, as we observed that TIGIT was commonly upregulated in tumors, we investigated whether protein expression of TIGIT in blood correlated with the individual patient's tumor, an attractive possibility given the relatively easy accessibility of blood samples. We performed CyTOF on the peripheral white blood cell (PBMC) component in 36 pancreatic cancer patients, 18 healthy volunteers, and 8 patients with chronic pancreatitis (Supplemental Figure 2.6A). Cellular subtyping and frequency of circulating immune cells present are shown in Supplemental Figure 2.7B–E. Principal component analysis failed to show any major distinction between our three patient populations (Supplemental Figure 2.6G). Blood from both PDA and chronic pancreatitis patients had fewer circulating CD8$^+$ T cells, but higher expression of TIGIT CD8$^+$ T cells (Figure 2.8F, 2.8G and Supplemental Figure 2.6F). PD1 and CTLA4 protein expression was elevated in PDA circulating CD8$^+$ and CD4$^+$ T cells, respectively, compared to healthy subjects (Figure 2.8G). We then analyzed the subset of patients for whom we had matched mass

cytometry of tumor and PBMCs and found a positive correlation of TIGIT expression, but not PD1 expression, in $CD8^+$ T cells (Figure 2.8H and 2.8I). Thus, different immune checkpoint molecules are prevalent in individual patients, and further validation of potential targets, including TIGIT, is warranted.

Figure 2.8 CyTOF and immunofluorescence protein validation of immune checkpoint expression in human pancreatic tissues and PBMCs.

(A) Violin plots, where each dot represent a single cell, of select dendritic cell lineage markers across all 9 identified subsets. **(B)** Immune checkpoint ligand expression heatmap within dendritic subclusters. **(C)** Circos plot map of all putative ligand receptor interactions that are upregulated in PDA macrophages, **(D)** granulocytes, **(E)** dendritic cells, **(F)** endothelial cells **(G)** epithelial cells compared to adjacent/normal pancreas visualized by circos plot using the Circos software V0.69-9 (circos.ca). The heatmap within the circos plots is the scaled average expression of each gene within PDA tissue cell populations. The interactions plotted are those in which the expression level of either the ligand, the receptor, or both are increased in expression in PDA samples compared to adjacent/normal tissue. **(H)** Violin plots for the normalized expression of TIGIT, CD96, and CD226 in CD8+ T cells in PDA (red) compared to adjacent/normal pancreas (blue). Between adj/norm and PDA groups, the asterisk indicates $P<0.0001$, and exact P=4.8E-32. For Figure 6 panels A through H, n=3 adj/norm samples were examined and n=16 PDA patients were analyzed. **(I)** Dot plot analysis of TIGIT family members within PDAC tissue. Color of dot represents average expression, while the size of the dot represents percent expression. Dot plot represent n=16 PDA patients gene expression.

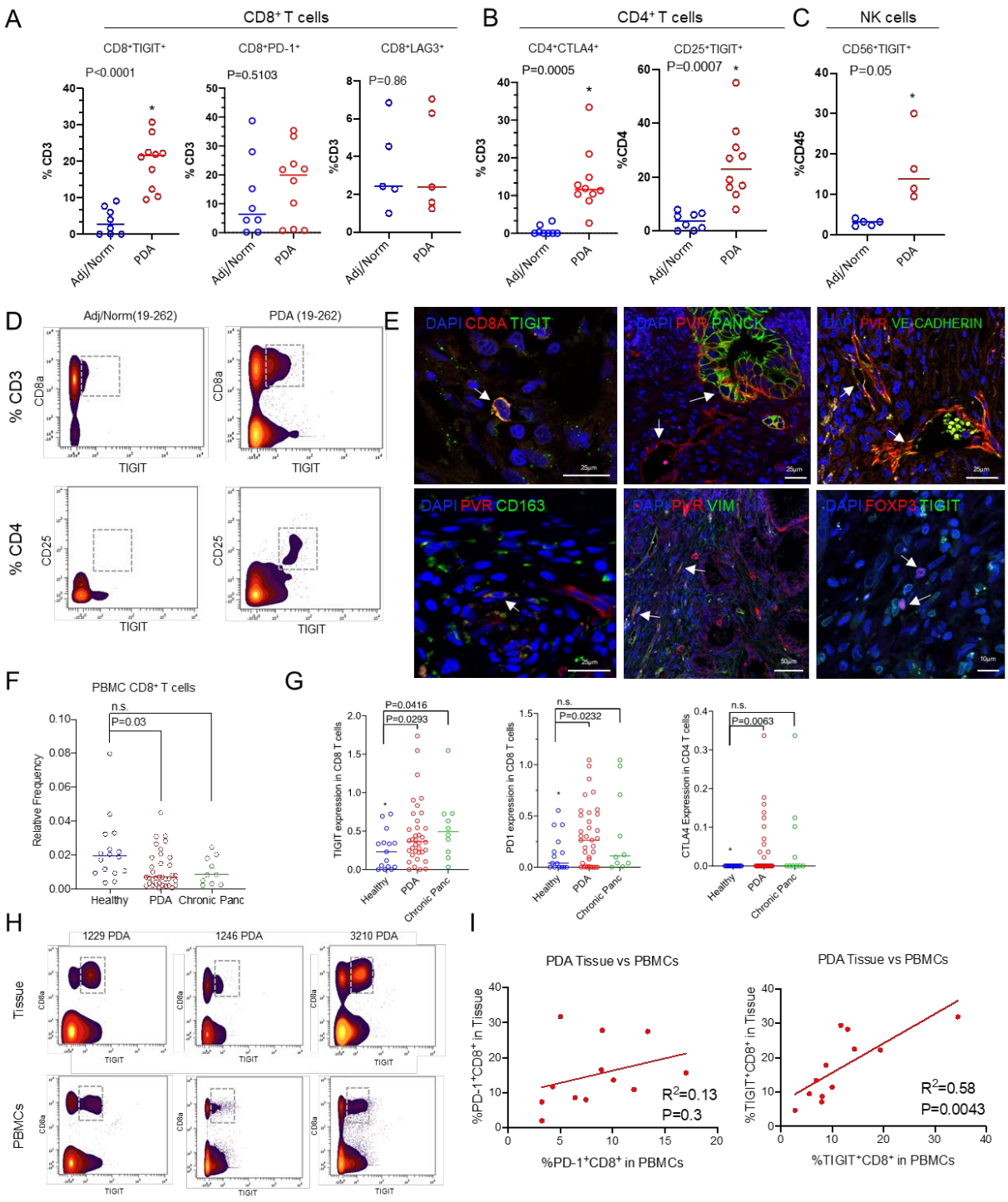
A
CD8+ T cells
CD8+TIGIT+
P<0.0001
CD8+PD-1+
P=0.5103
CD8+LAG3+
P=0.86
% CD3
Adj/Norm
PDA
B
CD4+ T cells
CD4+CTLA4+
P=0.0005
CD25+TIGIT+
P=0.0007
%CD4
C
NK cells
CD56+TIGIT+
P=0.05
%CD45
D
Adj/Norm(19-262)
PDA (19-262)
% CD3
% CD4
CD8a
CD25
TIGIT
E
DAPI CD8A TIGIT
DAPI PVR PANCK
DAPI PVR VE-CADHERIN
DAPI PVR CD163
DAPI PVR VIM
DAPI FOXP3 TIGIT
F
PBMC CD8+ T cells
n.s.
P=0.03
Relative Frequency
Healthy
PDA
Chronic Panc
G
P=0.0416
P=0.0293
TIGIT expression in CD8 T cells
n.s.
P=0.0232
PD1 expression in CD8 T cells
P=0.0063
CTLA4 Expression in CD4 T cells
H
1229 PDA
1246 PDA
3210 PDA
Tissue
PBMCs
I
PDA Tissue vs PBMCs
%PD-1+CD8+ in Tissue
%PD-1+CD8+ in PBMCs
R2=0.13
P=0.3
PDA Tissue vs PBMCs
%TIGIT+CD8+ in Tissue
%TIGIT+CD8+ in PBMCs
R2=0.58
P=0.0043

Discussion

Recent reports examining gene expression in pancreatic tumors by scRNAseq or high content in situ hybridization have largely focused on the complexity of the fibroblast populations (Elyada et al. 2019; Dominguez et al. 2020; Ligorio et al. 2019), however the heterogeneity of the immune reaction in PDA at a single cell level remained unclear. We have used a multi-modal approach combining CyTOF (Bendall et al. 2011; Amir et al. 2019), multiplex immunohistochemistry, and scRNA seq to map the immune infiltration, as well as the systemic immune response through patient blood, in human PDA (Stuart and Satija 2019).

Multiparameter mapping of the TME demonstrated a highly heterogeneous immune infiltration in individual patients, consistent with previous reports (Ingunn M. Stromnes et al. 2017), suggesting that immune-modulatory therapies should potentially be targeted to specific individuals based on their checkpoint expression profile within tumors. Both CyTOF and mfIHC also revealed an inverse correlation between infiltration of myeloid and $CD8^+$ T cells. scRNA seq analysis suggests that $CD8^+$ T cells express markers of exhaustion at levels that increase in advanced stages of disease, consistent with a recent study of peripheral T cells in pancreatic cancer patients showing diminished fitness (Xu et al. 2019). Importantly, we included fine needle biopsy samples for both single cell sequencing and CyTOF, which allowed us to study the immune infiltration in patients with unresectable advanced stages of disease. These tumors included $CD8^+$ T cells with a more pronounced exhaustion signature compared with early stage patients, a possible indication of progressive immune dysfunction.

We found differential expression of TIGIT, both at the gene and at the protein level, in patient $CD8^+$ T cells. We chose to focus on TIGIT in particular as one example of an immune checkpoint ligand/receptor pair given our ability to evaluate this relatively understudied checkpoint across multiple modalities. TIGIT expression was enriched specifically within $EOMES^{high}$ $CD8^+$ T cells, or exhausted T cells, similar to recent findings in human prostate, bladder, and kidney cancer (Jansen et al. 2019). TIGIT was also elevated in NK cells within the tumor, where its role is less understood, although there is at least some evidence TIGIT inhibition in NK cells might be beneficial (Qing Zhang et al. 2018). Elevated TIGIT expression is a feature of Tregs, and again its role in this cell population is not well understood. However, it has been proposed that inhibition of TIGIT on Tregs may suppress the secretion of the immunosuppressive cytokine IL-10 (Manieri, Chiang, and Grogan 2017). The expression of TIGIT, and other immune checkpoint receptors in multiple cellular compartments, as well as the observation that expression of immune checkpoints is highly heterogeneous across patients, will have to be further investigated as new combination immunotherapy approaches are devised for preclinical testing. Further, it is interesting to note that multiple cellular compartments express a variety of immune checkpoint ligands in a similar heterogeneous manner. At the protein level, we validated that PVR, the ligand for TIGIT, was expressed in tumor, endocrine, and endothelial cells (while low in non-malignant acinar cells). PVR and other immune checkpoint ligands were also upregulated in myeloid subsets, supporting the notion of myeloid cells as key mediators of immune suppression in PDA. Intriguingly, TIGIT protein expression in the blood correlated with TIGIT expression in the tumors of individual patients, although a similar correlation was not observed for

other immune checkpoints such as PD-1. Of note, while functional studies on the role of TIGIT in different patients and different cellular compartments within each tumor are still needed, TIGIT blocking agents are available and are currently being evaluated in clinical trials (Solomon and Garrido-Laguna 2018).

In summary, our study provides a multimodal characterization of the immune landscape in PDA, highlights the complexity of this disease in human patients, and provides a resource for future functional studies.

Materials and methods

Study Approval and Patient Consent

Patient Selection/Sample procurement: Medical chart review was used to screen for potential study patients with pancreatic disease at the University of Michigan. Fine needle biopsies: Patients over the age of 18 referred for diagnostic endoscopic ultrasound of a pancreas mass lesion suspected of PDA were consented according to IRB HUM00041280 or HUM00025339. Up to 2 extra passes using at 22 Gauge SharkCore™ needle were taken for research after biopsy obtained for clinical use. Surgical specimens: Surgical specimens of either tumor tissue or adjacent normal pancreas were obtained from patients referred for Whipple procedure or distal pancreatectomy according to IRB HUM00025339. Blood collection: Up to 40 cc of whole blood were collected pre-procedurally or intra-operatively for all patients consented. For patients not undergoing interventional procedures (i.e. chemotherapy visit), only whole blood was collected. Supplemental Table 2.2 contains extended clinical data associated with clinical samples.

Multiplex fluorescent immunohistochemistry (mfIHC) imaging, cell segmentation, and basic phenotyping

Images were taken using the Mantra™ Quantitative Pathology Work Station (Akoya Biosciences) as described in the Online Methods.

Cytometry Time-of-Flight (CyTOF) Immune Phenotyping and Data Analysis

For CyTOF, we collected 8 samples from non-malignant pancreas specimens, including non-involved pancreas tissue adjacent to a duodenal adenoma (1196, (patient ID)), ampullary carcinoma (1258), insulinoma (19–700), and non-involved pancreas tissue adjacent to PDA (1172, 19–262, 19–561, 19–732, 1252), all obtained surgically (Supplemental Figure 2.1A). PDA samples were collected from either surgical (n=7) or fine needle biopsy (FNB) (n=3) procedures, and clinical annotation is shown in Supplemental Figure 2.1A. Human patient tissues from FNB or surgery were immediately placed into DMEM media supplemented with Y27632 (Rho-Kinase inhibitor) for transport to the laboratory. Sample Preparation, Analysis and Data analysis are described in detail in the Online Methods.

Immunofluorescent staining

Patient tissue slides were rehydrated in xylene, 100% ethanol, 95% ethanol, then running deionized water sequentially. Antigen retrieval was performed with sodium citrate, pH 6.0. Tissue was blocked in 10% donkey serum overnight at 4°C. Primary antibodies (PVR/CD155 (1:100, Cell Signaling Technology), VE-Cadherin/CD144 (1:250, R&D), FOXP3 (1:100, Cell Signaling), Vimentin (1:100, Cell Signaling), CD163

(1:100, Novus Biologicals), or Pan Cytokeratin-488 (1:250, Thermo Fisher Scientific) were diluted in 5% donkey serum in PBST (DS/PBST) and incubated overnight at 4°C. For tissue co-stained for TIGIT-FOXP3 and PVR-Vimentin: the tyramide signal amplification kit with Alexa Fluor 488 (Thermo Fisher Scientific) was used following the manufacturer's recommendation to enhance signaling for PVR and FOXP3. Samples underwent a second citrate antigen retrieval and were then multiplexed with TIGIT and Vimentin following the aforementioned standard IFC protocol. A 1% BSA block was used throughout the TSA protocol and subsequent multiplex staining. Tissue was mounted with DAPI ProLong™ Gold Antifade Mountant (Thermo Fisher Scientific) and subsequently imaged by confocal microscopy on a Leica SP5. Supplemental Table 2.6 lists the antibodies used.

Statistical Analysis and Reproducibility

Significance was evaluated by the following statistical analyses: two-tailed, parametric, unpaired Student's t-test, Student's t-test with Welch's correction, Wilcoxon rank-sum test, or a Mann–Whitney U-test in GraphPad Prism (version 7) or JMP Pro software (version 14). The data were presented as means ± standard error (SEM) or means ± standard deviation (STDV). A p value of $p<0.05$ was considered statistically significant. Pearson correlation coefficients were used to measure R and R2. Intergroup comparisons (differential expression) of scRNA seq was performed using Wilcoxon ranked test and p-values were adjusted for multiple comparisons with the Bonferroni correction method. For the interactome analysis, differences of the ligand and receptors between groups were determined using Wilcoxon ranked test, and p-values were

adjusted for multiple comparisons with the Bonferroni correction method. Ligand/Receptor pairs were considered significantly different if the $p < 1.0 \times 10^{-4}$. Ligand/Receptor pairs were then sorted by the adjusted ligand expression p-value. No statistical method was used to predetermine sample sizes, experiments were not randomized and mass cytometric analysis of samples was not blinded. No data were excluded from the analyses. Each patient is considered an independent biological sample in the analyses. For comparison of differential abundance analysis of mass cytometry data, the edegR package (version 3.11) was used.

Data Availability

All raw data are publicly available without restrictions. All mass cytometry data used for this publication have been deposited in the FlowRepository. All fcs files of tissue (tumor and adjacent normal) have been uploaded to FlowRepository Experiment FR-FCM-Z2S4 and PBMC files have been uploaded to FlowRepository Experiment FR-FCM-Z2S3. Single cell RNA sequencing data with clinical metadata are available at NIH dbGAP database under the accession phs002071.v1.p1. Deidentified single cell RNA sequencing data are available at NIH GEO database under the accession GSE155698. Source data are available for this study. All other data supporting the findings of this study are available from the corresponding author on reasonable request.

Code Availability

Code is publicly available on GitHub.com (https://github.com/PascaDiMagliano-Lab/MultimodalMappingPDA-scRNASeq).

Multiplex fluorescent immunohistochemistry (mfIHC) imaging, cell segmentation, and basic phenotyping

Images were taken using the Mantra™ Quantitative Pathology Work Station (Akoya Biosciences) as described in the Online Methods. One image was taken of each patient core. All cube filters were used for each image capture (DAPI, CY3, CY5, CY7, Texas Red, Qdot) and the saturation protection feature was utilized. After all images were acquired, images were analyzed using inForm® Cell Analysis™ software versions 2.3.0 and 2.4.2 (Akoya Biosciences). Using this software, chronic pancreatitis specimens and PDA specimens were batch analyzed by their separate diagnoses. Cell segmentation was completed using DAPI as a basis of cell location and size and all cells segmented into the following subsets (nucleus, cytoplasm, and membrane). Using the automated training software, basic phenotypes (T cells, tumor epithelial cells, other cells, $CD163^{+}$ cells) were created. Software output consisting of mean fluorescent intensity (mfi) of each antibody-fluorophore pair, basic phenotypes, and x and y coordinates were acquired for further processing. A total of 34 chronic pancreatitis patients and 71 PDA patients were included in this study. Supplemental Table 2.3 details the antibodies used for mfIHC.

Cytometry Time-of-Flight (CyTOF) Immune Phenotyping

Tissues were mechanically minced and enzymatically digested with collagenase P (1mg/mL DMEM) at 37 degrees Celsius with gentle shaking and subsequently filtered through a 40μm mesh to obtain single cells. Whole blood was collected pre-operatively

into two 10mL EDTA tubes. EDTA tubes were inverted 10 times before centrifugation at room temperature (RT), 1700 × g for 20 minutes. Serum was removed and using a P1000 tip, the white layer of PBMCs at the interface between serum and RBCs was removed and placed into 15mL falcon tube. PBMCs were washed in 3X volume PBS centrifuged at RT, 300 × g for 15 minutes. Following centrifugation, the supernatant was removed, and 10ml ACK lysis buffer was added to lyse RBCs for 10 minutes at RT. Following this, PBMCs were centrifuged at 300 × g for 5 minutes. PBMC and tissue samples were washed twice with MaxPar® PBS (Fluidigm) prior to Cell-ID™ Cisplatin (Live/Dead staining). Cell-ID™ Cisplatin reagent (1.67μM) was incubated with tissue and PBMCs single cell suspensions for 5 minutes at RT. To quench this reaction, 4mL of Cell Staining Buffer (Fluidigm) was added to each sample and samples were centrifuged at 300 g for 5 minutes. The supernatant was removed, and cells were washed with 2 mL of MaxPar® Cell Staining Buffer. Cell fixation was achieved by removing the supernatant, and re-suspending the cell pellet in residual volume, prior to the addition of freshly prepared cell fixation buffer (1.6% Methanol-free Formaldehyde; Thermo Fisher 28906 in MaxPar® PBS) for 10 minutes at RT. After fixation, samples were washed twice with 2mL of MaxPar® Cell Staining Buffer and centrifuged at 300 g for 5 minutes. Samples were re-suspended in 1mL MaxPar® Cell Staining Buffer and stored at 4 degrees Celsius for up to one week prior to staining. Up to 3 million cells per sample were stained with cell surface antibody cocktail (All antibodies were purchased from Fluidigm and used at the following dilutions: (CD3 (1:200); CD19 (1:300); CD15 (1:400); CD163 (1:100); CD64 (1:100); CD16 (1:400); LAMP1 (1:100); CD66b (1:200); CCR2 (1:200); TIGIT (1:100); PD-1 (1:100); PD-L1 (1:100); CD8a (1:200); CD33

(1:200); CD45RO (1:200); CD34 (1:100); CD45RA (1:100); CD206 (1:100); CD25 (1:100); CTLA-4 (1:100); CD68 (1:100); PD-L2 (1:100); HLA-DR (1:400); CD14 (1:100); CD4 (1:100); CD11b (1:200); CD45 (1:200); LAG3 (1:100); CD23 (1:100); CD56 (1:100)). (see Supplemental Table 2.1 for additional antibody information) in 100µl volume of MaxPar® Cell Staining Buffer for 30 minutes at room temperature. After being washed once in 1mL MaxPar® Cell Staining Buffer cells were re-suspended in 2mL cell intercalation solution (125 nM Cell-ID Intercalator-Ir in MaxPar® Fix and Perm Buffer) and shipped to either the Flow Cytometry core at the University of Rochester Medical Center or the Indiana University Simon Cancer Center Flow Cytometry where CyTOF2 Mass Cytometer cell acquisition was performed.

CyTOF Data Preprocessing

Normalized FCS files were analyzed using the Premium CytoBank Software V7.3.0 (cytobank.org). Data were checked for quality of staining and normalized by the use of internal bead standards. Live singlet cells were identified using the combination of Ir191 DNA Intercalator, Event Length, and Pt195 Cisplatin staining intensity channels. Filtered live single cells were exported as new FCS files for downstream analysis.

CyTOF Analysis

Unbiased identification of cellular subpopulations was performed in parallel using multiple approaches – visualization through FlowSOM-viSNE in R, where an initial FlowSOM clustered cells into 100 initial nodes, followed by the ConsensusClusterPlus package which, along with manual annotation helped to further consolidate the clusters

based on cell surface marker expression (Nowicka et al. 2019), or Astrolabe Cytometry Platform (Astrolabe Diagnostics, Inc.), where single-cell data was clustered using the FlowSOM R package (Van Gassen et al. 2015) and labeled using the Ek'Balam algorithm (Amir et al. 2019). The hierarchical clustering for all heatmaps uses the Pearson's correlation as a distance metric. Differential abundance analysis was performed using the edgeR V3.11 R package (Mccarthy, Chen, and Smyth 2012; Robinson, Mccarthy, and Smyth 2010). We used a combination of manual gating validation and unbiased approaches to analyze our datasets and included samples with >3000 live singlets in clustering algorithms.

Treatment of Batch Effects

In order to avoid batch effects within the data analysis, the Astrolabe Cytometry Platform did not compare numerical intensities between samples (Amir et al. 2019). Each sample was analyzed separately, and then comparisons were done using either cell frequencies (such as comparing T Cell counts) or qualitative values ("CD3 high" versus "CD3 low"). The underlying assumption was that a given subset was the same regardless of if underlying marker intensity has shifted; in other words, a T Cell was defined as a T Cell whether the $CD3^+$ peak was centered around a transformed intensity of 4, or a transformed intensity of 6. This mirrors the approach utilized in manual gating analysis.

t-SNE Visualization

For the t-SNE maps, each sample was uniformly downsampled into at most 10,000 cells. Samples were then concatenated, and the complete data set was uniformly downsampled into at most 500,000 cells. t-SNE algorithm was run using the Rt-SNE package: https://github.com/jkrijthe/Rt-SN.

Single-cell RNA sequencing

Tissues were mechanically minced and enzymatically digested with collagenase P (1mg/mL DMEM) and subsequently filtered through a 40μm mesh to obtain single cells. Dead cells were removed using MACS® Dead Cell Removal Kit (Miltenyi Biotec Inc.). Single-cell cDNA libraries were prepared and sequenced at the University of Michigan Sequencing Core using the 10x Genomics Platform. Samples were run using paired end 50 cycle reads on HiSeq 4000 or the NovaSeq 6000 (Illumina) to a depth of 100,000 reads. The raw data were processed and aligned by the University of Michigan DNA Sequencing Core. Cellranger count version 3.0.0 with default settings was used, with an initial expected cell count of 10,000. In all cases the hg19 reference supplied with the cellranger software was used for alignment. R Studio V3.5.1 and R package Seurat version 3.0 was used for single cell RNA-seq data analysis similarly as previous described. Data were initially filtered to only include all cells with at least 200 genes and all genes in greater than 3 cells. Data were initially normalized using the NormalizeData function with a scale factor of 10,000 and the LogNormalize normalization method. Variable genes were identified using the FindVariableFeatures function. Data were assigned a cell cycle score using the CellCycleScoring function and a cell cycle difference was calculated by subtracting the S phase score from the G2M score. Data

were scaled and centered using linear regression on the counts and the cell cycle score difference. PCA was run with the RunPCA function using the previously defined variable genes. Violin plots were then used to filter data according to user-defined criteria. All tissue samples were batch corrected through the R package Harmony V1.0 (https://github.com/immunogenomics/harmony). Harmony is a flexible multi-dataset integration algorithm for scRNA-seq by correcting the low-dimensional embedding of cells from principal component analysis (PCA). It first uses soft clustering to find potential clusters, and then uses a soft k-means clustering algorithm to find clusters that favors the cells from multiple datasets and penalizes for any specified unwanted technical or biological factors. It then learns a simple linear adjustment function by computing cluster-specific linear correction factors, such as individual cell-types and cell state, from the cluster-specific centroids from each dataset. Each cell is weighted and corrected by its cell-specific linear factor. It then iterates the clustering and correction until the cell cluster assignments are stable. We used Harmony V1.0 to integrate our scRNA-seq patient data, correcting for individual scRNA-seq Run IDs (as each individual patient was each their own Run ID). Cell clusters were identified via the FindNeighbors and FindClusters function using a resolution of 1.2–2 for all samples and Uniform Manifold Approximation and Projection (UMAP) clustering algorithms were performed. FindAllMarkers table was created and clusters were defined by user-defined criteria. Code is publicly available on GitHub.com (https://github.com/PascaDiMagliano-Lab/MultimodalMappingPDA-scRNASeq).

Interactome

Ligand and receptor pairs were defined based off of a curated literature supported list in (Ramilowski et al. 2015). The average of expression of ligands and receptors (LR) in all the population for each group were calculated. LR pairs in each group (adjacent/normal and PDA) were determined to be expressed by setting the median average expression for all groups as a threshold. LR's above the threshold were considered as expressed in the group. LR pairs were then filtered out if the ligand and receptor in the LR pairs were not expressed in both groups. Differences of the LR's between groups were determined using Wilcoxon ranked test, and p-values were adjusted for multiple comparisons with the Bonferroni correction method. LR's were considered significantly different if the $p < 1.0\times10-4$. LR pairs were then sorted by the adjusted ligand expression p-value. The interactomes were visualized using the Circos software V0.69-9 and the heatmap values within the circos plots displays the average expression of each ligand/receptor within the PDA tissues (Krzywinski et al. 2009).

Acknowledgements

We thank Matthew Cochran and Terry Wightman at the Flow Cytometry core at the University of Rochester Medical Center and Andrea Michelle Gunawan at the Indiana University Simon Cancer Center Flow Cytometry for their support in cell CyTOF acquisition. We thank Vinicius Motta and Kevin Brown from Fluidigm for their assistance with panel design. We would like to thank Patricia Schnepp and Aquila Ahmed for their assistance with CyTOF experimental design. We would also like to thank Tricia Tamsen and Judy Opp from the University of Michigan Advanced Genomics Core. We would like to thank David Hill and Michael Czerwinski for their input on designing single cell analysis pipelines. We would very much like to thank Amir Gilado and Ido Amit for their

expertise in building our pancreatic interactome network. We would like to thank the Tissue Procurement Center at the University of Michigan. Thanks to Ed Stack formerly with Perkin Elmer for assistance with initial R introduction and basic training using inForm 2.3.0 and earlier versions. and staining strategies. We thank Philip Turncliff for the excellent graphics. We also thank Jason Spence for the VE-cadherin antibody gift.

Funding:

This project was supported by NIH/NCI grants R01CA151588, R01CA198074, U01CA224145, and the American Cancer Society to MPdM. This work was also supported by the University of Michigan Cancer Center Support Grant (P30CA046592), including an Administrative Supplement to HCC and MPdM. FB was funded by the Association of Academic Surgery Joel Roslyn Award. TLF was funded by K08CA201581. SK was supported by T32-GM113900 and NS, VS, KD were supported by T32-CA009676. EC is supported the American College of Gastroenterology Clinical Research Award and by T32-DK094775. NS is a recipient of the American Cancer Society Postdoctoral Award PF-19-096-01 and the Michigan Institute for Clinical and Healthy Research (MICHR) Postdoctoral Translational Scholar Program fellowship award. AR and ST were supported by institutional startup funds from the University of Michigan, a gift from Agilent Technologies, NCI grant R37CA214955 and a Research Scholar Grant from the American Cancer Society (RSG-16-005-01). The funders had no role in study design, data collection and analysis, decision to publish, or preparation of the manuscript.

References

1. Amir, El-Ad David, Brian Lee, Paul Badoual, Martin Gordon, Xinzheng V. Guo, Miriam Merad, and Adeeb H. Rahman. 2019. "Development of a Comprehensive Antibody Staining Database Using a Standardized Analytics Pipeline." Frontiers in immunology 10: 1315-1315. https://doi.org/10.3389/fimmu.2019.01315. https://pubmed.ncbi.nlm.nih.gov/31244854. https://www.ncbi.nlm.nih.gov/pmc/articles/PMC6579881/.
2. Arlettaz, Lionel, Sylvie Degermann, Casimir?De Rham, Eddy Roosnek, and Bertrand Huard. 2004. "Expression of inhibitory KIR is confined to CD8+ effector T?cells and limits their proliferative capacity." European Journal of Immunology 34 (12): 3413-3422. https://doi.org/10.1002/eji.200324756.
3. Balachandran, Vinod P., Marta Łuksza, Julia N. Zhao, Vladimir Makarov, John Alec Moral, Romain Remark, Brian Herbst, Gokce Askan, Umesh Bhanot, Yasin Senbabaoglu, Daniel K. Wells, Charles Ian Ormsby Cary, Olivera Grbovic-Huezo, Marc Attiyeh, Benjamin Medina, Jennifer Zhang, Jennifer Loo, Joseph Saglimbeni, Mohsen Abu-Akeel, Roberta Zappasodi, Nadeem Riaz, Martin Smoragiewicz, Z. Larkin Kelley, Olca Basturk, Mithat Gönen, Arnold J. Levine, Peter J. Allen, Douglas T. Fearon, Miriam Merad, Sacha Gnjatic, Christine A. Iacobuzio-Donahue, Jedd D. Wolchok, Ronald P. Dematteo, Timothy A. Chan, Benjamin D. Greenbaum, Taha Merghoub, and Steven D. Leach. 2017. "Identification of unique neoantigen qualities in long-term survivors of pancreatic cancer." Nature 551 (7681): 512-516. https://doi.org/10.1038/nature24462. https://www.ncbi.nlm.nih.gov/pmc/articles/PMC6145146.
4. Balli, David, Andrew J. Rech, Ben Z. Stanger, and Robert H. Vonderheide. 2017. "Immune Cytolytic Activity Stratifies Molecular Subsets of Human Pancreatic Cancer." Clinical Cancer Research 23 (12): 3129-3138. https://doi.org/10.1158/1078-0432.ccr-16-2128.
5. Beatty, Gregory L., Rafael Winograd, Rebecca A. Evans, Kristen B. Long, Santiago L. Luque, Jae W. Lee, Cynthia Clendenin, Whitney L. Gladney, Dawson M. Knoblock, Patrick D. Guirnalda, and Robert H. Vonderheide. 2015. "Exclusion of T Cells From Pancreatic Carcinomas in Mice Is Regulated by Ly6Clow F4/80+ Extratumoral Macrophages." Gastroenterology 149 (1): 201-210. https://doi.org/10.1053/j.gastro.2015.04.010. https://www.ncbi.nlm.nih.gov/pmc/articles/PMC4478138.
6. Bendall, Sean C., Erin F. Simonds, Peng Qiu, El-Ad D. Amir, Peter O. Krutzik, Rachel Finck, Robert V. Bruggner, Rachel Melamed, Angelica Trejo, Olga I. Ornatsky, Robert S. Balderas, Sylvia K. Plevritis, Karen Sachs, Dana Pe'Er, Scott D. Tanner, and Garry P. Nolan. 2011. "Single-Cell Mass Cytometry of Differential Immune and Drug Responses Across a Human Hematopoietic Continuum." Science 332 (6030): 687-696. https://doi.org/10.1126/science.1198704. http://europepmc.org/articles/pmc3273988?pdf=render.
7. Bengsch, Fee, Dawson M. Knoblock, Anni Liu, Florencia Mcallister, and Gregory L. Beatty. 2017. "CTLA-4/CD80 pathway regulates T cell infiltration into pancreatic cancer." Cancer Immunology, Immunotherapy 66 (12): 1609-1617. https://doi.org/10.1007/s00262-017-2053-4.
8. Brahmer, Julie R., Scott S. Tykodi, Laura Q.M. Chow, Wen-Jen Hwu, Suzanne L. Topalian, Patrick Hwu, Charles G. Drake, Luis H. Camacho, John Kauh, Kunle Odunsi, Henry C. Pitot, Omid Hamid, Shailender Bhatia, Renato Martins, Keith Eaton, Shuming Chen, Theresa M. Salay, Suresh Alaparthy, Joseph F. Grosso, Alan J. Korman, Susan M. Parker, Shruti Agrawal, Stacie M. Goldberg, Drew M. Pardoll, Ashok Gupta, and Jon M. Wigginton. 2012. "Safety and Activity of Anti–PD-L1 Antibody in Patients with Advanced Cancer." New England Journal of Medicine 366 (26): 2455-2465. https://doi.org/10.1056/nejmoa1200694.
9. Carlson, Corey M., Bart T. Endrizzi, Jinghai Wu, Xiaojie Ding, Michael A. Weinreich, Elizabeth R. Walsh, Maqsood A. Wani, Jerry B. Lingrel, Kristin A. Hogquist, and Stephen C. Jameson. 2006. "Kruppel-like factor 2 regulates thymocyte and T-cell migration." Nature 442 (7100): 299-302. https://doi.org/10.1038/nature04882. https://www.nature.com/articles/nature04882.pdf.

10. Carstens, Julienne L., Pedro Correa De Sampaio, Dalu Yang, Souptik Barua, Huamin Wang, Arvind Rao, James P. Allison, Valerie S. Lebleu, and Raghu Kalluri. 2017. "Spatial computation of intratumoral T cells correlates with survival of patients with pancreatic cancer." Nature Communications 8 (1): 15095. https://doi.org/10.1038/ncomms15095. https://www.ncbi.nlm.nih.gov/pmc/articles/PMC5414182.
11. Chan-Seng-Yue, Michelle, Jaeseung C. Kim, Gavin W. Wilson, Karen Ng, Eugenia Flores Figueroa, Grainne M. O'Kane, Ashton A. Connor, Robert E. Denroche, Robert C. Grant, Jessica McLeod, Julie M. Wilson, Gun Ho Jang, Amy Zhang, Anna Dodd, Sheng-Ben Liang, Ayelet Borgida, Dianne Chadwick, Sangeetha Kalimuthu, Ilinca Lungu, John M. S. Bartlett, Paul M. Krzyzanowski, Vandana Sandhu, Hervé Tiriac, Fieke E. M. Froeling, Joanna M. Karasinska, James T. Topham, Daniel J. Renouf, David F. Schaeffer, Steven J. M. Jones, Marco A. Marra, Janessa Laskin, Runjan Chetty, Lincoln D. Stein, George Zogopoulos, Benjamin Haibe-Kains, Peter J. Campbell, David A. Tuveson, Jennifer J. Knox, Sandra E. Fischer, Steven Gallinger, and Faiyaz Notta. 2020. "Transcription phenotypes of pancreatic cancer are driven by genomic events during tumor evolution." Nature Genetics 52 (2): 231-240. https://doi.org/10.1038/s41588-019-0566-9. https://doi.org/10.1038/s41588-019-0566-9.
12. Clark, Carolyn E., Sunil R. Hingorani, Rosemarie Mick, Chelsea Combs, David A. Tuveson, and Robert H. Vonderheide. 2007. "Dynamics of the Immune Reaction to Pancreatic Cancer from Inception to Invasion." Cancer Research 67 (19): 9518-9527. https://doi.org/10.1158/0008-5472.can-07-0175.
13. Cohen, Merav, Amir Giladi, Anna-Dorothea Gorki, Dikla Gelbard Solodkin, Mor Zada, Anastasiya Hladik, Andras Miklosi, Tomer-Meir Salame, Keren Bahar Halpern, Eyal David, Shalev Itzkovitz, Tibor Harkany, Sylvia Knapp, and Ido Amit. 2018. "Lung Single-Cell Signaling Interaction Map Reveals Basophil Role in Macrophage Imprinting." Cell 175 (4): 1031-1044.e18. https://doi.org/10.1016/j.cell.2018.09.009.
14. Collin, Matthew, and Venetia Bigley. 2018. "Human dendritic cell subsets: an update." Immunology 154 (1): 3-20. https://doi.org/10.1111/imm.12888. http://europepmc.org/articles/pmc5904714?pdf=render.
15. Das, Shipra, Beny Shapiro, Emily A. Vucic, Sandra Vogt, and Dafna Bar-Sagi. 2020. "Tumor Cell–Derived IL1β Promotes Desmoplasia and Immune Suppression in Pancreatic Cancer." Cancer Research 80 (5): 1088-1101. https://doi.org/10.1158/0008-5472.can-19-2080.
16. Denardo, David G., and Brian Ruffell. 2019. "Macrophages as regulators of tumour immunity and immunotherapy." Nature Reviews Immunology 19 (6): 369-382. https://doi.org/10.1038/s41577-019-0127-6.
17. Dominguez, Claudia X., Sören Müller, Shilpa Keerthivasan, Hartmut Koeppen, Jeffrey Hung, Sarah Gierke, Beatrice Breart, Oded Foreman, Travis W. Bainbridge, Alessandra Castiglioni, Yasin Senbabaoglu, Zora Modrusan, Yuxin Liang, Melissa R. Junttila, Christiaan Klijn, Richard Bourgon, and Shannon J. Turley. 2020. "Single-Cell RNA Sequencing Reveals Stromal Evolution into LRRC15+ Myofibroblasts as a Determinant of Patient Response to Cancer Immunotherapy." Cancer Discovery 10 (2): 232-253. https://doi.org/10.1158/2159-8290.cd-19-0644.
18. Ducimetière, Laura, Marijne Vermeer, and Sonia Tugues. 2019. "The Interplay Between Innate Lymphoid Cells and the Tumor Microenvironment." Frontiers in immunology 10: 2895-2895. https://doi.org/10.3389/fimmu.2019.02895. https://pubmed.ncbi.nlm.nih.gov/31921156. https://www.ncbi.nlm.nih.gov/pmc/articles/PMC6923277/.
19. Elyada, Ela, Mohan Bolisetty, Pasquale Laise, William F. Flynn, Elise T. Courtois, Richard A. Burkhart, Jonathan A. Teinor, Pascal Belleau, Giulia Biffi, Matthew S. Lucito, Santhosh Sivajothi, Todd D. Armstrong, Dannielle D. Engle, Kenneth H. Yu, Yuan Hao, Christopher L. Wolfgang, Youngkyu Park, Jonathan Preall, Elizabeth M. Jaffee, Andrea Califano, Paul Robson, and David A. Tuveson. 2019. "Cross-Species Single-Cell Analysis of Pancreatic Ductal Adenocarcinoma Reveals Antigen-Presenting Cancer-Associated Fibroblasts." Cancer Discovery 9 (8): 1102-1123. https://doi.org/10.1158/2159-8290.cd-19-0094.
20. Fourcade, Julien, Zhaojun Sun, Joe-Marc Chauvin, Mignane Ka, Diwakar Davar, Ornella Pagliano, Hong Wang, Sofiane Saada, Carmine Menna, Rada Amin, Cindy Sander, John M. Kirkwood, Alan J. Korman, and Hassane M. Zarour. 2018. "CD226 opposes TIGIT to disrupt Tregs in

melanoma." JCI Insight 3 (14). https://doi.org/10.1172/jci.insight.121157. https://www.ncbi.nlm.nih.gov/pmc/articles/PMC6124410.
21. Hegde, Samarth, Varintra E. Krisnawan, Brett H. Herzog, Chong Zuo, Marcus A. Breden, Brett L. Knolhoff, Graham D. Hogg, Jack P. Tang, John M. Baer, Cedric Mpoy, Kyung Bae Lee, Katherine A. Alexander, Buck E. Rogers, Kenneth M. Murphy, William G. Hawkins, Ryan C. Fields, Carl J. Deselm, Julie K. Schwarz, and David G. Denardo. 2020. "Dendritic Cell Paucity Leads to Dysfunctional Immune Surveillance in Pancreatic Cancer." Cancer Cell 37 (3): 289-307.e9. https://doi.org/10.1016/j.ccell.2020.02.008.
22. Huber, Samuel, Nicola Gagliani, Lauren A. Zenewicz, Francis J. Huber, Lidia Bosurgi, Bo Hu, Matija Hedl, Wei Zhang, William O'Connor, Andrew J. Murphy, David M. Valenzuela, George D. Yancopoulos, Carmen J. Booth, Judy H. Cho, Wenjun Ouyang, Clara Abraham, and Richard A. Flavell. 2012. "IL-22BP is regulated by the inflammasome and modulates tumorigenesis in the intestine." Nature 491 (7423): 259-263. https://doi.org/10.1038/nature11535. http://europepmc.org/articles/pmc3493690?pdf=render.
23. Jang, Jung-Eun, Cristina H. Hajdu, Caroline Liot, George Miller, Michael L. Dustin, and Dafna Bar-Sagi. 2017. "Crosstalk between Regulatory T Cells and Tumor-Associated Dendritic Cells Negates Anti-tumor Immunity in Pancreatic Cancer." Cell Reports 20 (3): 558-571. https://doi.org/10.1016/j.celrep.2017.06.062. https://doi.org/10.1016/j.celrep.2017.06.062.
24. Jansen, Caroline S., Nataliya Prokhnevska, Viraj A. Master, Martin G. Sanda, Jennifer W. Carlisle, Mehmet Asim Bilen, Maria Cardenas, Scott Wilkinson, Ross Lake, Adam G. Sowalsky, Rajesh M. Valanparambil, William H. Hudson, Donald McGuire, Kevin Melnick, Amir I. Khan, Kyu Kim, Yun Min Chang, Alice Kim, Christopher P. Filson, Mehrdad Alemozaffar, Adeboye O. Osunkoya, Patrick Mullane, Carla Ellis, Rama Akondy, Se Jin Im, Alice O. Kamphorst, Adriana Reyes, Yuan Liu, and Haydn Kissick. 2019. "An intra-tumoral niche maintains and differentiates stem-like CD8 T cells." Nature 576 (7787): 465-470. https://doi.org/10.1038/s41586-019-1836-5. https://pubmed.ncbi.nlm.nih.gov/31827286. https://www.ncbi.nlm.nih.gov/pmc/articles/PMC7108171/.
25. Kondo, Takaaki, Hiroshi Takata, and Masafumi Takiguchi. 2007. "Functional expression of chemokine receptor CCR6 on human effector memory CD8+ T cells." European Journal of Immunology 37 (1): 54-65. https://doi.org/10.1002/eji.200636251.
26. Krzywinski, Martin, Jacqueline Schein, İnanç Birol, Joseph Connors, Randy Gascoyne, Doug Horsman, Steven J. Jones, and Marco A. Marra. 2009. "Circos: An information aesthetic for comparative genomics." Genome Research 19 (9): 1639-1645. https://doi.org/10.1101/gr.092759.109. http://genome.cshlp.org/content/19/9/1639.full.pdf.
27. Lazarus, Jenny, Tomasz Maj, J. Joshua Smith, Mirna Perusina Lanfranca, Arvind Rao, Michael I. D'Angelica, Lawrence Delrosario, Alexander Girgis, Casey Schukow, Jinru Shia, Ilona Kryczek, Jiaqi Shi, Isaac Wasserman, Howard Crawford, Hari Nathan, Marina Pasca Di Magliano, Weiping Zou, and Timothy L. Frankel. 2018. "Spatial and phenotypic immune profiling of metastatic colon cancer." JCI Insight 3 (22). https://doi.org/10.1172/jci.insight.121932. https://www.ncbi.nlm.nih.gov/pmc/articles/PMC6302940.
28. Li, Jing, Yi He, Jing Hao, Ling Ni, and Chen Dong. 2018. "High Levels of Eomes Promote Exhaustion of Anti-tumor CD8(+) T Cells." Frontiers in immunology 9: 2981-2981. https://doi.org/10.3389/fimmu.2018.02981. https://pubmed.ncbi.nlm.nih.gov/30619337. https://www.ncbi.nlm.nih.gov/pmc/articles/PMC6305494/.
29. Ligorio, Matteo, Srinjoy Sil, Jose Malagon-Lopez, Linda T. Nieman, Sandra Misale, Mauro Di Pilato, Richard Y. Ebright, Murat N. Karabacak, Anupriya S. Kulkarni, Ann Liu, Nicole Vincent Jordan, Joseph W. Franses, Julia Philipp, Johannes Kreuzer, Niyati Desai, Kshitij S. Arora, Mihir Rajurkar, Elad Horwitz, Azfar Neyaz, Eric Tai, Neelima K.C. Magnus, Kevin D. Vo, Chittampalli N. Yashaswini, Francesco Marangoni, Myriam Boukhali, Jackson P. Fatherree, Leah J. Damon, Kristina Xega, Rushil Desai, Melissa Choz, Francesca Bersani, Adam Langenbucher, Vishal Thapar, Robert Morris, Ulrich F. Wellner, Oliver Schilling, Michael S. Lawrence, Andrew S. Liss, Miguel N. Rivera, Vikram Deshpande, Cyril H. Benes, Shyamala Maheswaran, Daniel A. Haber, Carlos Fernandez-Del-Castillo, Cristina R. Ferrone, Wilhelm Haas, Martin J. Aryee, and David T. Ting. 2019. "Stromal Microenvironment Shapes the Intratumoral Architecture of Pancreatic

Cancer." Cell 178 (1): 160-175.e27. https://doi.org/10.1016/j.cell.2019.05.012. http://www.cell.com/article/S0092867419305100/pdf.
30. Maj, Tomasz, Wei Wang, Joel Crespo, Hongjuan Zhang, Weimin Wang, Shuang Wei, Lili Zhao, Linda Vatan, Irene Shao, Wojciech Szeliga, Costas Lyssiotis, J Rebecca Liu, Ilona Kryczek, and Weiping Zou. 2017. "Oxidative stress controls regulatory T cell apoptosis and suppressor activity and PD-L1-blockade resistance in tumor." Nature Immunology 18 (12): 1332-1341. https://doi.org/10.1038/ni.3868. https://www.ncbi.nlm.nih.gov/pmc/articles/PMC5770150.
31. Manieri, N. A., E. Y. Chiang, and J. L. Grogan. 2017. "TIGIT: A Key Inhibitor of the Cancer Immunity Cycle." Trends Immunol 38 (1): 20-28. https://doi.org/10.1016/j.it.2016.10.002. https://www.ncbi.nlm.nih.gov/pubmed/27793572.
32. Mccarthy, Davis J., Yunshun Chen, and Gordon K. Smyth. 2012. "Differential expression analysis of multifactor RNA-Seq experiments with respect to biological variation." Nucleic Acids Research 40 (10): 4288-4297. https://doi.org/10.1093/nar/gks042. https://academic.oup.com/nar/article-pdf/40/10/4288/25335174/gks042.pdf.
33. Mcmahon, Christopher W., Allan J. Zajac, Amanda M. Jamieson, Laura Corral, Gianna E. Hammer, Rafi Ahmed, and David H. Raulet. 2002. "Viral and Bacterial Infections Induce Expression of Multiple NK Cell Receptors in Responding CD8+ T Cells." The Journal of Immunology 169 (3): 1444-1452. https://doi.org/10.4049/jimmunol.169.3.1444.
34. Moncada, Reuben, Dalia Barkley, Florian Wagner, Marta Chiodin, Joseph C. Devlin, Maayan Baron, Cristina H. Hajdu, Diane M. Simeone, and Itai Yanai. 2020. "Integrating microarray-based spatial transcriptomics and single-cell RNA-seq reveals tissue architecture in pancreatic ductal adenocarcinomas." Nature Biotechnology 38 (3): 333-342. https://doi.org/10.1038/s41587-019-0392-8. https://doi.org/10.1038/s41587-019-0392-8.
35. Nowicka, Malgorzata, Carsten Krieg, Helena L. Crowell, Lukas M. Weber, Felix J. Hartmann, Silvia Guglietta, Burkhard Becher, Mitchell P. Levesque, and Mark D. Robinson. 2019. "CyTOF workflow: differential discovery in high-throughput high-dimensional cytometry datasets." F1000Research 6: 748. https://doi.org/10.12688/f1000research.11622.3.
36. Nywening, Timothy M, Brian A Belt, Darren R Cullinan, Roheena Z Panni, Booyeon J Han, Dominic E Sanford, Ryan C Jacobs, Jian Ye, Ankit A Patel, William E Gillanders, Ryan C Fields, David G Denardo, William G Hawkins, Peter Goedegebuure, and David C Linehan. 2018. "Targeting both tumour-associated CXCR2+ neutrophils and CCR2+ macrophages disrupts myeloid recruitment and improves chemotherapeutic responses in pancreatic ductal adenocarcinoma." Gut 67 (6): 1112-1123. https://doi.org/10.1136/gutjnl-2017-313738. https://digitalcommons.wustl.edu/cgi/viewcontent.cgi?article=7871&context=open_access_pubs.
37. Panni, Roheena Z., John M. Herndon, Chong Zuo, Samarth Hegde, Graham D. Hogg, Brett L. Knolhoff, Marcus A. Breden, Xiaobo Li, Varintra E. Krisnawan, Samia Q. Khan, Julie K. Schwarz, Buck E. Rogers, Ryan C. Fields, William G. Hawkins, Vineet Gupta, and David G. Denardo. 2019. "Agonism of CD11b reprograms innate immunity to sensitize pancreatic cancer to immunotherapies." Science Translational Medicine 11 (499): eaau9240. https://doi.org/10.1126/scitranslmed.aau9240.
38. Perusina Lanfranca, Mirna, Yaqing Zhang, Alexander Girgis, Samantha Kasselman, Jenny Lazarus, Illona Kryczek, Lawrence Delrosario, Andrew Rhim, Lada Koneva, Maureen Sartor, Lei Sun, Christopher Halbrook, Hari Nathan, Jiaqi Shi, Howard C. Crawford, Marina Pasca Di Magliano, Weiping Zou, and Timothy L. Frankel. 2020. "Interleukin 22 Signaling Regulates Acinar Cell Plasticity to Promote Pancreatic Tumor Development in Mice." Gastroenterology 158 (5): 1417-1432.e11. https://doi.org/10.1053/j.gastro.2019.12.010.
39. Ramilowski, Jordan A., Tatyana Goldberg, Jayson Harshbarger, Edda Kloppmann, Marina Lizio, Venkata P. Satagopam, Masayoshi Itoh, Hideya Kawaji, Piero Carninci, Burkhard Rost, and Alistair R. R. Forrest. 2015. "A draft network of ligand–receptor-mediated multicellular signalling in human." Nature Communications 6 (1): 7866. https://doi.org/10.1038/ncomms8866. https://www.nature.com/articles/ncomms8866.pdf.
40. Robinson, M. D., D. J. Mccarthy, and G. K. Smyth. 2010. "edgeR: a Bioconductor package for differential expression analysis of digital gene expression data." Bioinformatics 26 (1): 139-140. https://doi.org/10.1093/bioinformatics/btp616. https://academic.oup.com/bioinformatics/article-pdf/26/1/139/443156/btp616.pdf.

41. Rosenberg, Steven A. 2014. "Entering the mainstream of cancer treatment." Nature Reviews Clinical Oncology 11 (11): 630-632. https://doi.org/10.1038/nrclinonc.2014.174. https://www.ncbi.nlm.nih.gov/pmc/articles/PMC6310157.
42. Royal, Richard E., Catherine Levy, Keli Turner, Aarti Mathur, Marybeth Hughes, Udai S. Kammula, Richard M. Sherry, Suzanne L. Topalian, James C. Yang, Israel Lowy, and Steven A. Rosenberg. 2010. "Phase 2 Trial of Single Agent Ipilimumab (Anti-CTLA-4) for Locally Advanced or Metastatic Pancreatic Adenocarcinoma." Journal of Immunotherapy 33 (8): 828-833. https://doi.org/10.1097/cji.0b013e3181eec14c.
43. Sanford, Dominic E., Brian A. Belt, Roheena Z. Panni, Allese Mayer, Anjali D. Deshpande, Danielle Carpenter, Jonathan B. Mitchem, Stacey M. Plambeck-Suess, Lori A. Worley, Brian D. Goetz, Andrea Wang-Gillam, Timothy J. Eberlein, David G. Denardo, Simon Peter Goedegebuure, and David C. Linehan. 2013. "Inflammatory Monocyte Mobilization Decreases Patient Survival in Pancreatic Cancer: A Role for Targeting the CCL2/CCR2 Axis." Clinical Cancer Research 19 (13): 3404-3415. https://doi.org/10.1158/1078-0432.ccr-13-0525.
44. Sckisel, Gail D., Annie Mirsoian, Christine M. Minnar, Marka Crittenden, Brendan Curti, Jane Q. Chen, Bruce R. Blazar, Alexander D. Borowsky, Arta M. Monjazeb, and William J. Murphy. 2017. "Differential phenotypes of memory CD4 and CD8 T cells in the spleen and peripheral tissues following immunostimulatory therapy." Journal for ImmunoTherapy of Cancer 5 (1). https://doi.org/10.1186/s40425-017-0235-4. https://doi.org/10.1186/s40425-017-0235-4.
45. Smith, Samantha L., Philippa R. Kennedy, Kevin B. Stacey, Jonathan D. Worboys, Annie Yarwood, Seungmae Seo, Everardo Hegewisch Solloa, Brandon Mistretta, Sujash S. Chatterjee, Preethi Gunaratne, Kimaada Allette, Ying-Chih Wang, Melissa Laird Smith, Robert Sebra, Emily M. Mace, Amir Horowitz, Wendy Thomson, Paul Martin, Steve Eyre, and Daniel M. Davis. 2020. "Diversity of peripheral blood human NK cells identified by single-cell RNA sequencing." Blood Advances 4 (7): 1388-1406. https://doi.org/10.1182/bloodadvances.2019000699.
46. Solomon, Benjamin L., and Ignacio Garrido-Laguna. 2018. "TIGIT: a novel immunotherapy target moving from bench to bedside." Cancer Immunology, Immunotherapy 67 (11): 1659-1667. https://doi.org/10.1007/s00262-018-2246-5.
47. Stromnes, Ingunn M, J Scott Brockenbrough, Kamel Izeradjene, Markus A Carlson, Carlos Cuevas, Randi M Simmons, Philip D Greenberg, and Sunil R Hingorani. 2014. "Targeted depletion of an MDSC subset unmasks pancreatic ductal adenocarcinoma to adaptive immunity." Gut 63 (11): 1769-1781. https://doi.org/10.1136/gutjnl-2013-306271. https://www.ncbi.nlm.nih.gov/pmc/articles/PMC4340484.
48. Stromnes, Ingunn M., Ayaka Hulbert, Robert H. Pierce, Philip D. Greenberg, and Sunil R. Hingorani. 2017. "T-cell Localization, Activation, and Clonal Expansion in Human Pancreatic Ductal Adenocarcinoma." Cancer Immunology Research 5 (11): 978-991. https://doi.org/10.1158/2326-6066.cir-16-0322.
49. Stuart, Tim, and Rahul Satija. 2019. "Integrative single-cell analysis." Nature Reviews Genetics 20 (5): 257-272. https://doi.org/10.1038/s41576-019-0093-7.
50. Tsujikawa, Takahiro, Sushil Kumar, Rohan N. Borkar, Vahid Azimi, Guillaume Thibault, Young Hwan Chang, Ariel Balter, Rie Kawashima, Gina Choe, David Sauer, Edward El Rassi, Daniel R. Clayburgh, Molly F. Kulesz-Martin, Eric R. Lutz, Lei Zheng, Elizabeth M. Jaffee, Patrick Leyshock, Adam A. Margolin, Motomi Mori, Joe W. Gray, Paul W. Flint, and Lisa M. Coussens. 2017. "Quantitative Multiplex Immunohistochemistry Reveals Myeloid-Inflamed Tumor-Immune Complexity Associated with Poor Prognosis." Cell reports 19 (1): 203-217. https://doi.org/10.1016/j.celrep.2017.03.037. https://pubmed.ncbi.nlm.nih.gov/28380359. https://www.ncbi.nlm.nih.gov/pmc/articles/PMC5564306/.
51. Van Gassen, Sofie, Britt Callebaut, Mary J. Van Helden, Bart N. Lambrecht, Piet Demeester, Tom Dhaene, and Yvan Saeys. 2015. "FlowSOM: Using self-organizing maps for visualization and interpretation of cytometry data." Cytometry Part A 87 (7): 636-645. https://doi.org/10.1002/cyto.a.22625. https://onlinelibrary.wiley.com/doi/pdf/10.1002/cyto.a.22625.
52. Veglia, Filippo, and Dmitry I Gabrilovich. 2017. "Dendritic cells in cancer: the role revisited." Current Opinion in Immunology 45: 43-51. https://doi.org/10.1016/j.coi.2017.01.002. https://www.ncbi.nlm.nih.gov/pmc/articles/PMC5449252.

53. Vonderheide, Robert H. 2018. "The Immune Revolution: A Case for Priming, Not Checkpoint." Cancer Cell 33 (4): 563-569. https://doi.org/10.1016/j.ccell.2018.03.008. https://www.ncbi.nlm.nih.gov/pmc/articles/PMC5898647.
54. Wherry, E. J., S. J. Ha, S. M. Kaech, W. N. Haining, S. Sarkar, V. Kalia, S. Subramaniam, J. N. Blattman, D. L. Barber, and R. Ahmed. 2007. "Molecular signature of CD8+ T cell exhaustion during chronic viral infection." Immunity 27 (4): 670-84. https://doi.org/10.1016/j.immuni.2007.09.006. https://www.ncbi.nlm.nih.gov/pubmed/17950003.
55. Xu, J., H. Sai, Y. Li, A.C. Jordan, S.E. Mcgettigan, J.-H. Chen, F. Bedoya, J.A. Fraietta, W.L. Gladney, J.Joseph Melenhorst, and G.L. Beatty. 2019. "Peripheral Blood T-Cell Fitness Is Diminished in Patients With Pancreatic Carcinoma but Can Be Improved With Homeostatic Cytokines." Cellular and Molecular Gastroenterology and Hepatology 8 (4): 656-658.e6. https://doi.org/10.1016/j.jcmgh.2019.07.008. https://doi.org/10.1016/j.jcmgh.2019.07.008.
56. Yu, Xin, Kristin Harden, Lino C Gonzalez, Michelle Francesco, Eugene Chiang, Bryan Irving, Irene Tom, Sinisa Ivelja, Canio J Refino, Hilary Clark, Dan Eaton, and Jane L Grogan. 2009. "The surface protein TIGIT suppresses T cell activation by promoting the generation of mature immunoregulatory dendritic cells." Nature Immunology 10 (1): 48-57. https://doi.org/10.1038/ni.1674.
57. Zhang, Qiming, Yao He, Nan Luo, Shashank J. Patel, Yanjie Han, Ranran Gao, Madhura Modak, Sebastian Carotta, Christian Haslinger, David Kind, Gregory W. Peet, Guojie Zhong, Shuangjia Lu, Weihua Zhu, Yilei Mao, Mengmeng Xiao, Michael Bergmann, Xueda Hu, Sid P. Kerkar, Anne B. Vogt, Stefan Pflanz, Kang Liu, Jirun Peng, Xianwen Ren, and Zemin Zhang. 2019. "Landscape and Dynamics of Single Immune Cells in Hepatocellular Carcinoma." Cell 179 (4): 829-845.e20. https://doi.org/10.1016/j.cell.2019.10.003.
58. Zhang, Qing, Jiacheng Bi, Xiaodong Zheng, Yongyan Chen, Hua Wang, Wenyong Wu, Zhengguang Wang, Qiang Wu, Hui Peng, Haiming Wei, Rui Sun, and Zhigang Tian. 2018. "Blockade of the checkpoint receptor TIGIT prevents NK cell exhaustion and elicits potent anti-tumor immunity." Nature Immunology 19 (7): 723-732. https://doi.org/10.1038/s41590-018-0132-0.
59. Zhang, Yaqing, Jenny Lazarus, Nina G. Steele, Wei Yan, Ho-Joon Lee, Zeribe C. Nwosu, Christopher J. Halbrook, Rosa E. Menjivar, Samantha B. Kemp, Veerin R. Sirihorachai, Ashley Velez-Delgado, Katelyn Donahue, Eileen S. Carpenter, Kristee L. Brown, Valerie Irizarry-Negron, Anna C. Nevison, Alekya Vinta, Michelle A. Anderson, Howard C. Crawford, Costas A. Lyssiotis, Timothy L. Frankel, Filip Bednar, and Marina Pasca Di Magliano. 2020. "Regulatory T-cell Depletion Alters the Tumor Microenvironment and Accelerates Pancreatic Carcinogenesis." Cancer Discovery 10 (3): 422-439. https://doi.org/10.1158/2159-8290.cd-19-0958.
60. Zhang, Yaqing, Ashley Velez-Delgado, Esha Mathew, Dongjun Li, Flor M Mendez, Kevin Flannagan, Andrew D Rhim, Diane M Simeone, Gregory L Beatty, and Marina Pasca Di Magliano. 2017. "Myeloid cells are required for PD-1/PD-L1 checkpoint activation and the establishment of an immunosuppressive environment in pancreatic cancer." Gut 66 (1): 124-136. https://doi.org/10.1136/gutjnl-2016-312078. https://www.ncbi.nlm.nih.gov/pmc/articles/PMC5256390.
61. Zhang, Yaqing, Wei Yan, Esha Mathew, Filip Bednar, Shanshan Wan, Meredith A. Collins, Rebecca A. Evans, Theodore H. Welling, Robert H. Vonderheide, and Marina Pasca Di Magliano. 2014. "CD4+ T Lymphocyte Ablation Prevents Pancreatic Carcinogenesis in Mice." Cancer Immunology Research 2 (5): 423-435. https://doi.org/10.1158/2326-6066.cir-14-0016-t.
62. Zhu, Yu, John M. Herndon, Dorothy K. Sojka, Ki-Wook Kim, Brett L. Knolhoff, Chong Zuo, Darren R. Cullinan, Jingqin Luo, Audrey R. Bearden, Kory J. Lavine, Wayne M. Yokoyama, William G. Hawkins, Ryan C. Fields, Gwendalyn J. Randolph, and David G. Denardo. 2017. "Tissue-Resident Macrophages in Pancreatic Ductal Adenocarcinoma Originate from Embryonic Hematopoiesis and Promote Tumor Progression." Immunity 47 (2): 323-338.e6. https://doi.org/10.1016/j.immuni.2017.07.014. http://www.cell.com/article/S1074761317303217/pdf.
63. Zhu, Yu, Brett L. Knolhoff, Melissa A. Meyer, Timothy M. Nywening, Brian L. West, Jingqin Luo, Andrea Wang-Gillam, S. Peter Goedegebuure, David C. Linehan, and David G. Denardo. 2014. "CSF1/CSF1R Blockade Reprograms Tumor-Infiltrating Macrophages and Improves Response to

T-cell Checkpoint Immunotherapy in Pancreatic Cancer Models." Cancer Research 74 (18): 5057-5069. https://doi.org/10.1158/0008-5472.can-13-3723.
64. Öhlund, Daniel, Abram Handly-Santana, Giulia Biffi, Ela Elyada, Ana S. Almeida, Mariano Ponz-Sarvise, Vincenzo Corbo, Tobiloba E. Oni, Stephen A. Hearn, Eun Jung Lee, Iok In Christine Chio, Chang-Il Hwang, Hervé Tiriac, Lindsey A. Baker, Dannielle D. Engle, Christine Feig, Anne Kultti, Mikala Egeblad, Douglas T. Fearon, James M. Crawford, Hans Clevers, Youngkyu Park, and David A. Tuveson. 2017. "Distinct populations of inflammatory fibroblasts and myofibroblasts in pancreatic cancer." Journal of Experimental Medicine 214 (3): 579-596. https://doi.org/10.1084/jem.20162024. http://repository.cshl.edu/34140/1/Tuveson%20et%20al%202017.pdf.

Chapter 3: Characterization of the Tumor Microenvironment of Pancreatic Liver Metastases

Summary

Pancreatic cancer is a deadly malignancy that is often only diagnosed as metastatic disease. Previous studies have primarily focused on the metastatic potential of primary tumors. These studies have characterized PDA as an aggressive, early metastasizing disease, prompting the need to better understand the biology of PDA metastases. Here, we perform single cell RNA sequencing on biopsies of human PDA liver metastases. We use the transcriptome of the cells captured and compare them to adjacent normal pancreas and PDA primary tumor samples. We identified the diverse population of cells that make up the LM TME and compared their transcriptomes to their counterparts in the PDA TME. We found that fibroblasts and myeloid cells have increased expression of pro-metastatic genes, decreasing expression of certain immunomodulatory genes present in the primary PDA TME. We found that there are a higher percentage of exhausted CD8 T cells in the LM TME and that the exhausted CD8 T cells express higher levels of exhaustion markers. Finally, we perform putative ligand-receptor interactome mapping, visualizing ligand-receptor pairs that are upregulated in the LM TME versus the PDA TME. We find that there are many mechanisms of immune suppression with potential to be activated between the multiple cell populations present in the LM TME. The goal of this work is to better characterize the LM TME using scRNAseq to find potential mechanisms of immune suppression to

validate in tissue samples to determine which mechanism is the primary driver of immunosuppression in the LM TME. Once the mechanism is determined, treatment plans can be developed to overcome immune suppression in both the primary and metastatic tumors to increase the efficacy of treatment systemically.

Introduction

Metastasis is the process by which tumor cells disseminate from the primary and grow in a secondary location [see review:(Welch and Hurst 2019; Lambert, Pattabiraman, and Weinberg 2017)]. The process of metastasis is highly inefficient as the metastatic cancer cells may encounter a variety of cellular environments different than the primary tumor they originate from and are subject to a variety of barriers and environmental stressors. This inefficiency can be overcome however, resulting in metastatic growth that is the primary cause of cancer related mortality. There are many sub-processes involved in formation of metastases, termed the invasion-metastatic cascade. The invasion-metastatic cascade begins within the primary tumor aberrantly activating pathways that promote the dissociation of cells from the primary tumor. This includes processes such as angiogenesis, immune suppression, and secretion of factors that can create a pre-metastatic niche, the modulation of a distal microenvironment that makes the site amenable to metastatic growth. Next, the tumor cells must disseminate from the primary tumor and leave the local microenvironment. This step is often aided by a process called epithelial-to-mesenchymal transition (EMT). Solid tumors are generally epithelial-like, expressing proteins like cadherins and keratins, proteins important in maintenance of cellular structure and cell-to-cell adhesion. EMT describes the process whereby tumor cells decrease expression of

these structural proteins in favor of proteins found in more motile cells, endowing increased migration capacity. The tumor cells then leave the local environment, either invading adjacent organs or intravasating into the body's lymphatic or circulatory systems. To complete the process of metastasis, the tumor cells must enter the secondary location and successfully colonize the new site. The requirements for successful colonization and growth differ between cancers and specific organs, but one observed process is the re-expression of epithelial markers in tumor cells at the secondary site, termed the mesenchymal-to-epithelial transition (MET). Different types of cancers demonstrate different organ tropism, preferentially growing in certain organs due to either physical factors, such as proximity and connection via vasculature, or due to the biological properties of the organ being more easily amenable to supporting metastatic growth. Metastasis introduces additional complexity to the successful treatment of cancer. Firstly, the distant colonization renders all forms of local therapy, such as radiation therapy and surgical resection, ineffective. Secondly, the microenvironment of the metastatic site may confer different selective pressures to the metastases, resulting in a metastatic tumor with different mutational and phenotypic properties than the primary tumor (Yachida et al. 2010; Campbell et al. 2010; Stein et al. 2019). Regardless of the primary tumor, advanced metastatic disease has proven to be incurable by current treatment regiments.

Pancreatic cancer is most frequently diagnosed when the disease is at the metastatic stage, commonly metastasizing to the liver, peritoneum, and lung (Siegel et al. 2021) [see review:(Mizrahi et al. 2020)]. There are many hypotheses to explain this. First, there is difficulty in diagnosing early disease due to a lack of specific symptoms

and biomarkers. Then, given that the only curative treatment is surgery, there is the possibility of unresected margins and/or undetectable microlesions. However, even surgical resection only has a five-year survival rate on 10-20%. The possibilities become even more complicated once metastasis is considered. There is evidence for and against early metastasis of PDA. Creating a phylogenetic tree detailing the series of mutations or epigenetic events that need to occur between the oncogenesis of the very first PDA tumor cell and the cell that make up the metastases portray PDA at an incredibly late metastasizing tumor, suggesting a decades long window for surgical resection (Campbell et al. 2010; Yachida et al. 2010). However, mathematical modeling using the growth kinetics and dissemination of PDA from patient data determined that cells bearing metastatic potential arose early in the primary tumor and that even patients that were diagnosed early enough to receive surgery would have harbored metastases at the time of diagnosis (Haeno et al. 2012; Rhim et al. 2012). Given the prevalence of metastases in PDA patients, it is important understand the biology of PDA tumor metastases.

Primary PDA tumors demonstrate activation of many pro-metastatic pathways [see review:(Kalluri and Weinberg 2009)]. KRAS, the most frequently mutated driving oncogene in PDA, regulates multiple pathways that can promote metastasis such as the PI3K and NF-κB pathways [see review: (Wang et al. 2021)]. While there are conflicting reports about the role of EMT and the specific EMT-inducing transcription factors involved in PDA, there is evidence that disseminated PDA tumor cells express more mesenchymal markers than primary tumor cells, regaining expression of epithelial markers (Rhim et al. 2012; Zheng et al. 2015; Aiello et al. 2016). Additionally, like the

primary PDA tumor, PDA metastases also demonstrate a similar infiltration of fibroblasts and immune cells. However, unlike the primary PDA tumor, the specific composition of the subpopulations present in the metastatic PDA TME is different than the primary tumor (Aiello et al. 2016). Here, we further characterize the differences between the primary and metastatic PDA TME, using single cell RNA sequencing to identify populations present in both TMEs and compare the transcriptomes of those populations to gauge similarities and differences in the functions of the cell types present. Our study offers preliminary insight into the transcriptional changes that occur between cells polarized by primary tumor cells and metastatic tumor cells, demonstrating the need to better understand the biology of PDA metastases to decide on systemic treatments that would be efficacious against both the primary tumor and metastases.

Results

Single cell RNA sequencing reveals a complex immune landscape with heterogenous expression of immune checkpoints and ligands in liver metastases of pancreatic cancer

We performed single cell RNA sequencing (scRNA-seq) on 16 primary PDA (PD) samples, 3 adjacent/normal (Adj/Norm) pancreas samples, and 5 PDA liver metastases (LM) (Figure 3.1A). To define the cell populations, we processed the data as previously described and identified the population clusters based on published lineage markers (Figure 3.1A and 3.1B) (N. G. Steele et al. 2020). We previously profiled the average expression of immune checkpoint receptors and ligands by cell types in the primary samples and found expression of multiple immune checkpoint receptors in T cells, with enriched expression of their cognate ligands expressed on myeloid cells. We similarly

profiled expression of immune checkpoint genes in the liver metastases. Similarly to the primary tumor, the CD8 and CD4 T cells in the liver metastases expressed TIGIT and PDCD1. LAG3 is more highly expressed in CD8 T cells and low in CD4 T cells. CTLA-4 expression was high in CD4 T cells and low in CD8 T cells. The cognate ligands of these immune checkpoints are expressed on multiple other cell types. Epithelial cells, fibroblasts, and endothelial cells express TIGIT ligand PVR. PD-1 ligand CD274 is expressed on myeloid cells, B and plasma cells, and appears to be expressed on CD4 and CD8 T cells in the liver metastases. LAG3 binds to the MHC-II proteins, of which HLA-DQA1 is expressed on myeloid, B and plasma cells. CTLA-4 ligands CD80 is expressed on myeloid cells, B cells, and CD4 T cells, and CD86 is expressed on myeloid cells. Combining this data with protein level expression would be necessary to confirm these findings. Next, we wanted to understand the expression of genes within specific subsets of cells.

Figure 3.1 The TME of liver metastases recapitulates the immunosuppressive TME of primary PDA tissue

(A) UMAP on 3 adjacent/normal pancreas (left) and 16 PDA patient (middle) tissues and 5 LM patient (right) tissues. Populations identified as follows: T cell (dark blue), epithelial (red), fibroblasts (green), B cells (brown), plasma cells (yellow), mast cells (purple), myeloid (orange), endothelial cells (hot pink), acinar (pink), and nerves (blue-grey). **(B)** Dot plot of key markers used to define the identified cell populations. Color of dot represents average expression, while the size of the dot represents percent expression. Dot plot represents merged n=3 adj/norm patients and n=16 PDA patients and n=5 LM patients gene expression of lineage markers. **(C)** Average expression of immune checkpoint ligands and receptors in the identified cell populations in n=5 LM tissue samples.

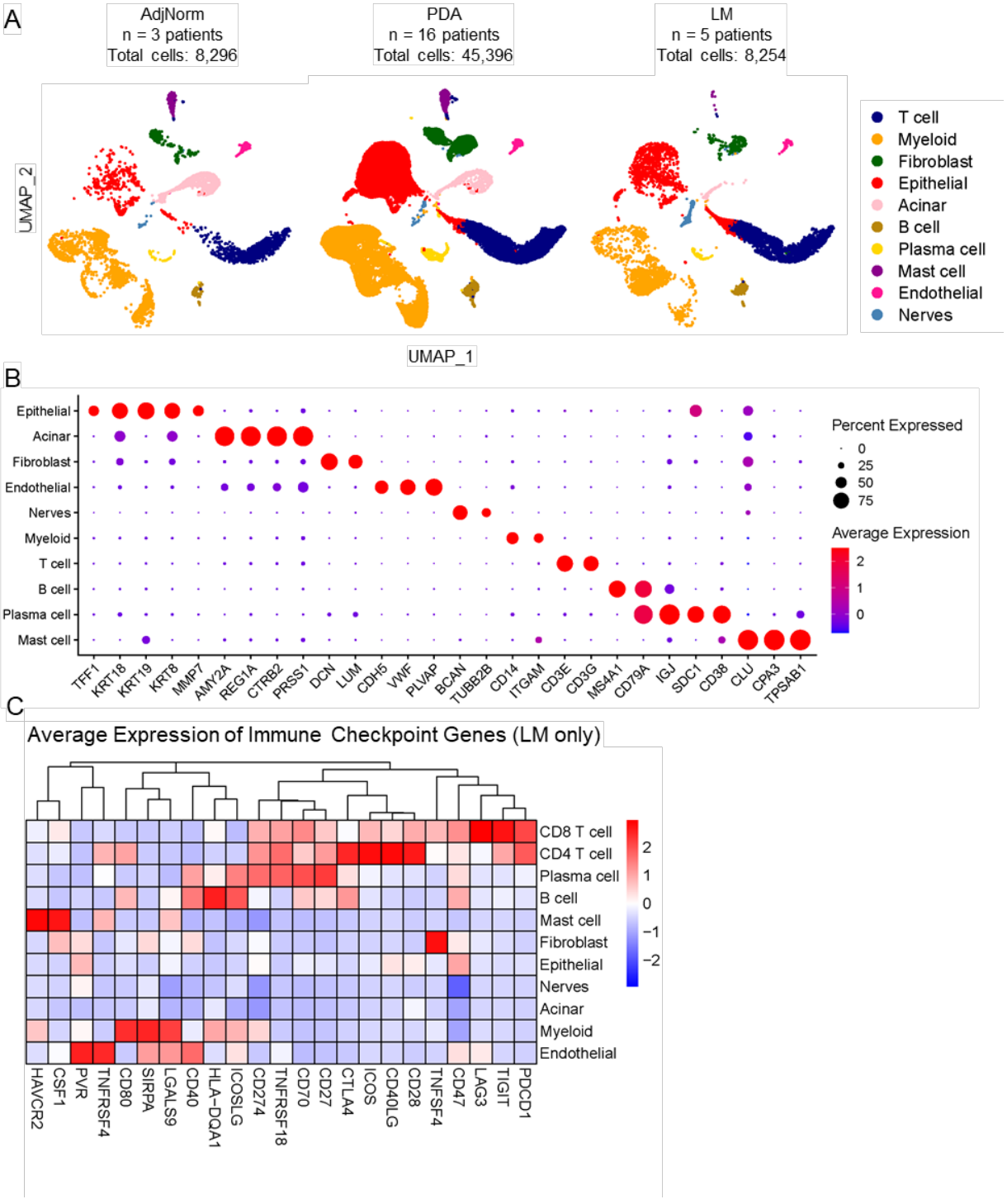
A
AdjNorm
n = 3 patients
Total cells: 8,296
PDA
n = 16 patients
Total cells: 45,396
LM
n = 5 patients
Total cells: 8,254
UMAP_2
UMAP_1
T cell
Myeloid
Fibroblast
Epithelial
Acinar
B cell
Plasma cell
Mast cell
Endothelial
Nerves
B
Epithelial
Acinar
Fibroblast
Endothelial
Nerves
Myeloid
T cell
B cell
Plasma cell
Mast cell
TFF1 KRT18 KRT19 KRT8 MMP7 AMY2A REG1A CTRB2 PRSS1 DCN LUM CDH5 VWF PLVAP BCAN TUBB2B CD14 ITGAM CD3E CD3G MS4A1 CD79A IGJ SDC1 CD38 CLU CPA3 TPSAB1
Percent Expressed
0
25
50
75
Average Expression
2
1
0
C
Average Expression of Immune Checkpoint Genes (LM only)
CD8 T cell
CD4 T cell
Plasma cell
B cell
Mast cell
Fibroblast
Epithelial
Nerves
Acinar
Myeloid
Endothelial
2
1
0
−1
−2
HAVCR2 CSF1 PVR TNFRSF4 CD80 SIRPA LGALS9 CD40 HLA-DQA1 ICOSLG CD274 TNFRSF18 CD70 CD27 CTLA4 ICOS CD40LG CD28 TNFSF4 CD47 LAG3 TIGIT PDCD1

Fibroblasts in PDA liver metastases upregulate pro-metastatic genes compared to primary PDA tumors

Fibroblasts are a major part of the primary PDA TME that have heterogenous subpopulations with distinct functions and characteristics. We sought out to characterize whether the cancer associated fibroblast (CAF) populations in the LM TME were similar to the populations found in the PDA TME [see review:(Biffi and Tuveson 2021)]. To define the cell populations, we processed the data as previously described and identified the fibroblast populations based on previously published markers (N. G. Steele et al. 2020; Nina G. Steele et al. 2021). We found the same populations as previously described, myCAFs, iCAFs, and apCAFs, additionally discovering a subset of pericytes (Figure 3.2A and 3.2B). We then performed differential expression analysis of the four populations to confirm their identity based on expression of genes related to their previously reported functions in the PDA tumor. Pericytes expressed pericyte specific genes such as RGS5 and FABP4 (Figure 3.2A-C). myCAFs are myofibril-like CAFs that function in depositing ECM in the PDA TME. As expected, many of the top expressed myCAF genes are ECM genes such as COL10A1, LUM, COL1A2, COL3A1, COL1A1, and COL11A1 (Figure 3.2C). iCAFs are inflammatory CAFs that function in secretion of immunomodulatory ligands, typically resulting in the promotion of an immunosuppressive TME in PDA. While genes for immunosuppressive ligands are present, such as CXCL12, the top most differentially expressed genes were involved in the complement system, C7 and C3 (Figure 3.2C). The final population of CAFs are the antigen-presenting CAFs, a rare population of MHC expressing CAFs, the function of which are still being elucidated. apCAFs are present in the LM, but differential

expression analysis did not reveal any expected expression of MHC in the apCAF population. We then performed differential expression analysis of the AdjNorm, PDA, and LM populations. We selected a few significantly (padj. > 0.05) differentially expressed genes to highlight potential differences between CAFs in the PDA and LM TMEs. We found that there was an increase in pro-metastatic genes in the LM CAFs. POSTN, VEGFC, and LOXL2 were increased in the LM CAF populations compared to PDA and AdjNorm, specifically being highly expressed in the myCAF population (Figure 3.2D and Supplemental Figure 3.1A). This demonstrates that while the cell types may be present and broadly phenotypically similar, they may have different nuances depending on the specific environmental niche they exist in.

Figure 3.2 LM Fibroblasts express higher levels of metastasis supportive genes

(A) UMAP on 3 adjacent/normal pancreas (left) and 16 PDA patient (middle) tissues and 5 LM patient (right) tissues. Populations identified as follows: myCAF (dark green), iCAF (light green), apCAF (teal), and pericytes (pink). **(B)** Dot plot of key markers used to define the identified cell populations. Color of dot represents average expression, while the size of the dot represents percent expression. Dot plot represents merged n=3 adj/norm patients and n=16 PDA patients and n=5 LM patients gene expression of lineage markers. **(C)** Single cell resolution heatmap analysis of top 20 genes for each identified fibroblast subset. **(D)** Panel of genes differentially expressed in fibroblasts in LM tissue (red) compared to primary PDA tissue (blue) adjacent/normal pancreas (black). Plots represent n=3 adj/norm and n=16 PDA patients and n=5 LM patients. Violin plots are shown as normalized expression. All violin plots in have an adjusted p-value of $p<0.05$ and are considered statistically significant.

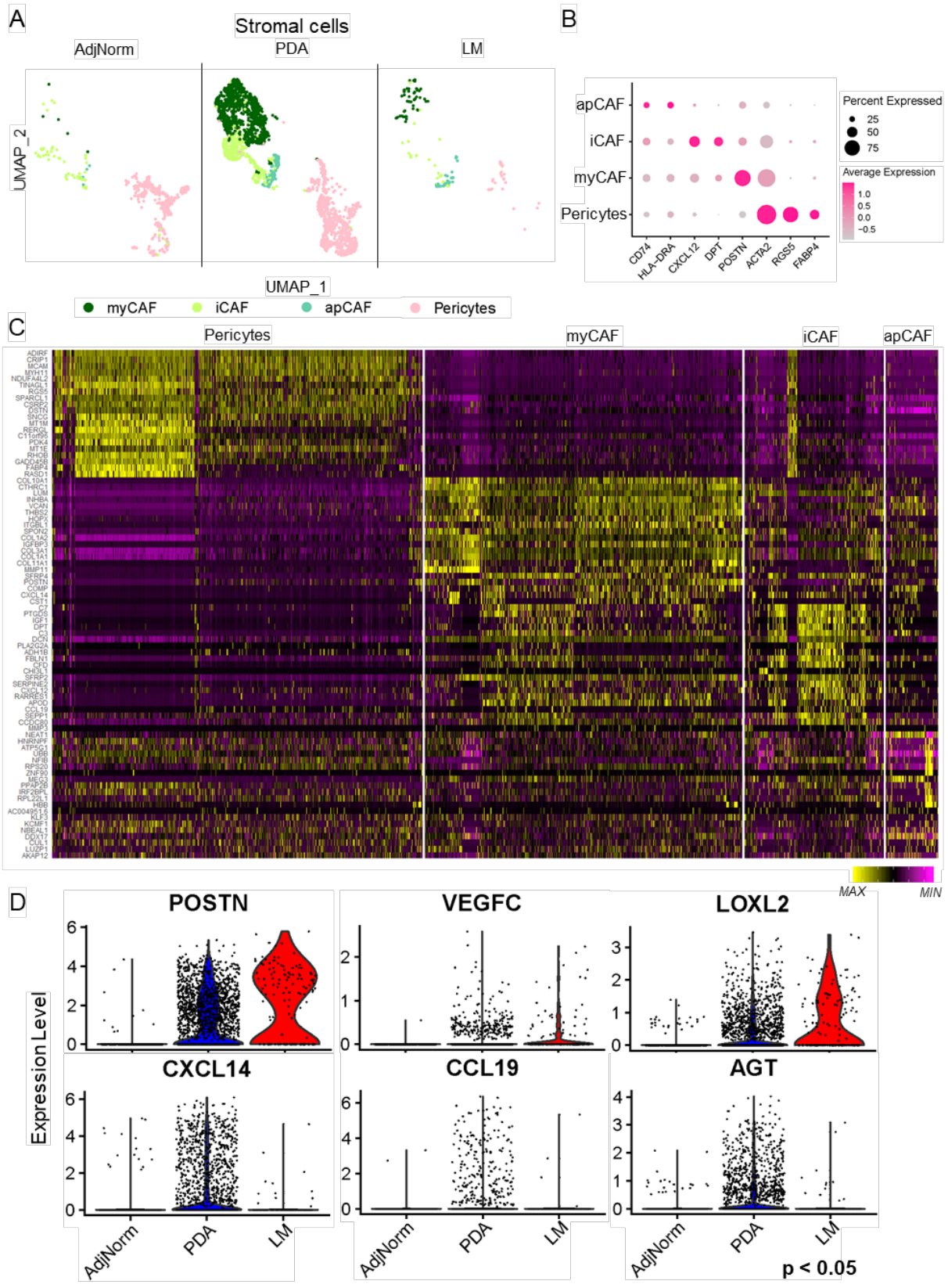
A
Stromal cells
AdjNorm
PDA
LM
UMAP_2
UMAP_1
myCAF
iCAF
apCAF
Pericytes
B
apCAF
iCAF
myCAF
Pericytes
CD74
HLA-DRA
CXCL12
DPT
POSTN
ACTA2
RGS5
FABP4
Percent Expressed
25
50
75
Average Expression
1.0
0.5
0.0
−0.5
C
Pericytes
myCAF
iCAF
apCAF
MAX
MIN
D
POSTN
VEGFC
LOXL2
CXCL14
CCL19
AGT
Expression Level
AdjNorm
PDA
LM
p < 0.05

Myeloid cells in PDA liver metastases upregulate pro-metastatic genes and express less immunomodulatory genes compared to primary PDA tumors

Myeloid cells demonstrate major immunosuppressive functions in the PDA TME. The myeloid cells found in the PDA TME are often polarized or recruited by the PDA tumor cells promote a more immunosuppressive phenotype. We sought out to characterize the myeloid populations in the LM TME and determine their polarization state and function. To define the cell populations, we processed the data as previously described and identified the fibroblast populations based on previously published markers (Elyada et al. 2019; N. G. Steele et al. 2020). We found granulocytes, macrophages, classical monocytes, and dendritic cells (DC) (Figure 3.3A and 3.3B). We then performed differential expression analysis of the four populations to confirm their identity based on expression of genes related to their previously reported functions in the PDA tumor. Granulocytes expressed previously reported markers such as FCGR3B and CXCR2 (Figure 3.3C). Macrophages expressed previously reported markers such as APOE as well as a multiple completement genes C1QB, C1QA (Figure 3.3C) (Samantha B. Kemp, Carpenter, et al. 2021; Samantha B Kemp, Steele, et al. 2021). Dendritic cells function as antigen presenting cells, and subsequently express many antigen presentation component genes such as HLA-DPB1, HLA-DPA1, HLA-DQA1 (Figure 3.3C). We next mapped immune checkpoint ligand expression with the various myeloid compartments. Some genes were more broadly expressed like HLA-DQA1, LGALS9, SIRPA, and CSF1R, while others were more specifically expressed like higher PVR in macrophages (Figure 3.3D). Next, we isolated the macrophage population to

determine the polarization status of the macrophage population. We found that the macrophages were extremely heterogenous in their expression, with some populations expressing high M1 pro-inflammatory markers such as HLA-DQB2 and IL2RA, while others expressing more M2 or TAM-associated markers such as MARCO and CCR2 (Figure 3.3E)[see review: (Martinez and Gordon 2014)](Elyada et al. 2019; N. G. Steele et al. 2020). We then performed differential expression analysis of the AdjNorm, PDA, and LM populations. We selected a few significantly (padj. > 0.05) differentially expressed genes to highlight potential differences between myeloid cells in the PDA and LM TMEs. We found that there was an increase in genes such as VCAN, CD52, CD36, S100A4, CD48, and CSF1R in the LM myeloid cells compared to PDA and AdjNorm (Figure 3.3F and Supplemental Figure 3.2A-B). These genes cover a wide array of functions related to metastasis, from anti-adhesion, to promotion and inhibition of angiogenesis, to both pro-inflammatory and anti-inflammatory functions [see reviews: (Wight et al. 2020; Rudnik et al. 2021; Febbraio, Hajjar, and Silverstein 2001; Helfman et al. 2005; Mcardel, Terhorst, and Sharpe 2016). There is a simultaneous decrease in expression of genes important in maintenance of immunosuppression in the primary PDA tumor, such as CD97, IL6R, CXCR2, SIRPA, and CSF3R [see review: (Safaee et al. 2013)]. The diversity and contradictory downstream functions of these genes demonstrate the need to better understand the LM TME to determine what the homeostatic phenotype of these antiparallel processes are.

Figure 3.3 Myeloid cells in liver metastases express levels of metastasis supportive genes

(A) UMAP on 3 adjacent/normal pancreas (left) and 16 PDA patient (middle) tissues and 5 LM patient (right) tissues. Populations identified as follows: macrophage (dark orange), monocyte (tan), granulocytes (orange), and dendritic cells (brown). (continued)

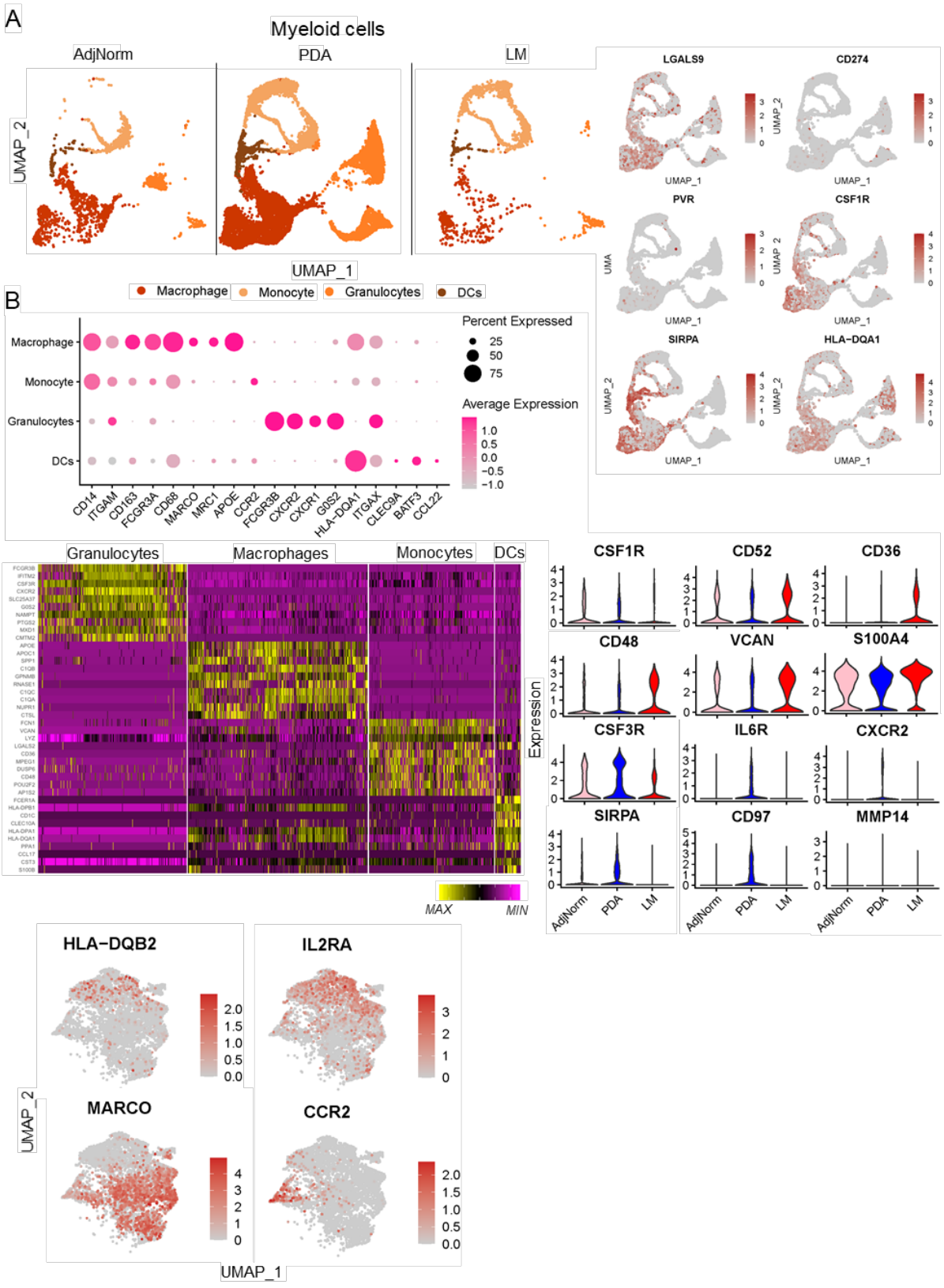
A
Myeloid cells
AdjNorm
PDA
LM
UMAP_2
UMAP_1
Macrophage
Monocyte
Granulocytes
DCs
LGALS9
CD274
PVR
CSF1R
SIRPA
HLA-DQA1
B
Percent Expressed
25
50
75
Average Expression
1.0
0.5
0.0
−0.5
−1.0
CD14
ITGAM
CD163
FCGR3A
CD68
MARCO
MRC1
APOE
CCR2
FCGR3B
CXCR2
CXCR1
G0S2
HLA-DQA1
ITGAX
CLEC9A
BATF3
COL22
Granulocytes
Macrophages
Monocytes
DCs
MAX
MIN
Expression
CSF1R
CD52
CD36
CD48
VCAN
S100A4
CSF3R
IL6R
CXCR2
SIRPA
CD97
MMP14
AdjNorm
PDA
LM
HLA-DQB2
IL2RA
MARCO
CCR2

(continued) **(B)** Dot plot of key markers used to define the identified cell populations. Color of dot represents average expression, while the size of the dot represents percent expression. Dot plot represents merged n=3 adj/norm patients and n=16 PDA patients and n=5 LM patients gene expression of lineage markers. **(C)** Single cell resolution heatmap analysis of top 20 genes for each identified fibroblast subset. **(D)** Selected feature plots of the immune checkpoints, *LGALS9*, *CD274*, *PVR*, *CSF1R*, *SIRPA*, *HLA-DQA1* in myeloid cells. **(E)** Selected feature plots of the macrophage polarization markers, *HLA-DQB2*, *IL2RA*, *MARCO*, and *CCR2* in macrophages. Panel of genes differentially expressed in myeloid cells that are up in **(F)** LM or in **(G)** PDA tissue. LM expression (red) is compared to PDA expression (blue) and adjacent/normal pancreas expression (black). Plots represent n=3 adj/norm and n=16 PDA patients and n=5 LM patients. Violin plots are shown as normalized expression. All violin plots in have an adjusted p-value of $p<0.05$ and are considered statistically significant.

CD8 T cells in PDA liver metastases demonstrate an exhausted phenotype

We have previously shown that CD8 T cells are present in the PDA TME, but that the majority of CD8 T cells present demonstrate an exhausted phenotype (N. G. Steele et al. 2020). We sought out to determine if the CD8 T cells in the LM TME demonstrated a similarly exhausted phenotype. To define the cell populations, we processed the data as previously described and determined the phenotype of the CD8 T cells based on expression of specific functional markers (Wherry et al. 2007; N. G. Steele et al. 2020). We discovered four CD8 T cell populations, the majority of which demonstrate and Effect or Exhausted phenotype (Figure 3.4A and 3.4B). We then performed differential expression analysis of the four populations to confirm their identity based on expression of genes related to their previously reported functions. As expected T_{eff} cells expressed genes like GZMB, the pro-apoptotic enzyme secreted by active CD8 T cells, while T_{ex} expressed genes related to exhaustion such as GZMK, EOMES, AND TIGIT (Figure 3.4C)(Wherry et al. 2007). We quantified the percentage of T cells we captured in our scRNA seq and found that there was a decrease in T_{eff} from AdjNorm to PDA and LM, and that there was a significant increase in T_{ex} between AdjNorm, PDA, and LM, with LM having the highest percentage of exhausted CD8 T cells (Figure 3.4D). We then performed differential expression analysis of the PDA, and LM populations. We selected

a few significantly (padj. > 0.05) differentially expressed genes to highlight potential differences between CD8 T cells in the PDA and LM TMEs. CD8 T cells in LM express a significantly higher amount of exhaustion genes than in the primary PDA tumor Figure 3.4E). Having identified and characterized many of the cell types present in the LM TME, we wanted to determine mechanisms these cell types could signal to each other.

Figure 3.4 CD8 T cells in liver metastases demonstrate an exhausted phenotype

(A) UMAP on 3 adjacent/normal pancreas (left) and 16 PDA patient (middle) tissues and 5 LM patient (right) tissues. Populations identified as follows: Naïve CD8 T cell (blue), T_{eff} (navy blue), T_{ex} (light blue), and $T_{mem/pec}$ (purple, bottom). **(B)** Selected feature plots of CD8 T cell phenotype markers, *GZMK*, and *EOMES*. **(C)** Single cell resolution heatmap analysis of top 6 genes for each CD8 T cell phenotype. **(D)** Quantitation of the percentage of CD8 T cell phenotypes (of total CD8 T cells) from scRNAseq of healthy, PDA, and LM patient tissue. Quantitation of data represent n=3 healthy, n=16 PDA, and n=5 LM patients. **(E)** Panel of genes differentially expressed in CD8 T cells that are up in LM tissue. LM expression (black) is compared to PDA expression (red). Plots represent n=16 PDA patients and n=5 LM patients. Violin plots are shown as normalized expression. All violin plots in have an adjusted p-value of $p<0.05$ and are considered statistically significant.

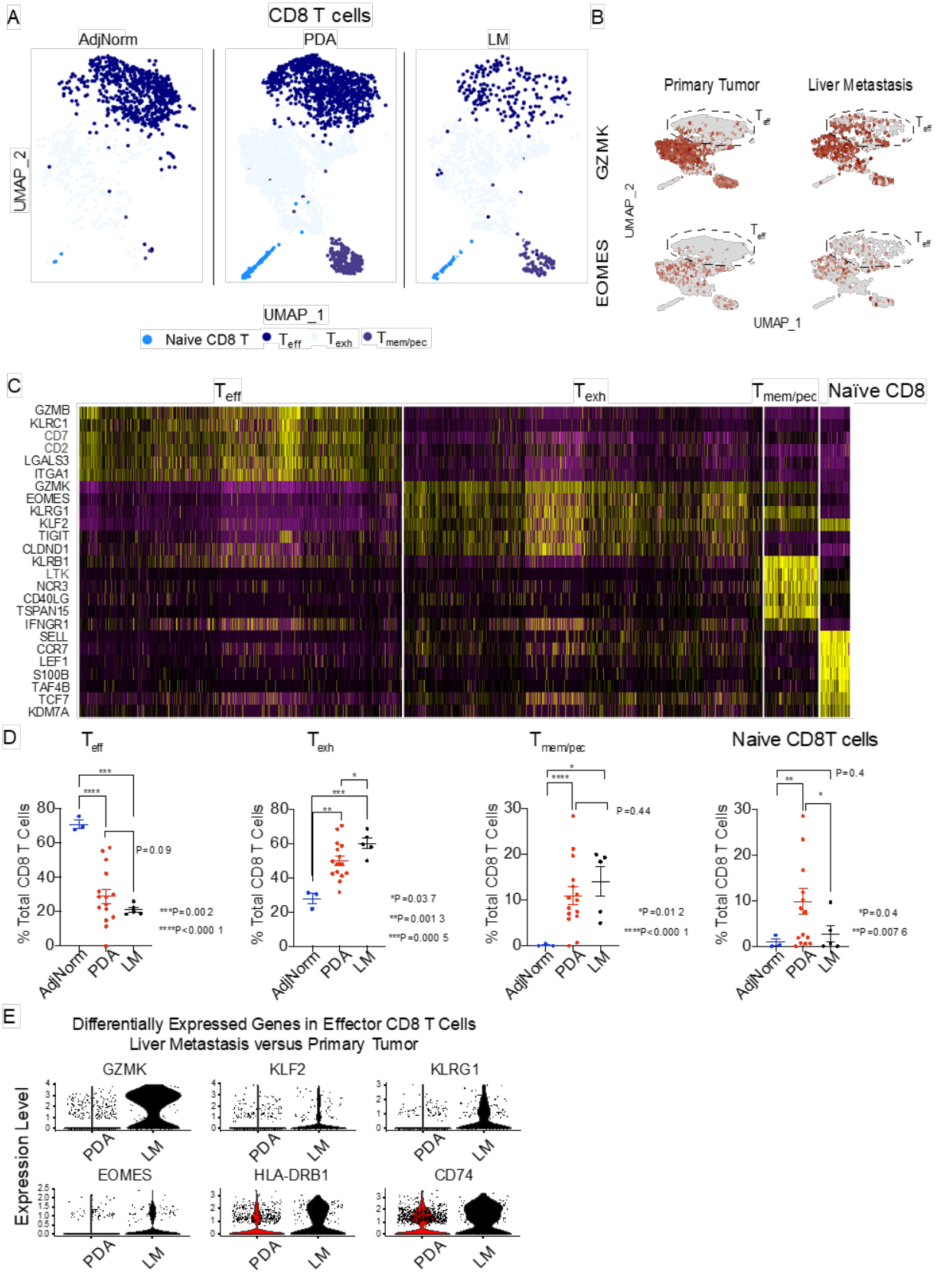
A
CD8 T cells
AdjNorm
PDA
LM
UMAP_2
UMAP_1
Naive CD8 T
T_eff
T_exh
T_mem/pec
B
Primary Tumor
Liver Metastasis
GZMK
EOMES
UMAP_2
UMAP_1
C
T_eff
T_exh
T_mem/pec
Naïve CD8
GZMB
KLRC1
CD7
CD2
LGALS3
ITGA1
GZMK
EOMES
KLRG1
KLF2
TIGIT
CLDND1
KLRB1
LTK
NCR3
CD40LG
TSPAN15
IFNGR1
SELL
CCR7
LEF1
S100B
TAF4B
TCF7
KDM7A
D
T_eff
T_exh
T_mem/pec
Naive CD8T cells
% Total CD8 T Cells
P=0.09
***P=0.002
****P<0.000 1
*P=0.03 7
**P=0.001 3
***P=0.000 5
P=0.44
*P=0.01 2
****P<0.000 1
P=0.4
*P=0.04
**P=0.007 6
AdjNorm
PDA
LM
E
Differentially Expressed Genes in Effector CD8 T Cells
Liver Metastasis versus Primary Tumor
GZMK
KLF2
KLRG1
EOMES
HLA-DRB1
CD74
Expression Level
PDA
LM

Predicted ligand receptor mapping shows immunosuppressive signaling networks upregulated in PDA liver metastases versus primary PDA tumors

To identify potential signaling between cell populations in the LM TME, we applied a predicted interaction algorithm based on known ligand-receptor (LR) pairs interacting with high affinity. We curated the list to specifically add immune checkpoints and limit the receptor-ligand pairs to cytokines, chemokines and specific signaling pathways [for a comprehensive list, see Supplemental Table 2.7]. We first plotted all the receptor-ligand interactions that were statistically higher in LM versus PDA samples, based on the level of ligand expression. Then we visualized connections between expressed ligands or receptors on a single cell type and their cognate binding partners on other cell types, filtering connections based on ligand and receptor expression. First, we visualized connections between epithelial cells and the major myeloid and lymphocytic subtypes, demonstrating putative inhibitory immune checkpoint signaling between epithelial PVR and TIGIT on CD8 T cells, or signaling that would promote immunosuppression such as recruitment of myeloid derived suppressor cells (MDSCs) through the IL-8:CXCR2 interaction from epithelial cells and granulocytes (Figure 3.5A). Next, we visualized putative signaling between macrophages and lymphocytes, with potential engagement of inhibitory immune checkpoints HLA-DQA1:LAG3 with CD8 and CD4 T cells and LGALS9:HAVCR2 with CD4 T cells (Figure 3.5B). Next, we looked at the interactions between the iCAF and myCAF populations and their interactions with myeloid cells. The two populations largely express the same ligands, but iCAFs exclusively express CCL20, IL33, TNFSF14, IL6, IL11, DLK1, CXCL5, CXCL3, CCL8,

and CCL5 while myCAFs exclusively express CX3CL1 and DLL1 (Figure 3.5C). Finally, we plotted CD8 T cell receptors versus the non-immune compartment, lymphocytes, and myeloid cell compartment to highlight the various potential mechanisms of immune suppression upregulated in the LM TME. TIGIT, PD-1, and LAG3 are all potentially engaged by multiple cell types in the LM TME (Figure 3.5D).

Figure 3.5 Predicted ligand receptor mapping shows putative signaling networks upregulated in liver metastases versus primary PDA tumors

(A) Circos plot map of all putative ligand receptor interactions that are upregulated in LM epithelial cells, **(B)** macrophages, **(C)** iCAFs and myCAFs compared to PDA and visualized by circos plot. **(D)** Circos plot map of all putative receptor ligand interactions that are upregulated in LM CD8 T cells. Plotted using the Circos software V0.69-9 (circos.ca). The heatmap within the circos plots is the scaled average expression of each gene within PDA tissue cell populations. The interactions plotted are those in which the expression level of either the ligand, the receptor, or both are increased in expression in LM samples compared to PDA.

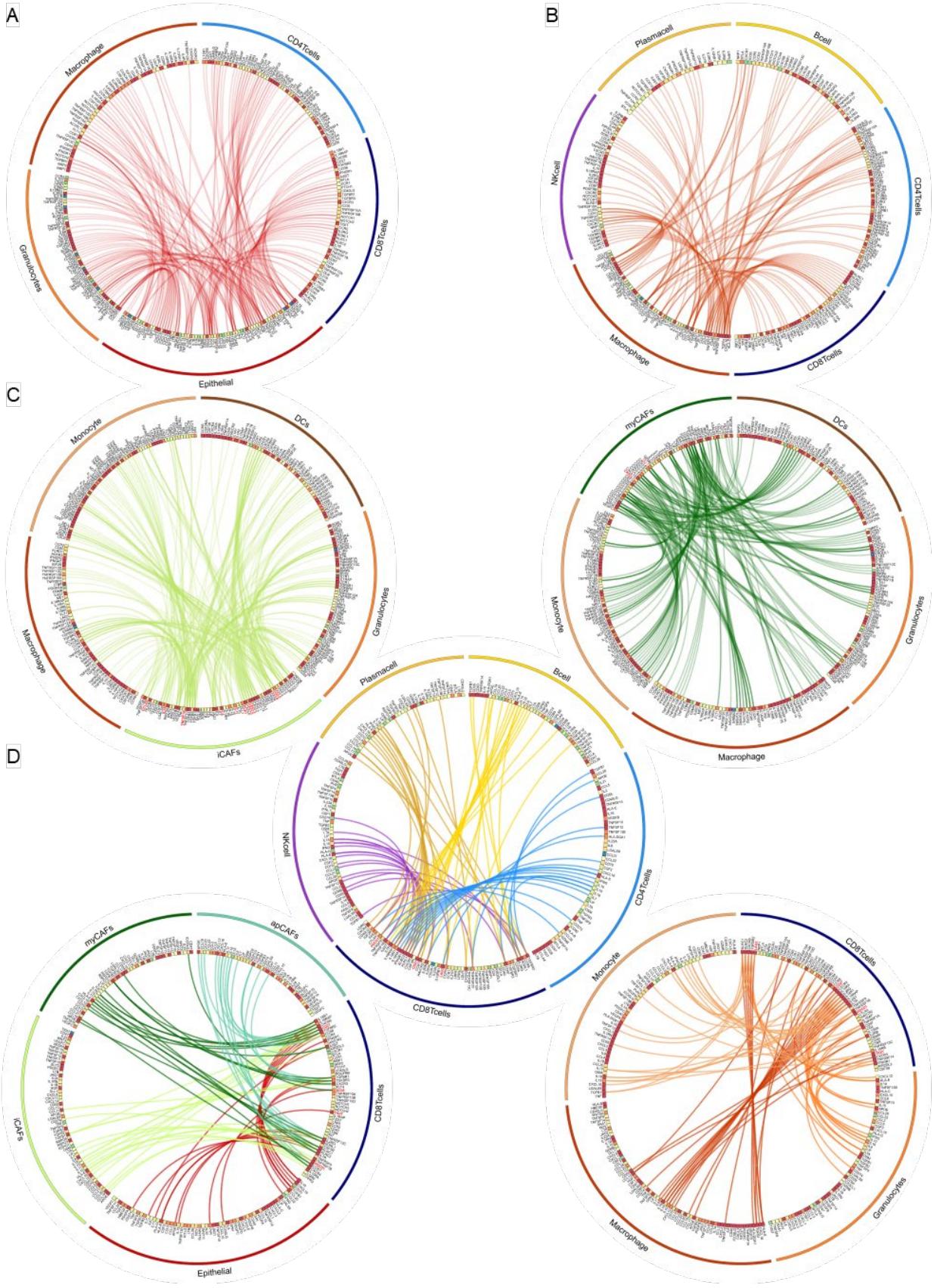
A
CD4Tcells
CD8Tcells
Epithelial
Granulocytes
Macrophage
B
Plasmacell
Bcell
CD4Tcells
CD8Tcells
Macrophage
NKcell
C
DCs
Granulocytes
iCAFs
Macrophage
Monocyte
myCAFs
DCs
Granulocytes
Macrophage
Monocyte
D
Plasmacell
Bcell
CD4Tcells
CD8Tcells
NKcell
myCAFs
apCAFs
CD8Tcells
Epithelial
iCAFs
CD8Tcells
Granulocytes
Macrophage
Monocyte

Discussion

This work represents the first step towards deeper understanding of the human LM TME. Most of the work previously done on the metastatic TME was done in metastatic mouse models of pancreas cancer. Previous studies of PDA metastasis were performed following rapid autopsy programs where the cell integrity would not have been high enough to perform single cell transcriptome studies, and mostly relied on bulk RNA sequencing of patient derived cell lines or protein-level analyses such as immunohistochemistry or proteomics (Yachida et al. 2010; Campbell et al. 2010; Law et al. 2020). The importance of being able to analyze PDA metastasis at this level cannot be understated. That being said, transcriptomic data is only the first step in validating the function of the various cell types detected. CD4 T cells, for example, are incredibly hard to subtype using scRNAseq data. In Supplemental Figure 4.3A, the grouped CD4 T cells demonstrate ligands for T_H1, T_H17, T_{reg}, and T_{FH} CD4 T cells. Proper identification of those subsets using flow cytometry or CyTOF are required in order to further complete this work. Protein-level verification is also necessary for any transcriptomic study, as there are many layers of regulation that occur after mRNA transcription that cannot be determined from a purely transcriptomic study. Even so, identification of potential pathways or genes of interest significantly narrow down the scope of work that needs to be done. Particularly interesting are the changes between the CAFs and myeloid cells between PDA and LM. First, protein level verification would be necessary to determine if the increased RNA-level expression results in increased protein expression. And if that is the case, culturing the fibroblasts or myeloid cells with media conditioned by a metastasis-derived PDA cell line vs a primary PDA cell could

determine if a secreted signaling from metastatic tumor cells is sufficient to increase expression of the protein of interest. If not, an overexpression vector can be knocked into an immortalized fibroblast cell line to determine the effect the upregulated protein has on the cell itself. If there is an increase in some cell signaling pathway, it would be interesting to co-culture the knock-in cells with primary PDA tumor cells and perform a motility/metastasis assay. This is just a hypothetical example of one way this data could be used. This major importance of this work is that it can be used to generate testable hypotheses that lead to translationally actionable targets.

Materials and methods

Study approvals

For human research, this study included a dataset that included patients over the age of 18 yr who received diagnostic endoscopic ultrasound for a suspected pancreas mass who were consented under the Institutional Review Board HUM00041280 (Two additional passes using a 22 Gauge SharkCore needle was performed for research once biopsy for clinical use was obtained). For surgically resected tissue, patients who underwent either Whipple of distal pancreatectomy were consented under Institutional Review Board HUM00025339. For liver metastasis samples, patients over the age of 18 referred for percutaneous liver biopsy of a mass suspected to be metastatic PDA were consented according to HUM00025339. Up to 2 extra biopsies were taken for research. All patients provided written consent and procedures and studies performed were carried out in accordance to ethical standards.

Single-cell RNA sequencing

Tissues were mechanically minced and enzymatically digested with collagenase P (1mg/mL DMEM) and subsequently filtered through a 40μm mesh to obtain single cells. Dead cells were removed using MACS® Dead Cell Removal Kit (Miltenyi Biotec Inc.). Single-cell cDNA libraries were prepared and sequenced at the University of Michigan Sequencing Core using the 10x Genomics Platform. Samples were run using paired end 50 cycle reads on HiSeq 4000 or the NovaSeq 6000 (Illumina) to a depth of 100,000 reads. The raw data were processed and aligned by the University of Michigan DNA Sequencing Core. Cellranger count version 3.0.0 with default settings was used, with an initial expected cell count of 10,000. In all cases the hg19 reference supplied with the cellranger software was used for alignment. R Studio V3.5.1 and R package Seurat version 3.0 was used for single cell RNA-seq data analysis similarly as previous described. Data were initially filtered to only include all cells with at least 200 genes and all genes in greater than 3 cells. Data were initially normalized using the NormalizeData function with a scale factor of 10,000 and the LogNormalize normalization method. Variable genes were identified using the FindVariableFeatures function. Data were assigned a cell cycle score using the CellCycleScoring function and a cell cycle difference was calculated by subtracting the S phase score from the G2M score. Data were scaled and centered using linear regression on the counts and the cell cycle score difference. PCA was run with the RunPCA function using the previously defined variable genes. Violin plots were then used to filter data according to user-defined criteria. All tissue samples were batch corrected through the R package Harmony V1.0 (https://github.com/immunogenomics/harmony). Harmony is a flexible multi-dataset integration algorithm for scRNA-seq by correcting the low-dimensional embedding of

cells from principal component analysis (PCA). It first uses soft clustering to find potential clusters, and then uses a soft k-means clustering algorithm to find clusters that favors the cells from multiple datasets and penalizes for any specified unwanted technical or biological factors. It then learns a simple linear adjustment function by computing cluster-specific linear correction factors, such as individual cell-types and cell state, from the cluster-specific centroids from each dataset. Each cell is weighted and corrected by its cell-specific linear factor. It then iterates the clustering and correction until the cell cluster assignments are stable. We used Harmony V1.0 to integrate our scRNA-seq patient data, correcting for individual scRNA-seq Run IDs (as each individual patient was each their own Run ID). Cell clusters were identified via the FindNeighbors and FindClusters function using a resolution of 1.2–2 for all samples and Uniform Manifold Approximation and Projection (UMAP) clustering algorithms were performed. FindAllMarkers table was created and clusters were defined by user-defined criteria. Code is publicly available on GitHub.com (https://github.com/PascaDiMagliano-Lab/MultimodalMappingPDA-scRNASeq).

Interactome

Ligand and receptor pairs were defined based off of a curated literature supported list in (Ramilowski et al. 2015). The average of expression of ligands and receptors (LR) in all the population for each group were calculated. LR pairs in each group (adjacent/normal and PDA) were determined to be expressed by setting the median average expression for all groups as a threshold. LR's above the threshold were considered as expressed in the group. LR pairs were then filtered out if the ligand and receptor in the LR pairs were not expressed in both groups. Differences of the LR's between groups were determined

using Wilcoxon ranked test, and p-values were adjusted for multiple comparisons with the Bonferroni correction method. LR's were considered significantly different if the $p < 1.0\times10^{-4}$. LR pairs were then sorted by the adjusted ligand expression p-value. The interactomes were visualized using the Circos software V0.69-9 and the heatmap values within the circos plots displays the average expression of each ligand/receptor within the PDA tissues (Krzywinski et al. 2009).

Statistics

GraphPad Prism V7 software was used for graphical representation and statistical analysis. Two-tailed Student's t-tests were performed. A $P < 0.05$ was considered statistically significant. Data are presented as means ± standard error (SEM). Differential expression analysis in single-cell RNA sequencing data was performed using Wilcoxon rank sum test, with adjusted P-values for multiple comparisons.

Acknowledgements

We would also like to thank Tricia Tamsen and Judy Opp from the University of Michigan Advanced Genomics Core. We would like to thank David Hill and Michael Czerwinski for their input on designing single cell analysis pipelines. We would like to thank the Tissue Procurement Center at the University of Michigan.

References

1. Aiello, Nicole M., David L. Bajor, Robert J. Norgard, Amine Sahmoud, Neha Bhagwat, Minh N. Pham, Toby C. Cornish, Christine A. Iacobuzio-Donahue, Robert H. Vonderheide, and Ben Z. Stanger. 2016. "Metastatic progression is associated with dynamic changes in the local microenvironment." Nature Communications 7 (1): 12819. https://doi.org/10.1038/ncomms12819. https://www.ncbi.nlm.nih.gov/pmc/articles/PMC5027614.
2. Biffi, G., and D. A. Tuveson. 2021. "Diversity and Biology of Cancer-Associated Fibroblasts." Physiol Rev 101 (1): 147-176. https://doi.org/10.1152/physrev.00048.2019. https://www.ncbi.nlm.nih.gov/pubmed/32466724.

3. Campbell, Peter J., Shinichi Yachida, Laura J. Mudie, Philip J. Stephens, Erin D. Pleasance, Lucy A. Stebbings, Laura A. Morsberger, Calli Latimer, Stuart Mclaren, Meng-Lay Lin, David J. Mcbride, Ignacio Varela, Serena A. Nik-Zainal, Catherine Leroy, Mingming Jia, Andrew Menzies, Adam P. Butler, Jon W. Teague, Constance A. Griffin, John Burton, Harold Swerdlow, Michael A. Quail, Michael R. Stratton, Christine Iacobuzio-Donahue, and P. Andrew Futreal. 2010. "The patterns and dynamics of genomic instability in metastatic pancreatic cancer." Nature 467 (7319): 1109-1113. https://doi.org/10.1038/nature09460. http://europepmc.org/articles/pmc3137369?pdf=render.
4. Elyada, Ela, Mohan Bolisetty, Pasquale Laise, William F. Flynn, Elise T. Courtois, Richard A. Burkhart, Jonathan A. Teinor, Pascal Belleau, Giulia Biffi, Matthew S. Lucito, Santhosh Sivajothi, Todd D. Armstrong, Dannielle D. Engle, Kenneth H. Yu, Yuan Hao, Christopher L. Wolfgang, Youngkyu Park, Jonathan Preall, Elizabeth M. Jaffee, Andrea Califano, Paul Robson, and David A. Tuveson. 2019. "Cross-Species Single-Cell Analysis of Pancreatic Ductal Adenocarcinoma Reveals Antigen-Presenting Cancer-Associated Fibroblasts." Cancer Discovery 9 (8): 1102-1123. https://doi.org/10.1158/2159-8290.cd-19-0094.
5. Febbraio, Maria, David P. Hajjar, and Roy L. Silverstein. 2001. "CD36: a class B scavenger receptor involved in angiogenesis, atherosclerosis, inflammation, and lipid metabolism." Journal of Clinical Investigation 108 (6): 785-791. https://doi.org/10.1172/jci14006.
6. Haeno, Hiroshi, Mithat Gonen, B. Davis, Meghan, M. Herman, Joseph, A. Iacobuzio-Donahue, Christine, and Franziska Michor. 2012. "Computational Modeling of Pancreatic Cancer Reveals Kinetics of Metastasis Suggesting Optimum Treatment Strategies." Cell 148 (1-2): 362-375. https://doi.org/10.1016/j.cell.2011.11.060. https://doi.org/10.1016/j.cell.2011.11.060.
7. Helfman, D M, E J Kim, E Lukanidin, and M Grigorian. 2005. "The metastasis associated protein S100A4: role in tumour progression and metastasis." British Journal of Cancer 92 (11): 1955-1958. https://doi.org/10.1038/sj.bjc.6602613. https://www.ncbi.nlm.nih.gov/pmc/articles/PMC2361793.
8. Kalluri, Raghu, and Robert A. Weinberg. 2009. "The basics of epithelial-mesenchymal transition." Journal of Clinical Investigation 119 (6): 1420-1428. https://doi.org/10.1172/jci39104.
9. Kemp, Samantha B, Nina G Steele, Eileen S Carpenter, Katelyn L Donahue, Grace G Bushnell, Aaron H Morris, Stephanie The, Sophia M Orbach, Veerin R Sirihorachai, Zeribe C Nwosu, Carlos Espinoza, Fatima Lima, Kristee Brown, Alexander A Girgis, Valerie Gunchick, Yaqing Zhang, Costas A Lyssiotis, Timothy L Frankel, Filip Bednar, Arvind Rao, Vaibhav Sahai, Lonnie D Shea, Howard C Crawford, and Marina Pasca Di Magliano. 2021. "Pancreatic cancer is marked by complement-high blood monocytes and tumor-associated macrophages." Life Science Alliance 4 (6): e202000935. https://doi.org/10.26508/lsa.202000935.
10. Kemp, Samantha B., Eileen S. Carpenter, Nina G. Steele, Katelyn L. Donahue, Zeribe C. Nwosu, Amanda Pacheco, Ashley Velez-Delgado, Rosa E. Menjivar, Fatima Lima, Stephanie The, Carlos E. Espinoza, Kristee Brown, Daniel Long, Costas A. Lyssiotis, Arvind Rao, Yaqing Zhang, Marina Pasca Di Magliano, and Howard C. Crawford. 2021. "Apolipoprotein E Promotes Immune Suppression in Pancreatic Cancer through NF-κB–Mediated Production of CXCL1." Cancer Research 81 (16): 4305-4318. https://doi.org/10.1158/0008-5472.can-20-3929.
11. Krzywinski, Martin, Jacqueline Schein, İnanç Birol, Joseph Connors, Randy Gascoyne, Doug Horsman, Steven J. Jones, and Marco A. Marra. 2009. "Circos: An information aesthetic for comparative genomics." Genome Research 19 (9): 1639-1645. https://doi.org/10.1101/gr.092759.109. http://genome.cshlp.org/content/19/9/1639.full.pdf.
12. Lambert, A. W., D. R. Pattabiraman, and R. A. Weinberg. 2017. "Emerging Biological Principles of Metastasis." Cell 168 (4): 670-691. https://doi.org/10.1016/j.cell.2016.11.037. https://www.ncbi.nlm.nih.gov/pubmed/28187288.
13. Law, Henry C.-H., Dragana Lagundžin, Emalie J. Clement, Fangfang Qiao, Zachary S. Wagner, Kimiko L. Krieger, Diane Costanzo-Garvey, Thomas C. Caffrey, Jean L. Grem, Dominick J. Dimaio, Paul M. Grandgenett, Leah M. Cook, Kurt W. Fisher, Fang Yu, Michael A. Hollingsworth, and Nicholas T. Woods. 2020. "The Proteomic Landscape of Pancreatic Ductal Adenocarcinoma Liver Metastases Identifies Molecular Subtypes and Associations with Clinical Response." Clinical Cancer Research 26 (5): 1065-1076. https://doi.org/10.1158/1078-0432.ccr-19-1496.

14. Martinez, Fernando O., and Siamon Gordon. 2014. "The M1 and M2 paradigm of macrophage activation: time for reassessment." F1000Prime Reports 6. https://doi.org/10.12703/p6-13.
15. Mcardel, Shannon L., Cox Terhorst, and Arlene H. Sharpe. 2016. "Roles of CD48 in regulating immunity and tolerance." Clinical Immunology 164: 10-20. https://doi.org/10.1016/j.clim.2016.01.008. https://www.ncbi.nlm.nih.gov/pmc/articles/PMC4860950.
16. Mizrahi, J. D., R. Surana, J. W. Valle, and R. T. Shroff. 2020. "Pancreatic cancer." Lancet 395 (10242): 2008-2020. https://doi.org/10.1016/S0140-6736(20)30974-0. https://www.ncbi.nlm.nih.gov/pubmed/32593337.
17. Ramilowski, Jordan A., Tatyana Goldberg, Jayson Harshbarger, Edda Kloppmann, Marina Lizio, Venkata P. Satagopam, Masayoshi Itoh, Hideya Kawaji, Piero Carninci, Burkhard Rost, and Alistair R. R. Forrest. 2015. "A draft network of ligand–receptor-mediated multicellular signalling in human." Nature Communications 6 (1): 7866. https://doi.org/10.1038/ncomms8866. https://www.nature.com/articles/ncomms8866.pdf.
18. Rhim, D., Andrew, T. Mirek, Emily, M. Aiello, Nicole, Anirban Maitra, M. Bailey, Jennifer, Florencia Mcallister, Maximilian Reichert, L. Beatty, Gregory, K. Rustgi, Anil, H. Vonderheide, Robert, D. Leach, Steven, and Z. Stanger, Ben. 2012. "EMT and Dissemination Precede Pancreatic Tumor Formation." Cell 148 (1-2): 349-361. https://doi.org/10.1016/j.cell.2011.11.025. https://www.ncbi.nlm.nih.gov/pmc/articles/PMC3266542.
19. Rudnik, Michał, Filip Rolski, Suzana Jordan, Tonja Mertelj, Mara Stellato, Oliver Distler, Przemysław Blyszczuk, and Gabriela Kania. 2021. "Regulation of Monocyte Adhesion and Type I Interferon Signaling by CD52 in Patients With Systemic Sclerosis." Arthritis & Rheumatology 73 (9): 1720-1730. https://doi.org/10.1002/art.41737.
20. Safaee, Michael, Aaron J. Clark, Michael E. Ivan, Michael C. Oh, Orin Bloch, Matthew Z. Sun, Taemin Oh, and Andrew T. Parsa. 2013. "CD97 is a multifunctional leukocyte receptor with distinct roles in human cancers." International Journal of Oncology 43 (5): 1343-1350. https://doi.org/10.3892/ijo.2013.2075. http://www.spandidos-publications.com/ijo/43/5/1343/download.
21. Siegel, Rebecca L., Kimberly D. Miller, Hannah E. Fuchs, and Ahmedin Jemal. 2021. "Cancer Statistics, 2021." CA: A Cancer Journal for Clinicians 71 (1): 7-33. https://doi.org/10.3322/caac.21654.
22. Steele, N. G., E. S. Carpenter, S. B. Kemp, V. Sirihorachai, S. The, L. Delrosario, J. Lazarus, E. D. Amir, V. Gunchick, C. Espinoza, S. Bell, L. Harris, F. Lima, V. Irizarry-Negron, D. Paglia, J. Macchia, A. K. Y. Chu, H. Schofield, E. J. Wamsteker, R. Kwon, A. Schulman, A. Prabhu, R. Law, A. Sondhi, J. Yu, A. Patel, K. Donahue, H. Nathan, C. Cho, M. A. Anderson, V. Sahai, C. A. Lyssiotis, W. Zou, B. L. Allen, A. Rao, H. C. Crawford, F. Bednar, T. L. Frankel, and M. Pasca di Magliano. 2020. "Multimodal Mapping of the Tumor and Peripheral Blood Immune Landscape in Human Pancreatic Cancer." Nat Cancer 1 (11): 1097-1112. https://doi.org/10.1038/s43018-020-00121-4. https://www.ncbi.nlm.nih.gov/pubmed/34296197.
23. Steele, Nina G., Giulia Biffi, Samantha B. Kemp, Yaqing Zhang, Donovan Drouillard, Lijyun Syu, Yuan Hao, Tobiloba E. Oni, Erin Brosnan, Ela Elyada, Abhishek Doshi, Christa Hansma, Carlos Espinoza, Ahmed Abbas, Stephanie The, Valerie Irizarry-Negron, Christopher J. Halbrook, Nicole E. Franks, Megan T. Hoffman, Kristee Brown, Eileen S. Carpenter, Zeribe C. Nwosu, Craig Johnson, Fatima Lima, Michelle A. Anderson, Youngkyu Park, Howard C. Crawford, Costas A. Lyssiotis, Timothy L. Frankel, Arvind Rao, Filip Bednar, Andrzej A. Dlugosz, Jonathan B. Preall, David A. Tuveson, Benjamin L. Allen, and Marina Pasca Di Magliano. 2021. "Inhibition of Hedgehog Signaling Alters Fibroblast Composition in Pancreatic Cancer." Clinical Cancer Research 27 (7): 2023-2037. https://doi.org/10.1158/1078-0432.ccr-20-3715.
24. Stein, Matthew K., Manjari Pandey, Joanne Xiu, Hongseok Tae, Jeff Swensen, Sandeep Mittal, Andrew J. Brenner, W. Michael Korn, Amy B. Heimberger, and Mike G. Martin. 2019. "Tumor Mutational Burden Is Site Specific in Non–Small-Cell Lung Cancer and Is Highest in Lung Adenocarcinoma Brain Metastases." JCO Precision Oncology (3): 1-13. https://doi.org/10.1200/po.18.00376.
25. Wang, Shun, Yan Zheng, Feng Yang, Le Zhu, Xiao-Qiang Zhu, Zhe-Fang Wang, Xiao-Lin Wu, Cheng-Hui Zhou, Jia-Yan Yan, Bei-Yuan Hu, Bo Kong, De-Liang Fu, Christiane Bruns, Yue Zhao,

Lun-Xiu Qin, and Qiong-Zhu Dong. 2021. "The molecular biology of pancreatic adenocarcinoma: translational challenges and clinical perspectives." Signal Transduction and Targeted Therapy 6 (1). https://doi.org/10.1038/s41392-021-00659-4.
26. Welch, Danny R., and Douglas R. Hurst. 2019. "Defining the Hallmarks of Metastasis." Cancer Research 79 (12): 3011-3027. https://doi.org/10.1158/0008-5472.can-19-0458.
27. Wherry, E. J., S. J. Ha, S. M. Kaech, W. N. Haining, S. Sarkar, V. Kalia, S. Subramaniam, J. N. Blattman, D. L. Barber, and R. Ahmed. 2007. "Molecular signature of CD8+ T cell exhaustion during chronic viral infection." Immunity 27 (4): 670-84. https://doi.org/10.1016/j.immuni.2007.09.006. https://www.ncbi.nlm.nih.gov/pubmed/17950003.
28. Wight, T. N., I. Kang, S. P. Evanko, I. A. Harten, M. Y. Chang, O. M. T. Pearce, C. E. Allen, and C. W. Frevert. 2020. "Versican-A Critical Extracellular Matrix Regulator of Immunity and Inflammation." Front Immunol 11: 512. https://doi.org/10.3389/fimmu.2020.00512. https://www.ncbi.nlm.nih.gov/pubmed/32265939.
29. Yachida, Shinichi, Siân Jones, Ivana Bozic, Tibor Antal, Rebecca Leary, Baojin Fu, Mihoko Kamiyama, Ralph H. Hruban, James R. Eshleman, Martin A. Nowak, Victor E. Velculescu, Kenneth W. Kinzler, Bert Vogelstein, and Christine A. Iacobuzio-Donahue. 2010. "Distant metastasis occurs late during the genetic evolution of pancreatic cancer." Nature 467 (7319): 1114-1117. https://doi.org/10.1038/nature09515. https://www.ncbi.nlm.nih.gov/pmc/articles/PMC3148940.
30. Zheng, Xiaofeng, Julienne L. Carstens, Jiha Kim, Matthew Scheible, Judith Kaye, Hikaru Sugimoto, Chia-Chin Wu, Valerie S. Lebleu, and Raghu Kalluri. 2015. "Epithelial-to-mesenchymal transition is dispensable for metastasis but induces chemoresistance in pancreatic cancer." Nature 527 (7579): 525-530. https://doi.org/10.1038/nature16064. https://www.ncbi.nlm.nih.gov/pmc/articles/PMC4849281.

Chapter 4: Comparisons of the L-iKras and P-iKras Mouse Models Demonstrate the Effects of KRAS^{G12D} Inhibition on the Primary and Premetastatic TME

Summary

Oncogenic Kras is a frequently mutated driver of cancer, including PDA and lung cancer. Creating drugs inhibiting the function of oncogenic KRAS is difficult and prone to the development of resistance. Our lab has previously generated and characterized the iKras model of PDA, a mouse model that allows for inducible, reversible expression of KRAS^{G12D}. This model demonstrated how dependent PDA is on oncogenic KRAS^{G12D} expression, as withdrawal of the oncogene results in tumor shrinking and can result in complete reversion to healthy pancreas. However, this model also demonstrated that withdrawal of KRAS^{G12D} does not lead to complete tumor clearance and that residual tumor cells can reactivate Kras signaling independently of induced expression, leading to tumor relapse. The iKras mouse model gives both a hopeful glimpse at the benefits of Kras inhibition, with the sobering reminder of how short lived those successes can be when evolutionary pressure is combined with high proliferation and high mutation rate. One potential mechanism of circumventing resistance to Kras inhibition is the co-activation of an effective anti-tumor immune response. The adaptive immune system can systemically detect and kill any recognized tumor cells. Unfortunately, one of the functions of oncogenic Kras is the generation of an immunosuppressive TME. Work in our lab has previously described the immunosuppressive TME in primary tumors and in

liver metastases. Here, we generate an inducible, reversible mouse model of lung cancer to model the progression, regression, and relapse of $Kras^{G12D}$ driven tumors. Firstly, we characterize the lung iKras mouse model and analyze the immune infiltration upon oncogenic Kras expression and withdrawal. We compare the changes in the LC TME caused by local KRAS modulation to changes in the immune population caused by distal KRAS modulation using the P-iKras model. Finally, we compared the immune infiltration of the LC TME during initial tumor progression to the immune infiltration during tumor relapse. By characterizing and comparing these two models, we hope to better understand the mechanisms of immune suppression promoted by both local and distal oncogenic KRAS as well as during primary tumor growth and relapse to determine which treatment regimens will need to be combined to eradicate tumors and metastasis, and what second-line treatments could be used upon the development of resistance.

Introduction

The mutational landscape of solid tumors has been described as a landscape made up of few mountains amongst multiple lower lying hills (Jones et al. 2008; Wood et al. 2007). The mountains represent the most frequently genes, typically the main oncogenic driver of the cancer, while the hills represent other genes important for progression that can vary due to pathway or functional redundancy, such as tumor suppressors. This is especially true for pancreatic cancer, where *KRAS* is the most mutated the gene, with the second most common mutations being a host of various tumor suppressor genes such *TP53*, *SMAD4*, and *CDKN2A* (Waddell et al. 2015). It was previously thought that KRAS was undruggable, but given its prevalence in multiple cancers, a massive effort was put towards making the undruggable druggable. Inhibitors

were designed against pathways downstream of KRAS, against the upstream mechanisms required for KRAS localization and signal transduction, and against KRAS itself. Some indirect inhibitors of KRAS were efficacious in certain contexts, with PI3K and MAPK inhibitors being commonly used. It was only recently that a direct inhibitor of KRAS was developed, and it is now FDA approved for treatment of Non-small cell lung cancer (NSCLC). However, this inhibitor only targets one specific point mutation encoding $KRAS^{G12C}$. There are multiple mutational hotspots on KRAS that can result in oncogenic activation. The codon 12 hotspot is the most frequently mutated codon on KRAS, with many of those point mutations able to drive cancer progression. $KRAS^{G12C}$ is the most frequently mutated isoform of oncogenic KRAS in NSCLC, but even so the majority of NSCLC tumors are driven by non- $KRAS^{G12C}$ isoforms (Cox et al. 2014). Another one of the major mutant isoforms of KRAS that can drive NSCLC is $KRAS^{G12D}$, which also drives most PDA tumors. Unlike $KRAS^{G12C}$, $KRAS^{G12D}$ does not have an available inhibitor. It is important, then, to understand the biology of oncogenic KRAS, to develop strategies against the specific oncogenic properties of KRAS in lieu of a direct inhibitor.

Activation of KRAS is the first step in multiple signaling pathways. KRAS normally exists in an inactive state, but upon extracellular stimulation, KRAS becomes activated, promoting the phosphorylation of downstream pathways. Oncogenic KRAS mutations abrogate the need for the activation step, resulting in constitutive activation of KRAS signaling. Two of the most well-described downstream targets of KRAS signaling are the MAPK and PI3K signaling pathways. In the context of the MAPK signaling cascade, activated KRAS promotes dimerization and phosphorylation of RAF kinase.

Activated RAF can then phosphorylate downstream kinase MEK, which continues a kinase cascade that ultimately promotes cellular growth and proliferation. In the context of PI3K signaling, activated Kras promotes the formation of the PI3K complex, which phosphorylates plasma membrane lipids that result in the colocalization of kinases such as PDPK1 and AKT. AKT is then phosphorylated and becomes active, potentially activating multiple downstream targets involved in promoting survival and inhibiting apoptosis, proliferation, or cell migration. There have been inhibitors developed for these downstream targets, with multiple MEK and PI3K inhibitors (MEKi and PI3Ki) approved for use in the treatment of many cancers. While these inhibitors can be extremely efficacious, there are multiple mechanisms of resistance that can occur. The target proteins can mutate and prevent functional drug binding, non-classical pathway activation may occur, or another signaling pathway may become upregulated as a compensatory mechanism. For example, the YAP/HIPPO signaling pathway can function as a mechanism of escape from in primary PDA tumors (Kapoor et al. 2014). Development of mechanisms of resistance are common in any therapy, but when the mechanism that is being targeted is as adaptive as the evolutionary pressure exerted by a tumor, there is a greater possibility of success.

Reactivation of the immune system against tumors through immunotherapy can be used as a parallel treatment modality to targeting signaling pathways. Oncogene addiction refers to the dependency tumor cells have on the pro-growth, pro-survival signals derived from the driving oncogene. The mutational burden and/or metabolic stress that tumor cells experience would normally trigger any number of cell death pathways in cells that were not actively inhibiting cell death pathways and upregulating

survival pathways. Effective blocking of oncogenic signaling will result in the death of tumor cells. The death of tumor cells is always something to be celebrated, but this is especially true when there is an active immune response. Cell death triggers an immune response, prompting immune surveillance and clearance of dead tissue by phagocytes. This presents a great window of opportunity for development of an anti-tumor immune response, as the phagocytosed tumor cells can lead to the detection and presentation of tumor neo-antigens which can be used to educate T cells to mount a productive T cell response. However, this concept is predicated on the assumption that the immune system can function properly in the TME. Unfortunately, it is known that oncogenic KRAS signaling promotes an immunosuppressive TME. Previous work in the lab has been done to characterize immunosuppression in human PDA, both at the level of the primary tumor and again within liver metastases (Steele et al. 2020). Both studies were carried out using established tumors, allowing for a comprehensive analysis of established tumors, but are not able to demonstrate the development of the immunosuppressive TME and what role KRAS has in promoting it.

The iKras mouse model accurately models the progression of PDA development and allows us to mimic the effect of KRAS inhibition on the PDA TME. Our lab developed an inducible, reversible model of $Kras^{G12D}$ driven PDA (Collins, Brisset, et al. 2012; Collins, Bednar, et al. 2012). Using this model, we found that PDA tumor cells are dependent on oncogenic KRAS for survival and progression, and that upon KRAS withdrawal PanINs regress back to normal pancreatic tissue, and established tumors significantly shrunk. Additionally, we found that oncogenic KRAS is similarly required in the development and maintenance of the immunosuppressive microenvironment. This

was most apparent when we compared the regression of PanIN lesions from mice pancreata after 3 versus 5 weeks of oncogenic Kras expression. After 3 weeks of oncogenic KRAS expression, the pancreas was able to almost fully recover, but after 5 weeks of oncogenic KRAS expression, a significant number of PanIN lesions remained after KRAS withdrawal, demonstrating that mechanisms against KRAS loss were already established in pre-invasive lesions. Having established the local effects KRAS has on the TME, we next wanted to understand the distal effects KRAS can impart on the microenvironment of the pre-metastatic niche.

It is known that certain cancers preferentially metastasize to certain locations. For PDA, those sites are the liver, peritoneum, and lung. This phenomenon has been described as the “seed and soil” hypothesis, that certain distal tissues are more amenable to supporting the growth of a metastasis than other tissues. Whether this preference is due to ease of migration or due to favorable growth conditions is context and cancer specific. There is a large body of evidence, however, that shows that this preference is not entirely passive on the part of the primary tumor. Rather, there is active, distant remodeling of the microenvironment by the primary tumor, preparing the distant site for metastatic colonization. We can use the iKras model to detect distal remodeling of the pre-metastatic niche, but lung metastases in the iKras model are infrequent. While we lack a reliable model of lung metastasis, we hypothesized that local expression of oncogenic Kras from cells in the lung may demonstrate a similar effect to local expression of oncogenic Kras from metastasized pancreas cells in the lung. To this end, we generated a mouse model of lung cancer (LC) in the same vein as the iKras mouse model of PDA.

There was a previously developed lung cancer iKras (L-iKras) model that demonstrated progression and regression of LC upon expression of oncogenic $KRAS^{G12D}$(Fisher et al. 2001). Similarly to the PDA iKras (P-iKras) model, expression of $Kras^{G12D}$ is driven by doxycycline-induced binding of rtTA to the Tet operon upstream of $Kras^{G12D}$. rtTA expression controlled by the CCSP promoter, a lineage marker of one of the cells of origin for LC (Jackson et al. 2001; Kim et al. 2005). Activation of oncogenic KRAS in the lung results in the infiltration of largely immunosuppressive immune cells (Ji et al. 2006; Lavin et al. 2017; Seo et al. 2018). Unlike the PDA iKras (P-iKras) model, there was almost complete regression to normal lung tissue regardless of the length of oncogenic KRAS expression. This is not unexpected, as the pancreas and lung have different functions and subsequently experience different levels of immune surveillance. The lung is a barrier organ while the pancreas is an internal secretory organ, so the removal of immune suppression in the lung has greater potential for anti-tumor immune activity. Yet, despite this immune presence, the expression of oncogenic KRAS locally and distally is sufficient to suppress an anti-tumor immune response that allows primary tumors to grow and metastases to seed.

The aim of this work is to use the L-iKras and P-iKras models in tandem to understand the microenvironmental remodeling by KRAS in the lung, using the two models to dissect the local and distal effects of oncogenic KRAS on the lung microenvironment both during tumor progression as well as upon KRAS withdrawal. The goal of this study is to understand the tissue specific effects of KRAS in the primary tumor and the mechanisms of distal remodeling in lung metastases. By understanding the mechanisms of KRAS driven immunosuppression on a local and distal level, we can

find strategies to reverse the immunosuppression and promote clearance of both primary and metastatic tumors.

Results

The L-iKras model demonstrates the requirement of oncogenic Kras^{G12D} in the maintenance of LC tumors

We generated the L-iKras mouse model by crossing CCSP-rtTA mice with TetO-*Kras*^{G12D} mice, resulting in double transgenic CCSP-rtTA;TetO- *Kras*^{G12D} L-iKras mice (Figure 4.1A). Additionally, we crossed in L-iKras mice with an LSL-*p53*^{R172H} cassette inserted into the endogenous *p53* locus, allowing for expression of mutant p53 upon treatment with Adenoviral Cre (AdCre) (details in Materials and Methods). The CCSP-rtTA cassette results in expression of rtTA in club cells (formerly known as Clara cells), one of the possible cells-of-origin for LC. rtTA remains inactive in the cell until doxycycline is supplied. Doxycycline activates the rtTA, which can then bind the Tet operon and initiate transcription of *Kras*^{G12D}. This transcription can be reversed upon doxycycline withdrawal from supplying the mice with regular water. We had generated

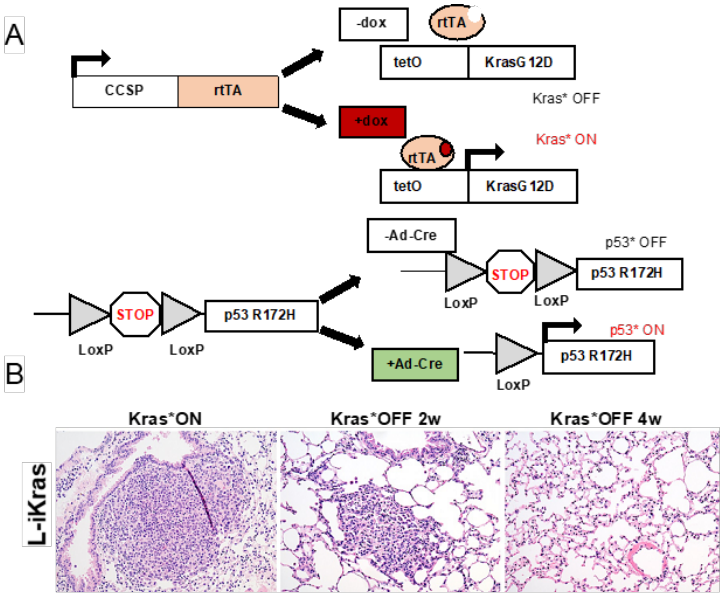

Figure 4.1 The L-iKras mouse demonstrates Kras dependent tumor progress and maintenance

(A) The genetic makeup of the L-iKras mouse model of lung tumorigenesis with CCSP-rtTA;TetO-*Kras*^{G12D};*LSL-p53*^{R172H}. **(B)** H&E staining of L-iKras murine lung after 20W treatment with doxycycline or with removal of doxycycline at indicated time points.

the P-iKras;LSL-*p53*^{R172H} as previously described (Supplemental Figure 4.1A and 4.1B) (Collins, Brisset, et al. 2012; Collins, Bednar, et al. 2012).

Next, we wanted to verify that the L-iKras model produced tumors in the lung as effectively as the previously described inducible model of *Kras*^{G12D} driven LC. We used single transgenic mice containing only the CCSP-rtTA or TetO- *Kras*^{G12D} cassette to confirm that doxycycline administration, expression of rtTA, and treatment with AdCre did not confer a noticeable phenotype to the mouse lungs. Additionally, we harvested the lungs of triple transgenic mice without doxycycline or AdCre to confirm that there was no aberrant expression of KRAS^{G12D} or p53^{R172H} without the administration of doxycycline or AdCre. Neither condition demonstrated a significant phenotype in the lung. We administered doxycycline and/or AdCre to a cohort of mice and generated a survival curve (Supplemental Figure 4.1C). Multiple LC lesions were observed in L-iKras mice after 20 weeks of doxycycline treatment regardless of p53 status (Figure 4.1B left panel). As previously reported, withdrawal of doxycycline resulted in smaller tumors, with most tumors completely cleared one month after withdrawal of doxycycline (Figure 4.1B middle and left panels). Having phenotypically confirmed the function of the L-iKras;p53 model, we next sought to understand the changes that occur in the TME during progression and regression of the LC tumor.

<u>Local expression of oncogenic Kras in the L-iKras mouse model effects a change in the LC TME</u>

We performed OPAL multiplex fluorescent immunohistochemistry (mfIHC) to understand the composition and spatial dynamics of the immune infiltration in L-iKras

mice upon modulation of KRAS expression. The ON context describes when L-iKras mice are treated with doxycycline until the treatment endpoint. The ON/OFF context describes when mice are initially given doxycycline until 20-24 weeks to allow for tumors to develop and are then taken off doxycycline for varying timepoints, allowing for tumors to regress or clear. We performed mfIHC with markers of epithelium (CK19), macrophages (F4/80), alternatively activated macrophages (ARG1), and CD8 T cells (CD3 and CD8) (details in Materials and Methods) (Figure 4.2A). One caveat to the data is that CK19 is also present on certain types of cells already present in the lung, so images were selected by their histological appearance rather than through more unbiased methods. Tumors were identified by their dense, disorganized mass of $CK19^{+}$ cells versus the typically more spacious alveolar structures that make up the lung. However, it was not uncommon for an atypical structure such as a pinched bronchiole or tertiary lymphoid structure to be mistaken for a tumor lesion. Nonetheless, most of the images selected appeared to be LC tumors that were cleared after withdrawal of $KRAS^{G12D}$, as expected. (Figure 4.2B). Next, we analyzed the population data that came from the phenotype maps. The presence of $F4/80^{+}$ macrophages was decreased upon withdrawal of Kras compared to the percentage of macrophages in (Figure 4.2C). While there was no significant change in the total number of T cells in the presence of $KRAS^{G12D}$, there was a surprising decrease in the percentage of CD8 T cells present after $KRAS^{G12D}$ withdrawal (Figure 4.2D). The advantage of mfIHC is the ability to use the phenotype mapping to generate spatial data. We computed two parameters, engagement and mean distance (Supplemental Figure 4.2A). While there were no significant changes in mean distance between both CD8 T cells and epithelial cells or

macrophages, there was an observed decrease in engagement (Figure 4.2E and Supplemental Figure 4.2C). This data paints a very contradictory picture of T cell presence and function in the presence of $KRAS^{G12D}$ in the L-iKras TME. T cells appear to be both present and engaged with tumor cells while simultaneously failing to initiate a productive tumor response. To explore this contradiction further, the exhaustion status of these T cells needs to be characterized.

Figure 4.2 mfIHC reveals changes in the lung TME upon modulation of oncogenic KRAS
(A) The OPAL mfIHC pipeline, using a tertiary lymphoid structure as example staining and phenotype mapping. **(B)** mfIHC composite images of formalin-fixed paraffin-embedded lung samples from L-iKras mice treated with doxycycline for 17w and removed from doxycycline for the indicated timepoints. Antibodies and colors are as followed: CK19 (teal), F4/80 (magenta), ARG1 (orange), CD3 (green), CD8 (yellow) and DAPI (blue). **(C)** Comparison of the macrophage composition between triplicate pictures of n=3 ON mice and triplicate pictures of n=1 ON/OFF mice per timepoint. **(D)** Comparison of the T cell composition between triplicate pictures of n=3 ON mice and triplicate pictures of n=3 ON/OFF mice **(E)** Comparison of the %CTL-Mac and %CTL-Epithelial engagement. Asterisk denotes a p-value less than 0.05, 2 asterisks denote less than 0.001, determined by Two-way ANOVA.

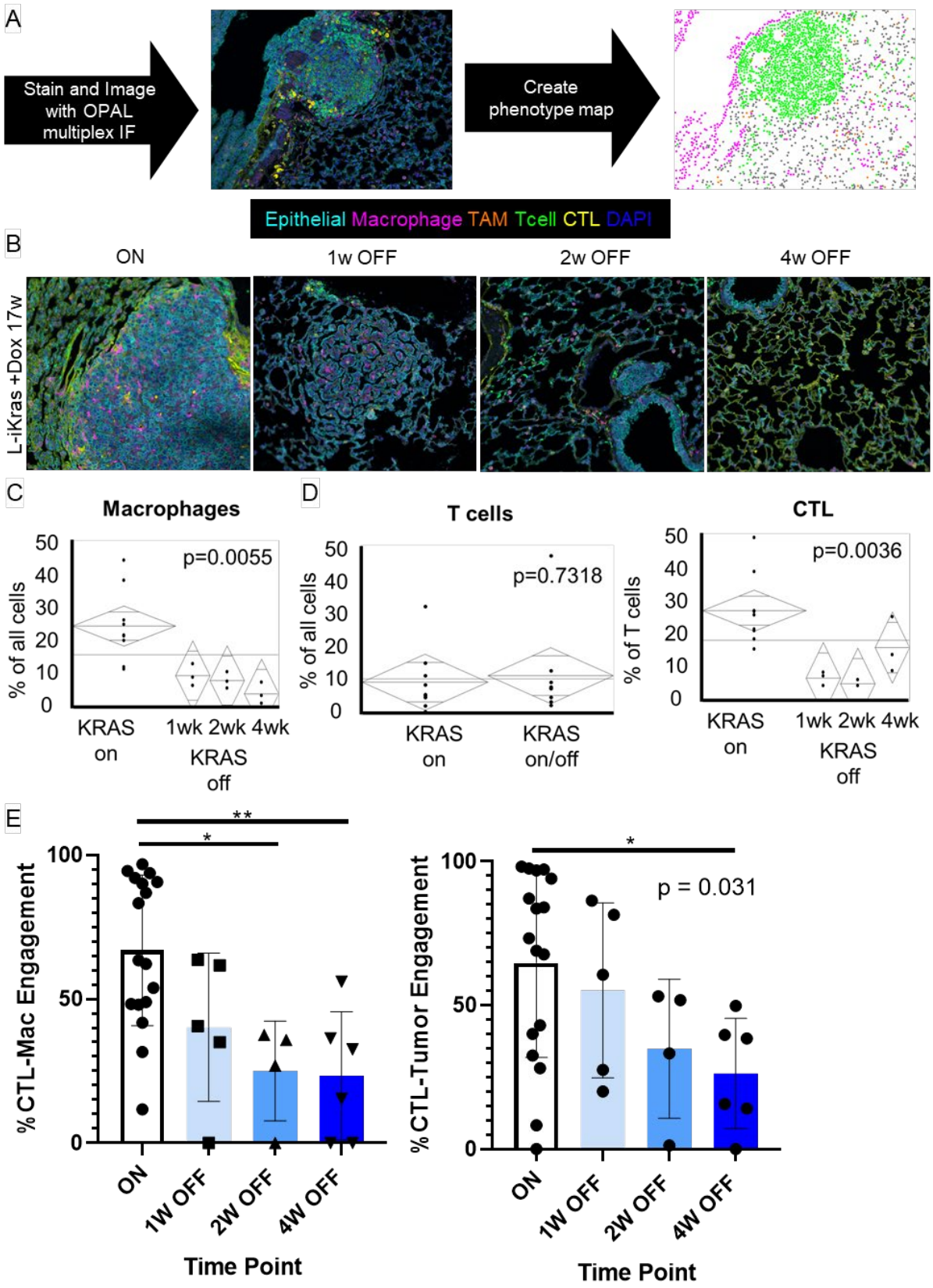
A
Stain and Image with OPAL multiplex IF
Create phenotype map
Epithelial Macrophage TAM Tcell CTL DAPI
B
ON
1w OFF
2w OFF
4w OFF
L-iKras +Dox 17w
C
Macrophages
% of all cells
p=0.0055
KRAS on
1wk 2wk 4wk KRAS off
D
T cells
% of all cells
p=0.7318
KRAS on
KRAS on/off
CTL
% of T cells
p=0.0036
KRAS on
1wk 2wk 4wk KRAS off
E
% CTL-Mac Engagement
**
*
ON
1W OFF
2W OFF
4W OFF
Time Point
% CTL-Tumor Engagement
*
p = 0.031
ON
1W OFF
2W OFF
4W OFF
Time Point

Models of L-iKras tumor relapse demonstrate different immune composition to initial tumor growth

We performed mass cytometry (cyTOF) of L-iKras lungs in different contexts of tumor growth. After 4 weeks, the mice are put back on doxycycline, representing a tumor relapse caused by resistance to oncogene inactivation. We compared both groups to untreated, triple transgenic control or to doxycycline treated single transgenic mice. First, we performed H&E staining to confirm the presence of lesions in the ON and ON/OFF/ON context and no lesions in the control and low or small lesions in the ON/OFF context. Then we performed cyTOF on the lungs and analyzed the immune populations present in the ON and ON/OFF/ON context compared to the controls. There was a striking increase in the myeloid derived suppressor cell (MDSC) population between the ON group and the controls (Figure 4.3B). MDSCs are immunosuppressive myeloid cells characterized by dual expression of LY6G and LY6C. This increase was not observed in the ON/OFF/ON cohort, which did not demonstrate an increase in the MDSC population at all. Instead, there was a trend that indicated a higher population of B cells in the ON/OFF/ON group than in the ON group (Figure 4.3C). No other cell type detected demonstrated a difference between control, ON, or ON/OFF/ON contexts (Supplemental Figure 4.3A-C). This data highlights the importance of MDSCs in the primary LC tumors represented by the ON context, but the absence od MDSCs in the ON/OFF/ON context demonstrate that MDSC-derived immunosuppression is not the mechanism of immune suppression in the TME of a relapsing tumor represented by the ON/OFF/ON context. Having described the changes in the LC TME upon local $KRAS^{G12D}$ modulation in primary tumor growth and relapse, we wanted to determine if

there were any changes to the lung microenvironment upon modulation of distal KRAS^{G12D}.

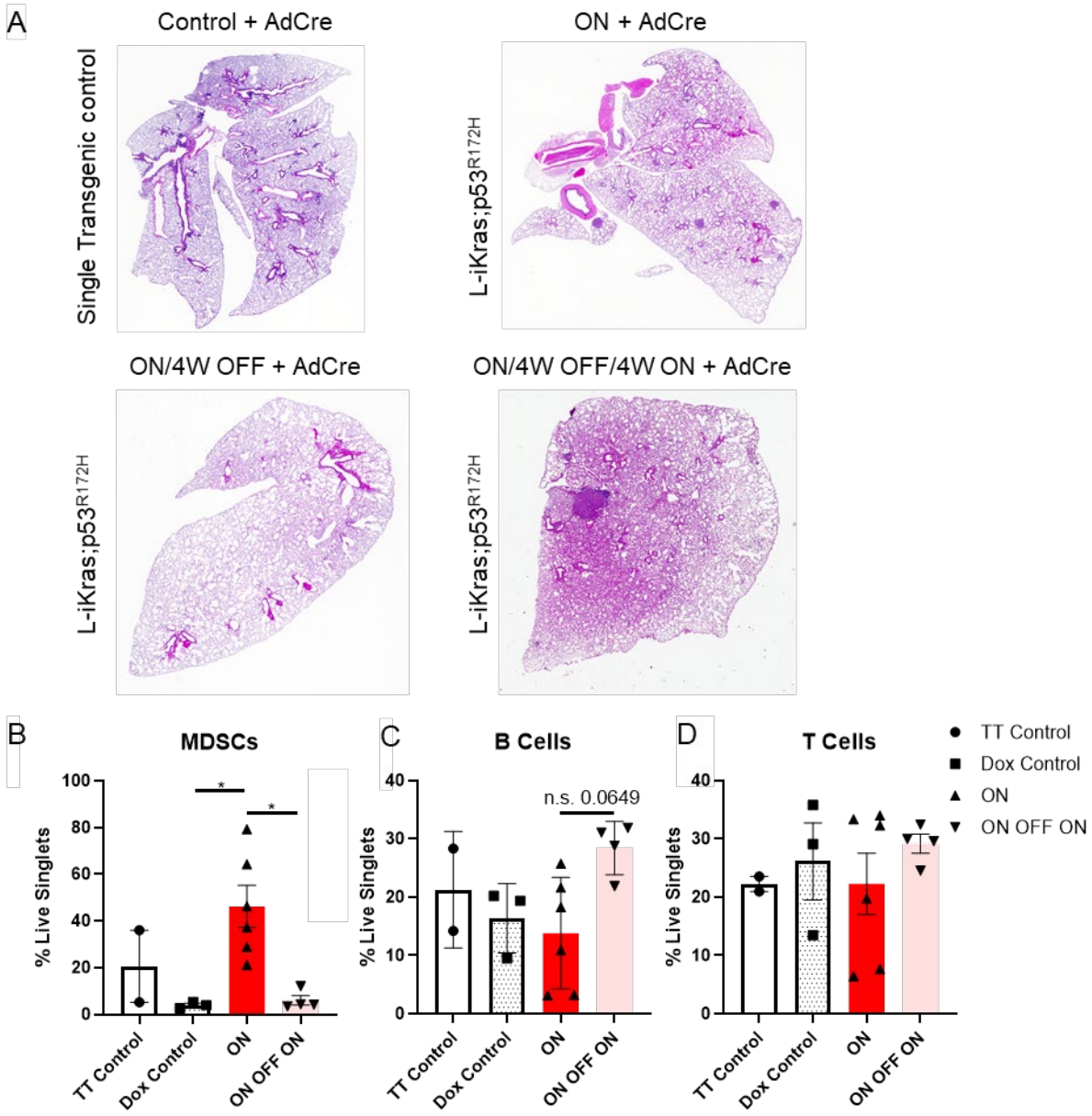

Figure 4.3 The L-iKras ON/OFF/ON TME differs from the ON TME

(A) H&E staining of iKras murine lung after 24 weeks treatment with doxycycline or 20 weeks with removal of doxycycline for 4 weeks. ON/OFF/ON mice were re-administered doxycycline for 4 weeks, resulting in tumor relapse. Triple transgenic (TT) mice were not treated with doxycycline. **(B-D)** Manual quantitation of MDSCs (LY6G$^{+/}$ LY6C^{+}), CD3^{+} T cells, and B cells. Manual gating included n = 5 control mice, n = 6 ON mice, and n = 4 ON/OFF/ON mice. Asterisk denotes a p-value less than 0.05 determined by two-sided Student's t-test.

Distal expression of oncogenic Kras in the P-iKras mouse model effects a change in the lung microenvironment during early carcinogenesis

We performed flow cytometry on the lungs of P-iKras mice to assess if modulation of distally expressed $KRAS^{G12D}$ effected the development of the premetastatic niche in the lung. Administration of doxycycline for three weeks resulted in a decrease in the CD8 T cells in the lung compared to control mice, demonstrating that even distally expressed $KRAS^{G12D}$ can affect immune suppression in a systemic manner (Figure 4.4A right panel). Upon withdrawal of KRAS there was a temporal increase in both CD8 and CD4 T cells, resulting in a higher proportion of total T cells in the lung than in control mice (Figure 4.4A left and middle panels). There was no observed change in the proportions of macrophage or $LY6G^{+}/LY6C^{+}$ myeloid populations (Figure 4.4B). Given the early prevalence of myeloid cells in the primary P-iKras tumor and even the L-iKras primary tumor, this lack of a change in the myeloid population demonstrates that myeloid recruitment is not the mechanism of immune suppression at this early stage of setting up the premetastatic niche in P-iKras mice. Further characterization of the polarization states of the myeloid cells as well as the proportions of the other metastatic niche supporting cells needs to be performed.

Figure 4.4 Modulation of $KRAS^{G12D}$ expression in P-iKras pancreatic tissue effects immune cell populations in the lung

(A-B) Flow cytometry analysis of immune cells, specifically T cells and $CD11b^{+}$ myeloid cells as a percentage of total cells in control or P-iKras* lung at the indicated time points. n = 6-12 mice per group, shown as mean ± SD, multiple comparison ANOVA and multiple comparison Kruskal Wallis.

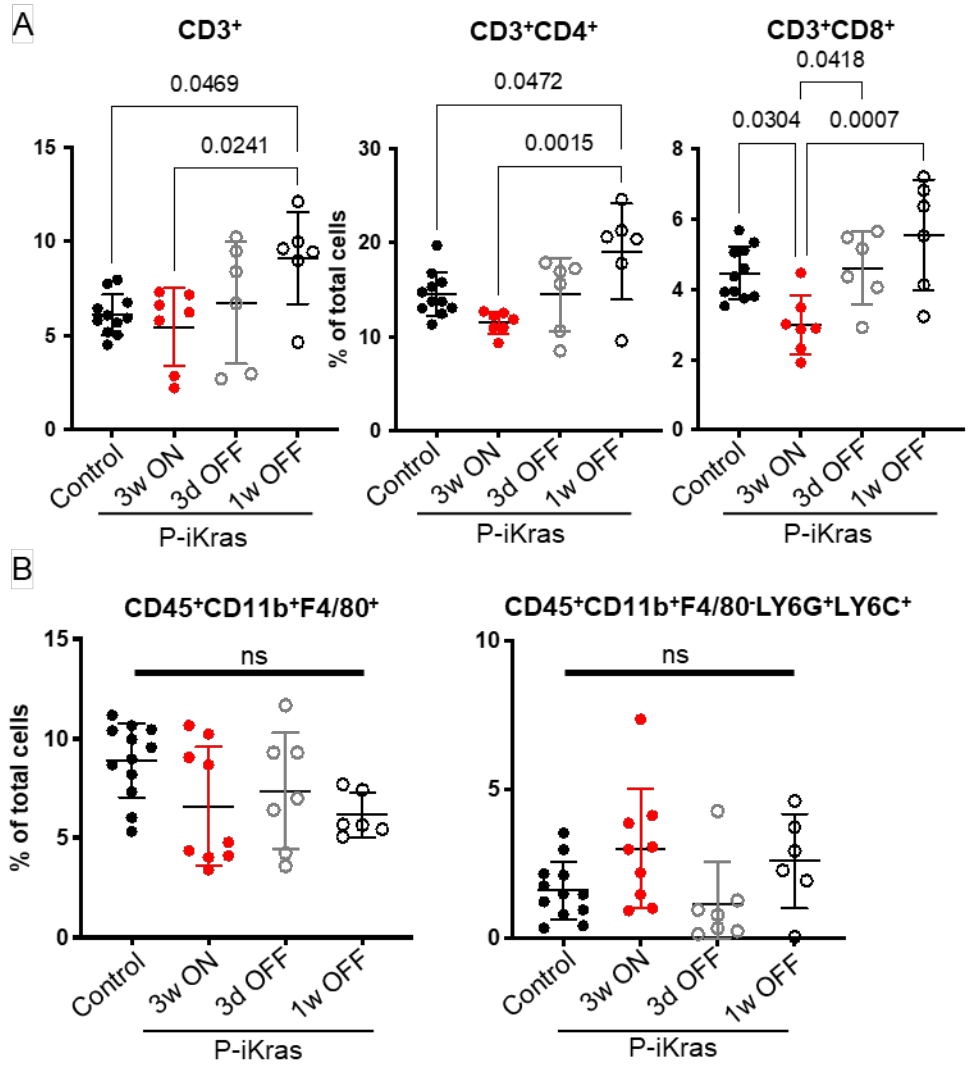

Discussion

While this project is still very much in its infancy, there are already some exciting implications for the work done. Characterization of the L-iKras model is a necessary baseline for designing future experiments. By understanding the mortality rate of the L-iKras model, we can better design experiments to fit the life expectancy of our experimental mice. We have carried out some of these experiments already, changing the temporal activation and withdrawal of doxycycline to mimic specific tumor contexts. We have cohorts of mice that stay on doxycycline to model continuous, untreated tumor

progression, the ON cohort. The ON/OFF cohort mimics successful inhibition of $KRAS^{G12D}$ and demonstrates the efficacy of inhibiting KRAS in both LC and PDA. This is important, as treatment with just inhibitors of MAPK signaling in the P-iKras model were efficacious in reversing tumor progression but did not promote tumor cell death, resulting in progression upon termination of inhibitor treatment (Collins et al. 2014). The ON/OFF/ON model is an effective model of $KRAS^{G12D}$ inhibitor resistance, demonstrating tumor relapse upon reactivation of $KRAS^{G12D}$ signaling. The preliminary characterizations from this study revealed some interesting immune phenotypes in the various LC TMEs. The prevalence of CD8 T cells in all stages of the tumor demonstrate a stark difference to the relative CD8 T cell paucity in PDA. In spite of CD8 T cell presence and engagement however, there is still tumor growth, hinting at an alternate mechanism of immune suppression. Previous studies have indicated that, similar to PDA, there is expression of myriad immune checkpoint proteins (Thommen et al. 2015). The expression of these proteins needs to be confirmed in the L-iKras model. While I have yet to analyze the data, we have already harvested cohorts of mice in the ON, ON/OFF, and ON/OFF/ON contexts for bulk RNA sequencing and a cohort of ON and ON-OFF mice for scRNA-Seq. The scRNA-Seq especially represents an exciting future development, as most of this work is focused on specific subsets of lymphocytes and myeloid cells, though previous studies have shown that the LC TME is as diverse and important to LC progression as the PDA TME is in PDA [see review: (Altorki et al. 2019)]. Comparison of a broader selection of cells present in the LC TME will be important to understanding the mechanisms of $KRAS^{G12D}$ driven immune cell recruitment and immune evasion in the lung, furthering understanding of $KRAS^{G12D}$ signaling in the lung,

as well as providing a comparison for how distal $KRAS^{G12D}$ expression promotes metastasis in lung tissues. Additionally, we presently only have short term changes in the lung premetastatic niche. In the pancreas, the PanIN formation after 3 weeks of doxycycline administration can still recover to phenotypically normal pancreas, though there are lesions that remain after 5 weeks of doxycycline administration (Collins, Bednar, et al. 2012). If there is a different phenotype at 3 vs 5 weeks of local $KRAS^{G12D}$ expression, it stands to reason that there may also be a similar shift in the lung premetastatic niche. It is also important to monitor changes in the lung premetastatic niche upon development of frank PDA and when there is metastatic growth in the lung. The L-iKras and P-iKras mouse models are invaluable models for understanding how $KRAS^{G12D}$ signaling supports tumor growth, survival, progression, and relapse that can be used in designing combinations of first-line and second-line treatments to bolster the efficacy of $KRAS^{G12D}$ inhibition and reduce the fatality of both primary LC and metastatic PDA.

Materials and methods

Mice

All animals were maintained in accordance with the University of Michigan's Institutional Animal Care and Use Committee (IACUC) guidelines approved protocol.

Doxy treatment

Doxycycline was administered in the drinking water at a concentration of 500mg/L in sterile water and replaced every 3–4 days.

Adenoviral-Cre administration

Stocks of Adenoviral-Cre are diluted in MEM with 10 mM $CaCl_2$ to $3x10^7$ PFU. 50 µL of diluted Adenovirla-cre is applied intranasally per mouse.

Pancreas histology

Pancreatic tissue from experimental and control mice were fixed in 10% neutral-buffered formalin (FisherBrand) overnight and then embedded in paraffin and sectioned into slides. Embedding and sections were performed by the University of Michigan histology core or by Daniel Lang from Howard Crawford laboratory at University of Michigan. Hematoxylin and eosin (H&E) was performed as previously described (Collins et al. 2012). Microscope: Olympus BX53F microscope, Olympus DP80 digital camera, and CellSens Standard software.

Lung harvesting scheme

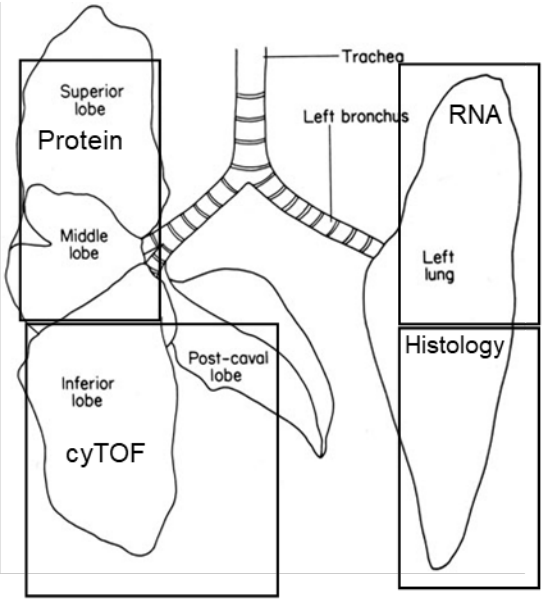

Figure 4.5 Lung tissue harvesting schema

Lung tissue from experimental and control mice were perfused with sterile PBS. fixed in 10% neutral-buffered formalin (FisherBrand) overnight and then embedded in paraffin and sectioned into slides. Embedding and sections were performed by the University of Michigan histology core or by Daniel Lang from Howard Crawford laboratory at University of Michigan. Hematoxylin and eosin (H&E) was performed as previously described (Collins et al. 2012). Microscope:

Olympus BX53F microscope, Olympus DP80 digital camera, and CellSens Standard software.

Multiplex IHC staining

Paraffin embedding for pancreatic tissue from experimental and control mice was performed by the University of Michigan histology core or by Daniel Lang from Howard Crawford laboratory at University of Michigan. Multiplex immunofluorescent staining was performed as follows. Slides were baked in a hybridization oven for one hour at 60 degrees Celsius, cooled for 10 minutes at room temperature, then dipped sequentially (x3) into xylene for 10 minutes each for removal of paraffin. Slides were then rehydrated in alcohol with dilutions of 100%, 95%, then 70% for 10 minutes each followed by a wash in deionized water for 2 minutes. Slides were then placed in neutral buffered formalin for 30 minutes. The slides were then washed for 2 minutes in deionized water then microwaved at 100% power in Rodent Decloaker (Biocare Medical) for 30 seconds, the power level was reduced to 20% and microwaving continued for an additional 10 minutes followed by a resting step of 15 minutes at room temperature. Microwaving continued at 10% power for an additional 10 minutes. Prior to microwaving with Rodent Decloaker, plastic wrap was secured on top of the microwave-proof slide box with rubber bands and a partial opening for steam escape to prevent loss of solution. After the last microwaving step, slides were left to cool until slides and solution achieved room temperature. The multiplex staining was performed for each primary-color combination. Sides were placed in a deionized water wash for two minutes followed by a TBST wash for 2 minutes. Slides were placed in a slide incubation chamber and Bloxall was applied for 10 minutes followed by an additional blocking step

of 1% BSA (in TBST) for 20 minutes, primary antibody was applied after tapping slide to remove the primary antibody and was left to incubate for 1 hour, slides were washed in TBST (x3) for 2 minutes each, secondary antibody was applied, followed by TBST wash (x3) for 2 minutes each, Opal color was applied for 10 minutes and a TBST wash (x3) for 2 minutes each was performed. The slides were then microwaved with either AR6 or AR9 for 45 seconds at 100% followed by 15 minutes at 20%. The previous steps were then repeated for each of the following antibodies and Opal colors in exact listed order: F480 at 1:600 (abcam ab6640), CD3 at 1:400 (Dako A0452)-TSA 520, CD8 at 1:400 (Cell Signaling 98941), Arg1 at 1:100 (Cell Signaling 93668), CK19 at 1:400 (Max Plank Institute Troma III). After the last application of multiplex was completed, sides were washed as above and placed in AR6, then microwaved. After cooling the slides were washed in deionized water followed by TBST for 2 minutes each. Opal spectral DAPI solution was applied (3 drops diluted in 1mL of TBST for 10 minutes followed by a wash in TBST for 30 seconds. Coverslips were mounted with Prolong Diamond, slides were left to lie flat overnight away from light. If the entire multiplex was not able to be completed without interruption, the slides were left in AR6 or AR9 after a microwaving step, covered from light until the next day. All primary antibodies were diluted in 1% BSA and all TSA Opal colors were diluted in TSA diluent at 1:50.

Multiplex fluorescent immunohistochemistry (mfIHC) imaging, cell segmentation, and basic phenotyping

Images were taken using the Mantra™ Quantitative Pathology Work Station (Akoya Biosciences) as described in the Online Methods. One image was taken of each patient core. All cube filters were used for each image capture (DAPI, CY3, CY5, CY7, Texas

Red, Qdot) and the saturation protection feature was utilized. After all images were acquired, images were analyzed using inForm® Cell Analysis™ software versions 2.3.0 and 2.4.2 (Akoya Biosciences). Using this software, chronic pancreatitis specimens and PDA specimens were batch analyzed by their separate diagnoses. Cell segmentation was completed using DAPI as a basis of cell location and size and all cells segmented into the following subsets (nucleus, cytoplasm, and membrane). Using the automated training software, basic phenotypes (T cells, F4/80$^+$ myeloid cells, CK19$^+$ epithelial cells) were created. Software output consisting of mean fluorescent intensity (mfi) of each antibody-fluorophore pair, basic phenotypes, and x and y coordinates were acquired for further processing. A total of n = 3 L-iKras ON mice and n = 3 L-iKras ON/OFF mice were included in this study. Supplemental Table 2.1 details the antibodies used for mfIHC.

Statistical Analysis and Reproducibility

Significance was evaluated by the following statistical analyses: two-tailed, parametric, unpaired Student's t-test, Student's t-test with Welch's correction, Wilcoxon rank-sum test, or a Mann–Whitney U-test in GraphPad Prism (version 7) or JMP Pro software (version 14). The data were presented as means ± standard error (SEM) or means ± standard deviation (STDV). A p value of $p<0.05$ was considered statistically significant.

Flow cytometry

Lung was harvested and disrupted to single cells by mincing the tissue finely using scissors and further disruption was completed using Collagenase IV (Sigma) for 30 minutes at 37°C while shaking to release the cells. A 40um mesh strainer was used to

force the cells into single cells. RBC lysis buffer was used to lyse all the red blood cells. Cells were stained for surface markers using antibodies listed in Supplemental Table 2.2. Cells were also fixed and permeabilized before intracellular staining using antibodies (Supplemental Table 2.2). Flow-cytometric analysis were performed on the Cyan ADP analyzer (Beckman coulter) and the ZE5 analyzer (Bio-Rad). Data was analyzed using the FlowJo v10 software.

Acknowledgements

This work would not have been possible without collaboration with Dr. Stefanie Galban and members of the Galban lab including Alexander Buschhaus, Cara Spencer, and Ranjit Mehta.

References

1. Altorki, Nasser K., Geoffrey J. Markowitz, Dingcheng Gao, Jeffrey L. Port, Ashish Saxena, Brendon Stiles, Timothy Mcgraw, and Vivek Mittal. 2019. "The lung microenvironment: an important regulator of tumour growth and metastasis." *Nature Reviews Cancer* 19 (1): 9-31. https://doi.org/10.1038/s41568-018-0081-9.
2. Collins, Meredith A., Filip Bednar, Yaqing Zhang, Jean-Christophe Brisset, Stefanie Galbán, Craig J. Galbán, Sabita Rakshit, Karen S. Flannagan, N. Volkan Adsay, and Marina Pasca Di Magliano. 2012. "Oncogenic Kras is required for both the initiation and maintenance of pancreatic cancer in mice." *Journal of Clinical Investigation* 122 (2): 639-653. https://doi.org/10.1172/jci59227.
3. Collins, Meredith A., Jean-Christophe Brisset, Yaqing Zhang, Filip Bednar, Josette Pierre, Kevin A. Heist, Craig J. Galbán, Stefanie Galbán, and Marina Pasca Di Magliano. 2012. "Metastatic Pancreatic Cancer Is Dependent on Oncogenic Kras in Mice." *PLoS ONE* 7 (12): e49707. https://doi.org/10.1371/journal.pone.0049707. https://journals.plos.org/plosone/article/file?id=10.1371/journal.pone.0049707&type=printable.
4. Collins, Meredith A., Wei Yan, Judith S. Sebolt–Leopold, and Marina Pasca Di Magliano. 2014. "MAPK Signaling Is Required for Dedifferentiation of Acinar Cells and Development of Pancreatic Intraepithelial Neoplasia in Mice." *Gastroenterology* 146 (3): 822-834.e7. https://doi.org/10.1053/j.gastro.2013.11.052. https://www.ncbi.nlm.nih.gov/pmc/articles/PMC4037403.
5. Cox, Adrienne D., Stephen W. Fesik, Alec C. Kimmelman, Ji Luo, and Channing J. Der. 2014. "Drugging the undruggable RAS: Mission Possible?" *Nature Reviews Drug Discovery* 13 (11): 828-851. https://doi.org/10.1038/nrd4389. https://www.ncbi.nlm.nih.gov/pmc/articles/PMC4355017.
6. Fisher, Galen H., Shari L. Wellen, David Klimstra, Joi M. Lenczowski, Jay W. Tichelaar, Martin J. Lizak, Jeffrey A. Whitsett, Alan Koretsky, and Harold E. Varmus. 2001. "Induction and apoptotic regression of lung adenocarcinomas by regulation of a K-Ras transgene in the presence and

absence of tumor suppressor genes." *Genes & Development* 15 (24): 3249-3262. https://doi.org/10.1101/gad.947701.
7. Jackson, Erica L., Nicholas Willis, Kim Mercer, Roderick T. Bronson, Denise Crowley, Raymond Montoya, Tyler Jacks, and David A. Tuveson. 2001. "Analysis of lung tumor initiation and progression using conditional expression of oncogenic K-ras." *Genes & Development* 15 (24): 3243-3248. https://doi.org/10.1101/gad.943001.
8. Ji, H, A M Houghton, T J Mariani, S Perera, C B Kim, R Padera, G Tonon, K Mcnamara, L A Marconcini, A Hezel, N El-Bardeesy, R T Bronson, D Sugarbaker, R S Maser, S D Shapiro, and K-K Wong. 2006. "K-ras activation generates an inflammatory response in lung tumors." *Oncogene* 25 (14): 2105-2112. https://doi.org/10.1038/sj.onc.1209237. https://www.nature.com/articles/1209237.pdf.
9. Jones, SiâN, Xiaosong Zhang, D. Williams Parsons, Jimmy Cheng-Ho Lin, Rebecca J. Leary, Philipp Angenendt, Parminder Mankoo, Hannah Carter, Hirohiko Kamiyama, Antonio Jimeno, Seung-Mo Hong, Baojin Fu, Ming-Tseh Lin, Eric S. Calhoun, Mihoko Kamiyama, Kimberly Walter, Tatiana Nikolskaya, Yuri Nikolsky, James Hartigan, Douglas R. Smith, Manuel Hidalgo, Steven D. Leach, Alison P. Klein, Elizabeth M. Jaffee, Michael Goggins, Anirban Maitra, Christine Iacobuzio-Donahue, James R. Eshleman, Scott E. Kern, Ralph H. Hruban, Rachel Karchin, Nickolas Papadopoulos, Giovanni Parmigiani, Bert Vogelstein, Victor E. Velculescu, and Kenneth W. Kinzler. 2008. "Core Signaling Pathways in Human Pancreatic Cancers Revealed by Global Genomic Analyses." *Science* 321 (5897): 1801-1806. https://doi.org/10.1126/science.1164368. http://europepmc.org/articles/pmc2848990?pdf=render.
10. Kapoor, Avnish, Wantong Yao, Haoqiang Ying, Sujun Hua, Alison Liewen, Qiuyun Wang, Yi Zhong, Chang-Jiun Wu, Anguraj Sadanandam, Baoli Hu, Qing Chang, C. Chu, Gerald, Ramsey Al-Khalil, Shan Jiang, Hongai Xia, Eliot Fletcher-Sananikone, Carol Lim, I. Horwitz, Gillian, Andrea Viale, Piergiorgio Pettazzoni, Nora Sanchez, Huamin Wang, Alexei Protopopov, Jianhua Zhang, Timothy Heffernan, L. Johnson, Randy, Lynda Chin, Alan Wang, Y., Giulio Draetta, and A. Depinho, Ronald. 2014. "Yap1 Activation Enables Bypass of Oncogenic Kras Addiction in Pancreatic Cancer." Cell 158 (1): 185-197. https://doi.org/10.1016/j.cell.2014.06.003. https://www.ncbi.nlm.nih.gov/pmc/articles/PMC4109295.
11. Kim, Carla F. Bender, Erica L. Jackson, Amber E. Woolfenden, Sharon Lawrence, Imran Babar, Sinae Vogel, Denise Crowley, Roderick T. Bronson, and Tyler Jacks. 2005. "Identification of Bronchioalveolar Stem Cells in Normal Lung and Lung Cancer." *Cell* 121 (6): 823-835. https://doi.org/10.1016/j.cell.2005.03.032. https://doi.org/10.1016/j.cell.2005.03.032.
12. Lavin, Y., S. Kobayashi, A. Leader, E. D. Amir, N. Elefant, C. Bigenwald, R. Remark, R. Sweeney, C. D. Becker, J. H. Levine, K. Meinhof, A. Chow, S. Kim-Shulze, A. Wolf, C. Medaglia, H. Li, J. A. Rytlewski, R. O. Emerson, A. Solovyov, B. D. Greenbaum, C. Sanders, M. Vignali, M. B. Beasley, R. Flores, S. Gnjatic, D. Pe'er, A. Rahman, I. Amit, and M. Merad. 2017. "Innate Immune Landscape in Early Lung Adenocarcinoma by Paired Single-Cell Analyses." *Cell* 169 (4): 750-765.e17. https://doi.org/10.1016/j.cell.2017.04.014. https://www.ncbi.nlm.nih.gov/pubmed/28475900.
13. Seo, Jeong-Sun, Ahreum Kim, Jong-Yeon Shin, and Young Tae Kim. 2018. "Comprehensive analysis of the tumor immune micro-environment in non-small cell lung cancer for efficacy of checkpoint inhibitor." *Scientific Reports* 8 (1). https://doi.org/10.1038/s41598-018-32855-8. https://www.nature.com/articles/s41598-018-32855-8.pdf.
14. Steele, N. G., E. S. Carpenter, S. B. Kemp, V. Sirihorachai, S. The, L. Delrosario, J. Lazarus, E. D. Amir, V. Gunchick, C. Espinoza, S. Bell, L. Harris, F. Lima, V. Irizarry-Negron, D. Paglia, J. Macchia, A. K. Y. Chu, H. Schofield, E. J. Wamsteker, R. Kwon, A. Schulman, A. Prabhu, R. Law, A. Sondhi, J. Yu, A. Patel, K. Donahue, H. Nathan, C. Cho, M. A. Anderson, V. Sahai, C. A. Lyssiotis, W. Zou, B. L. Allen, A. Rao, H. C. Crawford, F. Bednar, T. L. Frankel, and M. Pasca di Magliano. 2020. "Multimodal Mapping of the Tumor and Peripheral Blood Immune Landscape in Human Pancreatic Cancer." *Nat Cancer* 1 (11): 1097-1112. https://doi.org/10.1038/s43018-020-00121-4. https://www.ncbi.nlm.nih.gov/pubmed/34296197.
15. Thommen, Daniela S., Jens Schreiner, Philipp Müller, Petra Herzig, Andreas Roller, Anton Belousov, Pablo Umana, Pavel Pisa, Christian Klein, Marina Bacac, Ozana S. Fischer, Wolfgang Moersig, Spasenija Savic Prince, Victor Levitsky, Vaios Karanikas, Didier Lardinois, and Alfred

Zippelius. 2015. "Progression of Lung Cancer Is Associated with Increased Dysfunction of T Cells Defined by Coexpression of Multiple Inhibitory Receptors." *Cancer Immunology Research* 3 (12): 1344-1355. https://doi.org/10.1158/2326-6066.cir-15-0097.

16. Waddell, Nicola, Marina Pajic, Ann-Marie Patch, David K. Chang, Karin S. Kassahn, Peter Bailey, Amber L. Johns, David Miller, Katia Nones, Kelly Quek, Michael C. J. Quinn, Alan J. Robertson, Muhammad Z. H. Fadlullah, Tim J. C. Bruxner, Angelika N. Christ, Ivon Harliwong, Senel Idrisoglu, Suzanne Manning, Craig Nourse, Ehsan Nourbakhsh, Shivangi Wani, Peter J. Wilson, Emma Markham, Nicole Cloonan, Matthew J. Anderson, J. Lynn Fink, Oliver Holmes, Stephen H. Kazakoff, Conrad Leonard, Felicity Newell, Barsha Poudel, Sarah Song, Darrin Taylor, Nick Waddell, Scott Wood, Qinying Xu, Jianmin Wu, Mark Pinese, Mark J. Cowley, Hong C. Lee, Marc D. Jones, Adnan M. Nagrial, Jeremy Humphris, Lorraine A. Chantrill, Venessa Chin, Angela M. Steinmann, Amanda Mawson, Emily S. Humphrey, Emily K. Colvin, Angela Chou, Christopher J. Scarlett, Andreia V. Pinho, Marc Giry-Laterriere, Ilse Rooman, Jaswinder S. Samra, James G. Kench, Jessica A. Pettitt, Neil D. Merrett, Christopher Toon, Krishna Epari, Nam Q. Nguyen, Andrew Barbour, Nikolajs Zeps, Nigel B. Jamieson, Janet S. Graham, Simone P. Niclou, Rolf Bjerkvig, Robert Grützmann, Daniela Aust, Ralph H. Hruban, Anirban Maitra, Christine A. Iacobuzio-Donahue, Christopher L. Wolfgang, Richard A. Morgan, Rita T. Lawlor, Vincenzo Corbo, Claudio Bassi, Massimo Falconi, Giuseppe Zamboni, Giampaolo Tortora, Margaret A. Tempero, Anthony J. Gill, James R. Eshleman, Christian Pilarsky, Aldo Scarpa, Elizabeth A. Musgrove, John V. Pearson, Andrew V. Biankin, and Sean M. Grimmond. 2015. "Whole genomes redefine the mutational landscape of pancreatic cancer." *Nature* 518 (7540): 495-501. https://doi.org/10.1038/nature14169. http://europepmc.org/articles/pmc4523082?pdf=render.
17. Wood, L. D., D. W. Parsons, S. Jones, J. Lin, T. Sjöblom, R. J. Leary, D. Shen, S. M. Boca, T. Barber, J. Ptak, N. Silliman, S. Szabo, Z. Dezso, V. Ustyanksky, T. Nikolskaya, Y. Nikolsky, R. Karchin, P. A. Wilson, J. S. Kaminker, Z. Zhang, R. Croshaw, J. Willis, D. Dawson, M. Shipitsin, J. K. Willson, S. Sukumar, K. Polyak, B. H. Park, C. L. Pethiyagoda, P. V. Pant, D. G. Ballinger, A. B. Sparks, J. Hartigan, D. R. Smith, E. Suh, N. Papadopoulos, P. Buckhaults, S. D. Markowitz, G. Parmigiani, K. W. Kinzler, V. E. Velculescu, and B. Vogelstein. 2007. "The genomic landscapes of human breast and colorectal cancers." *Science* 318 (5853): 1108-13. https://doi.org/10.1126/science.1145720. https://www.ncbi.nlm.nih.gov/pubmed/17932254.

Chapter 5: Discussion and Future Directions

The sum of this work is to generate and demonstrate the use of a single cell RNA sequencing study pipeline to study the complex TME of PDA. First, we performed scRNAseq of biopsies of human PDA (Steele et al. 2020). This was important as previous human studies could only be done on resected PDA tumors. As resection was only ever done on patients with locally, non-advanced disease, there was a major gap in resources for the field due to the lack of patient samples from the most common, metastatic disease. By using biopsies, we were able to use samples from patients at any staging. Additionally, we used a combination of high-resolution techniques to interrogate the data we received. scRNAseq allowed us to capture an almost unbiased glimpse at the transcriptomes of the individual cells present in the human PDA TME. We were able to verify the composition of human PDA with CyTOF and mfIHC. Then, we are able to use the scRNAseq data to generate hypotheses (Kemp et al. 2021; Steele et al. 2020; Nina G. Steele et al. 2021). In this work, we presented the work looking for the mechanism of immune checkpoint inhibition in human PDA. We were able to use the scRNAseq to phenotype the CD8 T cells in human PDA and identify TIGIT as a uniquely expressed marker on exhausted CD8 T cells. Then, using CyTOF and IF, we were able to verify expression of TIGIT and its cognate ligand PVR. Previous immunotherapy trials had failed in treating human PDA, specifically PD-1. Here, we show that TIGIT expression may be the primary mechanism of immunosuppression

rather than PD-1. Subsequent work has been done by other labs in the functional validation of TIGIT in human PDA from which clinical trials are being designed (Freed-Pastor et al. 2021).

We then applied this model to study liver metastases of PDA, using our pipeline to characterize the cell types present and their phenotypes. Again, using biopsies instead of tissue from rapid autopsies or from a tissue bank has allowed us to perform scRNAseq on tissue that has never been analyzed at this resolution by another lab. While the project is still in the protein verification step, once the scRNAseq data has been validated, we will be able to use the data to derive hypotheses about PDA liver metastases, filling another huge gap in the resources required by the field. Finally, we seek to understand more about lung metastases of PDA tumors.

As there are no protocols for getting biopsies of human lung metastases, we used two mouse models we generated to gain understanding of the tumor in a different system. We previously generated the Pancreas-iKras mouse and have thoroughly characterized the importance of oncogenic $KRAS^{G12D}$ signaling in that model (Collins, Brisset, et al. 2012; Collins, Bednar, et al. 2012; Collins et al. 2014). Here, we generated the Lung-iKras model and began characterizing the model in the context of lung cancer. Similarly to the P-iKras mouse model, the L-iKras mouse model demonstrates a requirement for $KRAS^{G12D}$ in maintenance of the L-iKras tumor. We are still only beginning to characterize the changing L-iKras TME. We have even performed scRNAseq of L-iKras tumors, but the analysis of that data remains ongoing. We have some incredibly preliminary data demonstrating that modulation of $KRAS^{G12D}$ in the P-iKras mouse model results in a shift in the immune composition of the P-iKras lung. The

future directions for this project will be to describe the shift in the immune composition of the lung in the P-iKras model more thoroughly, to compare it to the shifts in the lung of the L-iKras mouse model. If the shifts in the immune composition are similar, we may be able to use the L-iKras mouse as a model for studying the requirement of $KRAS^{G12D}$ in PDA lung metastases. Generating this mouse model will simultaneously fill two unmet needs. There are no inhibitors available for $KRAS^{G12D}$, so generating a model of inducible, reversible $KRAS^{G12D}$ expression in the lung will help mimic the effects of $KRAS^{G12D}$ inhibition to discover potential mechanisms of resistance to $KRAS^{G12D}$ inhibition in lung cancer. Finally, the combination of these two mouse models could be a useful system for studying PDA lung metastases. If the TME of the distal P-iKras and the local L-iKras lungs are comparable, then the two autochthonous models can be used to test hypotheses about PDA metastases. It has previously been difficult to study metastases in PDA, but the result of this work is a good step forward in the development of tools to better understand this deadly malignancy.

References

1. Collins, Meredith A., Filip Bednar, Yaqing Zhang, Jean-Christophe Brisset, Stefanie Galbán, Craig J. Galbán, Sabita Rakshit, Karen S. Flannagan, N. Volkan Adsay, and Marina Pasca Di Magliano. 2012. "Oncogenic Kras is required for both the initiation and maintenance of pancreatic cancer in mice." *Journal of Clinical Investigation* 122 (2): 639-653. https://doi.org/10.1172/jci59227.
2. Collins, Meredith A., Jean-Christophe Brisset, Yaqing Zhang, Filip Bednar, Josette Pierre, Kevin A. Heist, Craig J. Galbán, Stefanie Galbán, and Marina Pasca Di Magliano. 2012. "Metastatic Pancreatic Cancer Is Dependent on Oncogenic Kras in Mice." *PLoS ONE* 7 (12): e49707. https://doi.org/10.1371/journal.pone.0049707. https://journals.plos.org/plosone/article/file?id=10.1371/journal.pone.0049707&type=printable.
3. Collins, Meredith A., Wei Yan, Judith S. Sebolt–Leopold, and Marina Pasca Di Magliano. 2014. "MAPK Signaling Is Required for Dedifferentiation of Acinar Cells and Development of Pancreatic Intraepithelial Neoplasia in Mice." *Gastroenterology* 146 (3): 822-834.e7. https://doi.org/10.1053/j.gastro.2013.11.052. https://www.ncbi.nlm.nih.gov/pmc/articles/PMC4037403.
4. Freed-Pastor, W. A., L. J. Lambert, Z. A. Ely, N. B. Pattada, A. Bhutkar, G. Eng, K. L. Mercer, A. P. Garcia, L. Lin, W. M. Rideout, W. L. Hwang, J. M. Schenkel, A. M. Jaeger, R. T. Bronson, P. M. K. Westcott, T. D. Hether, P. Divakar, J. W. Reeves, V. Deshpande, T. Delorey, D. Phillips, O. H. Yilmaz, A. Regev, and T. Jacks. 2021. "The CD155/TIGIT axis promotes and maintains

immune evasion in neoantigen-expressing pancreatic cancer." *Cancer Cell* 39 (10): 1342-1360.e14. https://doi.org/10.1016/j.ccell.2021.07.007. https://www.ncbi.nlm.nih.gov/pubmed/34358448.

5. Kemp, Samantha B., Eileen S. Carpenter, Nina G. Steele, Katelyn L. Donahue, Zeribe C. Nwosu, Amanda Pacheco, Ashley Velez-Delgado, Rosa E. Menjivar, Fatima Lima, Stephanie The, Carlos E. Espinoza, Kristee Brown, Daniel Long, Costas A. Lyssiotis, Arvind Rao, Yaqing Zhang, Marina Pasca Di Magliano, and Howard C. Crawford. 2021. "Apolipoprotein E Promotes Immune Suppression in Pancreatic Cancer through NF-κB–Mediated Production of CXCL1." *Cancer Research* 81 (16): 4305-4318. https://doi.org/10.1158/0008-5472.can-20-3929.
6. Steele, N. G., E. S. Carpenter, S. B. Kemp, V. Sirihorachai, S. The, L. Delrosario, J. Lazarus, E. D. Amir, V. Gunchick, C. Espinoza, S. Bell, L. Harris, F. Lima, V. Irizarry-Negron, D. Paglia, J. Macchia, A. K. Y. Chu, H. Schofield, E. J. Wamsteker, R. Kwon, A. Schulman, A. Prabhu, R. Law, A. Sondhi, J. Yu, A. Patel, K. Donahue, H. Nathan, C. Cho, M. A. Anderson, V. Sahai, C. A. Lyssiotis, W. Zou, B. L. Allen, A. Rao, H. C. Crawford, F. Bednar, T. L. Frankel, and M. Pasca di Magliano. 2020. "Multimodal Mapping of the Tumor and Peripheral Blood Immune Landscape in Human Pancreatic Cancer." *Nat Cancer* 1 (11): 1097-1112. https://doi.org/10.1038/s43018-020-00121-4. https://www.ncbi.nlm.nih.gov/pubmed/34296197.
7. Steele, Nina G., Giulia Biffi, Samantha B. Kemp, Yaqing Zhang, Donovan Drouillard, Lijyun Syu, Yuan Hao, Tobiloba E. Oni, Erin Brosnan, Ela Elyada, Abhishek Doshi, Christa Hansma, Carlos Espinoza, Ahmed Abbas, Stephanie The, Valerie Irizarry-Negron, Christopher J. Halbrook, Nicole E. Franks, Megan T. Hoffman, Kristee Brown, Eileen S. Carpenter, Zeribe C. Nwosu, Craig Johnson, Fatima Lima, Michelle A. Anderson, Youngkyu Park, Howard C. Crawford, Costas A. Lyssiotis, Timothy L. Frankel, Arvind Rao, Filip Bednar, Andrzej A. Dlugosz, Jonathan B. Preall, David A. Tuveson, Benjamin L. Allen, and Marina Pasca Di Magliano. 2021. "Inhibition of Hedgehog Signaling Alters Fibroblast Composition in Pancreatic Cancer." Clinical Cancer Research 27 (7): 2023-2037. https://doi.org/10.1158/1078-0432.ccr-20-3715.

Appendices

Appendix 1: Supplemental Figures

Supplemental Figure 2.1 CyTOF and multiplex fluorescent immunohistochemistry (mfIHC) mapping can be readily performed on patient tumor samples and show a heterogeneous immune infiltration in human pancreatic cancer.

(A) Patient breakdown and tumor characteristics of CyTOF performed on 8 adj/norm pancreas and 10 PDA tumor samples (surgical (7) vs. fine needle biopsy (FNB) (3)). **(B)** Representative H&E stains of samples DS20191258 (Adj/Norm), DS20191299 (PDA tumor from surgical resection), and DS20191324 (PDA tumor from fine needle biopsy). **(C)** The ConsensusClusterPlus and FlowSOM R packages were used to define the initial 22 clusters identified in the tissue CyTOF samples. **(D)** Final heatmap demonstrating marker expression used to define cell populations. **(E)** mfIHC composite image of PDA (left). Phenotype map with the following basic phenotypes at their x and y coordinates: T cell (green), epithelial cells (pink), APCs (orange), other cells (grey) (right). **(F)** Relative cellular composition by quantitation of mfIHC of surgical PDA tissue DS20181166 (PDA tumor from distal pancreatectomy), DS20181121 (PDA tumor from distal pancreatectomy) **(G)** Corresponding mfIHC images of DS20181166, and DS20181121.

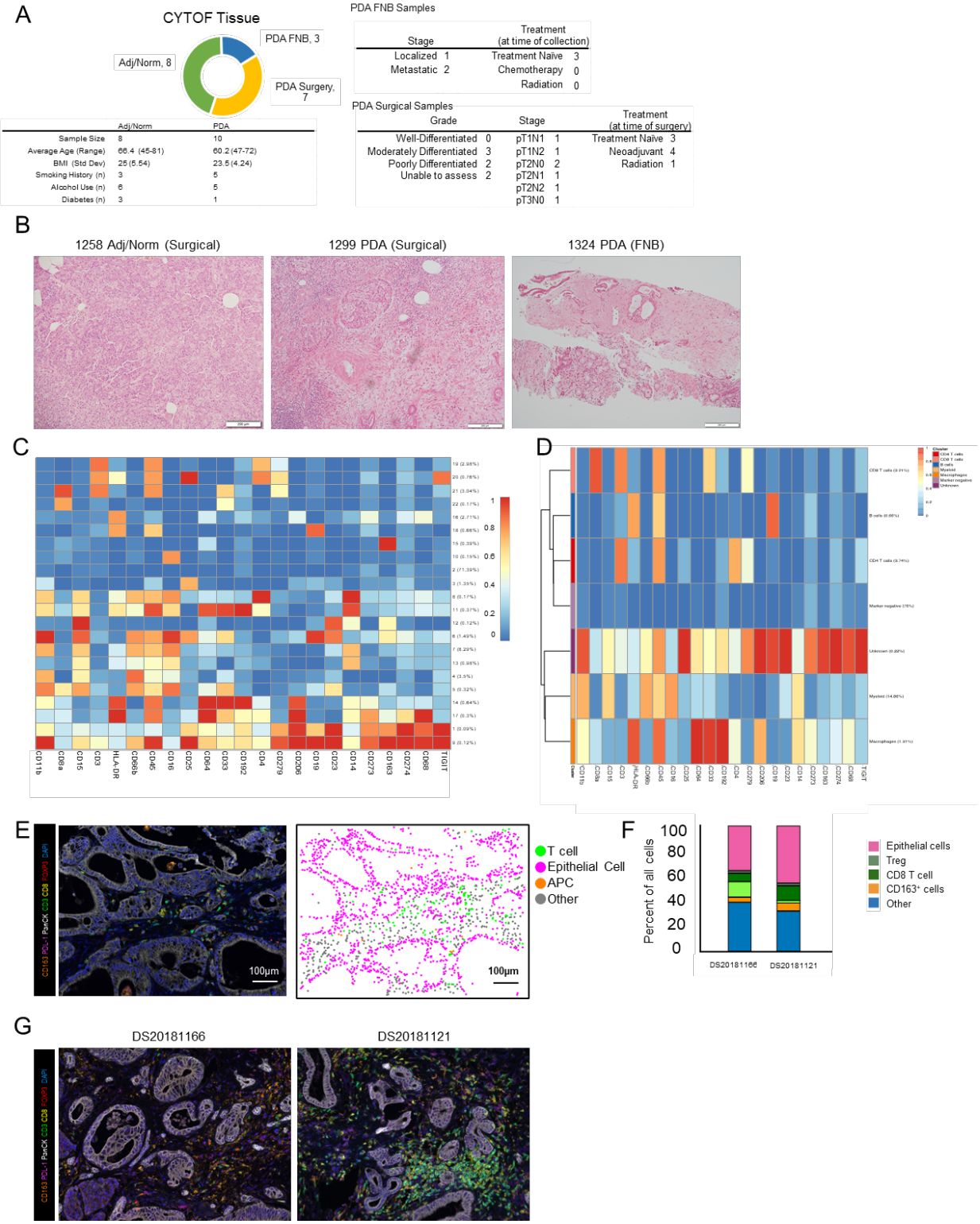
A
CYTOF Tissue
PDA FNB, 3
Adj/Norm, 8
PDA Surgery, 7
PDA FNB Samples
Stage
Localized 1
Metastatic 2
Treatment (at time of collection)
Treatment Naïve 3
Chemotherapy 0
Radiation 0
PDA Surgical Samples
Grade
Well-Differentiated 0
Moderately Differentiated 3
Poorly Differentiated 2
Unable to assess 2
Stage
pT1N1 1
pT1N2 1
pT2N0 2
pT2N1 1
pT2N2 1
pT3N0 1
Treatment (at time of surgery)
Treatment Naïve 3
Neoadjuvant 4
Radiation 1
Adj/Norm
PDA
Sample Size 8 10
Average Age (Range) 66.4 (45-81) 60.2 (47-72)
BMI (Std Dev) 25 (5.54) 23.5 (4.24)
Smoking History (n) 3 5
Alcohol Use (n) 6 5
Diabetes (n) 3 1
B
1258 Adj/Norm (Surgical)
1299 PDA (Surgical)
1324 PDA (FNB)
C
CD11b
CD8a
CD15
CD3
HLA-DR
CD66b
CD45
CD16
CD25
CD64
CD33
CD192
CD4
CD279
CD206
CD19
CD23
CD14
CD273
CD163
CD274
CD68
TIGIT
D
E
100μm
100μm
T cell
Epithelial Cell
APC
Other
F
Percent of all cells
100
80
60
40
20
0
DS20181166
DS20181121
Epithelial cells
Treg
CD8 T cell
CD163+ cells
Other
G
DS20181166
DS20181121

Supplemental Figure 2.2 Single Cell RNA Sequencing of PDA tissue reveals heterogeneous cellular composition and expression of immune checkpoints.

(A) Single cell RNA sequencing tissue sample breakdown (Adj/Norm, PDA tissue from fine needle biopsy, and PDA tissue from surgical resection), patient clinical data, and tumor characteristics (grade and stage) (Left panel). Breakdown of sequenced PBMC samples with corresponding patient clinical data (Right panel). (**B)** UMAP of the merged tissue colored by Patient ID prior to batch correction (Left panel) and post batch correction (Right panel). **(C)** UMAP of 3 individual adjacent/normal samples and **(D)** 16 PDA tissues. We distinguished two epithelial populations: tumor cells and acinar cells. In the non-epithelial compartment, we identified fibroblasts, $CD8^+$ T cells, $CD4^+$ T cells, Tregs, NK cells, B cells, plasma cells, mast cells, macrophages, granulocytes, dendritic cells, endothelial cells, and a small endocrine population.

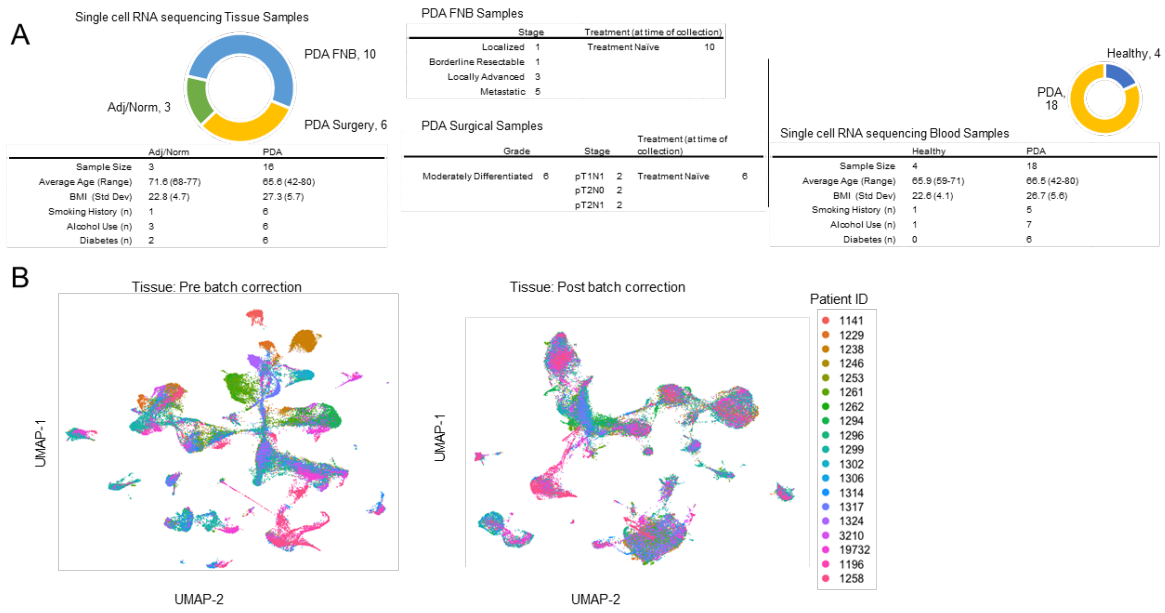
A
Single cell RNA sequencing Tissue Samples
PDA FNB, 10
Adj/Norm, 3
PDA Surgery, 6
Adj/Norm PDA
Sample Size 3 16
Average Age (Range) 71.6 (68-77) 65.6 (42-80)
BMI (Std Dev) 22.8 (4.7) 27.3 (5.7)
Smoking History (n) 1 6
Alcohol Use (n) 3 6
Diabetes (n) 2 6
PDA FNB Samples
Stage
Localized 1
Borderline Resectable 1
Locally Advanced 3
Metastatic 5
Treatment (at time of collection)
Treatment Naive 10
PDA Surgical Samples
Grade
Moderately Differentiated 6
Stage
pT1N1 2
pT2N0 2
pT2N1 2
Treatment (at time of collection)
Treatment Naive 6
Healthy, 4
PDA, 18
Single cell RNA sequencing Blood Samples
Healthy PDA
Sample Size 4 18
Average Age (Range) 65.9 (59-71) 66.5 (42-80)
BMI (Std Dev) 22.6 (4.1) 26.7 (5.6)
Smoking History (n) 1 5
Alcohol Use (n) 1 7
Diabetes (n) 0 6
B
Tissue: Pre batch correction
Tissue: Post batch correction
Patient ID
1141
1229
1238
1246
1253
1261
1262
1294
1296
1299
1302
1306
1314
1317
1324
3210
19732
1196
1258
UMAP-1
UMAP-2
C
Adj/Norm Pancreas
19732
1258
1196
D
PDA
1229
1238
1246
1253
1141
1261
1262
1264
1296
1299
1302
1306
1314
1317
1324
3210
CD4 T Cells
CD8 T Cells
Macrophage
Epithelial
Granulocyte
Mast Cells
Acinar
NK Cells
Plasma Cells
iCAF Fibroblast
B Cells
T Reg
myCAF Fibroblast
Endothelial
Dendritic Cell
Endocrine

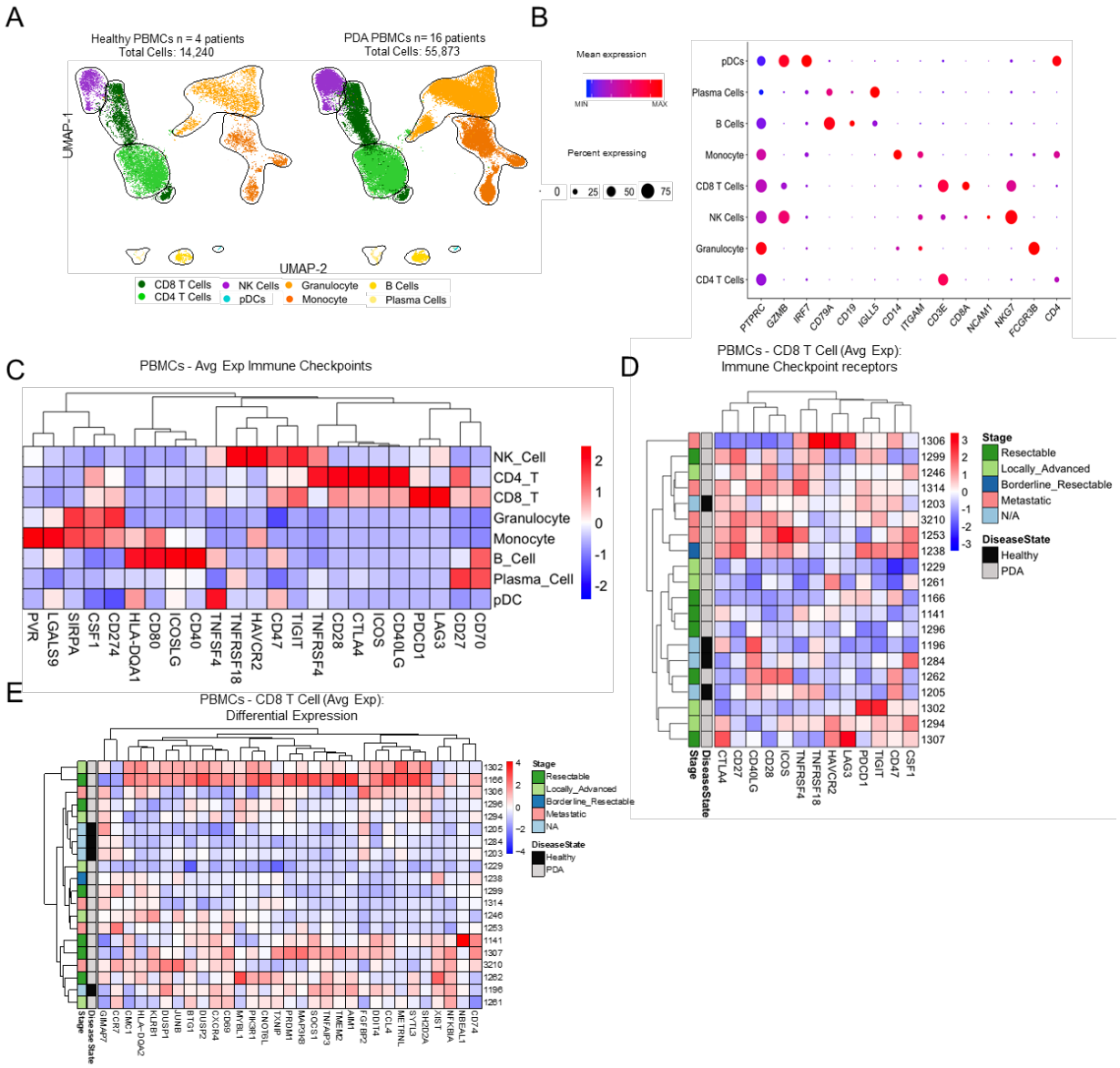

Supplemental Figure 2.3 Single Cell RNA Sequencing of PDA PBMCs reveals heterogeneous cellular composition and expression of immune checkpoints.

(A) Merged UMAP plots of PBMCs from 4 healthy donors and 16 PDA patients (total of 70,113 cells). CD8 T cells (green), CD4 T cells (light green), NK cells (purple), pDCs (blue), Granulocyte (light orange), Monocyte (orange), B cells (yellow), Plasma cells (light yellow). (**B)** Dot plot analysis of key markers to define the 8 identified cell populations. Color of dot represents average expression, while the size of the dot represents percent expression. **(C)** Average expression of immune checkpoint ligands and receptors in the identified cell populations in merged blood samples. **(D)** Average expression of immune checkpoint receptors on $CD8^+$ T cells in merged PBMCs. **(E)** Average expression of differentially expressed genes in $CD8^+$ T cells comparing healthy (black) to PDA (grey) PBMCs. Disease stage is plotted on the left.

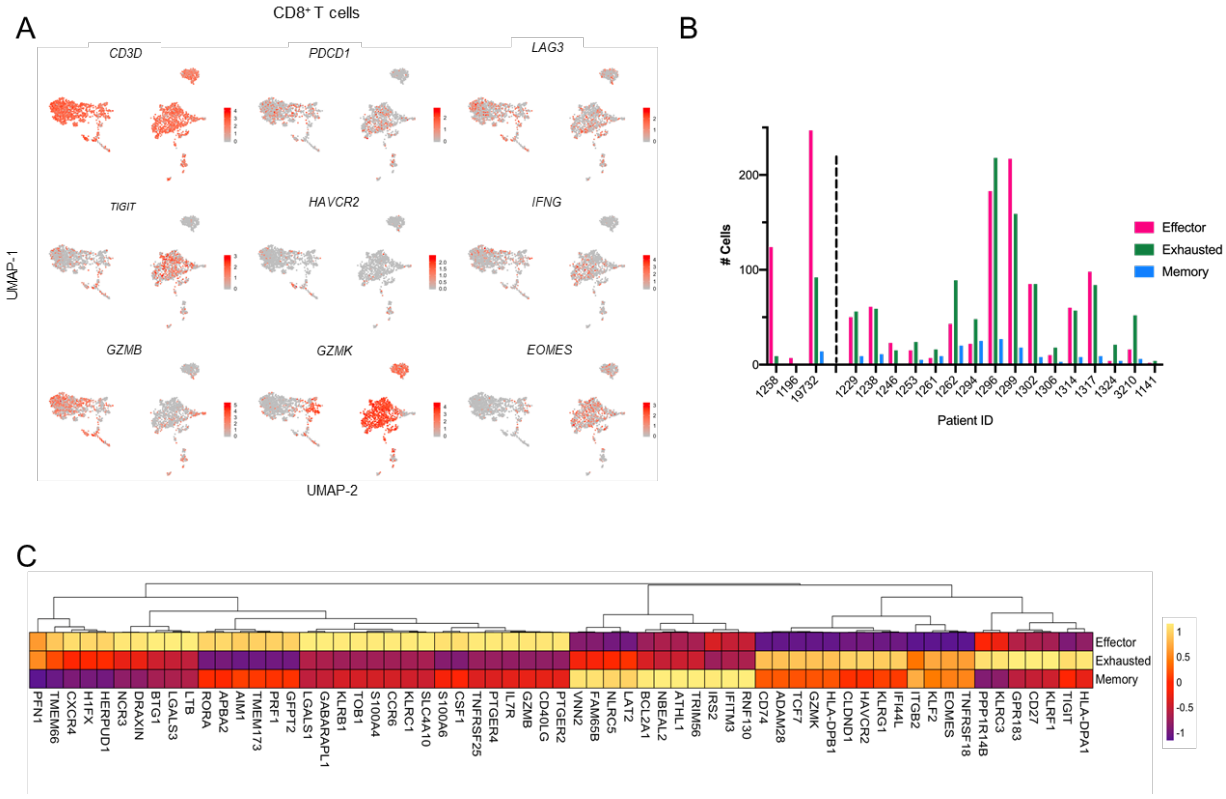

Supplemental Figure 2.4 Single cell RNA sequencing reveals 3 CD8+ T cell populations: effector, exhausted, and memory CD8+ T Cells.
(A) Feature plots of immune checkpoints (*PDCD1, LAG3, TIGIT, HAVCR2)*, activation markers (*IFNG, GZMB)*, and exhaustion markers *(GZMK, EOMES)* in CD8⁺ T cells. **(B)** Number of effector (pink), exhausted (green), and memory (blue) CD8⁺ T cells captured in each individual tissue sample by scRNA seq. **(C)** Average scaled expression heatmap of highly enriched genes by potential effector, exhausted, and memory cell populations.

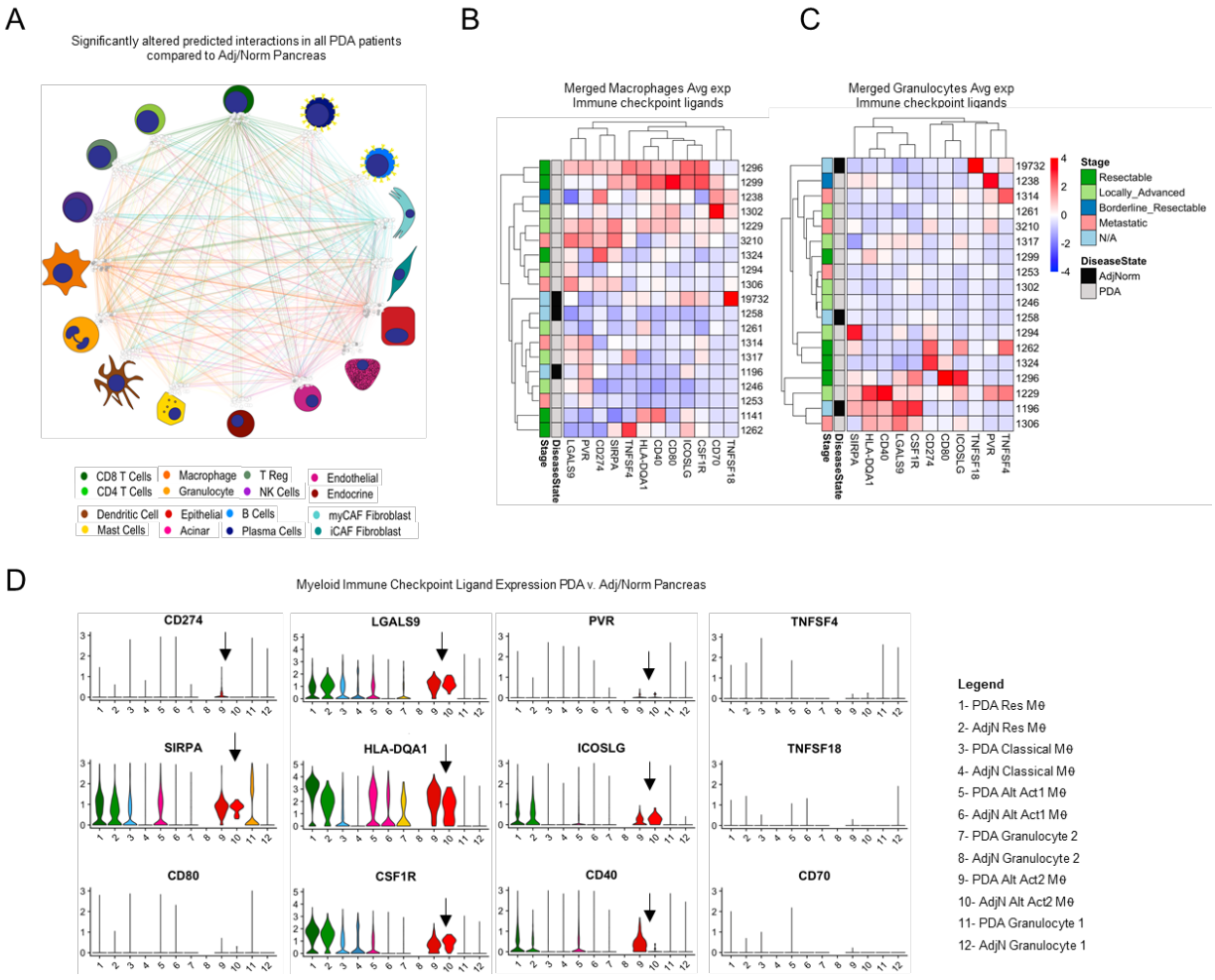

Supplemental Figure 2.5 Single cell RNA sequencing of myeloid subsets in human pancreatic cancer.
(A) Map of all putative ligand receptor differential interactions that are upregulated in 16 PDA compared to 3 adjacent/normal pancreas. The line color denotes cellular source of the ligand, and putative interactions were visualized in Cytoscape®. **(B)** Average expression heatmap of checkpoint ligands in merged macrophages (all cells expressing *CD68* within the myeloid population) and **(C)** merged granulocytes (all cells expressing *FCGR3B* within the myeloid population*)*. Left panels denote disease state (adjacent/normal vs. PDA tissue) and stage. **(D)** Violin Plots illustrating comparison of immune checkpoint ligands in myeloid clusters in PDA vs. adjacent normal/pancreas samples.

Supplemental Figure 2.6 CyTOF analysis of PBMCs from healthy, chronic pancreatitis, and PDA patients.

(A) Patient breakdown and characteristics of CyTOF performed on patient blood samples (healthy, chronic pancreatitis, and PDA). **(B)** t-SNE analysis of CyTOF of all merged PBMC samples with granulocytes ($CD66b^+$). **(C)** t-SNE analysis of CyTOF of all merged PBMC samples without granulocytes. Key marker t-SNE feature plots of CD3 (total T cells), CD4 (Helper $CD4^+$ T cells), CD8 (Cytotoxic T cells), CD19 (B cells), CD11b (Myeloid cells), CCR2, PDL-1, and CD68 (Macrophage marker). **(D)** Bar plots of relative cell type abundance (B cell, $CD4^+/CD8^+$ T cell, $CD4^+$ T cell, $CD4^-/CD8^-$ T cell, Dendritic cell, $CD14^+/CD16^+$ Monocyte, $CD14^+/CD16^-$ Monocyte, and $CD14^-$ $CD16^+$ Monocyte) from CyTOF of PBMCs of healthy, chronic pancreatitis, and PDA patients. **(E)** Quantification of unbiased analysis (Astrolabe pipeline) of PBMC immune populations in healthy (n=18), PDA (n=36), and chronic pancreatitis (n=8). **(F)** Relative CyTOF marker expression in $CD8^+$ T Cells from PDA tumor tissue. **(G)** PCA analysis of PBMCs at different disease states. Healthy (neon blue), PDA (red), and Chronic Pancreatitis (green).

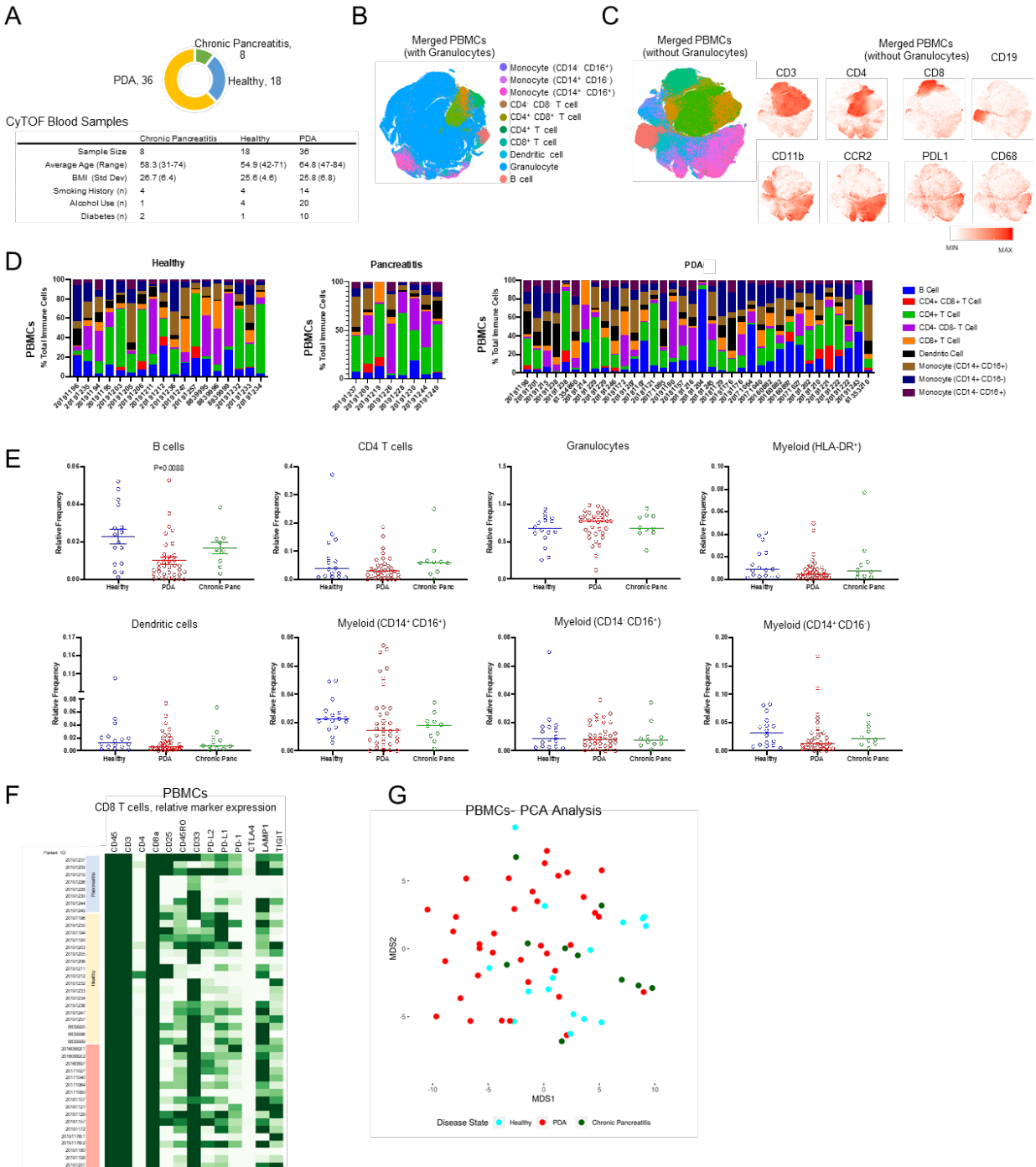

	Chronic Pancreatitis	Healthy	PDA
Sample Size	8	18	36
Average Age (Range)	58.3 (31-74)	54.9 (42-71)	64.8 (47-84)
BMI (Std Dev)	26.7 (6.4)	25.6 (4.6)	25.8 (6.8)
Smoking History (n)	4	4	14
Alcohol Use (n)	1	4	20
Diabetes (n)	2	1	10

Supplemental Figure 2.7 Immunofluorescence of immune checkpoints in pancreatic tumors.

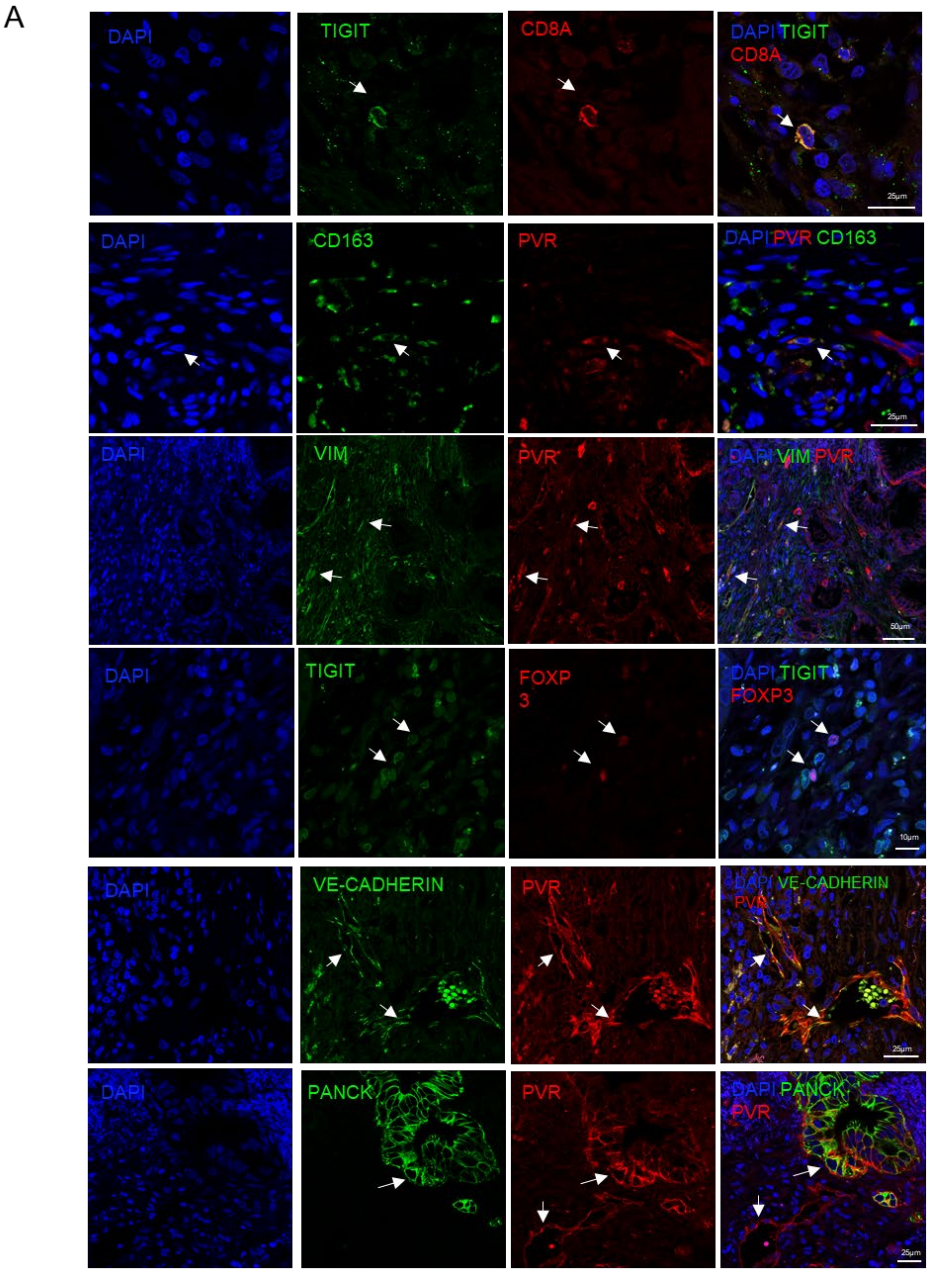

(A) Individual channels of immunofluorescent staining of patient tissues with antibodies specific for TIGIT/CD8A, TIGIT/FOXP3, PVR/Pan-cytokeratin, PVR/CD163, PVR/Vimentin, and PVR/VE-cadherin.

(B) Manual gating of PD-L1^{+} CD68^{+} macrophages in normal adjacent and PDA tissue. Representative individual CyTOF biaxial density plots from normal adjacent and PDA tissue of a matched patient (19-262) of PD-L1 expression in CD68^{+} macrophages (as a percentage of total CD11b^{+} cells).

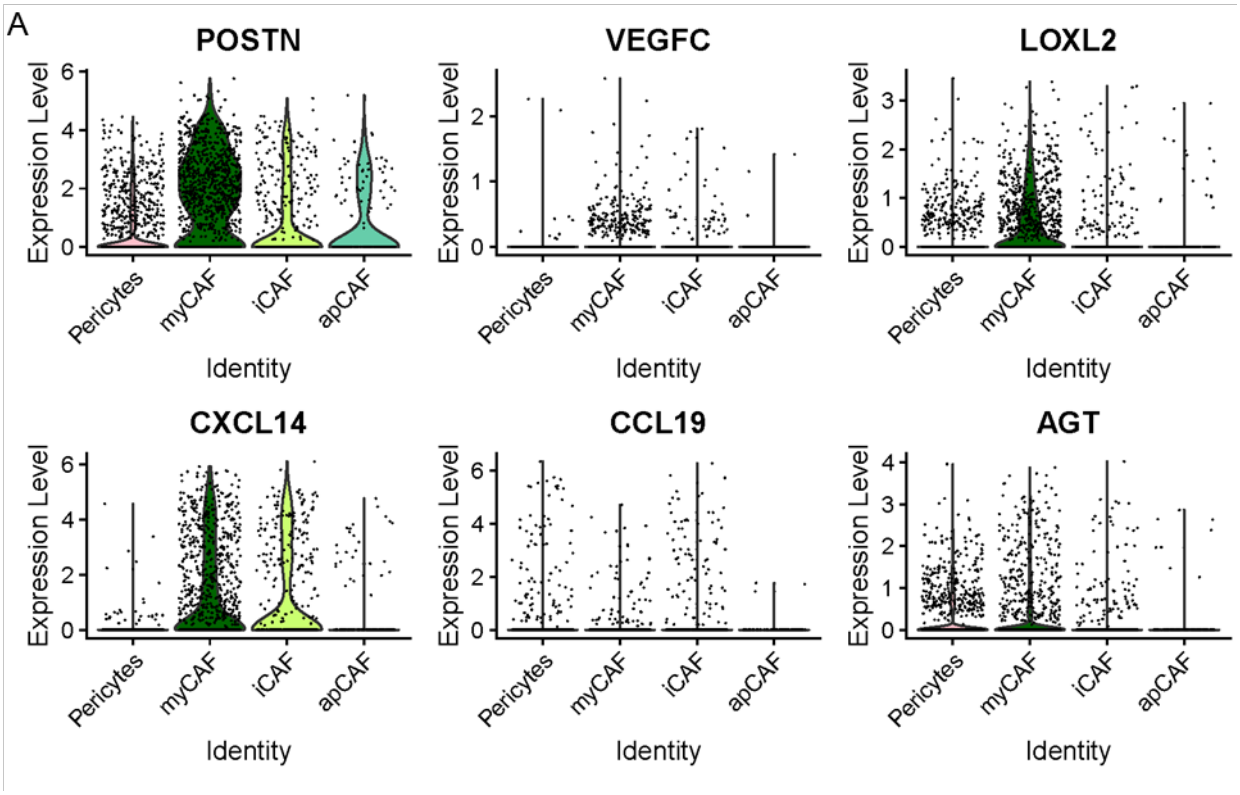

Supplemental Figure 3.1 myCAF signaling is more prevalent in upregulated LM genes
(A) Panel of genes differentially expressed in fibroblasts. Plots represent n=3 adj/norm and n=16 PDA patients and n=5 LM patients. Violin plots are shown as normalized expression. All violin plots in have an adjusted p-value of $p<0.05$ and are considered statistically significant.

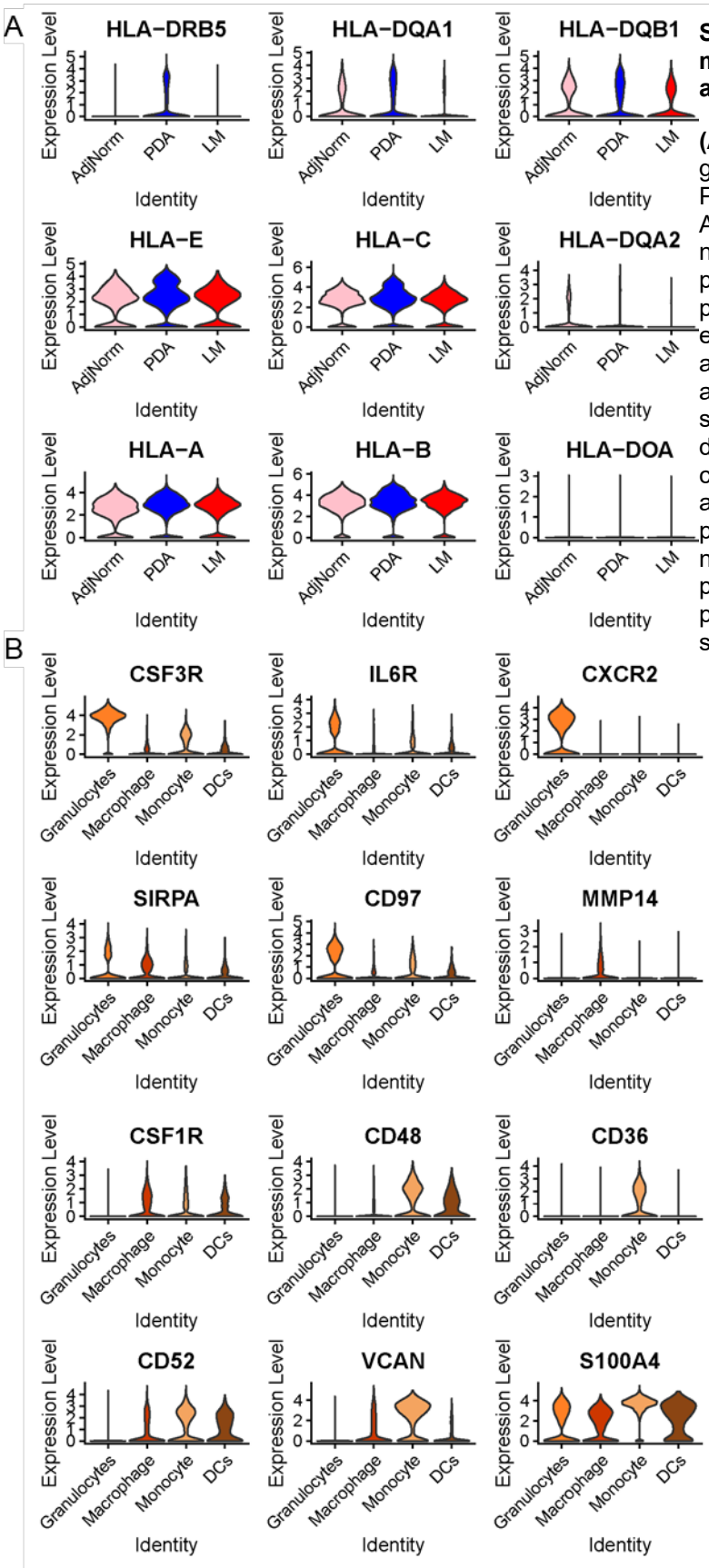

Supplemental Figure 3.2 LM myeloid cells express less antigen presentation genes

(A) Panel of antigen presentation genes differentially upregulated in PDA myeloid cells versus LM and Adj/Norm samples. Plots represent n=3 adj/norm and n=16 PDA patients and n=5 LM patients. Violin plots are shown as normalized expression. All violin plots in have an adjusted p-value of $p<0.05$ and are considered statistically significant. **(B)** Panel of genes differentially expressed in myeloid cells. Plots represent n=3 adj/norm and n=16 PDA patients and n=5 LM patients. Violin plots are shown as normalized expression. All violin plots in have an adjusted p-value of $p<0.05$ and are considered statistically significant.

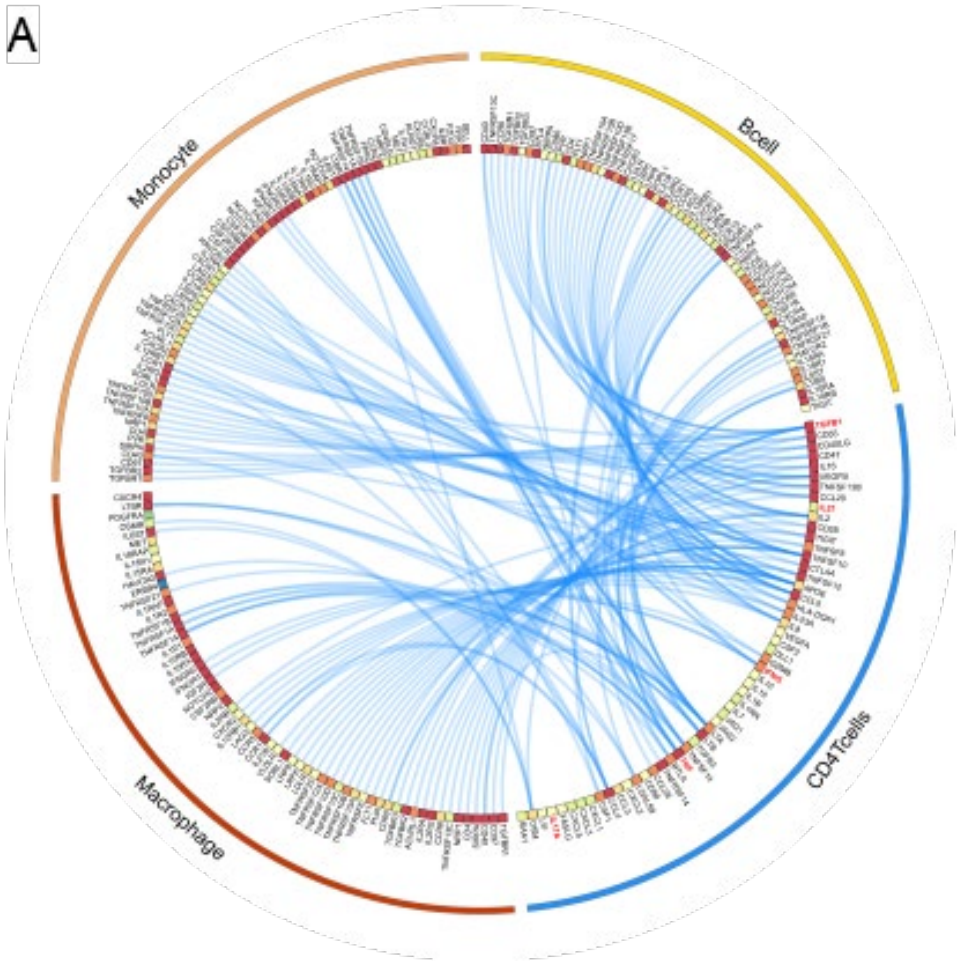

Supplemental Figure 3.3 CD4 interactome mapping demonstrates expression of multiple CD4 subsets

(A) Circos plot map of all putative ligand receptor interactions that are upregulated in LM CD4 T cells compared to PDA and visualized by circos plot. Plotted using the Circos software V0.69-9 (circos.ca). The heatmap within the circos plots is the scaled average expression of each gene within PDA tissue cell populations. The interactions plotted are those in which the expression level of either the ligand, the receptor, or both are increased in expression in LM samples compared to PDA.

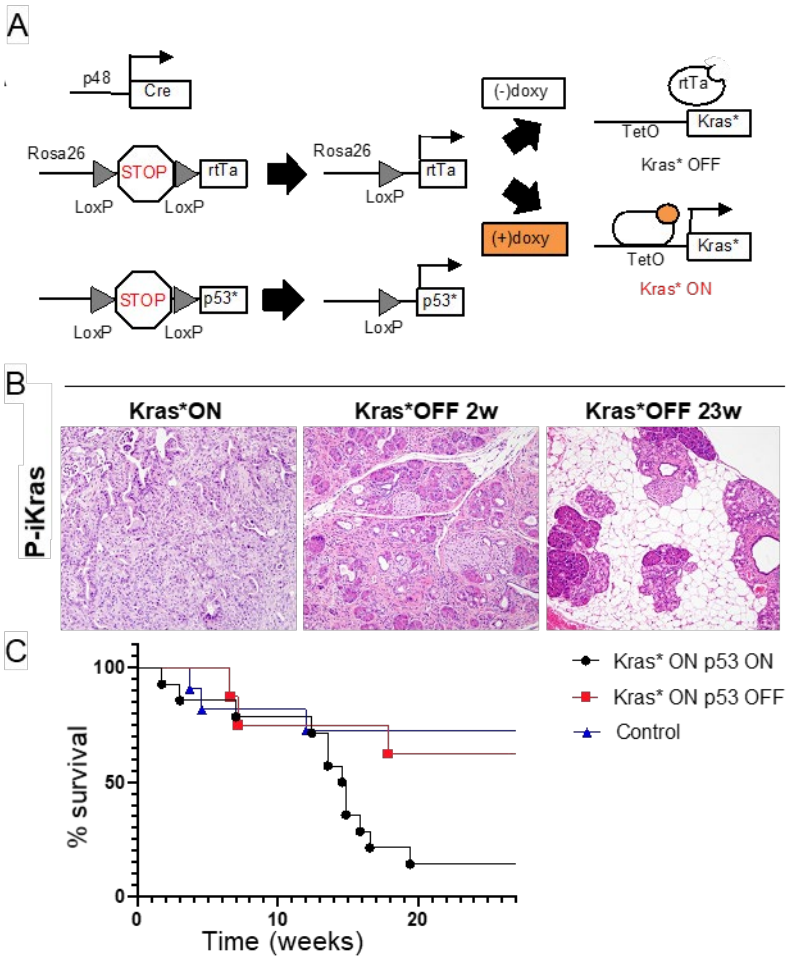

Supplemental Figure 4.1 Addition of mutant p53 results in worse survival for L-iKras mice

(A) The genetic makeup of the P-iKras mouse model of pancreas tumorigenesis with p48-Cre;R26-LSL-rtTA-IRES-EGFP;TetO-Kras^{G12D};LSL-p53^{R172H}. **(B)** H&E staining of P-iKras murine pancreas after treatment with doxycycline or with removal of doxycycline at indicated time points. **(C)** Survival curve of L-iKras mice ON doxycycline with p53 ON or OFF versus control.

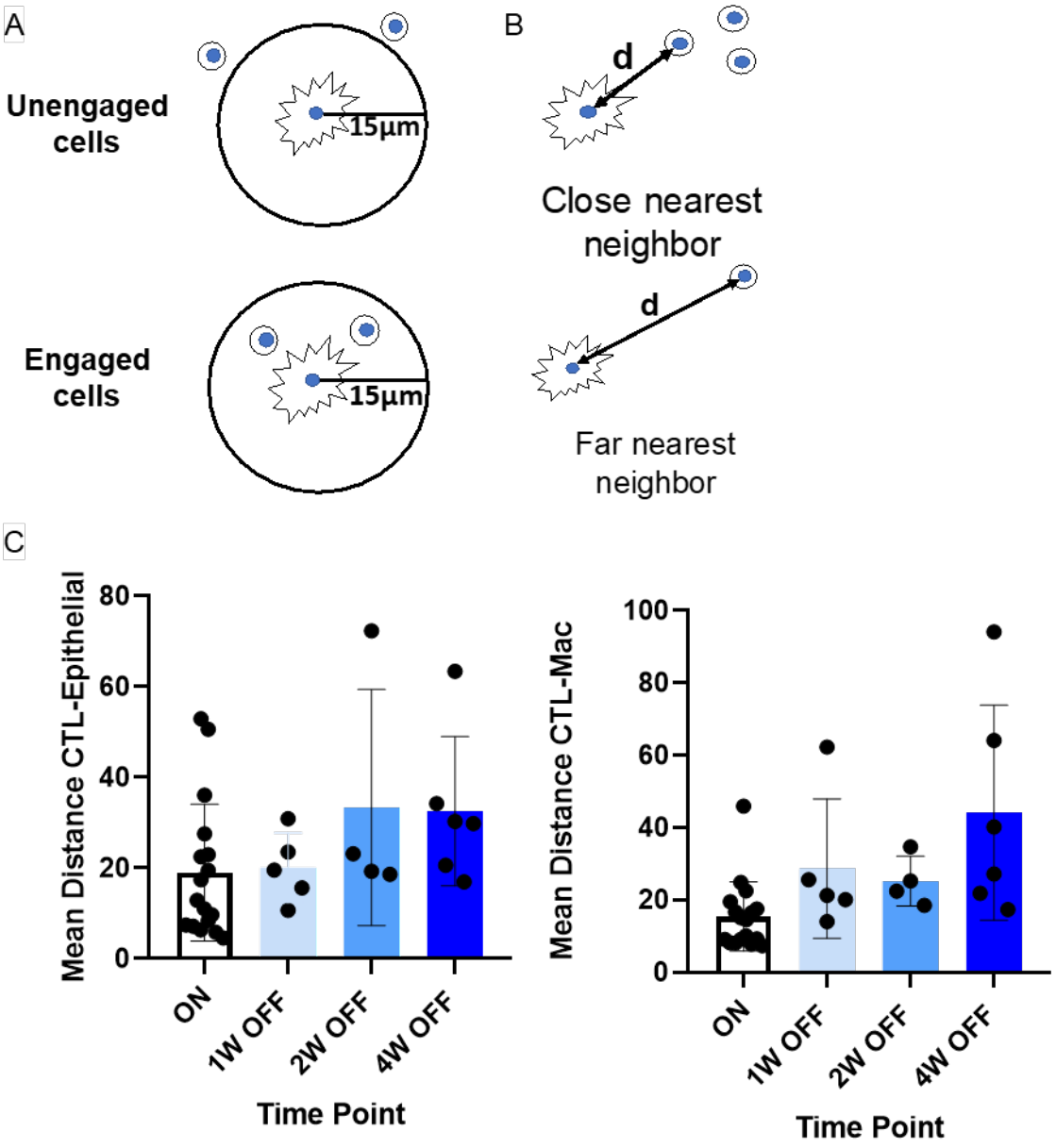

Supplemental Figure 4.2 mfIHC reveals steady T cell engagement in the L-iKras lung TME

(A) Schematic of inForn® Cell Analysis™ **(A)** engagement and **(B)** mean distance calculation. **(C)** Comparison of the mean CTL-Epithelial/Macrophage distance. No significant p value was found in these comparisons.

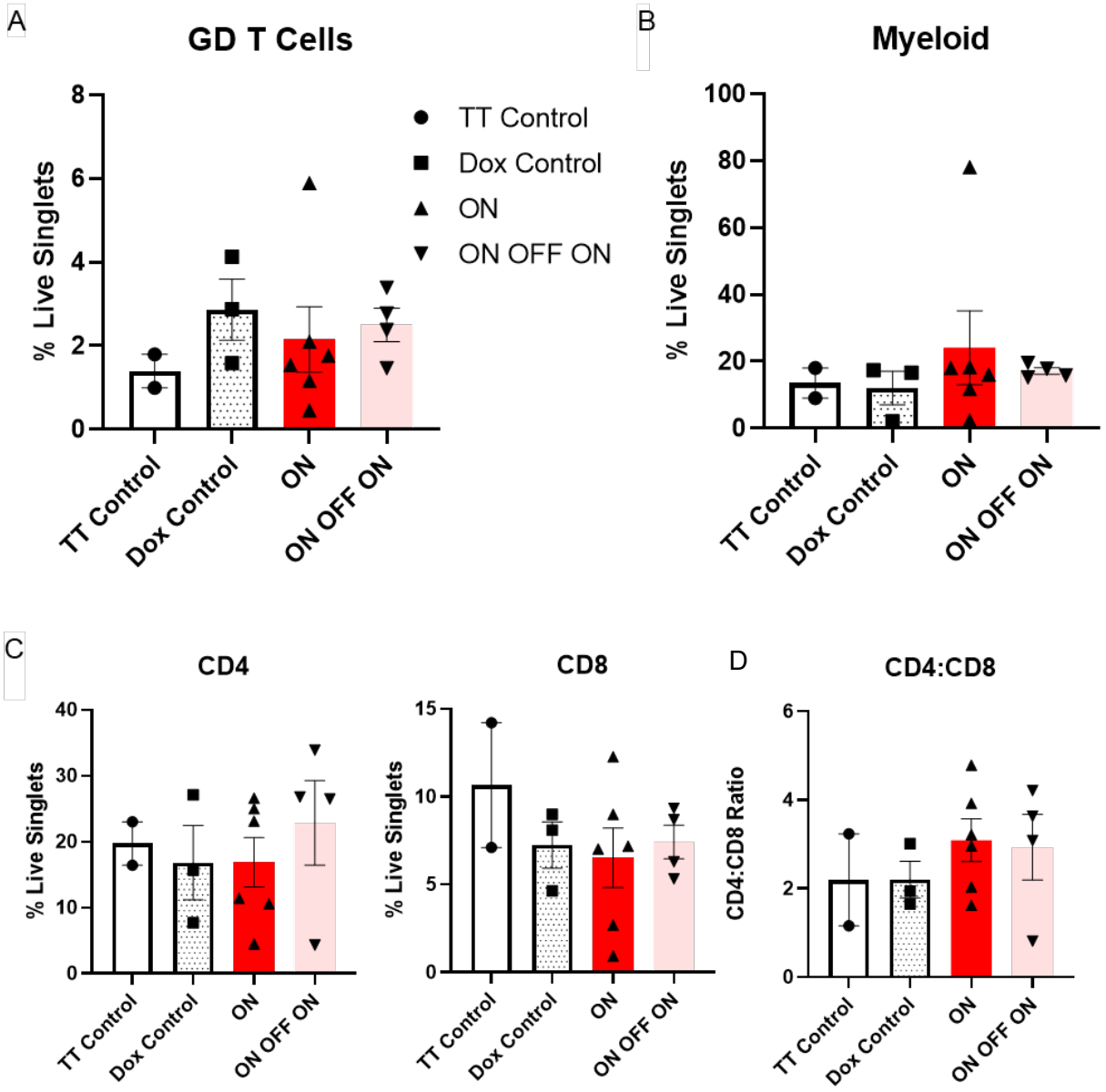

Supplemental Figure 4.3 T cells and myeloid cell levels remain steady during tumor regrowth

(A-C) Flow cytometry analysis of immune cells, specifically gd/CD4/CD8 T cells and CD11b+ myeloid cells as a percentage of total cells in control or P-iKras* lung at the indicated time points. **(D)** Ratio of CD4:CD8 T cells. n = 6-12 mice per group, shown as mean ± SD, multiple comparison ANOVA and multiple comparison Kruskal Wallis.

Appendix 2: Supplemental Tables

Supplemental Table 2.1 CyTOF antibody panel

Catalog Number	Metal Tag	Marker	Clone	Dilution	Source
3141019B	141Pr	CD3	UCHT1	1:200	Fluidigm
3142001B	142Nd	CD19	HIB19	1:300	Fluidigm
3144019B	144Nd	CD15 (SSEA-1)	W6D3	1:400	Fluidigm
3145010B	145Nd	CD163	GHI/61	1:100	Fluidigm
3146006B	146Nd	CD64	10.1	1:100	Fluidigm
3148004B	148Nd	CD16	3G8	1:400	Fluidigm
3151002B	151Eu	CD107a (LAMP1)	H4A3	1:100	Fluidigm
3152011B	152Sm	CD66b	80H3	1:200	Fluidigm
3153023B	153Eu	CD192 (CCR2)	K036C2	1:200	Fluidigm
3154016B	154Sm	TIGIT	MBSA43	1:100	Fluidigm
3155009B	155Gd	CD279 (PD-1)	EH12.2H7	1:100	Fluidigm
3156026B	156Gd	CD274 (PD-L1)	29E.2A3	1:100	Fluidigm
3162015B	162Dy	CD8a	RPA-T8	1:200	Fluidigm
3163023B	163Dy	CD33	WM53	1:200	Fluidigm
3165011B	165Ho	CD45RO	UCHL1	1:200	Fluidigm
3166012B	166Er	CD34	581	1:100	Fluidigm
201167A	167Er	CD45RA	HI100	1:100	Fluidigm
3168008B	168Er	CD206 (MMR)	15-2	1:100	Fluidigm
3169003B	169Tm	CD25 (IL-2R)	2A3	1:100	Fluidigm
3170005B	170Er	CD152 (CTLA-4)	14D3	1:100	Fluidigm
3171011B	171Yb	CD68	Y1/82A	1:100	Fluidigm
3172014B	172Yb	CD273 (PD-L2)	24F.10C12	1:100	Fluidigm
3173005B	173Yb	HLA-DR	L243	1:400	Fluidigm
3175015B	175Lu	CD14	M5E2	1:100	Fluidigm
3176010B	176Yb	CD4	RPA-T4	1:100	Fluidigm
3209003B	209Bi	CD11b (Mac-1)	ICRF44	1:200	Fluidigm
3089003B	89Y	CD45	HI30	1:200	Fluidigm
3150030B	150Nd	LAG3	11C3C65	1:100	Fluidigm
3160020B	160Gd	CD23	EBVCS-5	1:100	Fluidigm
3149021B	149Sm	CD56 (NCAM)	NCAM16.2	1:100	Fluidigm

Supplemental Table 2.2 Clinical information

Patient ID	Sex	Age	BMI	Disease State	Stage	Grade
20191245	M	58	23	PDAC	ypT1cN1	Well Differentiated
20191176t1	F	84	28	PDAC	ypT2N1Mx	Well Differentiated
20191176t2	F	84	28	PDAC	ypT2N1Mx	Well Differentiated
20181129	M	62	29	PDAC	ypT1N0Mx	Poorly Differentiated
20181157	F	65	17	PDAC	pT3N1R0	Poorly Differentiated
20191180	F	60	25	PDAC	pT3N1MX	Poorly differentiated
20191210	F	46	17	PDAC	Metastatic	Poorly Differentiated
20191225	F	58	16	PDAC	yoT2N1Mx	poorly Differentiated
20191231	M	58	26	PDAC	Metastatic	Poorly Differentiated
19-384	M	51	28	Bile Duct Carcinoma	pT2N1Mx	Poorly Differentiated
8839995	?	?	?	Healthy	N/A	N/A
8839996	?	?	?	Healthy	N/A	N/A
8839999	?	?	?	Healthy	N/A	N/A
20191194	F	63	35	Healthy	N/A	N/A
20191195	F	64	?	Healthy	N/A	N/A
20191196	F	70	18	Duodenal Adenoma	N/A	N/A
20191203	M	71	24	Healthy	N/A	N/A
20191205	M	63	26	Healthy	N/A	N/A
20191206	F	43	25	Healthy	N/A	N/A

Patient ID	Sex	Age	BMI	Disease State	Stage	Grade
20191209	F	64	37	Chronic Pancreatitis	N/A	N/A
20191211	M	45	?	Healthy	N/A	N/A
20191212	F	46	?	Healthy	N/A	N/A
20191219	F	74	29	Chronic Pancreatitis	N/A	N/A
20191226	M	31	29	Chronic Pancreatitis	N/A	N/A
20191228	M	58	23	Chronic Pancreatitis	N/A	N/A
20191230	F	57	28	Chronic Pancreatitis	N/A	N/A
20191232	F	57	?	Healthy	No	N/A
20191233	F	52	?	Healthy	No	N/A
20191234	M	70	?	Healthy	No	N/A
20191235	F	69	27	Duodenal Adenoma	N/A	N/A
20191236	F	42	23	Healthy	N/A	N/A
20191237	M	62	38	Chronic Pancreatitis	N/A	N/A
20191244	F	62	16	Chronic Pancreatitis	N/A	N/A
20191247	F	33	29	Healthy	N/A	N/A
20191249	M	40	25	Chronic Pancreatitis	N/A	N/A
20191257	F	65	24	Healthy	N/A	N/A

Patient ID	Sex	Age	BMI	Disease State	Stage	Grade
19-249	F	73	35	Serous Cystadenoma	N/A	N/A
19-469	M	74	31	IPMN	N/A	N/A
20171064	M	66	38	PDAC	Initially ypT3N0, now metastatic	Moderately differentiated
20171085	M	63	32	PDAC	pT3N1	Moderately differentiated
20181121	F	69	22	PDAC	pT2N1M0	Moderately differentiated
20191172	F	81	17	PDAC	pT1cN0	Moderately differentiated
20191204	M	60	22	PDAC	ypT1c N0	Moderately differentiated
20191207	M	74	28	PDAC	pT2N0	Moderately differentiated
20191262	F	63	29	PDAC	pT2 N0	Moderately differentiated
19-262	M	55	26	PDAC	pT2N2	Moderately differentiated
20191258	F	77	25	Ampullary Carcinoma	pT1b N1	Moderate to poorly differentiated

Patient ID	Sex	Age	BMI	Disease State	Stage	Grade
20191227	F	40	23	Metastatic Ovarian Carcinoma	IVB	High-grade
20191223	M	56	23	PDAC	ypT3N0M0	GX cannot be assessed
20181141	F	80	27	PDAC	pT2N1R1	G2 Moderately differentiated
20181107	F	49	19	PDAC	pT2N0M1	Cannot be assessed due to treatment effect
20160897	M	67	26	PDAC	Metastatic	?
20171027	F	53	30	PDAC	Metastatic	?
20171040	F	62	29	PDAC	Initially ypT3N1Mx, now Metastatic	?
20191198	F	47	34	PDAC	Borderline resectable	?
20191201	F	70	22	PDAC	Borderline resectable	?
20191202	F	74	19	PDAC	Metastatic	?
20191213	M	61	23	oncocytic IPMN, possible PDAC	Borderline resectable	?

Patient ID	Sex	Age	BMI	Disease State	Stage	Grade
20191214	M	54	40	PDAC	Localized	?
20191215	F	70	32	PDAC	Borderline resectable	?
20191216	M	68	23	PDAC	Resectable	?
20191221	M	76	19	PDAC	Metastatic	?
20191222	M	58	49	PDAC	Metastatic	?
20191229	M	65	21	PDAC	Localized	?
20191243	M	83	27	PDAC	Metastatic	?
20191246	M	47	30	PDAC	locally advanced	?
61353210	F	68	24	PDAC	Metastatic	?
61354860	F	73	20	PDAC	Borderline resectable	?
61619600	F	47	39	PDAC	Metastatic	?
20160882t1	F	71	22	PDAC	Metastatic	?
20160882t2	F	71	22	PDAC	Metastatic	?
20191222t2	M	58	49	PDAC	Metastatic	?
20191229 (6750)	M	65	21	PDAC	Localized	?
20191238t1	F	70	30	PDAC	Borderline resectable	?

Patient ID	Sex	Age	BMI	Disease State	Stage	Grade
20191238t2	F	70	30	PDAC	Borderline resectable	?

Patient ID	Collected on Surgery Day?	Pre-Surgical	s/p Surgery	Metastatic	Lymphovascular Invasion (in surgical samples)	Perineural Invasion (in surgical samples)
20191245	Yes	No	No	No	Yes	Yes
20191176t1	Yes	No	No	No	Yes	No
20191176t2	No	No	Yes	No	Yes	No
20181129	No	No	Yes	No	No	No
20181157	No	No	Yes	No	Yes	No
20191180	No	No	yes	No	Yes	Yes
20191210	No	No	No	Yes	N/A	N/A
20191225	Yes	No	No	No	Yes	Yes
20191231	No	N/A	No	Yes	N/A	N/A
19-384	Yes	No	No	No	Yes	Yes
8839995	No	N/A	No	N/A	N/A	N/A
8839996	No	N/A	No	N/A	N/A	N/A
8839999	No	N/A	No	N/A	N/A	N/A
20191194	No	N/A	No	N/A	N/A	N/A
20191195	No	N/A	No	N/A	N/A	N/A
20191196	Yes	N/A	No	N/A	N/A	N/A
20191203	No	N/A	No	N/A	N/A	N/A
20191205	No	N/A	No	N/A	N/A	N/A
20191206	No	N/A	No	N/A	N/A	N/A

Patient ID	Collected on Surgery Day?	Pre-Surgical	s/p Surgery	Metastatic	Lymphovascular Invasion (in surgical samples)	Perineural Invasion (in surgical samples)
20191209	No	N/A	No	N/A	N/A	N/A
20191211	No	N/A	No	N/A	N/A	N/A
20191212	No	N/A	No	N/A	N/A	N/A
20191219	No	N/A	No	N/A	N/A	N/A
20191226	No	N/A	No	N/A	N/A	N/A
20191228	No	N/A	No	N/A	N/A	N/A
20191230	No	N/A	No	N/A	N/A	N/A
20191232	No	N/A	N/A	N/A	N/A	N/A
20191233	No	N/A	N/A	N/A	N/A	N/A
20191234	No	N/A	N/A	N/A	N/A	N/A
20191235	Yes	N/A	No	N/A	N/A	N/A
20191236	No	N/A	No	N/A	N/A	N/A
20191237	No	N/A	No	N/A	N/A	N/A
20191244	No	N/A	No	N/A	N/A	N/A
20191247	No	N/A	No	N/A	N/A	N/A
20191249	No	N/A	No	N/A	N/A	N/A

Patient ID	Collected on Surgery Day?	Pre-Surgical	s/p Surgery	Metastatic	Lymphovascular Invasion (in surgical samples)	Perineural Invasion (in surgical samples)
20191257	No	N/A	No	N/A	N/A	N/A
19-249	Yes	No	No	N/A	N/A	N/A
19-469	Yes	No	No	N/A	N/A	N/A
20171064	No	No	Yes	Yes	Yes	Yes
20171085	No	No	Yes	No	Yes	Yes
20181121	No	No	Yes	No	Yes	No
20191172	Yes	No	No	No	No	No
20191204	Yes	No	No	No	No	No
20191207	Yes	No	Yes	No	Yes	Yes
20191262	Yes	No	No	No	Yes	Yes
19-262	Yes	No	No	No	Yes	Yes
20191258	Yes	N/A	N/A	No	N/A	N/A

Patient ID	Collected on Surgery Day?	Pre-Surgical	s/p Surgery	Metastatic	Lymphovascular Invasion (in surgical samples)	Perineural Invasion (in surgical samples)
20191227	Yes	No	yes - cyt	Yes	N/A	N/A
20191223	Yes	No	No	No	Yes	Yes
20181141	Yes	Yes	No	No	Yes	Yes
20181107	Yes	Yes	No	Yes, liver met extending to resected margin	Yes	Yes
20160897	No	N/A	Yes, Pall	Yes	N/A	N/A
20171027	No	N/A	No	Yes	N/A	N/A
20171040	No	No	Yes	Yes	N/A	N/A
20191198	No	Yes	No	No	N/A	N/A
20191201	No	Yes	No	No	N/A	N/A
20191202	No	No	No	Yes	N/A	N/A

Patient ID	Collected on Surgery Day?	Pre-Surgical	s/p Surgery	Metastatic	Lymphovascular Invasion (in surgical samples)	Perineural Invasion (in surgical samples)
20191213	No	Yes	Yes, dist	No	N/A	N/A
20191214	No	Yes	No	No	N/A	N/A
20191215	No	Yes	No	No	N/A	N/A
20191216	No	Yes	No	No	N/A	N/A
20191221	No	N/A	No	Yes	N/A	N/A
20191222	No	N/A	No	Yes	N/A	N/A
20191229	No	Yes	yes - pall	No	N/A	N/A
20191243	No	N/A	No	Yes	N/A	N/A
20191246	No	Yes	No	No	N/A	N/A
61353210	No	No	No	Yes	N/A	N/A
61354860	No	Yes	No	No	N/A	N/A
61619600	No	N/A	No	Yes	N/A	N/A
20160882t1	No	N/A	No	Yes	N/A	N/A
20160882t2	No	N/A	No	Yes	N/A	N/A

Patient ID	Collected on Surgery Day?	Pre-Surgical	s/p Surgery	Metastatic	Lymphovascular Invasion (in surgical samples)	Perineural Invasion (in surgical samples)
20191222t2	No	N/A	No	Yes	N/A	N/A
20191229 (6750)	No	Yes	No	No	N/A	N/A
20191238t1	No	Yes	No	No	N/A	N/A
20191238t2	No	Yes	No	No	N/A	N/A

Patient ID	Treatment	Prior Treatment	Current treatment Regimen
20191245	s/p neoadjuvant chemo -> Whipple	FOLFOXIRI -> nab-paclitaxel/gemcitabine-> Whipple	None
20191176t1	neoadjuvant gem/cap -> distal panc	N/A	None
20191176t2	neoadjuvant gem/cap -> distal panc ->adjuvant capecitabine/radation	N/A	Capecitabine
20181129	s/p neoadjuvant chemo, whipple	folfirinox -> Gem/abraxane	None
20181157	s/p whipple, adjuvant chemo	N/A	mFOLFIRINOX
20191180	s/p chemo and distal panc	Neoadjuvant modified FOLFIRINOX -> distal pancreatectomy -> FOLFOX	FOLFOX
20191210	s/p chemo	s/p nab-paclitaxel+gemcitabine +/- PegPH20 -> mFOLFIRINOX	mFOLFIRINOX
20191225	s/p neoadjuvant chemo -> distal panc	s/p gemcitabine/paclitaxel	None
20191231	Treatment Naïve	N/A	None
19-384	Treatment Naïve	N/A	Whipple
8839995	N/A	N/A	N/A
8839996	N/A	N/A	N/A
8839999	N/A	N/A	N/A
20191194	N/A	N/A	N/A
20191195	N/A	N/A	N/A
20191196	N/A	N/A	N/A
20191203	N/A	N/A	N/A
20191205	N/A	N/A	N/A
20191206	N/A	N/A	N/A

Patient ID	Treatment	Prior Treatment	Current treatment Regimen
20191209	N/A	N/A	N/A
20191211	N/A	N/A	N/A
20191212	N/A	N/A	N/A
20191219	N/A	N/A	N/A
20191226	N/A	N/A	N/A
20191228	N/A	N/A	N/A
20191230	N/A	N/A	N/A
20191232	N/A	N/A	N/A
20191233	N/A	N/A	N/A
20191234	N/A	N/A	N/A
20191235	N/A	N/A	N/A
20191236	N/A	N/A	N/A
20191237	N/A	N/A	N/A
20191244	N/A	N/A	N/A
20191247	N/A	N/A	N/A
20191249	N/A	N/A	N/A
20191257	N/A	N/A	N/A

Patient ID	Treatment	Prior Treatment	Current treatment Regimen
19-249	Treatment Naïve	N/A	distal pancreatectomy
19-469	N/A	N/A	distal pancreatectomy
20171064	s/p whipple -> chemo for recurrance	N/A	Gem/Abraxane
20171085	s/p whipple -> adjuvant chemo	N/A	Gem/Capecitabine
20181121	s/p distal pancreatectomy, chemo	Gem/capectabine, gem discontinued	Capecitabine
20191172	Treatment Naïve	N/A	distal pancreatectomy
20191204	s/p neoadjuvant chemo -> Whipple	Neoadjuvant gemcitabine and nab-□paclitaxel	None
20191207	s/p distal pancreatectomy	N/A	None
20191262	Treatment Naïve	N/A	distal pancreatectomy
19-262	Treatment Naïve	N/A	Whipple
20191258	Treatment Naïve Whipple	N/A	None

Patient ID	Treatment	Prior Treatment	Current treatment Regimen
20191227	s/p chemo and cytoreductive surgery	carboplatin/docetaxel -> cytoreduction surgery -> carboplatin and docetaxel -> niraparib	nirapanib
20191223	s/p neoadjuvant chemo and radiation -> distal panc	s/p mFOLFIRINOX -> chemoradiation with gemzar	None
20181141	Treatment naïve	N/A	None
20181107	s/p Liver resection, Partial pancreatectomy, partial gastrectomy, s/p chemo	neoadjuvant gem/abraxane	None
20160897	on chemo	N/A	Gem/Abraxane
20171027	s/p chemo	mFOLFIRINOX	Break (last chemo 2 months prior)
20171040	s/p neoadjuvant chemo -> whipple	s/p neoadjuvant gem/cis, whipple 8/2/17, adjuvent with gem/cap -> recurrance with metastatic disease	None, about to start mFOLFIRINOX
20191198	on neoadjuvant chemo	N/A	mFOLFIRINOX
20191201	on neoadjuvant chemo	N/A	mFOLFIRINOX
20191202	On chemo	FOLFIRINOX -> gemcitabine/Abraxane -> FOLFOX	FOLFOX
20191213	s/p distal pancreatectomy for IPMN, palliative gastro-jej	s/p distal pancreatectomy for IPMN, palliative gastro-jej	None

Patient ID	Treatment	Prior Treatment	Current treatment Regimen
20191214	Treatment Naïve	N/A	none, about to start mFOLFIRINIX
20191215	Treatment Naïve	N/A	none, about to start neoadjuvant mFOLFIRINIX
20191216	Treatment Naïve	N/A	none, about to start neoadjuvant mFOLFIRINIX
20191221	Treatment Naïve	N/A	None, about to start gemcitabine/abraxane
20191222	Treatment Naïve	N/A	None, about to start gemcitabine, cisplatin, and fluorouracil
20191229	s/p palliative gastrojej and ptc, neoadjuvant chemo	N/A	GAX-P - gamcitabine, abraxane, capecitabine, and cisplatin
20191243	s/p chemo/RT	gemcitabine-RT -> gemcitabine -> gemcitabine/capecitabine -> gemcitabine	Gemcitabine
20191246	Treatment Naïve	N/A	None
61353210	Treatment Naïve	N/A	None
61354860	Treatment Naïve	N/A	None
61619600	Treatment Naïve	N/A	None
20160882t1	on chemo	Mk1775+Gemcitabine -> FOLFOX6 -> Gem/Capecitadine -> progression -> abraxane monotherapy	Gem/Abraxane
20160882t2	on chemo	Mk1775+Gemcitabine -> FOLFOX6 -> Gem/Capecitadine -> progression -> abraxane monotherapy	Gem/Abraxane

Patient ID	Treatment	Prior Treatment	Current treatment Regimen
20191222t2	on chemo	N/A	gemcitabine, cisplatin, and fluorouracil
20191229 (6750)	Treatment Naïve	N/A	None
20191238t1	Treatment Naïve	N/A	None
20191238t2	s/p chemo	GAX (capecitabine, gemcitabine, abraxane)-> capecitabine/abraxane	capecitabine/Abraxane

Patient ID	Time point	Disease Years	CA19-9 Initial	Date Initial CA19-9	CA19-9 Current	Date current CA19-9	Associated IPMN
20191245	1	<1	203	3/29/2019			No
20191176t1	1	1	13	8/6/2018	4	12/13/2018	No
20191176t2	2	1	13	8/6/2018	4	12/13/2018	No
20181129	1	1	7	7/11/2018	21	4/15/2019	No
20181157	1	<1	5	11/30/2018	6	2/4/2019	No
20191180	1	<1	431	1/7/2019	40	3/19/2019	Yes
20191210	1	2	854	8/14/2017	627	3/12/2019	No
20191225	1	1	25	7/26/2018	6.1	2/4/2019	No
20191231	1	<1	199	3/13/2019			No
19-384	1	<1	N/A	N/A	N/A	N/A	No
8839995	1	N/A	N/A	N/A	N/A	N/A	N/A
8839996	1	N/A	N/A	N/A	N/A	N/A	N/A
8839999	1	N/A	N/A	N/A	N/A	N/A	N/A
20191194	1	N/A	N/A	N/A	N/A	N/A	N/A
20191195	1	N/A	N/A	N/A	N/A	N/A	N/A
20191196	1	N/A	N/A	N/A	N/A	N/A	N/A

Patient ID	Time point	Disease Years	CA19-9 Initial	Date Initial CA19-9	CA19-9 Current	Date current CA19-9	Associated IPMN
20191203	1	N/A	N/A	N/A	N/A	N/A	N/A
20191205	1	N/A	N/A	N/A	N/A	N/A	N/A
20191206	1	N/A	N/A	N/A	N/A	N/A	N/A
20191209	1	N/A	N/A	N/A	N/A	N/A	No
20191211	1	N/A	N/A	N/A	N/A	N/A	N/A
20191212	1	N/A	N/A	N/A	N/A	N/A	N/A
20191219	1	N/A	N/A	N/A	N/A	N/A	Yes
20191226	1	N/A	N/A	N/A	N/A	N/A	No
20191228	1	N/A	N/A	N/A	N/A	N/A	No
20191230	1	N/A	N/A	N/A	N/A	N/A	No
20191232	1	N/A	N/A	N/A	N/A	N/A	?
20191233	1	N/A	N/A	N/A	N/A	N/A	?
20191234	1	N/A	N/A	N/A	N/A	N/A	?
20191235	1	N/A	N/A	N/A	N/A	N/A	No
20191236	1	N/A	N/A	N/A	N/A	N/A	No
20191237	1	N/A	N/A	N/A	N/A	N/A	No

Patient ID	Time point	Disease Years	CA19-9 Initial	Date Initial CA19-9	CA19-9 Current	Date current CA19-9	Associated IPMN
20191244	1	N/A	N/A	N/A	N/A	N/A	No
20191247	1	N/A	N/A	N/A	N/A	N/A	No
20191249	1	N/A	N/A	N/A	N/A	N/A	No
20191257	1	N/A	N/A	N/A	N/A	N/A	No
19-249	1	N/A	N/A	N/A	N/A	N/A	Yes
19-469	1	N/A	N/A	N/A	N/A	N/A	Yes
20171064	1	2	310	5/8/2017	16,649	4/30/2019	Yes
20171085	1	2	484	8/8/2017	28	4/22/2019	No

Patient ID	Time point	Disease Years	CA19-9 Initial	Date Initial CA19-9	CA19-9 Current	Date current CA19-9	Associated IPMN
20181121	1	1	5	7/23/2018	9	8/10/2018	Yes
20191172	1	<1	<2	10/25/2018	<2	12/28/2018	No
20191204	1	1	218	7/23/2018	29	4/1/2019	Yes
20191207	1	<1	83	12/13/2018	73	1/14/2019	No
20191262	1	<1	59	5/9/2019			No
19-262	1	<1	159	2/11/2019	17	2/28/2019	No
20191258	1	<1	13	3/18/2019	N/A	N/A	No
20191227	1	4	N/A	N/A	N/A	N/A	No
20191223	1	1	7122	8/20/2018	289	3/18/2019	No
20181141	1	<1	2454	10/1/2018	N/A	N/A	Yes

Patient ID	Time point	Disease Years	CA19-9 Initial	Date Initial CA19-9	CA19-9 Current	Date current CA19-9	Associated IPMN
20181107	1	1	670	6/6/2018	182	1/29/2019	No
20160897	1	3	89	8/2/2016	2062	4/2/2019	No
20171027	1	2	1384	4/3/2017	152	4/29/2019	no
20171040	1	2	16	3/24/2017	54	4/17/2019	No
20191198	1	<1	10	3/11/2019	33	4/8/2019	No
20191201	1	<1	17	2/14/2019	20	4/23/2019	No
20191202	1	1	26,000	3/13/2019	17523	4/23/2019	No
20191213	1	<1	7	12/29/2014			Yes
20191214	1	<1	36	3/4/2019			No
20191215	1	<1	698	3/19/2019			No
20191216	1	<1	16	3/18/2019			No
20191221	1	<1	32	4/2/2019			No
20191222	1	<1	813853	3/18/2019			No

Patient ID	Time point	Disease Years	CA19-9 Initial	Date Initial CA19-9	CA19-9 Current	Date current CA19-9	Associated IPMN
20191229	2	<1	10	3/8/2019	24	4/19/2019	No
20191243	1	<1	312	10/16/2018	920	4/16/2019	No
20191246	1	<1	447	3/4/2019			No
61353210	1	<1	9	2/25/2019			No
61354860	1	<1	154	12/10/2018			No
61619600	1	<1	5767	10/29/2018			No
20160882t1	1	3	2402	8/1/2016	50305	4/30/2019	No
20160882t2	2	3	2402	8/1/2016	50305	4/30/2019	No
20191222t2	2	<1	813853	3/18/2019	240,473	5/13/2019	No
20191229 (6750)	1	<1	10	3/8/2019			No
20191238t1	1	<1	190	1/18/2019			No
20191238t2	1	<1	190	1/18/2019	42	4/5/2019	No

Patient ID	History of Pancreatitis	Hx diabetes (before prognosis)	Smoking (pack years)	Current Alcohol Use	Prior Cancer History	Family Hx Cancer
20191245	No	No	0	Yes	No	None
20191176t1	No	No	0	No	No	sister–colorectal cancer, brother–prostate cancer
20191176t2	No	No	0	No	No	sister–colorectal cancer, brother–prostate cancer
20181129	No	No	12, quit 1985	Yes	No	Father - pancreatic cancer, paternal grandmother - cancer, paternal grandfather - cancer
20181157	No	No	25	Yes	No	Mother - Colon cancer
20191180	No	No	1.25 pack years, quit 1985	Yes	No	Maternal grandmother–pancreatic cancer, maternal uncle–pancreatic cancer
20191210	No	No	0	Yes	No	Maternal grandmother - colon cancer
20191225	No	No	11.25, current	No	No	Maternal grandfather - lung cancer
20191231	No	No	40, currect	No	No	Mother - gastric cancer
19-384	No	Yes	0	No	No	None
8839995	?	?	?	?	?	?
8839996	?	?	?	?	?	?
8839999	?	?	?	?	?	?
20191194	No	Yes	?	?	?	?
20191195	?	?	?	?	?	?
20191196	No	No	0	Yes	Yes–basal cell	Mother–lung cancer, father–colon cancer,

Patient ID	History of Pancreatitis	Hx diabetes (before prognosis)	Smoking (pack years)	Current Alcohol Use	Prior Cancer History	Family Hx Cancer
					carcinoma	sister–breast cancer
20191203	No	No	1.8 pack years–quit 1992	No	No	Mother–breast cancer
20191205	No	No	0	No	No	None
20191206	No	No	0	Yes	No	None
20191209	Yes	No	0	No	No	None
20191211	?	?	?	?	?	?
20191212	?	?	?	?	?	?
20191219	Yes	Yes	60 pack years, quit 2014	No	No	Mother - cancer, brother - cancer
20191226	Yes	No	0	Yes	No	None
20191228	Yes	No	0	No	No	Mother - pancreatic cancer, father - colon cancer, sister - lung cancer, brother - brain cancer
20191230	Yes	Yes	? Quit 1999	No	No	Mother - colon cancer, brother - lymphoma
20191232	?	?	?	?	?	?
20191233	?	?	?	?	?	?
20191234	?	?	?	?	?	?
20191235	No	No	0	No	No	Father - colon cancer, sister - colon cancer, brother - bladder cancer
20191236	Yes, one episode of acute pancreatitis	No	17 pack years, quit 2014	Yes	No	Mother - Cancer, Grandmother - stomach cancer

Patient ID	History of Pancreatitis	Hx diabetes (before prognosis)	Smoking (pack years)	Current Alcohol Use	Prior Cancer History	Family Hx Cancer
20191237	Yes, one episode of acute pancreatitis <1 month prior	Yes	68 pack years, quit 2019	Yes	No	Mother - Cancer, brother -cancer
20191244	Yes	No	7.5 pack years, current	No	No	Mother - cancer
20191247	No	No	6.5 pack years, current	No	No	Mother - cancer
20191249	Yes	No	11 pack years, current	No	No	None
20191257	No	No	50 pack years, current	Yes	No	Brother - mouth cancer, stomach cancer, sister - basal cell carcinoma, sister - stomach cancer
19-249	No	No	15 pack years, quit 2006	Yes	No	Father - prostate cancer, sister - gallbladder cancer
19-469	No	No	5 pack years, quit 1975	Yes	No	None

Patient ID	History of Pancreatitis	Hx diabetes (before prognosis)	Smoking (pack years)	Current Alcohol Use	Prior Cancer History	Family Hx Cancer
20171064	No	No	0	Yes	No	Mother - lung cancer, father - cancer
20171085	No	Yes	0	Yes	No	Father - lung cancer, brother - liver cancer
20181121	No	No	0	No	No	None
20191172	Yes - Acute and chronic	Yes	0	No	N	Y - sister (sarcoma), mother (breast)
20191204	No	No	60 pack years– quit in 1990	No	No	Brother–throat cancer
20191207	No	Yes	120, quit 1997	Yes	Yes - Colon cancer	Sister - Breast Cancer, brother prostate cancer
20191262	No	No	0	No	No	None
19-262	No	No	38 pack years, quit 1/1/14	Yes	No	Mother - lung cancer
20191258	No	No	20 pack years, quit 1995	No	No	Mother - cancer
20191227	No	No	0	No	No	Mother - breast cancer, sister breast cancer, maternal Aunt - breast cancer,

Patient ID	History of Pancreatitis	Hx diabetes (before prognosis)	Smoking (pack years)	Current Alcohol Use	Prior Cancer History	Family Hx Cancer
						maternal aunt - uterine cancer,
20191223	No	Yes	0	Yes	No	Mother - colon cancer, sister - breast cancer, maternal grandmother - lymphoma
20181141	No	No	18 pack years, quit 2015 years a	No	No	Lung cancer in brother and maternal aunt
20181107	Yes	No	33 pack years, quit 2019	No	No	Mother - gallbladder cancer, father - lung cancer
20160897	No	Yes	0	Yes	No	Mother - pancreatic and colon cancer, father - prostate cancer
20171027	No	No	25 pack years, quit 2011	No	No	Mother - Breast cancer, maternal aunt Breast cancer, father Prostate cancer
20171040	No	No	0	No	No	Sister- pancreatic cancer, brother - pancreatic cancer
20191198	No	No	16 pack years, quit 2005	Yes	No	Maternal grandmother–colon cancer, maternal aunt–breast cancer, paternal aunt–breast cancer, paternal uncle–colon cancer

Patient ID	History of Pancreatitis	Hx diabetes (before prognosis)	Smoking (pack years)	Current Alcohol Use	Prior Cancer History	Family Hx Cancer
20191201	No	No	7 pack years, quit 1972	Yes	No	Father–cancer, brother–prostate cancer, brother–oral cancer
20191202	No	No	0	Yes	No	Father–colon cancer
20191213	No	Yes	0	No	No	Mother - pancreatic cancer
20191214	No	Yes	0	Yes	Yes - B Cell lymphoma	maternal grandmother - pancreatic cancer, mother - melanoma, father - prostate cancer and melanoma
20191215	No	Yes	0	Yes	No	Father - colon cancer, paternal grandmother - lung cancer, maternal uncle - lung cancer
20191216	No	Yes	0	No	No	Sister - breast cancer, father - colon cancer, maternal grandmother - breast cancer
20191221	No	No	0	No	No	Father - lung cancer
20191222	No	Yes	0	Yes	No	Mother - lung cancer, father - mesothelioma, maternal aunt - pancreatic cancer and lung cancer
20191229	No	No	0	Yes	No	Father - prostate cancer, sister - breast cancer
20191243	No	No	11 pack years, quit 1968	Yes	Yes - basal cell carcinoma	Mother - skin cancer, father - skin cancer

Patient ID	History of Pancreatitis	Hx diabetes (before prognosis)	Smoking (pack years)	Current Alcohol Use	Prior Cancer History	Family Hx Cancer
20191246	No	No	0	No	No	Mother - breast cancer, sister - breast cancer
61353210	No	No	7.5 pack years, quit 1986	Yes	No	Sister - Breast Cancer
61354860	No	No	15 pack years, quit 1989	Yes	No	None
61619600	No	No	0	Yes	No	Father - prostate cancer
20160882t1	No	Yes	0	No	No	Mother and brother - cancer
20160882t2	No	Yes	0	No	No	Mother and brother - cancer
20191222t2	No	Yes	0	Yes	No	Mother - lung cancer, father - mesothelioma, maternal aunt - pancreatic cancer and lung cancer
20191229 (6750)	No	No	0	Yes	No	Father - prostate cancer, sister - breast cancer
20191238t1	No	No	0	No	No	Father - lung cancer, brother - prostate cancer
20191238t2	No	No	0	No	No	Father - lung cancer, brother - prostate cancer

Supplemental Table 2.3 OPAL Antibodies

PRIMARY ANTIBODY	COMPANY-CATALOGUE NUMBER	CONCENTRATION	SECONDARY ANTIBODY	COMPANY-CATALOGUE NUMBER	OPAL TSA™ FLUOROPHORE
CD8	SpringBio-M5390	1:400	Opal Polymer®	ARH1A01EA	570
CD3	Dako-A0452	1:400	Opal Polymer®	ARH1A01EA	520
CD163	Leica-NCL-L-CD163	1:400	Opal Polymer®	ARH1A01EA	650
PD-L1	CST-13684	1:200	Opal Polymer®	ARH1A01EA	540
Pancytokeratin	Dako-M3515	1:500	Opal Polymer®	ARH1A01EA	690
FOXP3	CST-12653	1:400	Opal Polymer®	ARH1A01EA	620

Supplemental Table 2.4 OPAL Phenotypes for Chronic Pancreatitis

COMPLEX PHENOTYPES FOR CHRONIC PANCREATITIS	BASIC PHENOTYPE (inForm®)	MEAN FLUORESCENT INTENSITY (MFI)	CELL SEGMENT OF MFI	POSITIVE OR NEGATIVE MFI
Tumor epithelial cell (TC)	Epithelial cell	N/A	N/A	N/A
PD-L1^{+} TC	Epithelial cell	PD-L1 (5 mfi)	Membrane	Positive
PD-L1^{-} TC	Epithelial cell	PD-L1 (5 mfi)	Membrane	Negative
Antigen presenting cell (APC)	APC	N/A	N/A	N/A
PD-L1^{+} APC	APC	PD-L1 (5 mfi)	Membrane	Positive
PD-L1^{-} APC	APC	PD-L1 (5 mfi)	Membrane	Negative
$T_{regulatory}$ cell (T_{reg})	Tcell	FOXP3 (4.75 mfi) CD8 (3 mfi)	Nucleus Cytoplasm	Positive Negative
Cytotoxic Tcell (CTL)	Tcell	CD8 (3 mfi)	Cytoplasm	Positive
T_{helper} cell (T_h)	Tcell	CD8 (3 mfi) FOXP3 (4.75 mfi)	Cytoplasm Nucleus	Negative Negative

Supplemental Table 2.5 OPAL Phenotypes for PDA samples

COMPLEX PHENOTYPES FOR PDASAMPLES	BASIC PHENOTYPE (inForm®)	MEAN FLUORESCENT INTENSITY (MFI)	CELL SEGMENT OF MFI	POSITIVE OR NEGATIVE MFI
Tumor epithelial cell (TC)	Epithelial cell	N/A	N/A	N/A
PD-L1^{+} TC	Epithelial cell	PD-L1 (2 mfi)	Membrane	Positive
PD-L1^{-} TC	Epithelial cell	PD-L1 (2 mfi)	Membrane	Negative
Antigen presenting cell (APC)	APC	N/A	N/A	N/A
PD-L1^{+} APC	APC	PD-L1 (2 mfi)	Membrane	Positive
PD-L1^{-} APC	APC	PD-L1 (2 mfi)	Membrane	Negative
$T_{regulatory}$ cell (T_{reg})	Tcell	FOXP3 (2 mfi) CD8 (3 mfi)	Nucleus Cytoplasm	Positive Negative
Cytotoxic Tcell (CTL)	Tcell	CD8 (3 mfi)	Cytoplasm	Positive
T_{helper} cell (T_h)	Tcell	CD8 (3 mfi) FOXP3 (2 mfi)	Cytoplasm Nucleus	Negative Negative

Supplemental Table 2.6 Antibodies for Immunofluorescent Staining

Marker	Clone	Dilution	Source	Catalog Number
PVR/CD155	D8A5G	1:100	Cell Signaling Technology	Cat# 81254S
Recombinant Anti-TIGIT antibody	BLR047F	1:100	Abcam	Cat# ab243903
CD8α	C8/144B	1:100	Cell Signaling Technology	Cat# 70306S
Anti-human CD163	10D6	1:100	Novus Biologicals	Cat# NB110-59935SS
Pan Cytokeratin Monoclonal Antibody, Alexa Fluor 488	AE1/AE3	1:250	Thermo Fisher Scientific	Cat# 53-9003-82
FoxP3	D6O8R	1:100	Cell Signaling Technology	Cat# 12653S
Vimentin XP®	D21H3	1:100	Cell Signaling Technology	Cat# 5741S
VE- Cadherin/CD144	123413	1:250	R&D	#MAB9381

Supplemental Table 2.7 Literature Supported Receptor Ligand Pairs

Ligand.ApprovedSymbol	Receptor.ApprovedSymbol
APOB	LDLR
APOE	LDLR
APOE	LRP5
APOE	LRP8
APOE	SORL1
APOE	VLDLR
CCL11	ACKR2
CCL11	CCR2
CCL11	CCR3
CCL11	CCR5
CCL11	CXCR3
CCL13	ACKR2
CCL13	CCR1
CCL13	CCR2
CCL13	CCR3
CCL13	CCR5
CCL13	CXCR3
CCL14	ACKR2
CCL14	CCR1
CCL14	CCR5
CCL15	CCR1
CCL15	CCR3
CCL16	CCR1
CCL16	CCR2
CCL16	CCR5
CCL16	HRH4
CCL17	CCR4
CCL17	CCR8

Ligand.ApprovedSymbol	Receptor.ApprovedSymbol
CCL19	ACKR4
CCL19	CCR7
CCL19	CCRL2
CCL19	CXCR3
CCL1	CCR8
CCL20	CCR6
CCL20	CXCR3
CCL21	ACKR4
CCL21	CCR7
CCL21	CXCR3
CCL22	CCR4
CCL23	CCR1
CCL24	CCR2
CCL24	CCR3
CCL25	ACKR4
CCL25	CCR9
CCL26	CCR2
CCL26	CCR3
CCL27	CCR10
CCL28	CCR10
CCL28	CCR3
CCL2	ACKR2
CCL2	CCR1
CCL2	CCR2
CCL2	CCR3
CCL2	CCR4
CCL2	CCR5
CCL2	DARC
CCL3	CCR1
CCL3	CCR5

Ligand.ApprovedSymbol	Receptor.ApprovedSymbol
CCL4	ACKR2
CCL4	CCR1
CCL4	CCR5
CCL4	CCR8
CCL5	ACKR2
CCL5	CCR1
CCL5	CCR3
CCL5	CCR4
CCL5	CCR5
CCL5	CXCR3
CCL5	DARC
CCL5	GPR75
CCL7	ACKR2
CCL7	CCR1
CCL7	CCR2
CCL7	CCR3
CCL7	CCR5
CCL7	CXCR3
CCL8	ACKR2
CCL8	CCR1
CCL8	CCR2
CCL8	CCR3
CCL8	CCR5
CD24	SELP
CD34	SELL
CD40LG	CD40
CD55	CD97
CD70	CD27
CX3CL1	CX3CR1
CXCL10	CCR3

Ligand.ApprovedSymbol	Receptor.ApprovedSymbol
CXCL10	CXCR3
CXCL11	ACKR3
CXCL11	CCR3
CXCL11	CXCR3
CXCL12	ACKR3
CXCL12	CXCR3
CXCL12	CXCR4
CXCL13	CXCR5
CXCL16	CXCR6
CXCL1	CXCR1
CXCL1	CXCR2
CXCL1	DARC
CXCL2	CXCR1
CXCL2	CXCR2
CXCL2	XCR1
CXCL3	CXCR1
CXCL3	CXCR2
CXCL5	CXCR1
CXCL5	CXCR2
CXCL6	CXCR1
CXCL6	CXCR2
CXCL9	CCR3
CXCL9	CXCR3
GZMB	IGF2R
HLA-A	KIR3DL2
HLA-B	KIR3DL1
HLA-C	KIR2DL1
HLA-C	KIR2DL3
HLA-C	KIR2DS4
HLA-E	KLRC1

Ligand.ApprovedSymbol	Receptor.ApprovedSymbol
HLA-E	KLRC2
HLA-E	KLRD1
HLA-G	KIR2DL4
HLA-G	KLRC1
HLA-G	KLRD1
HLA-G	LILRB1
IFNG	IFNGR1
IFNG	IFNGR2
IL10	IL10RA
IL10	IL10RB
IL11	IL11RA
IL11	IL6ST
IL12A	IL12RB1
IL12A	IL12RB2
IL12B	IL12RB1
IL12B	IL12RB2
IL13	IL13RA1
IL13	IL13RA2
IL13	IL2RG
IL13	IL4R
IL15	IL15RA
IL15	IL2RB
IL15	IL2RG
IL16	CD4
IL17A	IL17RA
IL17B	IL17RB
IL18	IL18R1
IL18	IL18RAP
IL18	IL1RAPL1
IL19	IL20RA

Ligand.ApprovedSymbol	Receptor.ApprovedSymbol
IL19	IL20RB
IL1A	IL1R1
IL1A	IL1R2
IL1B	IL1R1
IL1B	IL1R2
IL1B	IL1RAP
IL1RN	IL1R1
IL1RN	IL1R2
IL20	IL20RA
IL20	IL20RB
IL20	IL22RA1
IL21	IL21R
IL21	IL2RG
IL22	IL10RA
IL22	IL22RA1
IL22	IL22RA2
IL23A	IL12RB1
IL23A	IL23R
IL24	IL20RA
IL24	IL20RB
IL24	IL22RA1
IL25	IL17RB
IL2	IL2RA
IL2	IL2RB
IL2	IL2RG
IL31	IL31RA
IL31	OSMR
IL3	CSF2RB
IL3	IL3RA
IL4	IL13RA1

Ligand.ApprovedSymbol	Receptor.ApprovedSymbol
IL4	IL2RG
IL4	IL4R
IL5	CSF2RB
IL5	IL5RA
IL6	IL6R
IL6	IL6ST
IL7	IL2RG
IL7	IL7R
IL8	CXCR1
IL8	CXCR2
IL8	DARC
IL9	IL2RG
IL9	IL9R
CCL11	ACKR4
CCL13	ACKR4
CCL14	CCR3
CCL16	CCR8
CCL17	DARC
CCL18	C14orf1
CCL19	ACKR2
CCL19	CCR10
CCL21	ACKR2
CCL25	ACKR2
CCL25	CCR10
CCL26	CCR1
CCL27	ACKR2
CCL28	ACKR2
CCL2	ACKR4
CCL2	CCR10
CCL3L1	CCR1

Ligand.ApprovedSymbol	Receptor.ApprovedSymbol
CCL3L1	CCR3
CCL3L1	CCR5
CCL3L3	ACKR2
CCL3L3	CCR5
CCL3	ACKR2
CCL3	CCR3
CCL3	CCR4
CCL4	CCR3
CCL5	ACKR4
CCL5	SDC1
CCL5	SDC4
CCL7	ACKR4
CCL7	CCR10
CCL7	DARC
CCL8	ACKR4
CCL8	DARC
CD14	ITGA4
CD14	ITGB1
CD55	CR1
CD5L	CD5
CXCL10	SDC4
CXCL12	CD4
CXCL12	ITGB1
CXCL13	ACKR4
CXCL13	CCR10
CXCL13	CXCR3
CXCL5	DARC
HLA-A	APLP2
HLA-A	ERBB2
HLA-A	KIR3DL1

Ligand.ApprovedSymbol	Receptor.ApprovedSymbol
HLA-A	LILRB1
HLA-A	LILRB2
HLA-B	CANX
HLA-B	KLRD1
HLA-B	LILRB1
HLA-B	LILRB2
HLA-C	LILRA3
HLA-C	LILRB1
HLA-C	LILRB2
HLA-G	LILRB2
IL12A	CD28
IL12B	IL23R
IL15	IL2RA
IL16	GRIN2C
IL16	GRIN2D
IL16	KCNA3
IL16	KCND1
IL16	KCND2
IL16	KCNJ10
IL16	KCNJ15
IL16	KCNJ4
IL17A	IL17RC
IL17F	IL17RA
IL18	IL1RL2
IL1A	IL1RAP
IL1B	ADRB2
IL1F10	IL1R1
IL22	IL10RB
IL27	IL27RA
IL2	CD53

Ligand.ApprovedSymbol	Receptor.ApprovedSymbol
IL2	NGFR
IL34	CSF1R
IL4	CD53
IL4	IL13RA2
IL8	SDC1
IL8	SDC2
CD274	PDCD1
CD80	CTLA4
LGALS9	HAVCR2
PVR	TIGIT
HLA-DQA1	LAG3
TNFRSF14	BTLA
ADORA1	ADORA2A
CD80	CD28
ICOSLG	ICOS
TNFSF9	TNFRSF9
TNFSF4	TNFRSF4
TNFSF18	TNFRSF18
CD47	SIRPA
CSF1	CSF1R